Thesis submitted for obtaining the degree of

Doctorate in Civil Engineering

Specialty: Modeling and Analysis of Structures

Macro Analyse, Statique Non-linéaire et Dynamique des Bâtiments en Béton Armé avec Murs de Remplissage en Zones Sismiques

Macro Analysis, Nonlinear Static and Dynamic, of Reinforced Concrete Buildings with Masonry Infill Walls in Seismic Zones

Presented by:

Abdelghaffar Messaoudi

Thesis defender publicity on: March 09th, 2023

The jury is composed of:

Mr. Hamadi Djamel	Professor	U. Biskra	President
Mr. Chebili Rachid	Professor	U. Biskra	Supervisor
Mr. Rodrigues Hugo F. P	Assoc. Professor	U. Aveiro. Portugal	Co-Supervisor
Mr. Kadid Abdelkarim	Professor	U. Batna 2	Examiner
Mr. Abdeddaim Mahdi	Assoc. Professor	U. Biskra	Examiner
Mr. Mabrouki Abdelhak	Professor	U. Biskra	Invited

Acknowledgements

It has been a really fruitful journey full of new experiences both academically and personally. However, as any other experiences in our life, this experience was not free of hard times, it would not have been possible without the contribution and support of the kind people who accompanied me throughout this process. In the following paragraphs, I would like to express my most sincere gratitude and appreciation for those who have helped me in completing this journey.

Firstly, I would like to acknowledge my sincere gratitude to my supervisor, **Professor Chebili Rachid**, for providing the guidelines of the most work I have been doing since our first meeting, which put me on the right path. I also grateful to him for giving me the freedom to pursue independent work and explore things on my own. I am also grateful to him for his skilful supervision, continuous encouragement, and unconditional support during the preparation of this thesis. For being an exceptional Professor and Supervisor.

Second, I would like to express a special gratitude to **Professor Hugo Rodrigues** from Aveiro University, Portugal. I Acknowledge him for giving me the opportunity to complete this long and challenging journey under his Co-supervision. I will never forget all the opportunities, all the confidence, and all the knowledge that He shared with me for his unconditional support and friendship. always with a unique enthusiasm and an enormous willingness to speak about science and life.

Thirdly, I am grateful to the president of the jury, **Professor Hamadi Djamal**, who honoured me with his presence and chairing the defence jury.

I would also like to express my sincere thanks to the jury members **Professor Kadid Abdelkarim** and **Dr. Abdeddaim Mahdi** as examiners for the honour by accepting to examine this thesis and for the time and the interest that they brought to this work by agreeing to examine it.

I would like to express my deepest gratitude to **Professor Hossameldeen Mohamed** from Aswan University, Egypt, for his strong and close support that made it possible to complete this PhD. I will not forget all the efforts to ensure that everything was going well. For his friendship

and concern during all this period. For all the opportunities. For all the knowledge shared with me, for his contributions along the development of this work and enthusiastic ideas. For thousand reasons that it is impossible to express in words. " My Allah rewards you all good "

I would like to express a special gratitude to **Dr. Abdesslam Issam** one of my best friends during all these years. I will never forget all the support every single day during this period. All the advice, the concern, the friendship. An inspiration and an example for me. He always knows how to push my best capacities and how to motivate me, for all the adventures during all these years, and for other thousand reasons that I think it is not possible to express in words, Thank you.

I would like to acknowledge my sincere gratitude to **Professor Mabrouki Abdelhak** and **Professor Taallah Bachir** for their motivations during difficult periods. I appreciate their friendly behaviour, unconditional support, and fully encouraging innovative ideas.

A special thanks to **Dr. Kechai Abdelhak** for his support and assistance to me in preparing the PNE2019/2020 scholarship file and for his support and fruitful suggestion.

I would also like to express my sincere thanks to **Dr Belarbi M. Ouejdi**, **Dr. Yakoub Mohamed** and **Dr Zine Ali**, for their friendship and help. Their opinions, encouragement and optimism were fundamental during this journey.

Deep appreciation is extended in order to thank **Dr. Haouara Selma**, **Dr. Chabi Samia**, **Dr. Kadri Karima**, **Dr. Meghazi. I. Larafi** and **Dr. Djedoui Nassim** for their precious help, their opinions, encouragement, and optimism.

I want to thank **Professor Guettala Abdelhamid**, Director of the Laboratory of Civil Engineering, for his warm welcome within his research team and unconditional support.

A special acknowledgement to **Dr. Andre Furtado**, University of Porto (FEUP). For his precious help, his opinion, encouragement, and optimism, as well as for receiving me in the civil engineering laboratory at the University of Porto.

I would also like to express my deep appreciation to colleagues and friends from the Civil Engineering Research Laboratory, Civil Engineering Department, University of Biskra.

To all my friends in the IPL laboratory (Leiria, Portugal) and To my friends in the laboratory of civil engineering University of Aveiro (Portugal), whom I was fortunate to work with them in the same office and who made the working environment very friendly, I would like to express my deep thank to all of them for their companionship and friendship which made this experience in a foreign country more pleasant and enjoyable.

Because family is the support of our lives, this work would not be possible without the support and inspiration of my mother, father, sisters, and brother. All of them were present in each word of this thesis. They were the base of my force and ambition since I was born. Thanks for being always there for me. To my wife, for everything you did for me, I am also deeply grateful to her for help in editing some paragraphs in this dissertation.

I would like to express my thanks and deep appreciation to the Rector of Biskra University, **Professor Boutarfaia Ahmed** - *My Allah have mercy on him*- for his continuous encouragement and unconditional support. ⟨ *O Allah, forgive him and have mercy on him*⟩ .

I would like to extend my sincere thanks and gratitude to **Mr. Ariech Said** a deputy in the National People's Assembly, for his continuous support and for always standing by my side. Likewise, To **Mr. Bouznada Abdelbari** has a deputy in the Council of the Nation for his providing the unconditional support and fully encouraging.

Finally, it was a long process, which gave me the opportunity to get in touch with several professors, colleagues and people who shared in this work even by a kind word, to those may not be mentioned in these acknowledgements I would like to express deep appreciations.

Messaoudi Abdelghaffar

To my beloved family,

Abstract

The developed research aimed to understand the influence of masonry panels on the global behaviour of reinforced concrete frame buildings and in particular the effect of mechanical properties, openings, and the changing in the distribution. For this purpose, calibration procedures are used for defining the parameters of different types of simplified infill modelling based on available experimental work. The reliability of the proposed calibration procedures is evaluated based on available experimental data gathered from the literature. Then, a pushover analysis is carried out to evaluate the seismic performance, assess the behaviour of infilled RC, and study the results related to the capacity curve, maximum inter-storey drift (ISD_{max}) and energy absorbed.

To provide a comprehensive view regarding the effect of the infill and their configurations, the proposed study provided an extended parametric study and assumptions regarding the effect of the infill configuration and spatial distribution of the infill walls on final fragility curves. Numerical models of the structures were developed to obtain the fragility data, simulating the infill structures using single strut models. The models were analyzed in the context of nonlinear dynamic analysis using incremental dynamic analysis (IDA). The intensity measure IM-based procedures were adopted to drive the fragility functions. The driven fragility functions were then used to compare the performance of the studied cases and assess the effect of the infill configuration on the overall performance. Noticeable remarks and findings in terms of distributing masonry panels within a frame are observed and several recommendations concerning the current practice might be essential to be considered.

Keywords: Reinforce Concrete, OpenSees, masonry infill walls; Openings; Non-linear static analysis, Incremental dynamic analysis, Fragility curve.

الملخص

يهدف البحث المطوَّر إلى فهم تأثير ألواح البناء على السلوك العام للمباني ذات الإطار الخرساني المسلح وعلى وجه الخصوص تأثير الخواص الميكانيكية والفتحات والتغيير في التوزيع. لهذا الغرض، يتم استخدام إجراءات المعايرة لتحديد خصائص الأنواع المختلفة لنمذجة الحشو المبسطة بناءً على التجربة المتاحة. يتم تقييم موثوقية إجراءات المعايرة المقترحة بناءً على البيانات التجريبية المتوفرة التي تم جمعها من الأدبيات. بعد ذلك، يتم إجراء تحليل انسيابي لتقييم الأداء الزلزالي وتقييم سلوك RC المملوءة ودراسة النتائج المتعلقة بمنحنى السعة و ISD max والطاقة الممتصة.

لتوفير نظرة شاملة فيما يتعلق بتأثير الملء وتكويناته، قدمت الدراسة المقترحة *مسمار حدودي ممتد* وافتراضات فيما يتعلق بتأثير تكوين الحشو وتوزيع *جدران الردم* على منحنيات الهشاشة النهائية. تم تطوير النماذج العددية للهياكل للحصول على بيانات الهشاشة، ومحاكاة هياكل الحشو باستخدام نماذج الدعامة المفردة. تم تحليل النماذج في سياق التحليل الديناميكي غير الخطي باستخدام التحليل الديناميكي التزايدي (IDA). تم اعتماد الإجراءات القائمة على قياس الكثافة لقيادة وظائف الهشاشة. ثم تم استخدام وظائف الهشاشة المدفوعة لمقارنة أداء الحالات المعنية المدروسة وتقييم تأثير التعبئة على الأداء العام. يتم ملاحظة النتائج فيما يتعلق بتوزيع ألواح البناء داخل إطار وقد يكون من الضروري النظر في العديد من التوصيات المتعلقة بالممارسة الحالية.

الكلمات المفتاحية: خرسانة مسلحة، OpenSees، جدران حشو البناء، الفتحات، التحليل الستاتيكي اللاخطي، التحليل الديناميكي التزايدي، منحى الهشاشة.

Contents

List of figures

Chapter 1. Introduction

Chapter 2. Literature review

Chapter 3. Seismic Evaluation Methods for RC structures

Chapter 4. Numerical simulation of RC infilled frames

Chapter 5. Static Non-Linear Analysis of Infilled RC Structures

Chapter 6. Seismic vulnerability assessment of RC frames with masonry infills.

List of Tables

Chapter 6. Seismic vulnerability assessment of RC frames with masonry infills.

List of Abbreviations

ADRS	Acceleration Displacement Response Spectrum
ASCE	American Society of Civil Engineers
ATC	Applied Technology Council
Avg Sa	Average Spectral acceleration
CCMPA	Canadian Concrete Masonry Producers Association
CEB	Comité Euro-international du Béton.
COV	Coefficient Of Variation
CQC	Complete Quadratic Combination
EDP	Engineering Demand Parameters
FEMA	Federal Emergency Management Agency
IDA	Incremental Dynamic Analysis
IM	Intensity Measure
ISD	Inter-storey Drift
LNEC	Laboratório Nacional de Engenharia Civil (Portugal)
LVDT	Linear Variable Differential Transformer
MDOF	Multi-Degree-Of-Freedom
MRF	Moment-Resisting Frame
MSJC	Masonry Standards Joint Committee
NZS	New Zealand masonry Code
PGA	Peak Ground Acceleration
PGD	Peak Ground Displacement
PGV	Peak Ground Velocity
RC	Reinforced Concrete
RPA	Algerian Seismic Regulations
SDOF	Single-Degree-Of-Freedom
SEAOC	Structural Engineers Association Of California
SRSS	Square Root of the Sum of Squares
TEC	Turkish Code for Buildings in Seismic Zones
URM	Unreinforced masonry

Chapter 1.

Introduction

1.1 General Overiew

Reinforced concrete (RC) frame structures with masonry infills are common in use around the globe including countries with medium/high seismic hazards [1.2]. The Mediterranean Sea countries are a distinct example for these countries, including Algeria. Even though, the ability of infill walls to carry lateral loads during the earthquakes are obviously seen in several post-earthquake investigation (e.g., see [3] among others) and in several numerical and experimental studies [4].

Masonry infill walls may take a large part of the seismic forces in the initial stages of the earthquake action. Still, with the increase in the seismic demand, the infill walls may undergo the first cracks and may be separate from the structure. Therefore, the influence of the walls on the local and global behaviour of the structure and their contribution to the capacity and stiffness remains dependent on the characteristics of these walls.

The question generally asked is to know the influence of the infill masonry walls on the structure's building strength and energy dissipation capacity, its way of undergoing post-elastic deformations, its initial stiffness, and the failure mechanisms. Knowing that the failure mechanism recommended by the RPA [5] is a global failure mechanism, obtained by designing these self-stable structures in such a way that the plastic hinges are formed in the beams rather

than in the columns, to dissipate by plastic deformations, a maximum of seismic energy without collapsing.

In Algeria, the use of masonry is limited; it is often used only as filling material in the construction of the reinforced concrete building. In analysis, masonry's influence on building behaviour is commonly neglected. However, the masonry infill walls have an important influence on the characteristics of the structures; this practice consisting in neglecting the influence of the masonry was imposed by the lack of a practical method of calculation as well as of an appropriate regulatory tool.

1.2   Motivation and Objectives

Reinforced concrete (RC) frame buildings with masonry infills have been widely used to construct commercial, residential and industrial buildings. Such buildings have been mostly designed and constructed following different specifications and construction codes without accounting for the interaction between RC frames and the infill panels. Even though the infill panels were not intended to be a part of the structural system, masonry or infill panels increase the lateral stiffness of the structure. Furthermore, infill panels can introduce brittle shear failure mechanisms or short column effects due to infill panel and frame interactions, as shown in Figure1.1to Figure 1.3. Generally, it can be seen that infill panels can change the global characteristics of the structure and the failure mechanism in case of an earthquake. Therefore, the real performance of these structures and their ability to withstand earthquakes must be evaluated. Although, there is a vast body of literature that, over the past decades, tried to fully understand the dynamic response of RC infilled frames, either experimentally or numerically, there is still no consensus on the complete set of effects that masonry infill walls have on the global structural behaviour.

Figure1.1: Captive column failure Managua 1972 [6].

(a) Moderate damage to RC frame and infill wall   *(b) Infill damage and minor damage to the RC frame*

Figure 1.2: Effect of solid infill walls on the behaviour of the bounding RC frame [7].

(c) Infill damage and minor damage to the RC frame

Figure 1.2 (Continued): Effect of solid infill walls on the behaviour of the bounding RC frame [7].

(a) Infill compression and shear and minor frame
damages

(b) Infill shear and minor frame damages

Figure 1.3: Damages of masonry infilled RC frames after the Wenchuan earthquake [7].

(c) Infill compression and minor frame damages

(d) Infill compression and major frame damages

(e) Infill compression and shear and moderate framedamages

(f) Infill shear and major frame damages

Figure 1.3 (Continued): Damages of masonry infilled RC frames after the Wenchuan earthquake [7].

Most of the former research concentrated on the behaviour of the masonry panel and on assessing the structural interaction between the infill and the RC frame. Recently, enhanced modelling techniques to capture the physical behaviour of the relation between the infill and the frame have been investigated [8]. Due to the large number of structures and the potential fatalities and losses involved in high seismic regions, there is an urgent need to develop the tools needed to assess the performance of these buildings, more specifically within a performance-based probabilistic framework [9].

Therefore, the current study aims to analyse and assess the performance of RC infilled frames under seismic loading with a sequential methodology. This methodology can be summarized in three main steps as follows:

1. **Calibration of existing macro-models:**

   - Selection of the best modelling approaches for masonry infill involving equivalent strut models based on their calibration with experimental data.
   - Proposal of a configuration for a macro-model to model the behaviour of the partially infilled RC frames relying on numerical results obtained from the micro-models studied in the first step.
   - Verification of the parameters of the selected strut models considering the available experimental data.

2. **Performance analysis of RC infilled frames under lateral load:**

   - Definition of several RC infilled and bare frames with different characteristics and infill wall distribution configurations.
   - Study the seismic behaviour of RC infilled frames using the non-linear static analysis (Pushover), considering the influence of the mechanical propriety (i.e., thickness and compressive strength) on the global behaviour of RC frame structures.
   - Study the seismic behaviour of RC infilled frames using the non-linear static analysis (Pushover), considering the effect of openings and the variability of the presence of masonry panels on the global behaviour of RC frame structures.

3. **Seismic vulnerability assessment of RC frames with masonry infills:**

   - Definition of several RC infilled and bare frames with different characteristics and configurations, considering the variation in the distribution of the infill walls of the buildings.
   - Selection of real ground motions using advanced selection criteria to carry out nonlinear dynamic analyses.
   - Incremental dynamic analysis (IDA) of the selected frames.

- Statistical analysis of the structural and non-structural response of the frames.
- Definition of fragility curves for the frames for different performance levels (i.e., slight, light, moderate, extensive, partial collapse, and collapse).
- Addresses the probabilistic performance and vulnerability assessment of several masonry infilled RC frames.

1.3   Dissertation Outline

This thesis project consists of seven chapters. After this first introductory chapter, the **second chapter** presents a literature review of the past research conducted on the behaviour of masonry infilled RC frames. First, experimental research is presented, followed then by a discussion on existing analytical research and on the different modelling approaches that have been used for masonry panels, including micro-modelling and macro-modelling approaches. **Chapter two** also reports some of the failure modes of masonry infilled RC frames to motivate the study of the seismic performance of these buildings.

In the **third chapter** a description of the analysis's methods, especially the nonlinear static analysis method, Pushover, and the Incremental Dynamic Analysis, which were used in this study.

In the **fourth chapter**, an analysis of the studied models in the literature is carried out using OpenSees's software potentialities with the main objective of assessing the behaviour of detailed masonry infill structures under a set of variables and comparing the numerical results with available experimental data performed by *Kakaletsis et al* (2008), *Marta et al. (2021)*, *André Furtado et al. (2021)* and *Maria Teresa et al. (2022),* in the Laboratory of Earthquake and Structural Engineering (LESE, Portugal).

The **fifth chapter** presents the performance analysis of several 2D frames with different infill panel configurations, where it aims to focus on studying the influence of the mechanical proprieties, the impact of the presence of openings and the effect of the variability of the presence of masonry panels on the global behaviour of buildings and its effect on the structural response. For this, a pushover analysis is carried out to evaluate the seismic performance, assess the behaviour of infilled RC, and study the results related to capacity curve, inter-story drift and energy.

Chapter six presents the probabilistic performance analysis of several 2D frames with different infill panel configurations. It considers the difference in the distribution of the infill walls, and the proposed study examines the various structural modelling parameters and assumptions about probabilistic modelling that affect the final fragility curves. Numerical models of the structures were developed to obtain the fragility data, simulating the infill structures using single strut models. The models were analysed in the context of nonlinear dynamic analysis using incremental dynamic analysis (IDA). The study analyses the differences between the fragility curves of different infilled RC frames for several limits' states.

The final chapter, c**hapter seven,** briefly presents a summary of the main conclusions and findings of the previous chapters, along with proposals and recommendations for future research on some of the topics addressed in this thesis.

<div style="text-align: right">

Chapter 2.

Literature review

</div>

2.1 Preface

One of the most prevalent structural systems are reinforced concrete (RC) frames with unreinforced masonry (URM) in many nations, including seismically active areas. Despite being built as non-structural elements, these infill masonry walls' behavior during earthquakes is integrated with that of RC frames. This chapter gives an overview of the literature on the structural behavior and failure modes of infilled wall frames. After that, a review of prior analytical and experimental studies on this kind of structure is also included, along with an explanation of the benefits and drawbacks of each method.

2.2 Failure modes of RC frames with infill walls

Since there are so many different variables, the failure mechanism of masonry infill walls frames are highly complicated. Based on experimental studies that have been conducted over the last decades, as demonstrated in Figure 2.1, there are many different typologies of infilled RC frame failure modes. To organize the different masonry infilled RC frame failure modes into categories and to make understanding the phenomenon more straightforward, a substantial quantity of research has been done. Following, is a basic description of how different modes of failure are classified. Mehrabi [10] identified twenty-four various in-plane failure mechanisms

for infill wall frames based on fourteen half-scale tested frames. As depicted in Figure 2.2, Stavridis [11] recently divided these in-plane failure mechanisms into three primary mechanisms:

- Infill with diagonal cracking and column shear failure
- Masonry sliding horizontally with a column, flexural or shear failure.
- Infill corner crushing with column flexural failure.

a)

b) c)

d)
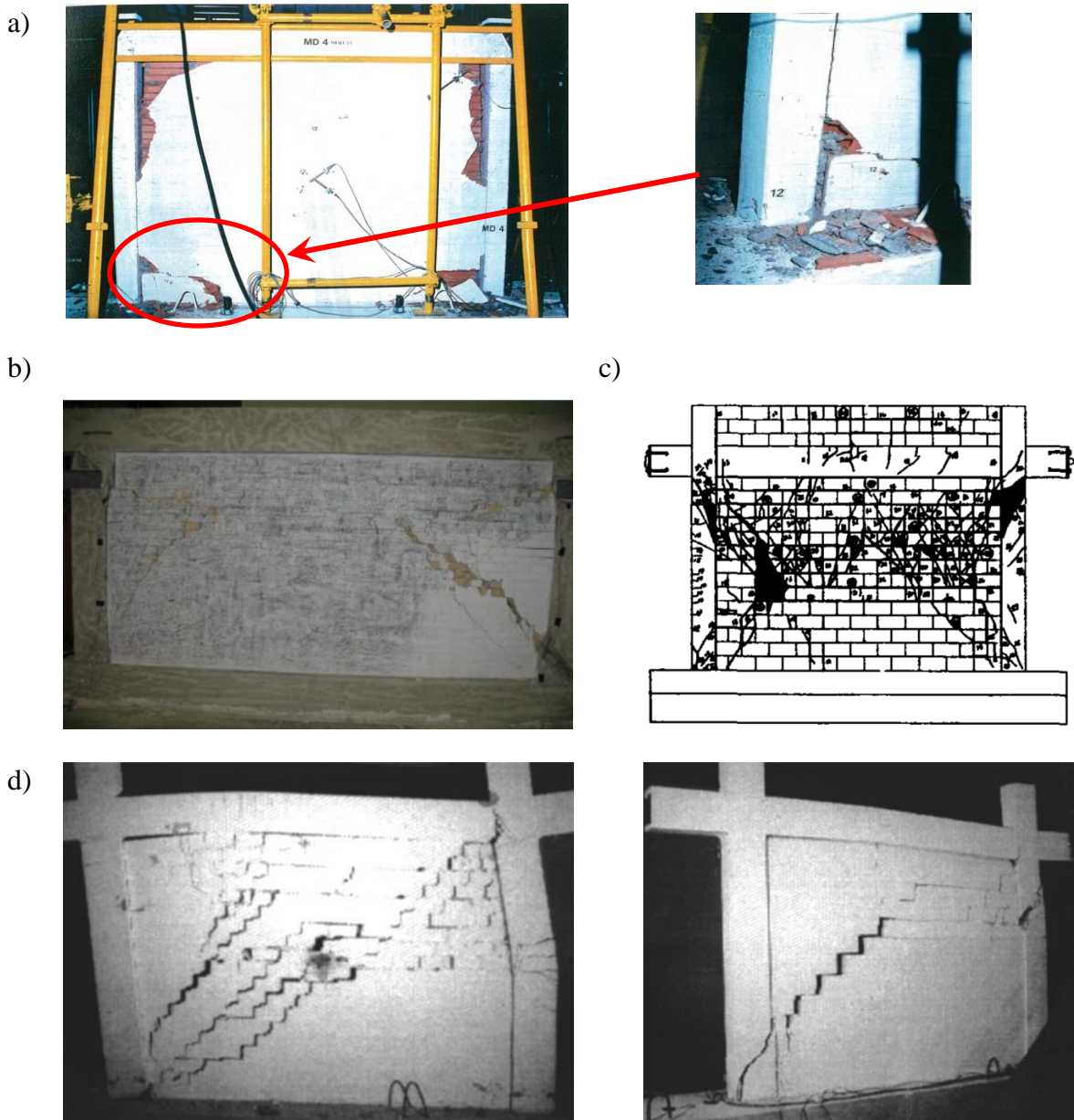
Figure 2.1: Experimental observations on infilled frames failure mechanisms (a) Corner failure mechanism (LNEC) [12] (b)Top corner failure (Blackard et al.) [13] (c)Shear failure in columns and masonry crushing (Mehrabi et al.)[14] (d) Splitting in bed and head joint through diagonal of the infill (Al-Chaar et al.) [15].
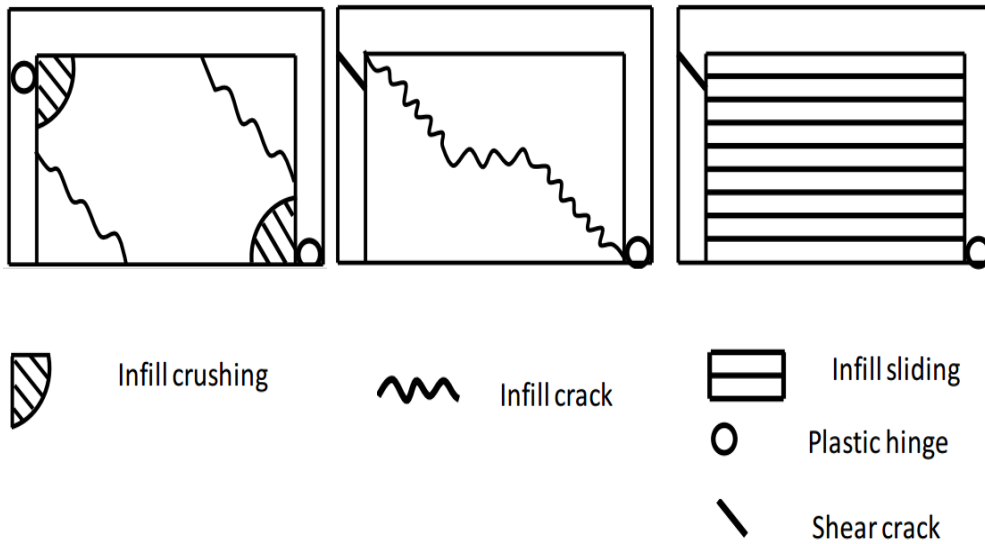
Figure 2.2:Failure mechanisms of masonry infill walls frames (Mehrabi) [10].

Based on experimental and analytical findings gathered, El-Dakhakhni, et al. [16] categorized the failure modes of masonry infilled frames according to five separate modes in the same context:

- *CC mode (Corner crushing),* in which at least one masonry wall panel corner is crushed.
- *DC mode(Diagonal compression) illustrates* the central region of the infill being crushed.
- *DK mode (Diagonal Cracking),* a crack forms across the infill panel's compressed diagonal.
- *SS mode (Sliding shear),* this mechanism involves shear sliding through a masonry infill's bed joint.
- *FF mode (Frame failure),* plastic hinges are created in columns, beam-column joints, in this mode.
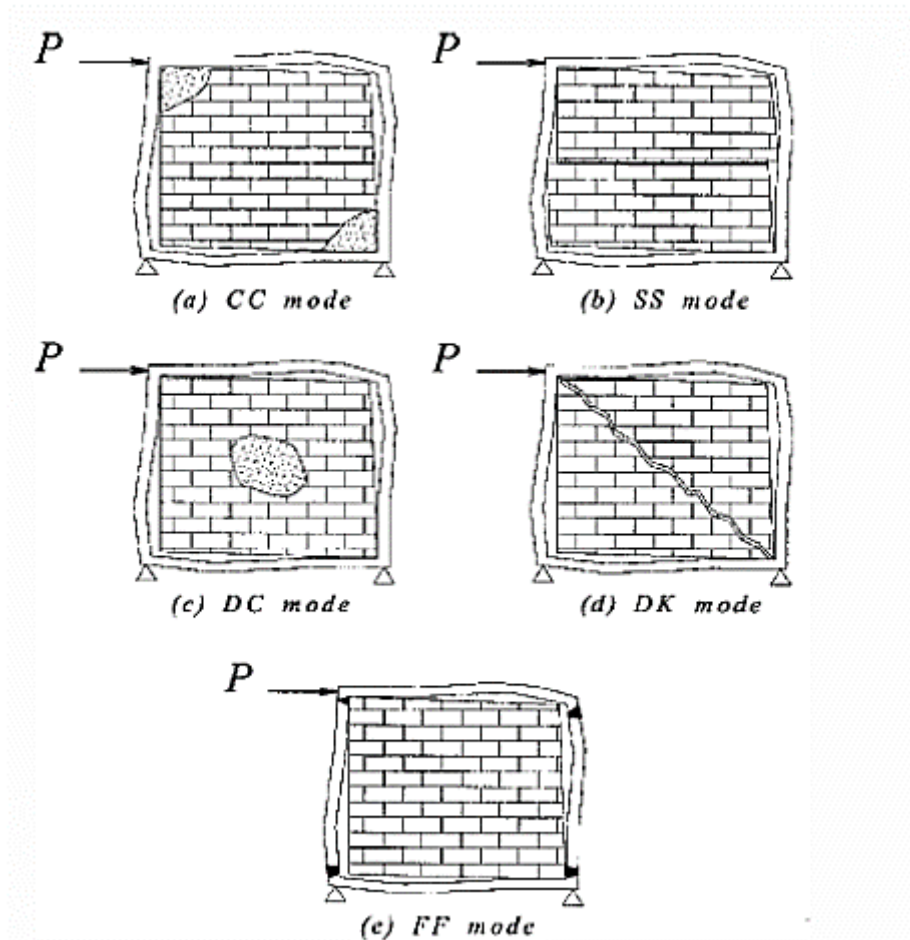
Figure 2.3: Different failure modes of the infilled frames: (a) corner crushing; (b) sliding shear;(c) diagonal compression; (d) diagonal cracking; and (e) frame bending failure (El-Dakhakhni etal.) [16].

Using numerical models based on the finite element method, including interface elements between the frame and the infill panel, Ghosh, *et al.* [17] confirmed the order of occurrence of the five distinct failure modes. On the other hand, CEB [18] mentioned that of the five modes, only the CC and SS modes are of practical importance,while the second mode (DC) occurs very rarely and requires a high slenderness ratio of the infill to result in out-of-plane buckling of the infill under in-plane loading and most infills are not slender (El-Dakhakhni, *et al.*) [16]. Asteris, *et al.*) [8] stated that (DK) should not be considered a failure mode because of the post-cracking capacity of the infill to carry additional load while (FF) is related to the failure of the frame and is particularly important when analysing existing structures that, in many cases, exhibit structural weaknesses [19].

a. CC mode (Corner crushing)

b. DC mode (Diagonal compression)

c. DK mode (Diagonal Cracking)

d. SS mode (Sliding shear)

e. FF mode (Frame failure)
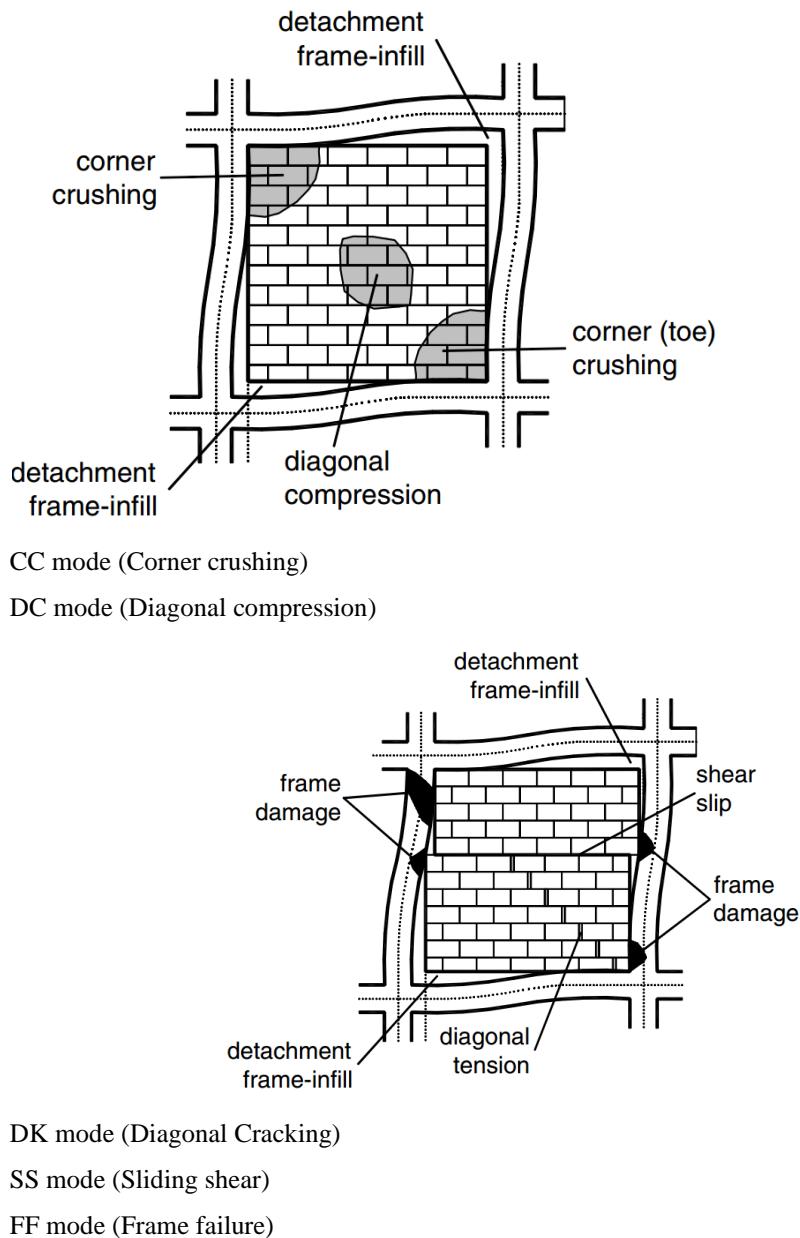
Figure 2.4 : Modes of failure of masonry in-filled frames (Asteris, et al.) [8].

2.3 Failure modes of RC infilled frames with openings

Figure 2.5 illustrates how the presence of an openingin in the infill panel affects the infill wall behaviour and, consequently, the failure mechanisms. The openings may prevent the infill wall and the development of the diagonal strut (diagonal bracing), Asteris, et al. (2011b) [20] divided the failure mechanisms for masonry infill walls frames with openings into three major categories based on ten tests using 1:3 scale one-bay frames with various sizes, types, and positions of openings.

➢ The presence of a window opening in a weak infill results in a plastic hinge failure mechanism at the ends of the columns, with shear sliding above and below the window, of the masonry zones, and internal crushing between columns and window, of the masonry segments, as illustrated in Figure 2.5.

➢ According to Figure 2.6, Plastic hinges at both ends of the columns govern the failure mechanism of the frame with a door opening in a weak infill, corner crushing due to rocking of the infill walls segment between the door and the column in tension, internal crushing of the other masonry segment between the door and the column, and shear sliding of the masonry zone above the door.

➢ Because the main compressive strut is not formed, the existence of an opening across the diagonal of the infill walls eliminates the well-known failure modes of (DC) Diagonal Compression and (DK) Diagonal Cracking.

a)

b)

c)

d)

e)

f)
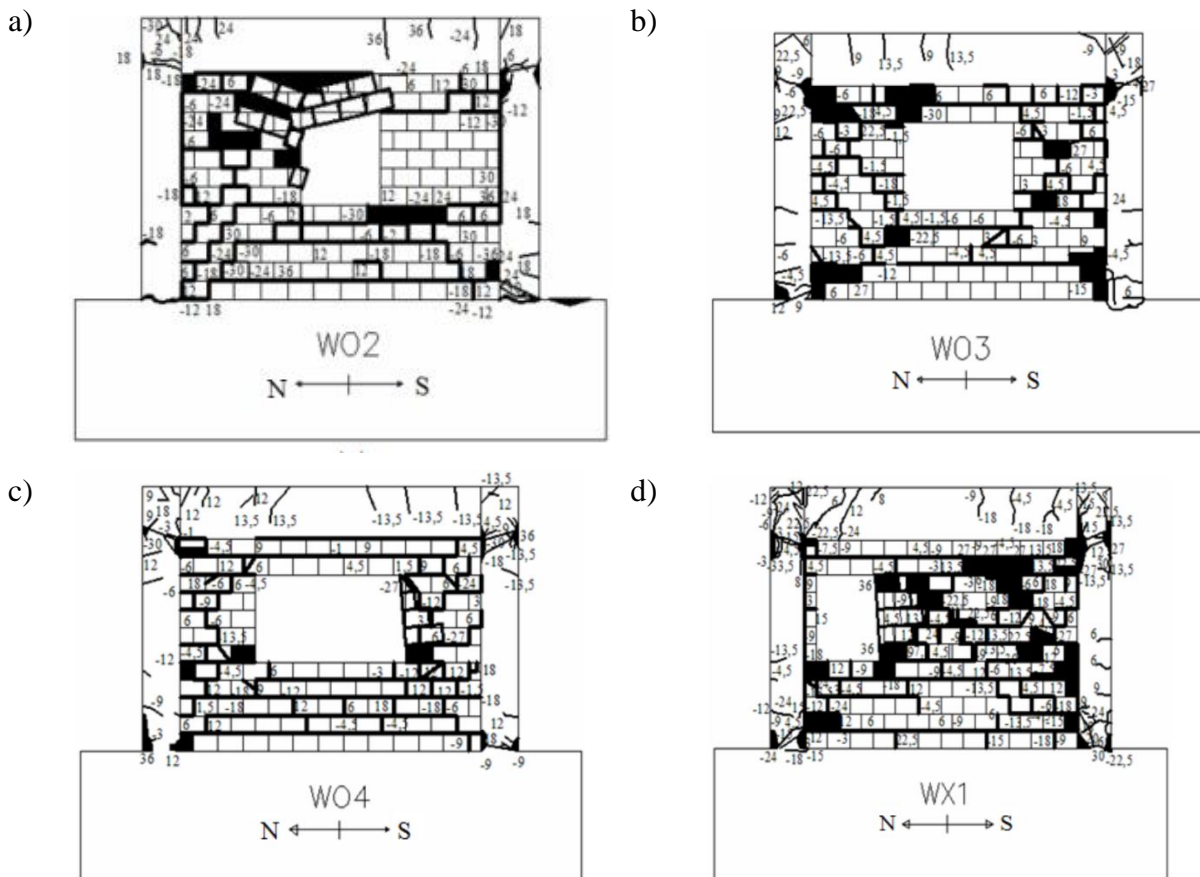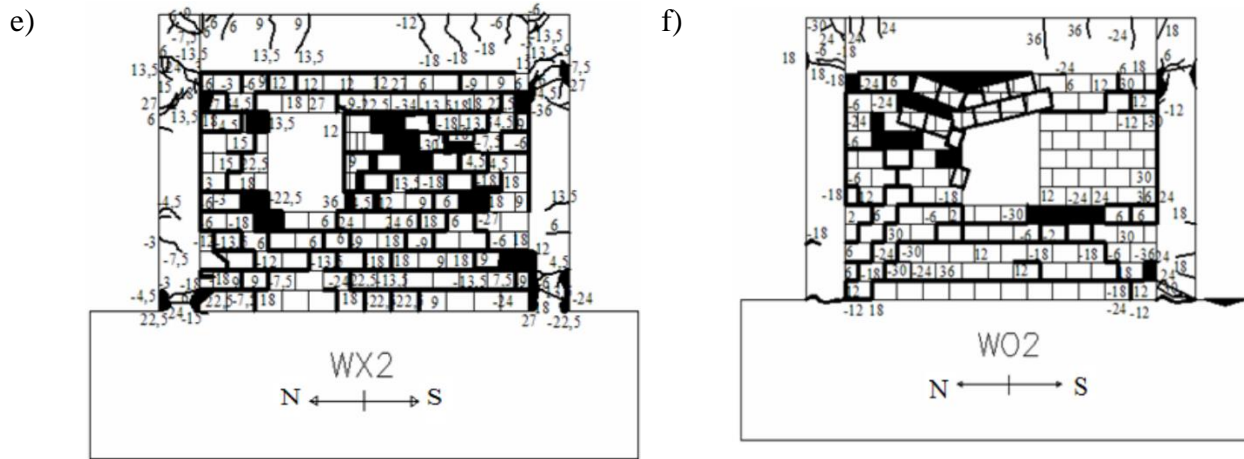
Figure 2.5: Different failure modes of masonry infilled frames with window openings observed by Asteris, et al. [20].

a)

b)

c)
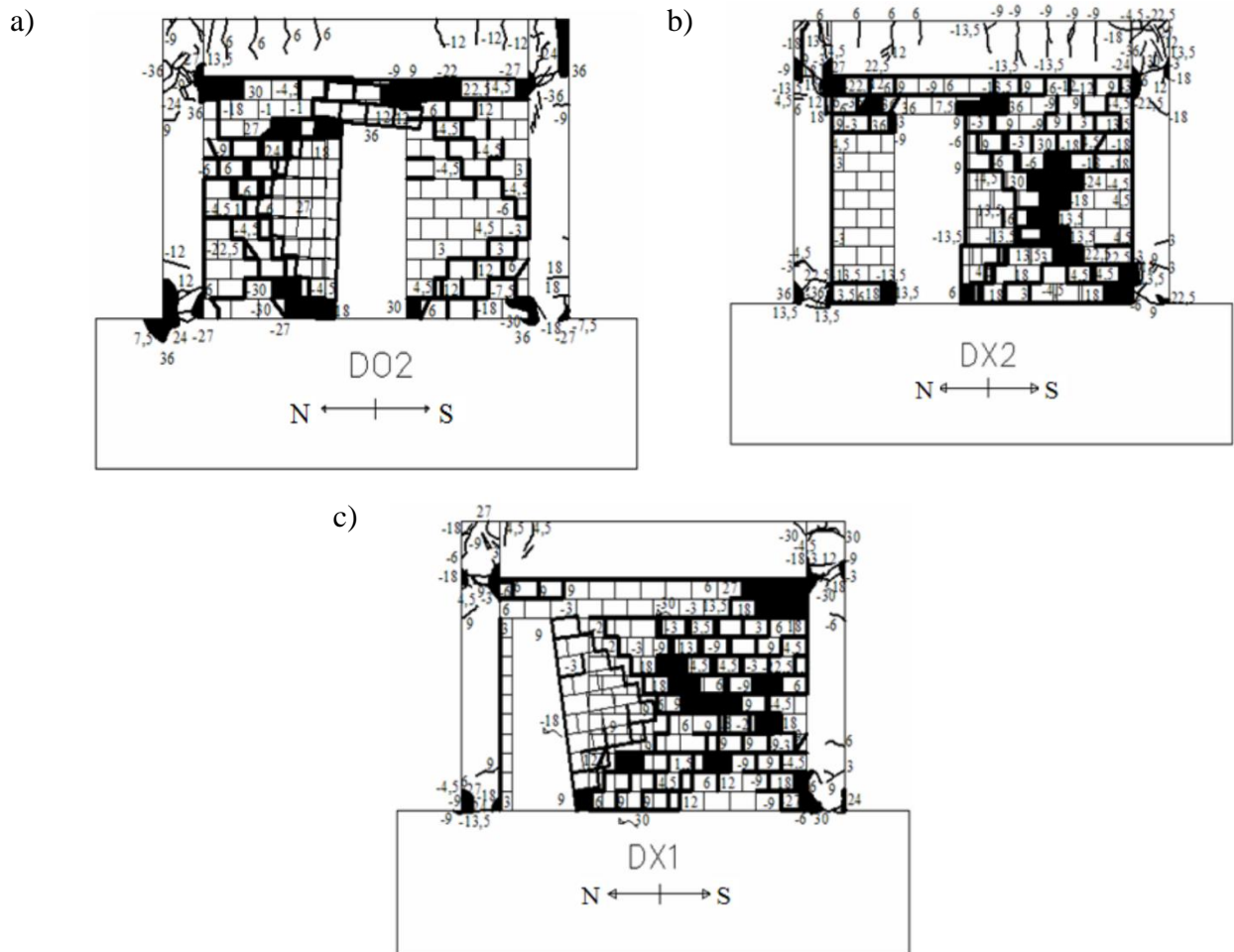
Figure 2.6: Different failure modes of masonry infilled frames with door openings by Asteris, *et al.* [20].

2.4 Experimental Research

This section addresses several experimental studies which have analysed the influence of masonry infill on the in-plane behaviour of RC frames. The experimental tests on RC infilled frames helped researchers to get a rational understanding of the behaviour of masonry infilled frames under different loading types. The referred experimental studies are presented in chronological order.

Polyakov (1956) [21] performed experimental tests on masonry infilled steel frames and suggested that the masonry infill wall acts as frame bracing by forming compression "struts", as seen in Figure 2.7. Because of the low tensile strength of the masonry infill material, these struts are assumed to be unable to carry tensile loads.
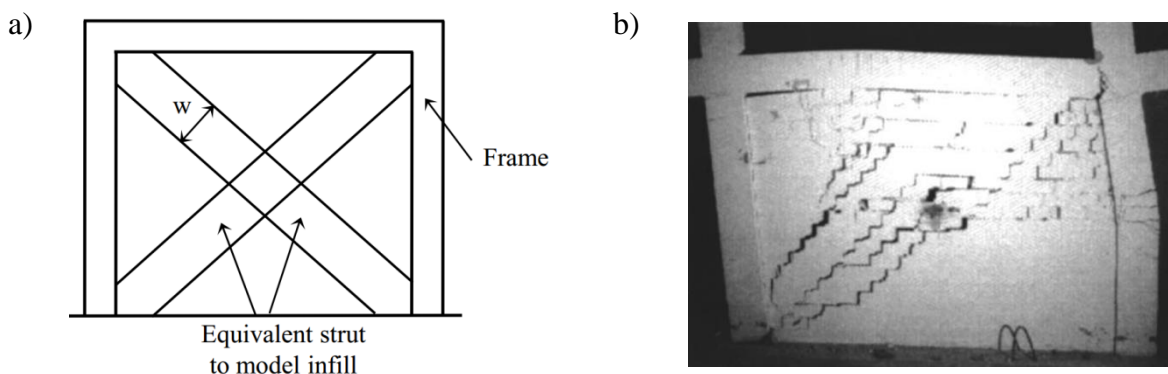
Figure 2.7: (a) Equivalent strut model, (b) experimental findings demonstrating strut production (Al-Chaar, et al.) [15].

Later Sachanski (1960) [22] to calibrate a theoretical technique to evaluate the contributions of masonry infill walls in the combined stiffness and load distribution of structures, he performed a series of monotonic static tests on full scale infilled RC frame models. Sachanski created a theoretical approach to analyse infilled RC frames using his collected experimental data. Assuming that there is no difference between the frame and the infill wall and that the infill wall has elastic, homogenous, isotropic behaviour, this method is applied to an infilled frame. These presumptions could not, however, be totally accurate.

Holmes (1961) [23] carried out tests on steel frames with masonry infill subjected to shear loads, Holmes confirmed the formation of the linkage mechanism in masonry, and based on the experimental tests, he proposed that the width of the equivalent linkage should be taken as one-third of the diagonal length.

Mainstone (1971) [24] and Mainstone et al. (1972) [25] carried out monotonic tests on steel and concrete frames with masonry walls; they also confirmed the formation of connecting rods in masonry infill panels and proposed an empirical equation to calculate the effective width of the equivalent diagonal as a function of the relative stiffness of the frame and infills and the diagonal length of the infill walls.

Fiorato et al. (1970) [26] carried out tests on RC frames with masonry infill; the models differed in terms of the number of storeys (one, two and five storeys), the number of bays (one and two bays), and also in the amount of reinforcement in the frame elements, the axial load and the existence of openings in the infill walls. They concluded that masonry infills increased the stiffness and strength but decreased the ductility of this type of structure. Klingner and Bertero (1978) [27] tested an 11-storey building at 1/3 scale to study the performance of structures with masonry infill. Their study concluded that the reinforced infill panels reduced the risk of collapsing reinforced concrete structures.

Zarnic and Tomazevic (1988) [28] performed cyclic tests on 28 models including bare frames and frames with infill, varying the scale (1/2 and 1/3), type of infill (clay brick and unreinforced concrete), reinforced walls and walls with openings, they prepared nine specimens after the tests using different techniques of repairing the infill panels (injected epoxy, and combination of exposed-injected and reinforced cement coating). After studying the different reinforcement techniques, they found that the infills resulted in increased stiffness and strength and a significant reduction in ductility with a significant reduction in the stiffness of the bare frames compared to the filled frames in the cyclic response.

Seven models were evaluated by Pires (1990) [29] in a 2:3 scale, including one-story, one-bay RC frames, six with brick masonry walls within, and one bare frame. In order to analyse the findings from the infilled models, the later model served as a reference. In order to display the effects of gravity loads, the tests included cyclic horizontal displacements applied at the level of the beam centreline and vertical forces applied at the top of the columns. This study also includes an analysis of how certain parameters namely, those related to model construction methods, frame reinforcement, and masonry characteristics affect the behaviour of the models. The study also looked at how the drift affected the frame.

Mehrabi (1994) [10] carried out twelve tests on half-scale one-bay one-story specimens, including two bare frames and frames with different infill conditions in terms of materials, loading procedures and reinforcement arrangement. After the tests, the frames were also

repaired to analyse the efficiency of the repair procedures. The test results were used widely to calibrate numerical models due to the comprehensive data available from the tests, including data required for developing micro-models and the experimental explanation of the failure mechanisms. The current report considered two of these specimens to calibrate the developed numerical models.

Mosalem et al. (1998) [30] performed pseudo-dynamic tests on steel frames with masonry infill for the evaluation of the seismic performance of two-story, two-frame frames; the results of their tests show the formation of diagonal crack patterns and the overall response similar to the results of static tests performed in the past, in the same line, Bounopane and Blanc (1999) [31] performed pseudo-dynamic tests on a two storey, two frames reinforced concrete frame, with two openings in the second level. They found that compression struts were formed at low force intensities. However, for higher-intensity forces, the contribution of the diagonal decreased and the stress distribution path changed due to the sliding bed at several locations in the infill wall. This change in the infill's stress path implies using another diagonal rod configuration in the modeling. They also suggest using different spaces for accounting for the effect of openings in the infill walls.

Al-chaar et al. (2002) [15] tested four frames with masonry infill (1/2 scale) and anbare frame under monotonic static loading. The samples differed in terms of the number of bays (one, two and three bays) and the type of infill (concrete blocks and bricks). The results showed a significant increase in the stiffness and fracture resistance of the infilled frames compared to the bare frames. It was also reported that increasing the number of bays increases the maximum stiffness and strength of the infilled frame.

Lee and Woo (2002) [32] performed monotonic static and dynamic tests at a 1:5 scale on a three-story non-ductile concrete portal frame with masonry infill walls. They reported a large increase in strength, stiffness and inertia force due to the added mass of the infilled frames compared to the bare frames. They concluded that the increase in inertial force due to the existence of the infill element and the increase in strength explains the improved seismic response of the infill wall frame compared to the bare frame. They also observed a shear failure of the columns in the low level of the filled frame; the bare frame has a flexible mechanism due to the formation of plastic hinges in the columns.

Hashemi, et al. (2006) [33] evaluated a 3:4 scale one-bay masonry infill wall of the RC frame that served as a model for the foundation of a five-story prototype using a shaking table.

They concluded that the presence of unreinforced masonry infill, in addition to having a positive impact on stiffness and strength, also resulted in a 50% reduction in the natural period of the tested structure and an increase in the damping coefficient from 4 to 5-12%, depending on the level of excitation.

Anil and Altin (2007) [34] conducted cyclic tests (1/3 scale) of RC frames with partial infill walls and different configurations and positions of openings, their results showed an increase in the strength of frames with infill as the aspect ratio (fill length/height) increases. Furthermore, they observed that frames with connections between the infill and the frame (interaction elements) shear springs and anchors have a better strength performance and frames with full infill have a high energy dissipation capacity (seven times) the dissipation capacity of bare frames.

Blackard et al. (2009) [35] carried out cyclic tests on RC frames with masonry infill walls (2/3 scale). The specimens differed in terms of openings' existence, configuration and position. In addition, the samples were retrofitted with an engineered cement composite (ECC), a material applied to the infill wall facades. In the case of small openings, they observed a small difference in the stiffness and strength of frames with openings in the infill walls compared to frames without openings. However, frames with large window openings result in lower stiffness and strength values.

Stavridis et al. (2012) [36] dynamically tested a RC frame with a three-story masonry infill walls at a 2/3 scale. This frame was filled in one bay and with window openings in the other bay. They found shear failure of the columns and considerable (but still repairable) damage to the structure when the spectra intensity became 43% greater than the maximum earthquake considered for the Los Angeles area. Stavridis et al. [36] concluded that the infilled frame could perform safely in high seismicity regions.

Six one-story, one-bay RC frame specimens were evaluated by Sigmund et al. (2013) [37] to determine the impact of openings presence and configuration on the structural aspects of infilled frames. One bare frame, one with a solid panel, and the remaining specimens with infill panels with openings of various sizes, locations, and types were evaluated. This study suggested correction parameters for the bare frame's behaviours that consider the opening's type and location to establish the behaviour of the infill panels with opening.

Mansouri et al. (2014) [38] also conducted experiments to assess openings' effect on the lateral behaviours of low-shear strength masonry infilled RC frames. Six half-scale single-story single-bay frame specimens were tested under in-plane lateral loading. They focused on the effect of the openings' shape, size, and location. They concluded that openings alter the failure mode, raise the damage level, and reduce the ductility, strength, and stiffness of the infilled frame. They also calculated the reduction in strength and energy dissipation capacity caused by openings in the infill panels. Based on the results of these tests, they proposed empirical equations for estimating the overall stiffness and strength reductions of infilled frames.

2.5 Analytical Research

Many researchers proposed analytical models to capture the characteristic features of infilled frame structures. This section provides a chronological overview of what has been done in this context over the last five decades, including the finite element (micro) modelling of masonry infill walls frames utilizing continuum elements, which is how this study categorizes analytical studies based on their infilled structure modelling method and the macro modelling approach of struts in masonry infill panels.

2.5.1 Masonry Infilled Frames Using Finite Element (Micro) Modelling (continuum elements)

The most practical strategy for researchers is the experimental testing of reinforced concrete frames with masonry infill walls. The experimental approach is sometimes impractical due to the high expense of such processes and the large diversity in the material properties, fabrication methods, and geometry. Researchers attempted to create a different strategy known as micro-models that use finite elements in response to the significant increase in the processing power of computers. Micro models need to model the elements of the frame, the masonry bricks, the interface between the bricks, and the joints ,between the infill wall and the frame. The presence of exceptionally brittle materials makes modelling of this portion of the structure extremely difficult.

2.5.2 Modelling levels for masonry infill walls in micro models

Bricks and mortar are typically used as common components in URM infills. The representation of such materials and their interactions can be divided into three categories based on the amount of modelling accuracy [19]:

- *Micro-continuum model: this method, which is illustrated in Figure 2.8(a), models the brick and mortar joints as continuum elements, with the interaction between the two elements being modelled as a set of interfaces or contact elements. Nonlinear stress-strain relations may be used to define the behaviours of both continuum and interface elements.*

- *Meso-continuum models, which are less detailed than micro models. The mortar joint and its interface with the bricks are modelled together as an interface element, as seen in Figure 2.8,(b) even though continuum components represent bricks. Because of this modest simplification, this model form may be analysed considerably more quickly than the micro-model relations, which was the type before it.*

- *Macro-continuum model: in this method, the behaviours of the brick, mortar, and brick-mortar contact are modelled as one continuum element with similar properties of materials, as illustrated in Figure 2.8. (c). The relationship between the infill and the frame might be modelled to be continuous at all linked points or specific places, or it can be represented via interface contact elements.*

(a)

Head joint (Mortar Material)

Bricks Material
Mortar Material
Interface elements

Bed joint (Mortar Material)

(b)

Bricks Material

—·— Interface elements

(c)

continuum element with
equivalent material properties
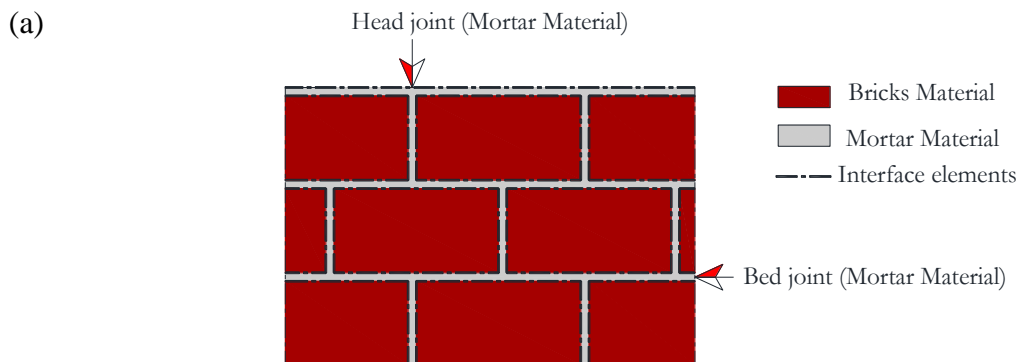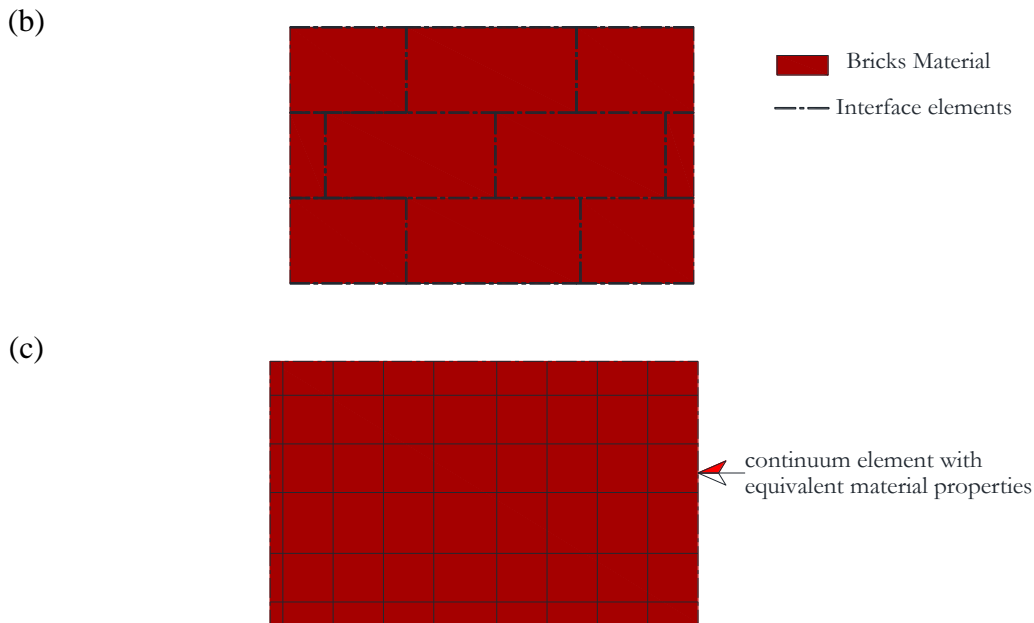
Figure 2.8: Continuum models for masonry infill (a) Micro-continuum model, (b) Meso-
continuum model and (c) Macro-continuum model [19].

2.5.3 A review of masonry infill applications using continuum modeling

This section examines earlier research that modelled the behaviours of infilled frame constructions using continuous finite element models. A pioneering numerical study that attempted to create continuum models for infill constructions was carried out. by Malick and Severn (1967) [39] and Malick and Garg (1971) [40] suggested the first finite element approach for the analysis of portal frames with infills. To solve the problem, an adequate representation of the interface conditions between the frame and the infill was required, the infill panels were simulated by means of linear elastic finite elements of rectangular type with two degrees of freedom at each of the four nodes, the frame was simulated by bar elements neglecting the axial deformation, this is a consequence of the assumption that the interaction forces between the frame and the infill along their interface consisted only of normal forces, shear and friction forces are considered in the contact areas.

Dhanasekhar, *et al.* (1986) [41] made one of the first studies in this area. The infill wall was modelled with a common homogeneous element, a 1D element to model the separation and shear failure of the joint. They developed an orthotropic nonlinear failure surface to capture the failure of the masonry infill walls. The nonlinear material properties of the masonry infill walls were defined based on the results of the bi-axial tests on square panels. They verified their

model by comparing the results of tests on a steel frame with masonry infill. They found that the masonry's tensile and shear strength greatly influence the structure's behaviours regarding the load-deflection law, the resistance to failure, and the mode of failure.Lotfi et Shing (1991) [42] investigated the reliability of a distributed cracking model to simulate the response of a reinforced masonry wall. In the distributed cracking model, the uncracked material is considered an isotropic material and the cracked material is modelled by an orthotropic nonlinear behaviour model. They showed that the distributed cracking model could accurately capture the flexural failure of aninfill wall. However, they showed that the brittle behaviour of the infill wall in shear from diagonal cracking could not be reproduced correctly for a lightly reinforced panel using this method.

Instead of using a homogeneous approach, Lotfi and Shing (1994) [43] developed a nonlinear constitutive interface model to account for the combined normal and shear stresses and also for the expansion observed in experiments, in combination with their smeared crack model for masonry bricks. They evaluated the performance of their interface model by comparing their results with available experimental data and showed the correct prediction of shear and expansion capacity. (Dilatancy is defined as the vertical displacement of the bricks under shear force.

To define a rational unit-joint model able to describe the cracking, slipand crushing of the masonry material, Lourenço and Rots (1997) [44] developed an elastoplastic behaviour model for the interface element. They showed the ability of their model to capture the behaviour of the masonry wall in terms of shear, peak loading and post-peak behaviour by comparing their results with experimental results on masonry walls .Mehrabi and Shing (1997) [45] have also shown the ability of their model to predict the load capacity, mode of failure, ductility, and crack profile of a non-ductile infill wall (masonry block or concrete).

Mehrabi and Shing (1997) [45] developed a behaviour model for mortar joints in masonry infill panels. Their model was used to examine the nonlinear stiffening behaviour of the interface, the reversal of shear expansion under cyclic loading, and the contraction of the interface under shear slip due to particle loss. To model the bricks, they used 4node and 9node distributed cracking elements to model the bricks in their finite element model for a RC portal frame with masonry infill. They used the distributed cracking model to simulate the infill panels' cracking, crushing and sliding. They also compared their simulation results with the

experimental results of cyclic and monotonic tests and found good agreement between the simulated and observed lateral resistance. In the same year,

Oliveira and Lourenço (2004) [41] developed an interface element-based behaviour model to simulate the cyclic behaviour of the interface element. They used a continuous 8-node element in plane stress to model the masonry elements. They compared their simulation results with static cyclic test results on three masonry walls (without frames). They showed the ability of their model to capture the stiffness degradation, energy dissipation, and deformation of masonry walls.

Stavridis and Shing (2010) [42] developed a nonlinear finite element model for reinforced concrete frames with masonry, combining distributed cracking (for masonry units) and discrete cracking (for mortar joints) to compensate for the limitations of the distributed cracking model in capturing the brittle shear failure of mortar joints in masonry and reinforced concrete frames. They used this new element to model the behaviour of concrete, brick and mortar. They used the 4-node element to model brick masonry. They showed that their model could capture the different failure modes observed in experiments, such as diagonal cracking, sliding, and crushing of the infill and bending and shear failures of concrete columns, as shown in Figure 2.9.

Koutromanos, *et al.* (2011) [48] followed the Stavridis (2009) [11] model, as shown in Figure 2.10, used the cohesive crack interface model and an improved distributed crack model to capture the cyclic behaviour of a frame with masonry infill. They validated their results by comparing them with quasi-static tests, they found a good match between the numerical simulation and the experimental results for both tests in terms of hysteretic behaviour and failure mechanism.
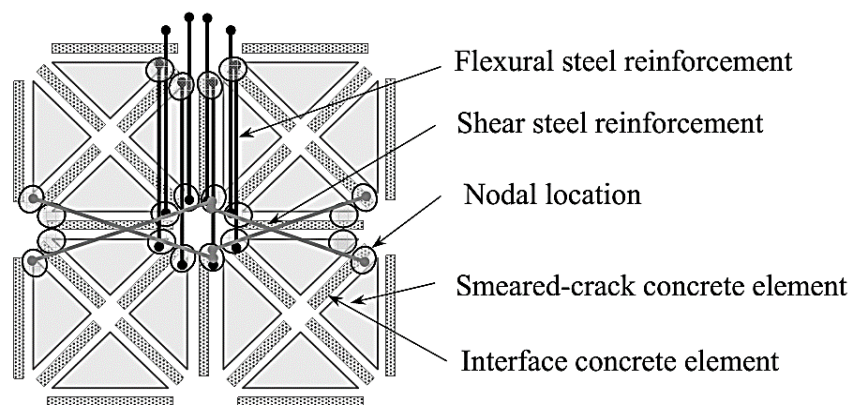
Figure 2.9: Finite element discretization of RC members proposed by Stavridis [11].
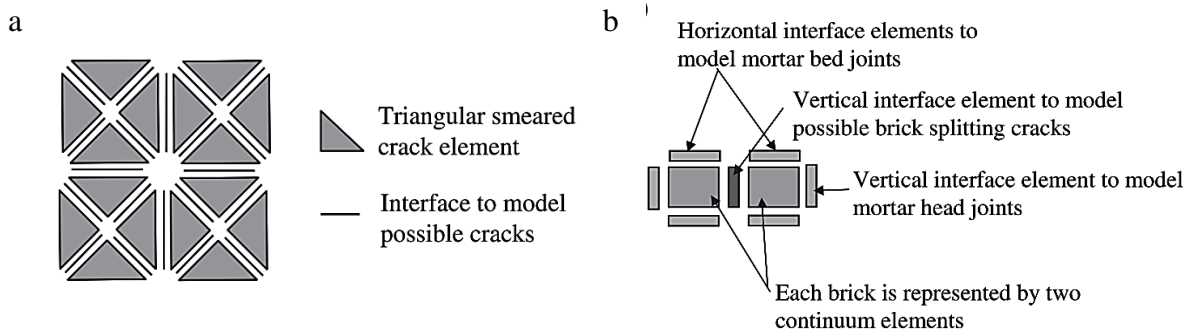
Figure 2.10: Discretization scheme employed in finite element models by Koutromanos, *et al.* [48]: a) reinforced concrete columns and b) unreinforced masonry panels.

2.5.4 Macromodels for masonry infill panels (strut models)

Due to their intrinsic simplicity, macro-models are one of the most useful approaches to represent the behaviours of infill walls, particularly for design reasons. The diagonal strut theory merely substitutes an equivalent pinned diagonal strut system for the infill panel, as seen in Figure 2.11. The primary structural characteristics of the diagonal strut, such as its weadth, stiffness, constitutive behaviours, and optimal number of struts, have been the subject of extensive investigation. A discussion of these studies is provided in this section. In this presentation, the single diagonal strut model's characteristics and the evolution to a multiple stru models with further revisions to this modelling strategy, and several constitutive models that have been developed are all covered.
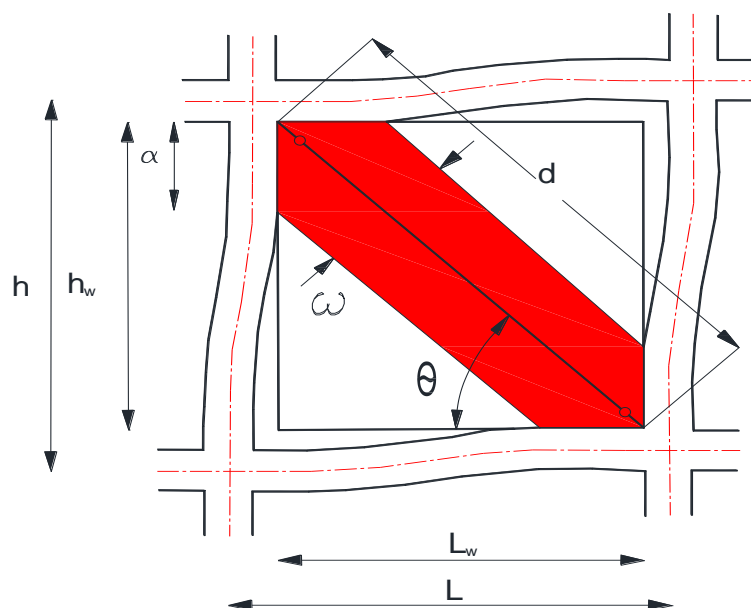
Figure 2.3:Formulation of the diagonal strut and its necessary parameters.

2.5.4.1 Single-Strut Model properties

The use of a single or double strut model is an appealing stratergy to include the global infill wall behaviour in the structural response. As a result, several studies have been done to identify the links between the simplified model and the infilled frame system's properties. The diagonal strut models has different properties based and are used in different analysis porpuse (e.g., linear elastic or nonlinear) and the loading method (monotonic, cyclic or transient loading).The potential of considering the infilled panel's effect as an equivalent diagonal bracing was raised by Polyakov (1956) [21]. This idea was then taken by Holmes (1961) [23], who put forth a linear equivalent compressive strut model. Holmes replaced the infilled panel with a diagonal strut made of the same material and thickness, with the proposed strut's width determined using the following equation.

$$w = \frac{1}{3}d \tag{2.1}$$

where d, as shown in Figure 2.11 is the diagonal length of the infill panel.

By analyzing the interaction between the frame and the infill to determine the effective width of the strut, Smith et al. (1969) [49] advanced the equivalent strut theory. According to their proposal, the effective width of the strut depends on the relative stiffness of the column and the infill, the proportion of the infill's length to height, the material's stress-strain properties, and the magnitude of the diagonal load acting on the infill. The following determines the length of contact between the infill and the frame:

$$\frac{\alpha}{h} = \frac{\pi}{2\lambda h} \tag{2.2}$$

Where h signifies the height of the column between the beam centrelines in millimetres, and λ is a characteristic stiffness parameter $\left(mm^{-1}\right)$ given by:

$$\lambda = \sqrt[4]{\frac{E_I t \sin 2\theta}{4EIh_w}} \tag{2.3}$$

Where E_I is the masonry panel's modulus of elasticity, EI is the columns' flexural stiffness; t is the infill panel's thickness and equivalent strut, h_w is the panel's height and θ slope of the infill

diagonal (degrees). The stiffness parameter and the effective width of an analogous strut are related by a series of empirical curves that they also created.

Mainstone (Mainstone, 1971 [24], Mainstone, 1974 [50]) studied all factors probable to have a significant impact on the infill walls contribution to the strength of a sidesway mechanism in multi-story buildings and suggested new different formulas to evaluate the equivalent strut width, for brick and concrete infills, use Equations (2.4) and (2.5) for infills between 4 and 5 and Equations (2.6) and (2.7).

$$w = 0.175 \, d \, \lambda_h^{-0.4} \qquad Brick \tag{2.4}$$

$$w = 0.115 \, d \, \lambda_h^{-0.4} \qquad Concrete \tag{2.5}$$

$$w = 0.16 \, d \, \lambda_h^{-0.3} \qquad Brick \tag{2.6}$$

$$w = 0.11 \, d \, \lambda_h^{-0.3} \qquad Concrete \tag{2.7}$$

Decanini, et al. (1987) [51] offered two sets of formulae to calculate for cracked and uncracked panels the equivalent diagonal strut width, based on the status of the infill panel with consideration to cracking as follows:

$$\text{Uncracked panel } w = \begin{cases} \left(\dfrac{0.748}{\lambda_h} + 0.085 \right) d & \text{if } \lambda_h \leq 7.85 \\[3mm] \left(\dfrac{0.393}{\lambda_h} + 0.130 \right) d & \text{if } \lambda_h > 7.85 \end{cases} \tag{2.8}$$

$$\text{Cracked panel } w = \begin{cases} \left(\dfrac{0.707}{\lambda_h} + 0.010 \right) d & \text{if } \lambda_h \leq 7.85 \\[3mm] \left(\dfrac{0.470}{\lambda_h} + 0.040 \right) d & \text{if } \lambda_h > 7.85 \end{cases} \tag{2.9}$$

Figure 2.12 shows the equations as a function of a parameter. The main benefit of the Decanini, et al. (1987) [51] method is that values in Eqs. (2.10) and (2.11) have been evaluated

based on Eq. (2.3), equivalent to various panel states. This distinction between them is shown in Figure 2.13 and is defined to impact the equivalent diagonal strut properties substantially.
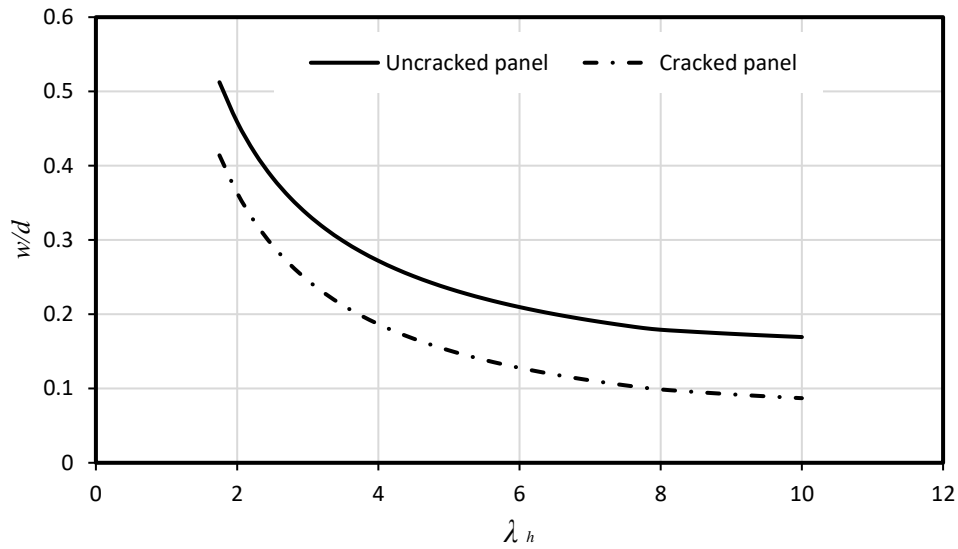
Figure 2.4:Variance of the ratio w/d with λ_h depending on Decanini, *et al.* [51]
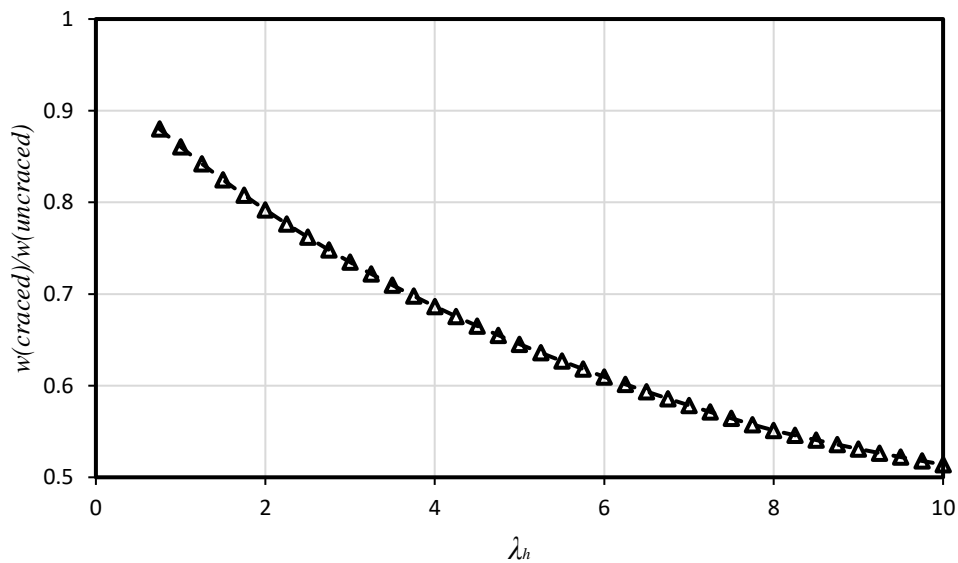
Figure 2.5. Reduction of the equivalent width due to cracking of the masonry panel according to Decanini, *et al.* [51].

Moghaddam, et al. (1988) [52] presented the following straightforward relation between the diagonal equivalent strut length and its width based on experimental findings of infilled frames scaled brick:

$$w = \frac{1}{6}d \tag{2.10}$$

Compressive strut models for unreinforced masonry already have the potential to model the infill's initial stiffness and low-level behaviours before significant bed joint cracking emerge. Hendry (1990) [53], the effective strut width is associated with the contact lengths by:

$$w = 0.5\sqrt{\alpha_l^2 + \alpha_h^2} \tag{2.11}$$

Where α_h and α_l are the horizontal and vertical contact lengths, as determined by the equations below:

$$\alpha_h = \frac{\pi}{2} \sqrt[4]{\frac{4(EI)^* h_w}{E_l t \sin 2\theta}} \tag{2.12}$$

$$\alpha_l = \frac{\pi}{2} \sqrt[4]{\frac{4(EI)^* l_w}{E_l t \sin 2\theta}} \tag{2.13}$$

Which (EI) terms are related to columns and beams, respectively, in Eqs. (2.14) and (2.15). The remaining parameters included in equations (2.14) and (2.15) are those that are likewise defined in (2.3).

According to Paulay et al. (1992) [54], a high value of the strut width will result in a stiffer structure and larger seismic responses. They suggested utilizing the following statement for earthquake design purposes:

$$w = \frac{1}{4} d \tag{2.14}$$

Durrani, et al. (1994) [55] developed semi-empirical formulas to evaluate the width of the equivalent diagonal strut, which may be determined using the following equations in light of prior research and empirical fitting of finite element data.

$$w = \gamma d \sin(2\theta) \tag{2.15}$$

$$\gamma = 0.32 \left[\frac{h^4 E_w t_w}{m E_c I_c h_w} \right]^{-0.1} \left[\sqrt{\sin 2\theta} \right] \tag{2.16}$$

$$m = 6 \left(1 + \frac{6 E_b I_b h}{\pi E_c I_c L} \right) \tag{2.17}$$

Where E_b and E_c are the corresponding elasticity moduli for the beam and column, respectively, were I_b and I_c are the respective moments of inertia for the beam and column.

Al-Chaar (2002) [15] states that Eqs. (2.21) to (2.23) can be used to estimate the equivalent width of the infill strut in the elastic range. It should be noted that for aspect ratios between 1.0 and 1.5, linear interpolation is necessary.

$$w = 0.0835Cd\left(1+\frac{2.574}{\lambda_h}\right) \quad For \; l_w/h_w \geq 1.5 \tag{2.18}$$

$$w = 0.1106d\left(1+\frac{6.027}{\lambda_h}\right) \quad For \; l_w/h_w = 1.0 \tag{2.19}$$

$$where \quad C = -0.3905\left(\frac{l_w}{h_w}\right)+1.7829 \tag{2.20}$$

To show the masonry infill for stiffness and power calculations, the New Zealand masonry code (NZS, 2004) [56], Design of RC Masonry Structures Standard, suggests adopting an analogous diagonal strut. Additionally, it means setting the strut's width at one-quarter the diagonal's length.

The contact length between the infill wall, the beam, and the column was used by Chethan et al. (2009) [57] to adjust the width of the corresponding strut;

$$w = \sqrt{\alpha_l^2 + \alpha_h^2} \tag{2.21}$$

Where α_h and α_l are the corresponding horizontal and vertical contact lengths, as determined by Equations (2.14) and (2.15), respectively. According to Khaja.M, et al. (2013) [58], the contact length between the infill wall and beam is almost equivalent to half of the beam span length. Additionally, CCMPA (2009) [59] modified the formulae to calculate the diagonal strut width using Eq. (2.24), as well as the expressions provided by:

$$\alpha_h = \frac{\pi}{2} \sqrt[4]{\frac{4(EI)_{column}\, h_w}{E_I t \sin 2\theta}} \tag{2.22}$$

$$\alpha_l = \pi \sqrt[4]{\frac{4(EI)_{beam}\, l_w}{E_I t \sin 2\theta}} \tag{2.23}$$

The following equations should be used to reflect the structural impact of infill walls that used an equivalent diagonal strut, according to the recommendations of the Masonry Standards Joint Committee (MSJC) (ACI, 2011) [60]:

$$w = \frac{0.30}{\lambda \cos \theta} \qquad\qquad (2.24)$$

Turgay, et al. (2014) [61] alternative expressions have recently been proposed to better estimate the stiffness and deformability of infilled RC frames. They suggest that the following expression gives the diagonal strut width:

$$w = 0.18 \frac{d}{\sqrt[4]{\lambda_h}} \qquad\qquad (2.25)$$

The ratio h/l considered in this study ranged from 1.2 to 2.

2.5.4.2 Modification of the diagonal Strut Model.

The equivalent diagonal strut can represent the infill panel, specifically in terms of its overall influence on the structural behaviours of constructions, based on the research reported in the preceding section. A single diagonal strut linking the two loaded corners of the frame, therefore, is insufficient to accurately represent the bending moments and shear forces in the frame members [62-64]. Due to these factors, more complicated macro-models were suggested to improve the behaviours of single strut models by adding extra struts and changing the way they are arranged, as seen in Figure 2.14.

Leuchars, et al. (1976) [65] proposed the model shown in Figure 2.14(a) to explain the reaction of infilled buildings when horizontal shear sliding occurs between masonry stages. The twin struts represent the bending moments and shear forces created in the column's central zone. Additionally, the friction mechanism that forms along the cracks and primarily regulates the system's strength can be considered. This model, therefore, was just offered as a recommendation because neither the authors nor any other researcher had used it to confirm its correctness.

Zarnic, et al. (1988) [66] noted during their experimental testing on infill frames that the damage in the higher zone of the masonry panel occurred offset from the diagonal. As a result,

they changed Figure 2.14 (b) to indicate a lower attachment point for the diagonal strut . This model might be used in situations when a shear failure at the top of the column is anticipated.

Schmid et al. (1973) [67] and Syrmakezis et al. (1986) .'s [68] models with many struts are seen in Figures 2.14 (c) and (d), respectively. Despite their increased complexity, these models' key benefit is their better ability to capture the internal forces in the frame. For instance, the five-strut model may demonstrate the important impact of contact lengths on the distribution of bending moments in frame components [68].
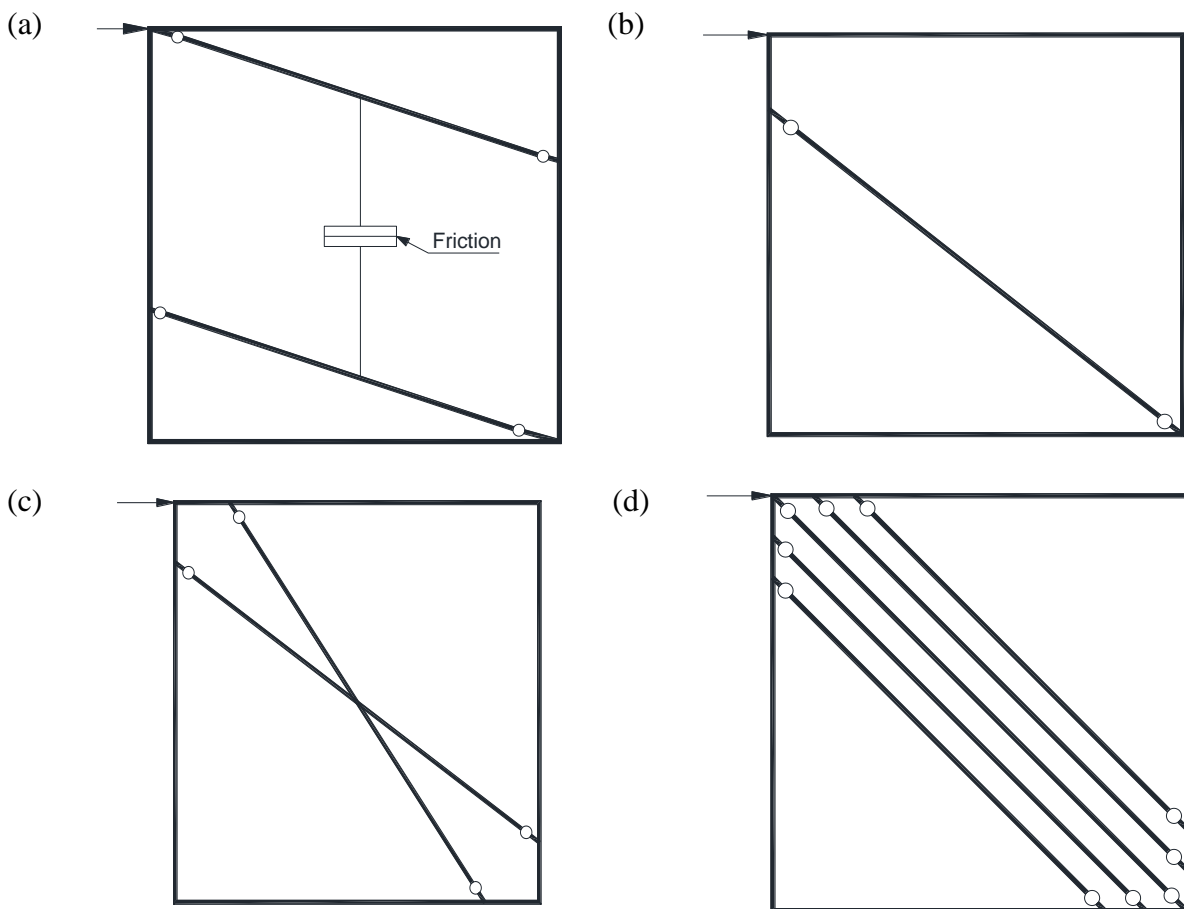
Figure 2.6: Modified systems for the diagonal strut model.

Generalizing the corresponding diagonal strut theory, Andreaus et al. (1985) [69] proposed that a truss-like structure may substitute brickwork to produce a type of finite element mesh made up of "cells," as seen in Figure 2.15. Every cell contains a four-node element, and each element's mechanical behavioursare determined by two truss members positioned along the element's diagonal direction. Although it is based on an analogous diagonal strut system, this model may be regarded as a micro-model due to the degree of refinement needed.
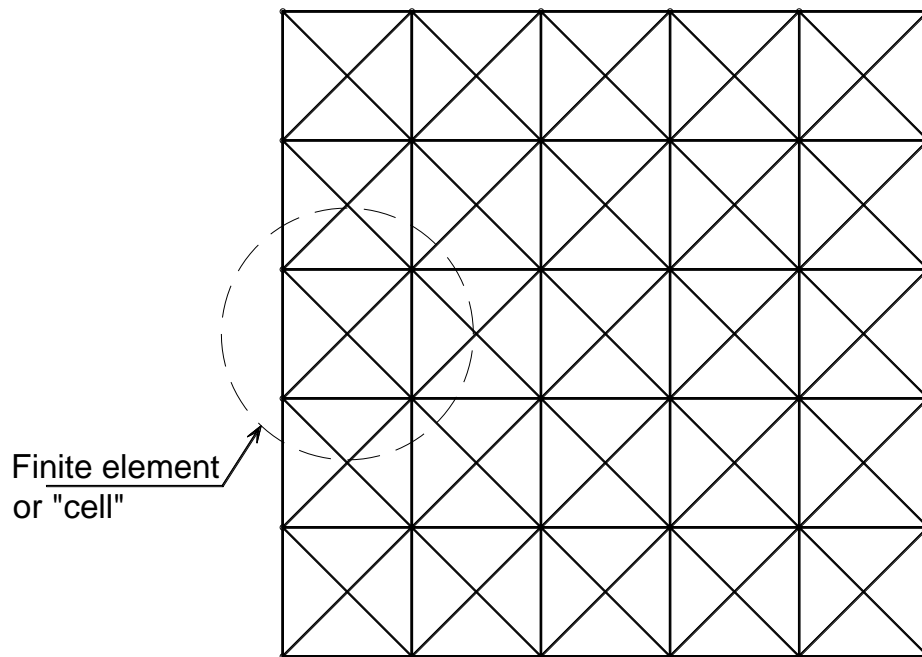
Figure 2.7: The finite element model suggested byAndreaus, et al. [69] based on the diagonal strut concept

As indicated in Figure 2.16, Chrysostomou (1991) [70] and Chrysostomou et al. (1992) [71] changed the infill panel with a six-diagonal strut arrangement. Three parallel struts were employed at every diagonal direction, with off-diagonal ones placed at important positions along the frame members. These locations are defined by parameters and correspond to the spot where a plastic hinge will form in a beam or a column. Theoretically, the assessment of these factors (i.e. and) is based on the work of Te-Chang et al. (1984) [72]. It should be observed

that only one set (three struts) of these struts is active at any given instant of the calculation, and the struts are shifted to the other direction once their compressive stress is lowered to zero.
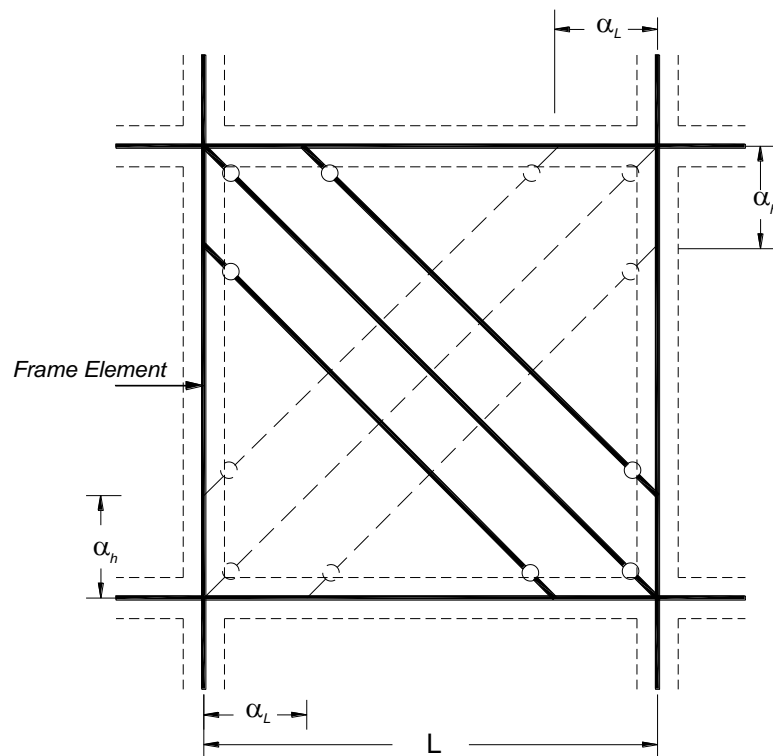
Figure 2.8: Six-strut model for masonry-infill panels in frame structures(Chrysostomou) [70]

Crisafulli (1997) [73] studied the effect of utilizing a varying number of diagonal struts on the structural result in terms of stiffness and forces in the frame's perimeter by making a comparison from single, double, and triple strut models with those from a detailed finite element model, as seen in Figure 2.17. His remarks can be paraphrased as follows:

- The structure's lateral stiffness was comparable in all situations studied, with lower values for two- and three-strut models.The stiffness of multi-strut models varies greatly related to strut separation distance.

- The bending moment of a single-strut model is underestimated because a truss mechanism predominantly resists lateral forces. In the two-strut, the values obtained with the finite element model are less than those obtained with the two-strut model.

- The three-strut model by Chrysostomou [70], depicted in Figure 2.16 gives a better approximation, albeit minor discrepancies appear at both columns' ends.

- The triple-strut model is more precise, even if the single-strut model is adequate for predicting the overall response.

Crisafulli (1997) [73] suggested utilizing the double-strut model technique since it is sufficiently accurate and simpler than the other mode.
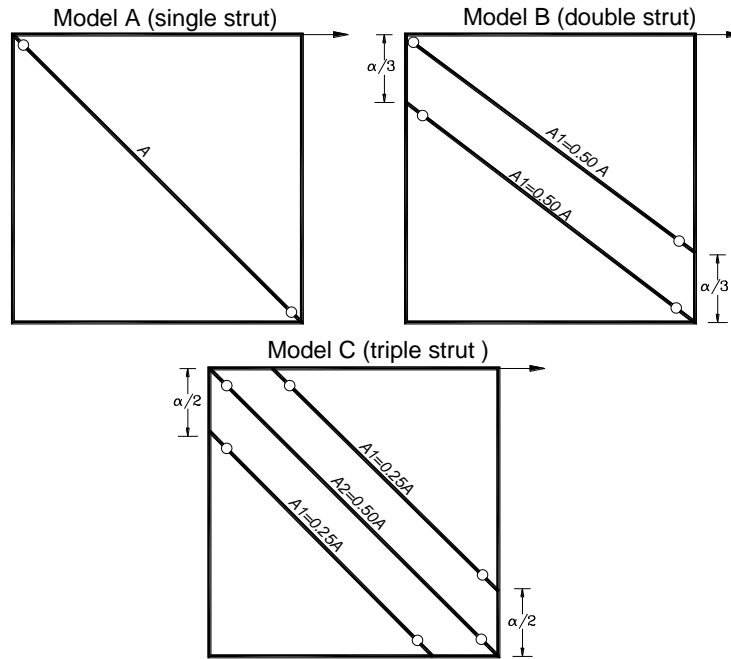
Figure 2.9: The strut models were studied by Crisafulli [73].

El-Dakhakhni et al. (2003) [16] also proposed utilizing two sets of struts, every group consisting of diagonal struts with two offset struts, to model steel frames infilled with concrete or masonry, as shown in Figure 2.18. The following formula gives the overall area of the suggested strut system:

$$A = \frac{(1-\alpha_c)\alpha_c h}{\cos\theta} t$$

(2.26)

Where α_c is the ratio between the height and column contact length and is denoted by Eq (2.31).
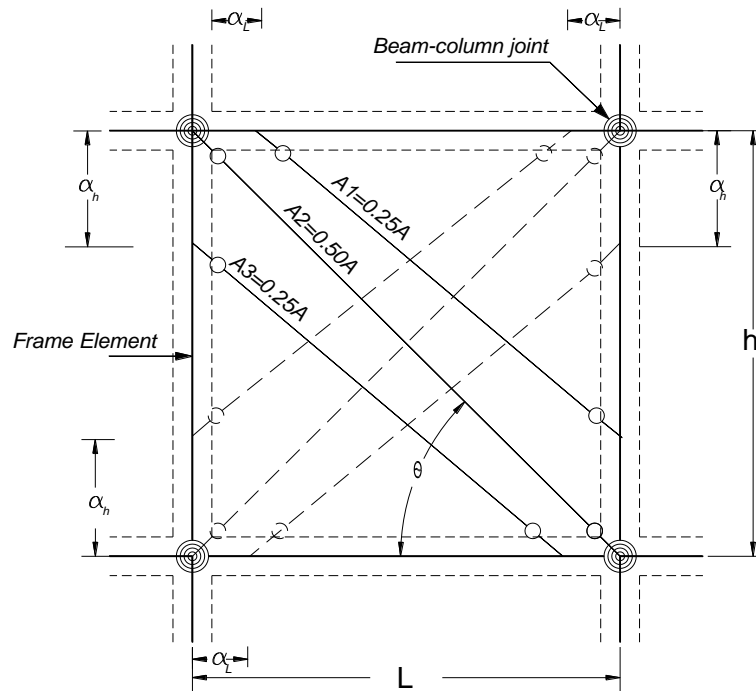
Figure 2.10. Six-strut model for masonry-infill panels in steel frame structures (El-Dakhakhni*, et al.*) [16].

Rodrigues et al. (2010) [74] suggested an updated equivalent bi-diagonal compression strut model with a central strut element to continue improving the behaviours of the equivalent diagonal strut system to capture the behaviours of infill frame constructions (Figure 2.19). Rodrigues et al. (2010) [69] concluded that their model could represent the performance of the structures from where displacement evolution, global shear-drift for every storey, and cumulative dissipated energy after calibrating it from different results of experimental.
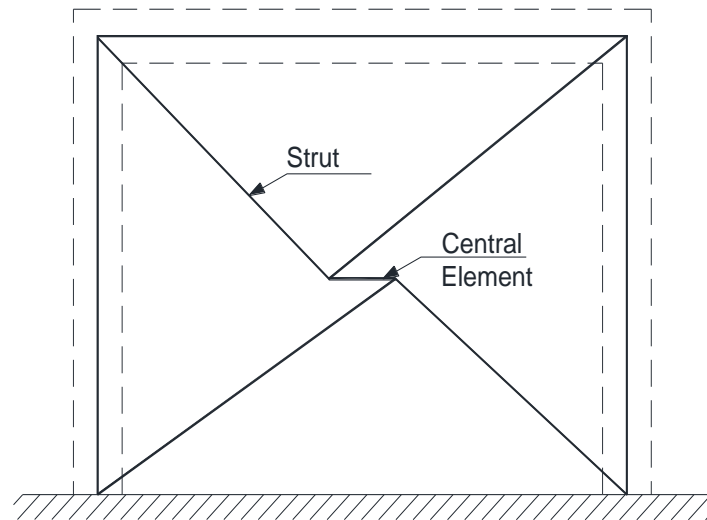
Figure 2.19: Macro- model suggested by Rodrigues, *et al.*[74].

　　Asteris, et al. (2011a) [8] concluded that the two-strut model was better suited to capturing the behaviour of the examined infilled frame with openings than the single-strut model, after comparing the analytical macro model that used a single and double-strut systems with the Pinto, et al. (2006) [75] experimental appears to result.

2.6. Final Remarks

　　From the overview provided, it is clear that estimating the behaviours of the structure of masonry-infilled frames is difficult owing to the parameters high number and phenomena involved and the substantial uncertainty involved in many parameters. To comprehend and analyse the complicated behaviour of these structures under seismic loads, experimental testing of masonry-filled RC frames, however, yields significant findings that confirm the structural parameters of the macro-models (strut models). Several experiments were conducted to evaluate the behaviour of the infilled RC frames. These studies took into different structural features of infilled RC frames, including the infill material, the configurations of the infill panels (such as with openings (window or/and door) with various dimensions and placements), the loading mode (for example, monotonic or cyclic loading), and the condition of the infilled panels (i.e. repaired or not). The experimental approach is sometimes impractical due to the high expense of such processes and the enormous variety in material characteristics, building methods, and geometry.

The macro-models are the most practical approach to representing the infill panel. According to the presented review in this chapter, the single-strut model, although very simple to implement in general-purpose finite-element commercial software, cannot capture the interaction between the bounding frame and the infill wall. Furthermore, unless it involves a hysteretic model, it cannot be used for response history analysis. On the other hand, multiple-strut models can provide an acceptable representation of the infill panel action on the surrounding frame behaviour. However, they cannot be used in general-purpose finite-element software because of the complexities involved in their implementation. Therefore, it can be concluded that the issue of modelling infill walls still needs more research. Eventually, as referred before, several codes and standards recommended using strut models to analyse the behaviour of RC infilled frames. To illustrate this, Table 2.7 shows the equations employed to estimate the stiffness and strength of the equivalent diagonal strut according to various codes.

Table 2-1. Summary of strut models developed for infill panels according to various codes

Model	Equivalent strut model	Strength model	Notations
ASCE/SEI 41-06 (ASCE, 2007) **[76]**	$\lambda_h = \sqrt[4]{\dfrac{E_I t \sin 2\theta}{4(EI)_{column} h_w}} h$ $w = 0.175 \ d \ \lambda_h^{-0.4}$ $E_I = 550 f_m'$	$V_u = 0.24(t_m + t_p)/l$	t_m =effective wall thickness. t_p =thickness of infill panel and equivalent strut;
(TEC, 2007) **[77]**	$\lambda_h = \sqrt[4]{\dfrac{E_I t \sin 2\theta}{4(EI)_{column} h_w}} h$ $w = 0.175 \ d \ \lambda_h^{-0.4}$ $E_I = 200 f_m'$	$V_u \le \begin{cases} 0.24(t_m + t_p)l \\ 0.22l(t_m f_m' + t_p f_p') \end{cases}$	f_m' compressive strength of masonry based on gross area;
(CCMPA, 2009) **[59]**	$w = \sqrt{\alpha_l^2 + \alpha_h^2}$ $\alpha_h = \dfrac{\pi}{2} \sqrt[4]{\dfrac{4(EI)_{column} h_w}{E_I t \sin 2\theta}}$ $\alpha_l = \pi \sqrt[4]{\dfrac{4(EI)_{beam} l_w}{E_I t \sin 2\theta}}$ $w_e \le \begin{cases} w/2 \\ d/4 \end{cases}$ $E_I = 850 f_m'$	$V_u \le \begin{cases} 0.85 \chi \phi_m w_e (f_m' t_{net}) \\ 0.16 \phi_m \sqrt{f_m'} t_{net} d_v \sqrt{1 - 0.9\phi_m \tan\theta} \end{cases}$ χ, factor used to account for direction of compressive stress in a masonry member relative to the direction used for determination of f_m', γ_g is factor to account for partially grouted or ungrouted walls that are constructed of hollow or semi-solid	$d_v = 0.80 \ l$; P, vertical component of compression forced carried by the diagonal strut; P$_d$ self-weight and ϕ_m resistance factor for masonry
(ACI, 2011) **[60]**	$\lambda_h = \sqrt[4]{\dfrac{E_I t \sin 2\theta}{4(EI)_{column} h_w}} h$ $w = \dfrac{0.30}{\lambda \cos\theta}$ $E_I = 700 f_m' \quad for\,clay$	$V_u \le \begin{cases} 00.33 \ l\left(t_m \sqrt{f_m'} + t_p \sqrt{f_p'}\right) \\ 0.83(t_m + t_p) \ l \\ 0.41(t_m + t_p) \ l + 0.45p \end{cases}$	p =compressive force acting normal to masonry infill wall

Chapter 3.

Seismic Evaluation Methods for RC structures

3. Methods of Analysis

Conventional methods for seismic design are intended to evaluate the seismic demand on reinforced concrete structures and to provide sufficient strength and deformation (ductility) capacity to preserve human life and to limit displacements under service loads to control the damage that may occur [78]. The design criteria are defined by the limiting stresses and forces evaluated in the structural elements from the prescribed levels of applied lateral shear. Consequently, Consequently, four main types of analysis methods are available and used depending on the desired level of structural response [79]:

- Linear static analyses
- Linear dynamics analyses (response spectrum or Time-history)
- Nonlinear static analyses (Pushover analysis)
- Nonlinear dynamics time history analyses (with possibility of using incremental dynamic, cloud, or multiple stripe analysis).

3.1. Linear static procedure

The linear static procedure uses the force-based evaluation methodology and is the oldest and simplest method of structural analysis. It assumes that the fundamental vibration mode controls the structural behaviour. The horizontal distribution of statically applied loads should be close to the first mode, representing a significant simplification. An equivalent static analysis can evaluate seismic structural performance. However, these analysis procedures are only appropriate for mid-rise and regular buildings where the effects of the higher modes are not significant [80]. To account for the energy dissipation capacity of the structure, the design spectrum is simply the elastic spectrum corrected with a reducing coefficient R, also known as the behaviour coefficient. According to FEMA 356 [81], structures are analyzed and evaluated using this method with linearly elastic damping and stiffness values at or near the plasticity level.

3.2. Linear dynamic procedure

When the contribution of higher modes to the structural response is significant, linear dynamic procedures are appropriate methods and their results are more accurate than those of linear static procedures. According to FEMA 356 [81], the linear method should be used when buildings are modeled with equivalent viscous damping values and linearly elastic stiffness at or near the plasticity level of this method. FEMA 356 [81] suggests the spectral modal method and the temporal dynamic analysis. In these methods, a linear elastic analysis based on the superposition principle is used to obtain the internal displacements and forces of the system.

This method is widely recognized as powerful for computing the linear dynamic response of elastically damped systems. This method is interesting because the response of multi-degree-of-freedom (MDOF) systems is expressed through a modal superposition, the response of each mode is determined from the spectral analysis of single-degree-of-freedom (SDOF) systems. The modal analysis combines the different modes' responses by superposition rules to obtain the average of the maximum structural response.

The analysis of the linear dynamic response is done by direct integration in time of the equations of motion. One of this procedure's main advantages is keeping the responses with their

respective signs. Nevertheless, it gives only a limited insight into the inelastic structural response under a severe earthquake.

3.3. Nonlinear static procedure

3.3.1. Background of the pushover analysis method

Pushover analysis generally refers to nonlinear static procedures applied to evaluate the seismic performance of existing structures and the design of new buildings [82]. Pushover analysis is a powerful tool for performance-based design methodology, which is presented in several recent seismic regulations and guidelines [81,83-85]. Pushover analysis is performed by applying a series of inelastic static analyses on the building using a pre-selected lateral loading mode based on the first vibration mode of the structure or the equivalent static lateral loading modes in the seismic regulations.

The loading mode remains unchanged during the pushover analysis, but its magnitude increases gradually until the building reaches a specific target displacement. Typically, this target displacement represents the displacement at the top of the building when it experiences seismic excitation. The pushover analysis results are used to estimate the capacity of the building by plotting the variation of the top displacement against the shear force at the base of the building [86]. This curve is known as the "capacity curve", as shown in Figure 3.1.
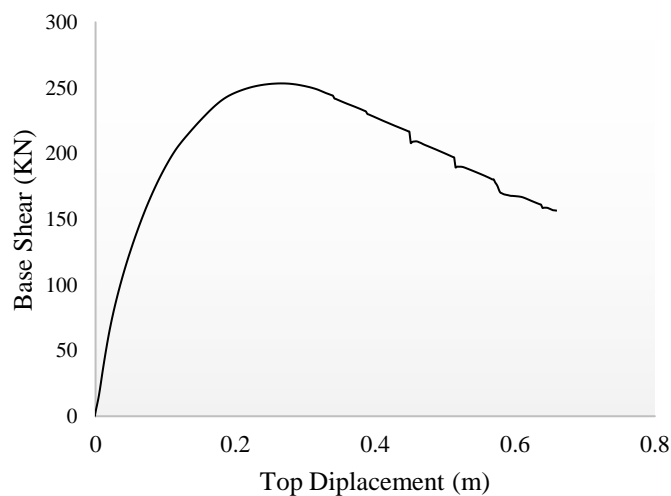
Figure 3.1: Pushover curve showing the variation of the shear force at the base as a function of the displacement at the top of the building.

Pushover analysis does not have a rigorous theoretical basis. It assumes that the structure's response can be related to an equivalent single-degree-of-freedom system. This is because a single mode dominates the response, and the shape of this mode remains constant throughout the analysis Figure 3.2.
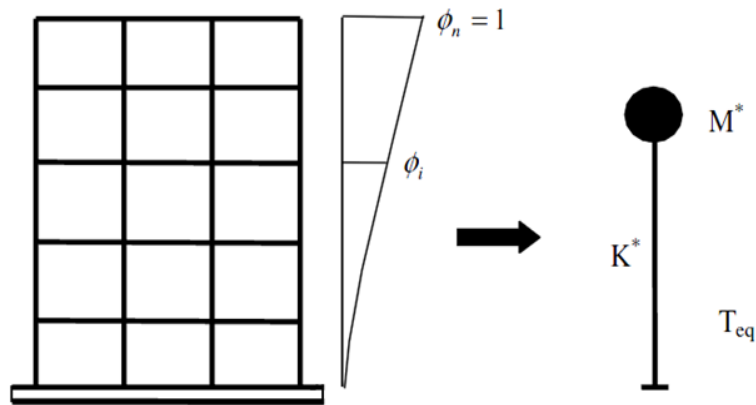
Figure 3.2: Concept diagram for transformation from multi-degree-of-freedom system to single-degree-of-freedom system [87].

Both assumptions are incorrect [87]. Still, pilot studies undertaken by many researchers have indicated that these assumptions lead to pretty good predictions of the correct maximum seismic response of a multi-degree-of-freedom system, provided that their response is dominated by a single mode [88].

The formulation of the equivalent single-degree-of-freedom system is not unique. Still, the fundamental assumption known to all approaches is that the deformed form of the multi-degree-of-freedom system can be represented by an eigenvector $\{\phi\}$ that remains constant throughout the analysis regardless of the level of deformation.

The differential equation of the multi-degree-of-freedom system can be written in the form:

$$M\ \ddot{\mu} + C\ \dot{\mu} + q = -M\ \{1\}\ddot{\mu}_g \qquad\qquad 3.2$$

Where M and C are the mass and damping matrices of the building, respectively, q is the force vector in the levels, {1} is the unit vector, μ is the relative displacement vector, and $\ddot{u}_g$ is the seismic action.

In the pushover analysis, the building response is assumed to be dominated by a single eigenvector $\{\phi\}$ which remains constant throughout the analysis.

The relative displacement vector can be expressed in terms of $\{\phi\}$ and the displacement at the top of the building (Δ) as follows:

$$\mu = \{\phi\}\,\Delta \qquad\qquad 3.3$$

Substituting equation (3.2) into equation (3.3) and multiplying by $\{\phi\}^T$ we obtain:

$$\{\phi\}^T M\,\{\phi\}\ddot{\Delta} + \{\phi\}^T\,C\{\phi\}\dot{\Delta} + \{\phi\}^T q = -\{\phi\}^T M\{1\}\ddot{u}_g \qquad\qquad 3.4$$

We define the reference displacement of the single degree of freedom system μ* by

$$\mu^* = \frac{\{\phi\}^T M\,\{\phi\}}{\{\phi\}^T M\,\{1\}}\Delta \qquad\qquad 3.5$$

And then, replacing (Δ) in equation (3.4) using equation (3.5), we obtain the following differential equation for the response of an equivalent single degree of freedom system:

$$m^*\ddot{\mu}^* + C^*\dot{\mu}^* + q^* = -m^*\ddot{u}_g \qquad\qquad 3.6$$

m*, C* and q* represent the properties of the equivalent single degree of freedom system and are given by :

$$m^* = \{\phi\}^T M\,\{1\} \qquad\qquad 3.7$$

$$C^* = \{\phi\}^T\,C\{\phi\}.\frac{\{\phi\}^T M\,\{1\}}{\{\phi\}^T M\,\{\phi\}} \qquad\qquad 3.8$$

$$q^* = \{\phi\}^T q \qquad\qquad 3.9$$
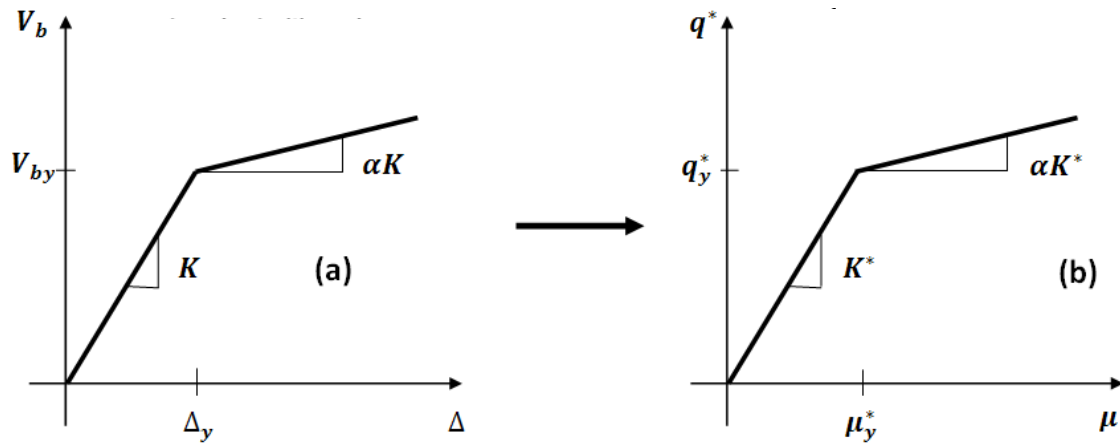
Figure 3.3: Force-displacement characteristics of multi-degree-of-freedom system and equivalent single-degree-of-freedom system [79].

Assuming, that the eigenvector $\{\phi\}$ is known, the force-displacement characteristics of the equivalent single-degree-of-freedom system (the relationship $q^* - \mu^*$) (see Fig. 3.3.b) can be determined from the results of an incremental nonlinear analysis of the multi-degree-of-freedom system which results in a shear force at the base-displacement at the top diagram as shown in Fig. (3.3.a). For the purpose of identifying the overall design strength and displacements, the multilinear diagram $(V_b\text{-}\Delta)$ must be represented by a bilinear relationship that defines a plastic strength V_{by}, an effective elastic stiffness $K_e = \dfrac{V_{by}}{\Delta y}$ and a stiffened or softened stiffness $K_s = \alpha K_e$ for the structure [87].
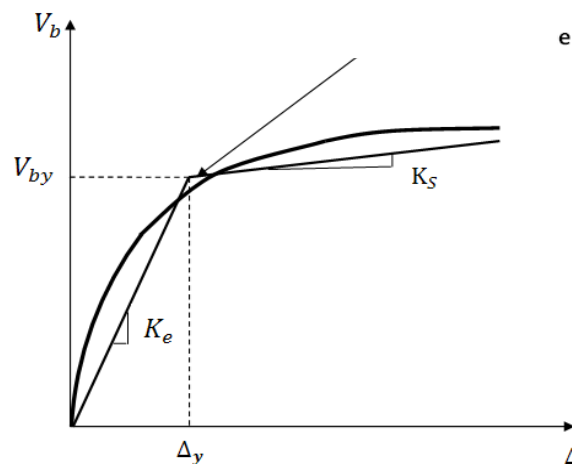
Figure 3.4: Idealized bilinear pushover curve [87].

This simplified bilinear curve (base shear - top displacement), which is shown in Figure (3.4), is required to define the properties of the equivalent single degree of freedom system.

The value of the base shear force and the corresponding top displacement from Figure (3.3. a) are used together with equations (3.5) and (3.9) to calculate the force-displacement relationship for the equivalent single degree of freedom system as follows:

$$\mu_y^* = \frac{\{\varphi\}^T M \{\varphi\}}{\{\varphi\}^T M \{1\}} \Delta y \qquad\qquad 3.10$$

Where, q_y is the vector of level forces at the non-linear incursion, in other words:

$$q_y^* = \{\varphi\}^T q_y \qquad\qquad 3.11$$

The initial period of the equivalent single degree of freedom system is given by:

$$V_{by} = \{1\}^T q_y) \qquad\qquad 3.12$$

$$T_{eq} = 2\pi \sqrt{\frac{m^* \mu_y^*}{q_y^*}} \qquad\qquad 3.13$$

The basic properties of an equivalent single degree of freedom system are now known.

The pushover analysis is performed until a target displacement is reached at which the seismic performance of the building is evaluated. The target displacement is like an estimate of the overall expected building displacement under a design earthquake [89]. It can be estimated by applying the nonlinear (chronological) analysis on an equivalent single degree of freedom system [90]. This requires first the construction of the inelastic displacement demand to determine the target displacement since the pushover analysis is a design tool. The ground motion execution is represented by an elastic response spectrum rather than its true response spectrum. The basic properties of an equivalent single degree of freedom system are now known.

In this case, the inelastic displacement demand must be deduced from the spectral data and auxiliary information that explains the differences between the elastic and inelastic displacement demand. Several studies focus on this point and devise practical relationships between elastic and inelastic displacement demand [91].

The elastic displacement demand S_d can be directly determined from the pseudo acceleration S_a of the response spectrum as follows:

$$S_d = \frac{T^2}{4\pi^2} S_a \qquad\qquad 3.14$$

Where T is the natural period of vibration of the single degree of freedom system.

This displacement demand is the baseline for predicting the inelastic displacement demand, which must be accomplished with consideration given to the plastic strength and hysteretic characteristics of the single degree of freedom system [87].

Alternatively, the inelastic response and design spectra for the displacement demand can be constructed using an equivalent single degree of freedom system [92]. In this case, the building capacity curve represented by the force-displacement relationship of the equivalent single degree of freedom system and the demand curve represented by the inelastic spectrum is plotted on the same graph, considering the (ADRS) Pseudo Acceleration Displacement format as shown in Figure 3.5.

The point of intersection of these two curves represents an adequate approximation of the maximum displacement of the equivalent single degree of freedom system, which, after conversion, gives a reasonable estimate of the target displacement of the pushover analysis for the building.

Once the target displacement is estimated, the building is pushed incrementally using a predefined lateral loading mode until the displacement at the top of the building reaches the target displacement.

At this state, the responses and induced forces are expected to represent in fair proportion to the response quantities of the building under the design earthquake excitation [79].
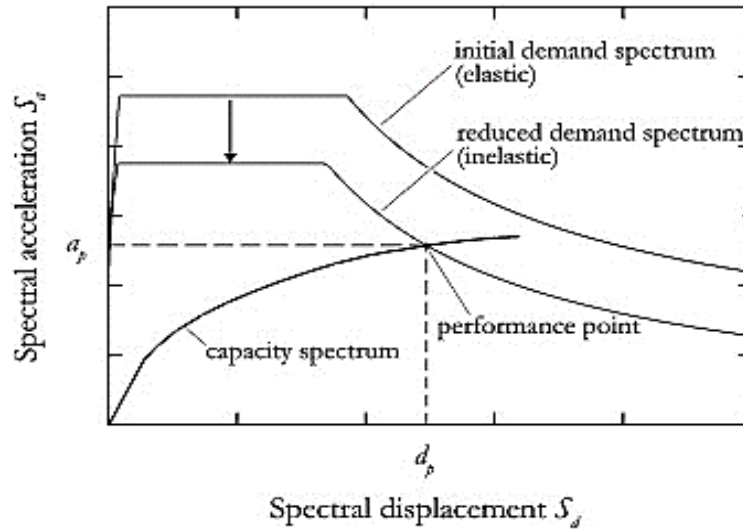
Figure 3.5: Response spectrum and capacity curve in ADRS format [79].

3.3.1.1 Pushover analysis methods according to the lateral loading mode

The participation of the upper mode of vibration in the response of the structure was the focus of many studies that led to the need to consider the effect of higher vibration mode in the nonlinear static analysis, especially for high-height structures that have long periods of vibration, for long periods. The participation of the higher modes in the response will influence the behaviour of the structure and the mechanism of its collapse.

The researchers are interested in developing this side of the nonlinear static analysis to make it more reliable and to have the possibility of its use in the design and evaluation of tall structures based on performance. Pushover analysis methods are beginning to emerge, but they do not just use the fundamental mode of vibration mode of vibration in the calculation of lateral loading, and take into consideration the participation of several vibration modes, pushover analysis methods can be classified according to can be classified according to the mode of lateral loading into three main groups [93]:

1- The conventional pushover method, which uses the constant and increasing lateral loading mode monotonically increasing lateral loading mode during the analysis, which is often cited in in seismic codes.

2- The modal pushover analysis method, which uses the monotonically increasing constant lateral loading mode during the analysis, takes into consideration the participation of

multi-modes of vibration. This method is named in some references: the multi-mode pushover analysis method. In this study, we are interested in this analysis method, especially its application to three-dimensional structures.

        3- The adaptive pushover analysis method is a variable (adaptive) lateral loading shape changes during the analysis stages according to the change in the structure's dynamic modal characteristics.

3.3.1.1.1 Modal pushover analysis:

        Goel and Chopra [94] have confirmed that any of the forms of the static lateral load distribution cannot represent the participation of the higher modes than the first mode in the response. Also, it cannot represent the redistribution of inertial forces, which is the result of the non-linear behaviour of the structural elements, nor it can represent changes in the vibration characteristics of the structure after non-linear incursions. These problems can be overcomed by using adaptive loading modes, which vary with the variation of the inertial forces during the analysis. But this analysis type is complicated, time-consuming, and unsuitable for professional use.

        For this purpose, **Goel and Chopra** [94] proposed the Pushover analysis method based on the principles of dynamic analysis while keeping the simplicity of the constant loading mode pushover method. The proposed method consists of an independent nonlinear static analysis for the system under study for each vibration mode, using the lateral loading mode according to that vibration mode of vibration. After that, the total responses of the vibration modes to be studied are combined according to the static SRSS method.

The proposed method starts with the analysis of the modal response history which, in turn, starts from the differential equation of the response of the elastic system with degrees of freedom, subjected to the ground acceleration ü. The differential equation is presented as follows:

$$m\ddot{u} + c\dot{u} + ku = -mi\ddot{u}g(t) \qquad\qquad 3.15$$

u: displacement vector of the N levels

k: stiffness matrix

m: mass matrix

c: system damping matrix.

i: unit influence vector

The right-hand side of this equation, shown, is the effective force of the excitation

$$P_{eff}(t) = mi\ddot{u}g(t) \tag{3.16}$$

The vector **S** and the ground acceleration define the spatial distribution of this effective force over the height. The spatial distribution is expressed as the sum of the modal inertia forces.

$$mi =$$
$$\sum_{n=1}^{N} S_n = \sum_{n=1}^{N} \Gamma m\phi_n \tag{3.17}$$

Were

ϕ_n: Is the n-mode vector of the structure.

Effective forces can be expressed as follows:

$$P_{eff}(t) = \sum_{n=1}^{N} P_{effn}(t) = \sum_{n=1}^{N} -S_n \ddot{u}g(t) \tag{3.18}$$

$$P_{eff}(t) = \sum_{n=1}^{N} -S_n \ddot{u}g(t) \tag{3.19}$$

If we consider that the response of the multi-degree-of-freedom system to the effective force is totally according to the vibration mode n, the displacements of the levels are as follows:

$$U_n(t) = \phi_n q_n(t) \tag{3.20}$$

Where the modal coordinate $q_n(t)$ is given by the following relationship:

$$q_n(t) = \Gamma_n D_n(t) \tag{3.21}$$

Where $D_n(t)$ is the displacement of the equivalent linear system of mode n, it is given by the following relation the following relationship:

$$\ddot{D}_n(t) + 2\xi_n w_n D_n + w_n D_n = -\ddot{u}g(t) \tag{3.22}$$

Substituting equation (3.21) into equation (3.20) the overall displacement is:

$$U_n(t) = \Gamma_n \phi_n D_n(t) \tag{3.23}$$

After that, any response r_n is possible, to calculate it and this by multiplication of the response, resulting from the modal static analysis under the effect of loading S_n, by the pseudo acceleration $A_n(t)$ of the linear system with one degree of freedom of mode n as follows of freedom of mode n as follows:

$$r_n(t) = r_n^{st} A_n(t) \tag{3.24}$$

Were

$$A_n(t) = w_n^2 D_n(t) \tag{3.25}$$

Where **w** is a natural frequency.

The two analyses that lead to r_n for the inelastic system are schematically in Figure 3.6
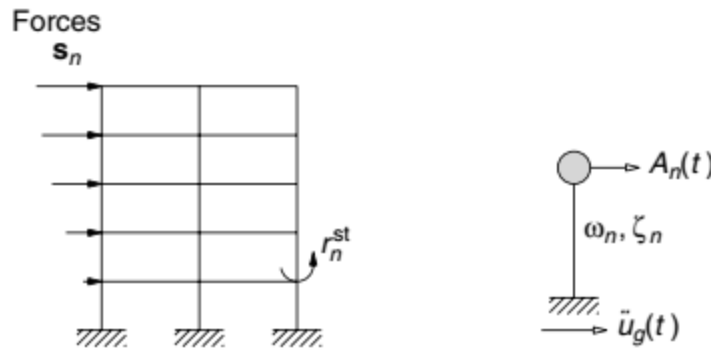
Figure 3.6: Principle of modal time analysis [94].

The global displacement and the global response of the effective force P_{eff}, at time (t) are given by the following relations:

$$U(t) = \sum_{n=1}^{N} U_n(t) = \sum_{n=1}^{N} \Gamma_n \phi_n D_n(t) \tag{3.26}$$

$$r(t) = \sum_{n=1}^{N} r_n(t) = r_n^{st} A_n(t) \tag{3.27}$$

The relationship between the applied lateral force s F and the lateral displacements u is nonlinear for nonlinear systems. Therefore, the governing relationship of the motion of the nonlinear system will be as follows:

$$m\ddot{u} + c\dot{u} + f_s(u, sign\dot{u}) = -S_n\ddot{u}g(t) \tag{3.28}$$

It is possible to solve this equation by the decoupled modal time analysis method analysis method based on the following two assumptions: neglecting the coupling between the N equations in modal coordinates and neglecting the participation of modes different from the n mode, in the nonlinear response corresponding to the n mode.

This mode n is considered the least dominant mode when subjected to the forces. P_{eff}, the equation of the inelastic system is expressed by:

$$\ddot{D}_n(t) + 2\xi_n w_n\dot{D}_n + \frac{F_{sn}}{L_n} = -\ddot{u}g(t) \tag{3.29}$$

Where F_{sn} is the nonlinear hysteretic function:

$$F_{sn} = F_{sn}(D_n, signD_n) = \phi_n^T f_s(D_n, signD_n) \tag{3.30}$$

The solution of this equation requires the determination of the relationship between the forces and displacements $(\frac{F_{sn}}{L_n} - D_n)$, this is possible by the nonlinear static analysis of the system under distributed lateral loading system under the effect of distributed lateral loading: $S_n^* = m\phi_n$ hen convert the capacity curve $(V_{bn}-U_m)$ to $(\frac{F_{sn}}{L_n} - D_n)$,

By the following two relations:

$$F_{sn} = \frac{V_{bn}}{\Gamma_n}, D_n = \frac{U_{rn}}{\Gamma_n\phi_{rn}} \tag{3.31}$$

From these two relationships, the corresponding values for the limit state elastic limit state D_{ny},

$\frac{F_{sn}}{L_n}$

Were,

$$D_{ny} = \frac{U_{rny}}{\Gamma_n \phi_{rn}}, \frac{F_{sny}}{L_n} = \frac{V_{bny}}{M_n^*} \qquad 3.32$$

$$\Gamma_n = \frac{L_n}{M_n}, L_n = \phi_n^T mi, M_n^* = \phi_n^T m \phi_n \qquad 3.33$$

D_{ny} and F_{sny} are related by the relationship:

$$\frac{F_{sny}}{L_n} = w_n^2 D_{ny} \qquad 3.34$$

Thus, it is possible to determine $D_n(t)$ from equation (3.29) and consequently the pseudo acceleration $A_n(t)$ and then the calculation of the global response as in linear systems.

   Chopra and Goel [94] have established the principles of the Pushover modal analysis method according to the following steps:

1- Determine the dynamic linear free vibration characteristics of the system under study.

2- Perform the pushover analysis for the system, for mode n, using the **Sn** lateral loading distribution and plot the capacity curve.

3- Convert the capacitance curve into a bilinear curve.

4- The idealized pushover curve should be converted to the force-displacement of a single-degree-of-freedom displacement of a single degree of freedom system for the inelastic mode n.

5- Determination of the maximum value of Dn By a nonlinear dynamic analysis or an elastic or inelastic response spectrum.

6- Calculate the maximum peak displacement of the structure in the direction associated with the n mode of equivalent single degree of freedom system using

$$U_m = \Gamma_n . \phi_m . D_n \qquad 3.35$$

7- Steps 2 to 6 should be repeated for enough modes.

8- Determine the overall response for the combination of maximum responses for the selected modes, using a static combination method (SRSS or CQC).

The proposed modal pushover method was applied to nine-level steel structures, taking into consideration the participation of the second and third modes, these results were more accurate for the responses compared to the conventional pushover analysis method, by the uniform loading mode. But the error in its estimation of plastic rotations was greater.

3.3.1.1.2. Adaptive pushover analysis

It is known that during the exposure of buildings to strong earthquakes, they begin to respond within the elastic behaviour and then move to the non-linear behavior and the change of the specifications of the total stiffness matrix of the structure and the accompanying change in the dynamic properties of the structure, i.e., its natural frequencies and the importance oof vibration modes. Which leads to a continuous change in the distribution of inertia forces during the period of elastic response. Adaptive analysis methods that rely on lateral loads of a fixed shape throughout the analysis period cannot express this change acceptably, but this requires a lateral load of variable shape with the change of the properties of the facility and the contributions of the patterns Figure 3.7. This aspect has been addressed Mainly in Adaptive Pushover analysis methods and presented below.

> **Adaptive Modal Combination**

As shown in Figure 3.7, one method of doing the static analysis that allows for changes in the inertial force distribution along the global drift is the adaptive pushover analysis. The fundamental drawbacks of the traditional pushover, which requires steady force during the analysis, are addressed by this technique. Like how traditional pushover analysis findings do not accurately capture the inelastic properties of buildings, such as displacements and horizontal forces [95].
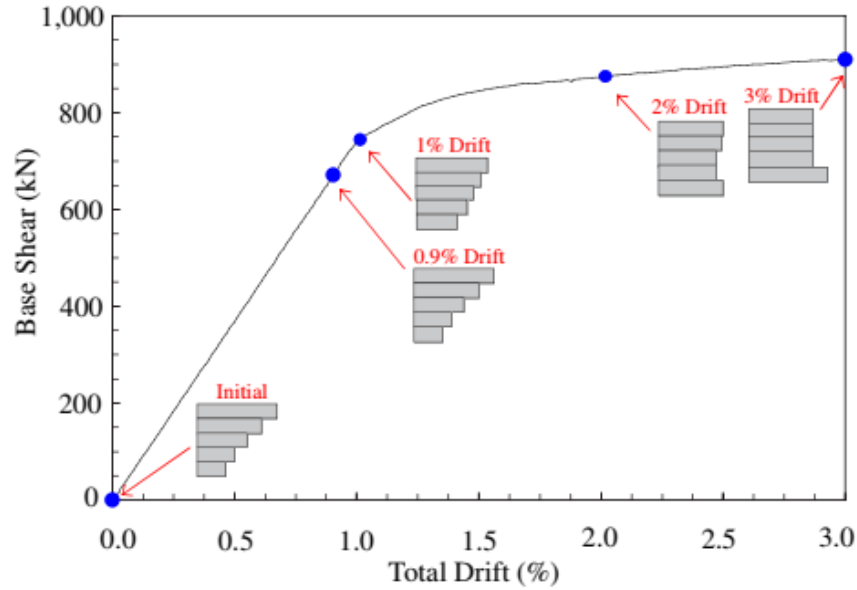
Figure 3.7: Changes of the distribution of inertial forces in a regular framed building (adaptive force distribution) [95]

Elnashai and Di Sarno [95] outlined the many stages that must be taken to do an adaptive pushover analysis of the structural system.

a) Apply the gravitational loads all at once.

b) Analyse the structure's eigenvalues at the present stiffness level. For the first stage, you can utilize the elastic stiffness. It computes eigenvalues and eigenvectors.

c) For the jth mode, ascertain the modal participation factors Γ_j used this formula:

$$\Gamma_j = \frac{L_j}{M_i^*}$$
                                                                                    3.36

Where M_i^* is the generalised mass indicated as:

$$M_i^* = \phi_j^T M \phi_j$$
                                                                                    3.37

$$L_j = \phi_j^T M_i$$
                                                                                    3.38

d) Determine the modal storey forces for every floor level and for N modes that are thought to fulfill a mass participation between 85 and 90% of the overall mass. These forces $F_{i,j}$ are calculated for the jth mode (being $1 \leq j \leq N$) at the ith level as shown below :

$$F_{ij} = \Gamma_j M_i \phi_{ij} g$$
                                                                                    3.39

Where: g is the acceleration brought on by gravity, M_i is the seismic mass of the ith level.

    e)   Carry out a static pushover on the structure while it is subjected to the individual story forces for each mode calculated in step 4.

    f)   For the kth analysis step, computing the element (or local) and structural (or global) forces and displacements using the square root of the sum of squares (SRSS) combining for every modal quantity. The relevant quantity of the $(k-1)^{th}$ step should be adjusted by the forces mentioned above and displacements.

    g) At both the local and global levels, compare the amounts established in step 6 to the limiting values for the defined performance targets. Till the desired performance is achieved, go back to step 2.

➢ Adaptive Spectra-based Pushover

Gupta, Kunnath [96] explained the change of inertial forces at the height of the structure during the response by studying the seismic response of a group of buildings existing in the United States with various structures between the frame and shear walls up to 22 floors and equipped with measuring devices responses in the floors during exposure to the Northridge earthquake 4771 and ground accelerations exceeding (2.25 g). The change was clear and significant as the height of the building increased during exposure to the earthquake, with confirmation that the lateral load of a constant shape throughout the analysis period could not express this change in the adaptive analysis. Therefore, the researchers sought to develop a method through which to control the shape of the increasing lateral load during the steps of the batch analysis, in other words, the shape of the lateral load continues to change during the analysis steps depending on the instantaneous dynamic properties of the studied facility. This method is called adaptive analysis based on spectra, and this method is distinguished from the traditional methods by the following [96]:

1- The response spectra of the studied site are used to form the lateral load.

2- A lateral load of continuously variable shape is used according to the change of instantaneous dynamic properties.

3- It allows considering the effect of multiple patterns in the final response through statistical grouping.

The stages of the method are summarized in the following steps:

1. Establishing the mathematical model and determining the various elements' nonlinear behaviour (strength-deformation) relationship.

2. Finding the elastic response spectrum of the studied site with an equivalent damping of 5%.

3. Analyse the eigenvalues of the model using its current stiffness, which is the initial stiffness in the first step (the stiffness matrix considers only the degrees of freedom of lateral movement of the floors) and find the dynamic properties of the roles and mode of vibration and the contributing factors of the mode.

$$\Gamma_j = \frac{1}{g}\sum_{i=1}^{i=N} W_i\, \phi_{ij}$$ 3.40

Γ_j : modal participation factor for $j^{\text{th mode}}$.

ϕ_{ij}: mass normalized mode shape value at i^{th} level and j^{th} made.

Wi: weight of Ith story.

g: acceleration due to gravity.

N: number of stories.

4. Calculate the forces at each story levelr (i) for each vibration mode *n* to be included in the response (j) of the relationship.

$$f_{ij} = \Gamma_j m \phi_{ij} S_a(j)$$ 3.41

f_{ij}: lateral story force at i^{th} level for j^{th} mode (1<j<n)

Sa: spectral acceleration corresponding to j^{th} mode.

5. Calculate the base shear *Vj* and combine them using SRSS to compute building base shear (V) as show below:

$$V = \sqrt{\sum_{i=1}^{N} V_j^2}\qquad\qquad V_j = \sqrt{\sum_{i=1}^{N} f_{ij}}$$ 3.41

6. The story forces computed in step 6 are uniformly scaled using the scaling factor *Sn* indicated below:

$$V_j = S_n V_j \qquad\qquad 3,42$$

Where:

$$S_n = \frac{V_B}{N_s V} \qquad\qquad 3.43$$

And V_B is the base shear estimate for the entire for the entire structure and Ns is the number of uniform steps over which the base shear is to be applied.

7. Performing a static analysis using the scaled incremental story forces computed in the previous step corresponding to each mode independently.

8.Collecting the resulting responses for each mode of element forces and floor displacements using the SRSS method and then adding them to the values calculated in the previous step.

9. Compute element forces, displacement, story drift … etc., by an SRSS combination of the respective modal quantities for this step and add these to the same from previous step.

10. Comparing the forces of the elements calculated cumulatively at the end of each step with the yield limit for each of them, recalculating the stiffness matrix by considering the elements that reached the yield limit, and re-analyzing starting from step 3.

11. The analysis continues until a maximum value for the basal shear is reached or the global drift exceeds the specified limit.

3.4. Nonlinear Dynamic Time History Analysis

Nonlinear dynamic time history analyses can generate results with high accuracy and relatively low uncertainty using a combination of seismic accelerations [97]. When nonlinear dynamic time history procedures are applied for the evaluation of the seismic performance of the structure, a mathematical model directly incorporating the nonlinear deformation characteristics of individual components and ground motions, which represent the severity of the earthquake, are applied to the structural elements [81]. Nonlinear dynamic analysis is the most accurate and

reliable approach to seismic analysis, which in practice consumes a great deal of time and requires enormous computational effort.

3.4.1. Temporal nonlinear dynamic analysis method:

This method evaluates structural seismic performance by applying a series of ground motion accelerations to the structure. In this procedure, the ground motion acceleration is applied to the structure to evaluate the displacement of each portal frame to estimate the possible performance limit states for each portal frame. Three steps are required to select the seismic records. First, the design response spectrum must be specified based on the seismic code related to the building location, then several seismic records are selected corresponding to the site characteristics and the seismic design spectrum. Finally, the selected seismic records are loaded and then, considering a loading case, selected acceleration series are applied to the structure to evaluate the seismic performance of the structure [98].

Since a structure deforms in its inelastic region, where the equation of motion of a multi-degree-of-freedom system governing the dynamic response is denoted by equation (x), the restoring force and damping force vectors cannot remain proportional to displacement or velocity, respectively. In addition, the acceleration of the ground motion varies arbitrarily with time; the numerical solution of equation (x) is generally impossible. As a result, the nonlinear responses of a multi-degree-of-freedom system generally require a numerical procedure for integrating the differential equations.

$$[M]\{\ddot{u}(t)\} + [C]\{\dot{u}(t)\} + \{Fr(t)\} = \text{-}[M]\{r\}\ddot{x}g(t)$$

Where [M] is the mass matrix, [C] is the viscous damping matrix, $\{Fr(t)\}$ is the nonlinear restoring force vector at time t; $\{\{\ddot{u}(t)\}, \{\dot{u}(t)\}, \{u(t)\}\}$ are the acceleration, velocity, and displacement response vectors respectively; {r} is the support influence vector; $\ddot{x}g(t)$ is the ground acceleration at time t.

3.4.2. Incremental dynamic analysis method:

Incremental dynamic analysis is a parametric structural analysis approach proposed to predict structures' behaviour under seismic loading.

Incremental dynamic analysis can estimate the limit state capacity and seismic demand of structures from elasticity to collapse by performing a series of nonlinear time analyses under a series of multi-scale accelerogram records of ground motion acceleration. To evaluate the seismic capacity, the selected ground motion intensity is incremented until the overall structural system's predicted limit state seismic capacity is reached. Vamvatsikos and Cornell [99] stated that incremental dynamic analysis has great potential and is not only a solution for earthquake engineering. In other words, it can extend far beyond and give researchers more accurate predictions of structural behaviour under seismic loading. Incremental dynamic analysis is a widely applicable and versatile tool for evaluating structural performance that can accurately predict the responses of structures under a wide range of intensities. In addition, it contains a measure of intensity (i.e., the first spectral acceleration mode, Sa) versus a measure of damage (maximum inter-story relative displacement ratio). The main objectives of the incremental dynamic analysis are summarized below:

- ➢ Better understanding of the structural behaviour under high levels of ground motion.
- ➢ Prediction of the seismic structural capacity level of the structure.
- ➢ Complete understanding of the range of responses or demands over the range of potential levels of a ground recording.
- ➢ Illustrate the dispersion of the nature of the structural response in increasing earthquake intensity.
- ➢ Derive a multi-record curve from the incremental dynamic analysis to demonstrate the stability and variability of different seismic ground motion records.

According to FEMA 440 [97], the large scatter in the engineering demand parameters is due to the variability in ground motion. FEMA 440 [97] illustrates this problem by showing Figure 3.8. The figure demonstrates the results obtained from the research work by Vamvatsikos & Cornell [99], in which a series of nonlinear time analyses were performed by setting a selected earthquake extended to several intensity levels.
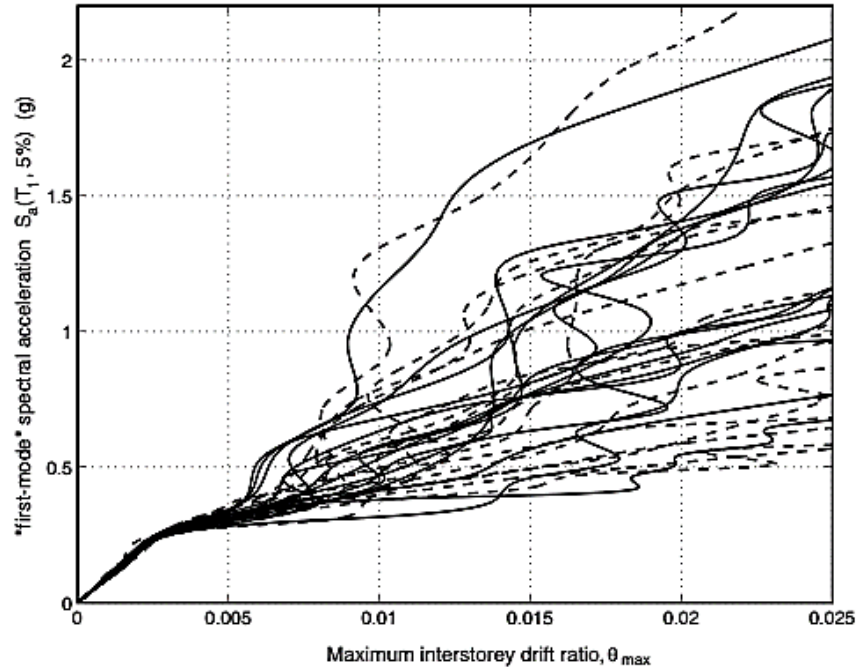
Figure 3.8: Incremental dynamic analysis curve using thirty ground motion records
(Vamvatsikos and Cornell) [99].

The various steps considered for obtaining IDA from each earthquake record, defined by Elnashai and Di Sarno [95] are as follows:

1. Define a suitable earthquake record consistent with the design scenario.

2. Define a monotonic scaleable ground-motion intensity measure, e.g., the PGA, PGV, PGD or a combination.

3. Define a damage measure or structural state variable: force-base (maximum base shear, bending moment or axial load) or deformation-based (maximum storey drifts or member rotations) parameters. Energy-based quantities, such as ductility and/or hysteretic energy are also suitable damage indices.

4. Define a set of scale factors to apply for the selected intensity measure in 2.

5. Scale the sample record in 1 to generate a set of records that will test the structure throughout its response range, from elastic response to collapse.

6. Perform response history analysis of the structural model subjected to the scaled accelerogram at the lowest intensity measure.

7. Evaluate the damage measure in 3 corresponding to the scaled intensity measure in 2.

8. Repeat step 6 to 7 for all the scaled intensity measures.

3.4.2.1. Drift limit states

The performance of a structure under earthquake motion can be analyzed using vulnerability curves. Vulnerability curve represents the probability of exceeding a certain damage limit state in terms of selected intensity of ground motion. One way of representing/plotting the vulnerability of the structure at different peak ground acceleration (PGA) can be obtained by plotting maximum inter-storey drift (%) with PGA, however other EDP can be used. Tiziana Rossetto and A. Elnashai [100] proposed analytical displacement-based vulnerability curves for the case of low rise, infilled RC frames with inadequate seismic provisions. ATC 40 [83] and FEMA-356 [81] proposed four limit states based on global behaviour (inter-storey drift) as well as element deformation (plastic hinge). They proposed performance level for structures with ductile moment resisting frame (ductile MRF). Similarly, Erberic [101], Papaila [102] also proposed in their study four limit states considering only inter-storey drift used for limit states global drift. The various performance level proposed by different codes and researchers are discussed below from Table 3.1 to Table 3.4.

Table 3.1: Performance level proposed by Tiziana Rossetto, A. Elnashai for a homogenized reinforced concrete (HRC) damage scale for infill RC frame structures [100].

Damage State	Slight damage	Light damage	Moderate damage	Extensive damage	Partial collapse	Collapse
Max. ISD(%)	0.05	0.08	0.30	1.15	2.80	> 4.36

Table 3.2: Storey Drift ratio (%) limit proposed with various damage levels (Ghobarah) [103].

Damage Of State	Ductile MRF	Non-ductile MRF	MRF with infill	Ductile walls
No damage	<0.2	<0.1	<0.1	<0.2
Repairable		/		
a)Light damage	0.4	0.2	0.2	0.4
b)Moderate damage	<1.0	<0.5	<0.4	,0,8
Irreparable damage >yield point	>1.0	>0.5	>0.4	>0.8
Servere damage – life safety – Partial Collapse	1.8	0.8	0.7	1.5
Collapse	>3.0	>1.0	>0.8	>0.25

Table 3.3: Performance level given by SEAOC –VISION 2000 based on inter-storey drift (%) [104].

Performance Level	Overall building damage	Max. Inter-storey drift (%)
Fully operational	Negligible	<0.2
Operational	Light	0.5-1.5
Near Collapse	Severe	1.5-2.5
Collapse	Complete	>2.5

Table 3.4: Storey drift limit based on FEMA-356 [81]

Damage State	Performance level			
	Immediate Occupancy	Damage control	Life safety	Collapse prevention
Max.ISD (%)	1%	1-2%	2%	>4%

3.5. Conclusion

The seismic performance of the selected buildings was evaluated through two methods: the nonlinear static method and dynamic time history analyses considering the nonlinear material response. In the dynamic time history analysis, the structures were subjected to a large number of real or artificial ground motion accelerations or earthquakes. Hence, this approach can be considered as the most reliable tools to examine the seismic performance of the buildings but requires large computational time and it is hard to interpret the results. On the other hand, The IDA is a non-linear dynamic analysis that offers an immense possibility to evaluate the seismic responses of the structure and takes into account the effects of energy intensity, duration and frequency contained in an accelerogram, and produces the effect of these parameters on the inter-story displacement and maximum displacements in a structure, unlike the Pushover analysis which is a static analysis that gives only a small insight into the seismic responses on the structure. The occurrence of damage with different degrees is a random process, therefore, the only appropriate tool to predict the expected damage distribution would be probabilistic. Therefore, we propose to establish fragility curves based on the data of the incremental dynamic analysis in order to define with precision a sequential pattern of damage.

Figure 3.9 summarizes the methods of structural analysis used in earthquake engineering. The studied methods are grouped as static or dynamic methods applied in elastic and inelastic response analysis.
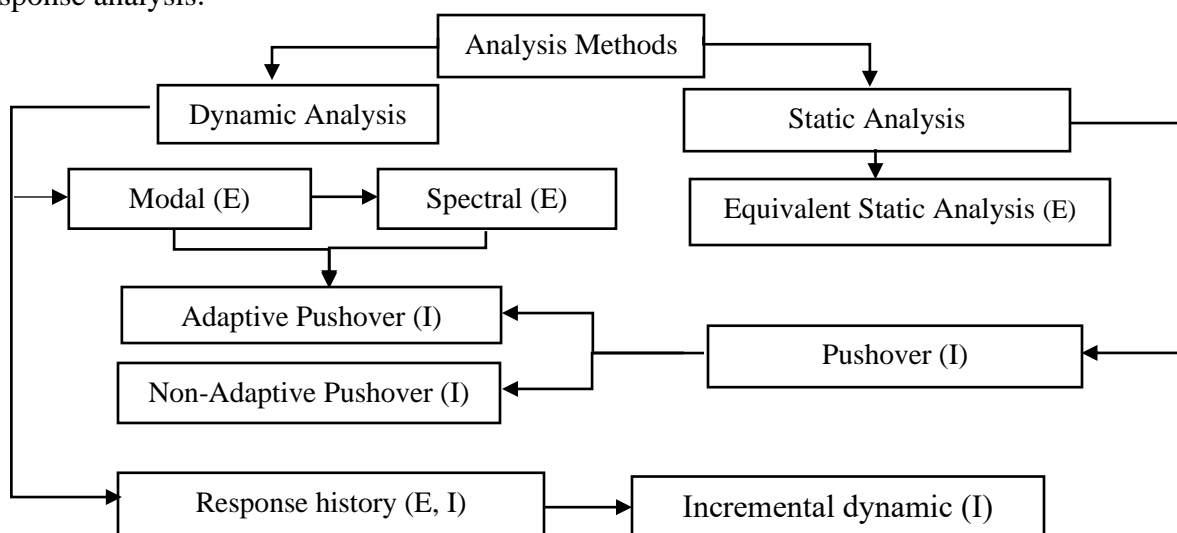
Figure 3.9: Common methods of structural analysis used in earthquake engineering [95].

Chapter 4.

Numerical simulation of RC infilled frames

4.1. Introduction

The present chapter describes a briefly the experimental tests that have been used to calibrate the numerical model used in the seismic assessment of infilled RC frames. These tests were selected due to the comprehensive data available for them, including data required for developing micro-models and the experimental explanation of failure mechanisms. The geometry, mechanical properties and all relevant parameters of those tests are presented with more detail in this chapter. In the end each test is compared with the numerical results, and it can be observed the accuracy of the considered modelling strategy in representing different types of masonry elements (strong and weak units) and with and without openings. Based on the validated simulated approach the strut properties can be used later in the simulation of infilled frame buildings.

4.2. Macro-model approach

Macro-models, such as strut-type models, have been used, combined with experimental observations, to represent the overall force-displacement relation of this type of structures in computationally efficient models. However, the properties of such models can be difficult to determine based on experiments.

This difficulty is due to different reasons, especially the uncertainties in the material properties of the different components of the infilled frame used in the experiment, which prevent a direct comparison between the experiment and the macro-model in the calibration process. These reasons motivated researchers to develop micro-models using finite element analysis tools to represent complex aspects of the behaviour of masonry infilled frames, including brittle failure mechanisms in the infill at mortar joints and the infill-frame interaction. Micro-models provide an alternative tool to simulate the detailed response of masonry infilled frames with different configurations at a lower cost, when compared to the cost of experimental tests, which can be used for the macro-model calibration process. Moreover, micro-models can potentially represent the multiple failure modes which can occur in the infill or in the frame.

4.3. Procedure for masonry infill wall modelling in OpenSees.

4.3.1 Numerical model description details

OpenSees software [105] provides a straightforward platform to model structural elements reliably and flexibly [106]. Furthermore, its ability to integrate with other software to input or postprocessing data is prominent. As such, the numerical models were generated using OpenSees software. Figure 4.1 shows an overall description of the adopted modelling strategy for the RC elements. As can be seen, beam with Hinges element from OpenSees element library was used to model the RC elements. This element has the capability to specify plastic hinge lengths at the element ends. By using Modified Radau Hinge Integration method [107,108], two-point Gauss integration is used on the element interior while two-point Gauss-Radau integration is applied over lengths of two hinges. To accommodate any extended plasticity beyond the hinge zones, fibre sections were also considered in the central part of the element. The length of hinges at the end of each element has been quantified using the following proposal [109]:

$$lp = 0.08l_e + 0.022d_b \, f_y \tag{4.1}$$

Where l_e is the length of the element, d_b is the diameter of the longitudinal steel rebar, and f_y is the yield strength of the used steel in MPa.
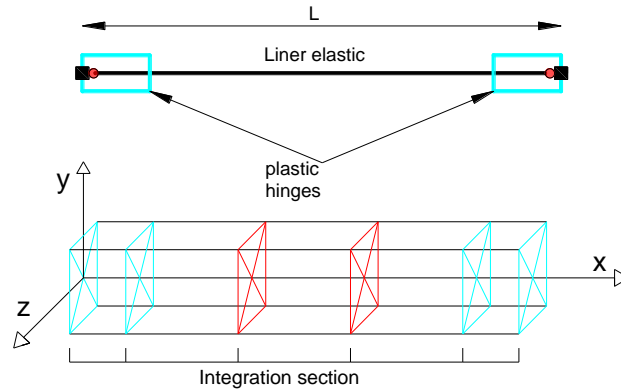
a)   Beam with hinge element general description
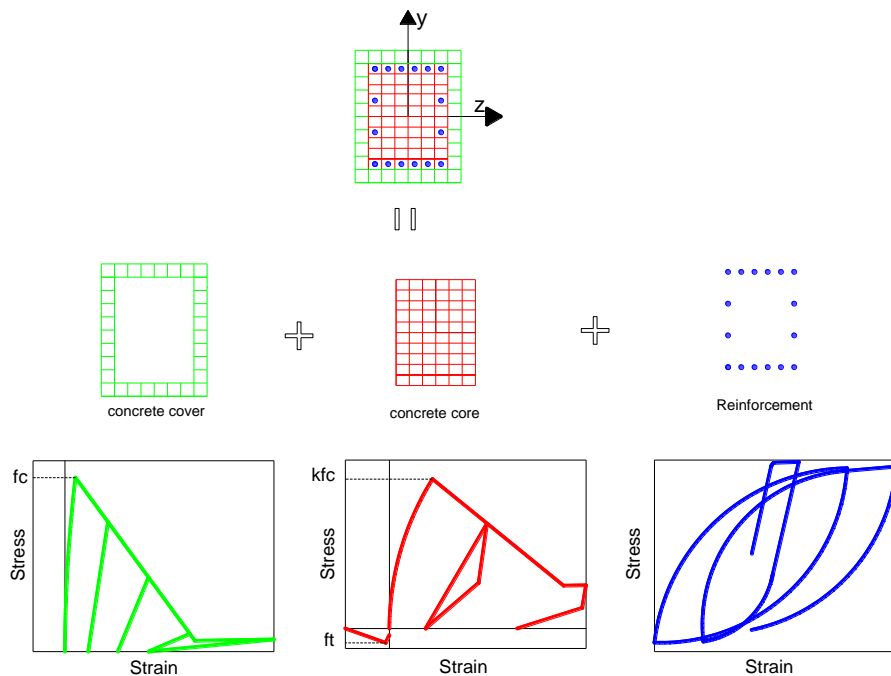
i. unconfined concrete (Concrete01)   *ii. confined concrete (concrete02)*   *iii. Steel material (steel02)*

b) Fibre section discretization

Figure 4.1.: Adopted strategy for modelling RC elements.

As can be seen in Figure 4.1b) the RC section was discretized in three different materials to accommodate the expected behaviour of each ingredient of the RC. For the cover, where the concrete has no confinement, a zero tensile concrete model known as Concrete01 has been used. On other hand, to account for the effect of steel stirrups, the confined ratio has been considered for

the middle region. The modified concrete strength has been used to define the concrete parts confined by stirrups. Concrete02 model in OpenSees was used to model the confined concrete with a tensile strength of 10% of the compressive strength of the concrete. Longitudinal rebars were modelled using uniaxial Giuffre- Menegotto-Pinto model [110] with isotropic hardening, known as Steel02 in OpenSees. Eventually, to account for beam-column connection, a rigid end-offset joint model was applied for the beam-column joints [111]. The lengths of the rigid parts were half of the depth of the perpendicular element.

The infills were modelled using a single compressive strut element with an area evaluated based on the expression that is proposed by Hendry [53] using the constitutive model for masonry, which matches the shape of the Concrete01 constitutive model. The constitutive model proposed by Hendry [53] is given by the following expression:

$$\sigma_m = f_m' \left[2 \frac{\varepsilon_m}{\varepsilon_{crm}} - \left(\frac{\varepsilon_m}{\varepsilon_{crm}} \right)^2 \right] \tag{4.2}$$

where ε_m and σ_m are the compressive strain and the corresponding compressive stress of the masonry, respectively, f_m' is the maximum compressive strength of the masonry and ε_{crm} is the compressive strain at the onset of failure, which according to [112] ranges from 0.0015~0.002. In these analyses, the value of ε_{crm} was 0.002 in all models.

4.3.2. The partially infilled frame (reduction factor)

Partially infilled RC frame can be defined as the RC frame with infill wall that has an opening (e.g., window, door or any construction opening). The existence of such openings effects the ability of infill wall to distribute loads and, therefore, reduces the panel's stiffness, ultimate strength, and capacity for dissipating energy. Based on the existing experimental tests, different proposal was found to model the partially infilled walls. These proposals can be categorized into two main groups [113]; single/multiple diagonal strut system with a reduced strength [114,115] and truss configurations that consist of several crossed struts, e.g., see [116-180]. Given that the latter modelling strategy comes with a high computational cost [113] , the former strategy was found more common in use in literature. As such several proposals found in literature to quantify the reduction factor to count for the infill walls (e.g., see among others [113,118-120] .These

models account for different parameters of the opening such as size, aspect ratio, type, and position. Based on assessment of the reliability of the existing models, Mohamed and Romão [113] presented a new model that showed adequacy performance compared to the other models. In this study this model will be used to quantify the reduction factor.

4.4. Kakaletsis, et al. tests.

4.4.1. Geometry specimens' details

In order to investigate the influence of the infill panel with openings, Kakaletsis*, et al.* [121],tested a set of specimens with a 1:3 scale made of single-storey and single-bay frames subjected to reversed cyclic quasi-static horizontal loading up to a drift of 4%. As illustrated in Table 4.1 one of these specimens is a bare frame which is the reference model, and the rest of the specimens were infilled with clay brick infills. Only one of the infilled specimens has a fully infilled panel while the rest of the specimens have partially infilled panels. Partially infilled specimens have openings with different types (i.e., door and window) Figure 4.2.

Table 4.1: Characteristics of the test specimens.

Specimen notation	Opening shape		Opening size $La / L =0.25$	Opening location $X / L = 0.5$	Masonry Type	
	Window	Door			Weak	Strong
B	Bare frame	Bare frame	-----	------		
S	Solid	Solid	-----	------	■	
IS	Solid	Solid	-----			■
WO2	■		■	■	■	
IWO2	■		■	■		■
DO2		■	■	■	■	
IDO2		■	■	■		■

(a)

(b)

(c)

(d)

Figure 4.2: Description of the specimens (all dimension in millimetre).

The design details for the bare frame (reference frame) are shown in Figure 4.3. The beam and the column cross sections were 100x200 mm^2 and 150x150 mm^2, respectively. The dimensions correspond to 1/3-scale of the prototype frame sections, 300x600 mm^2 for the beam and 450x450 mm^2 for the column, respectively. The column had closer ties throughout the length and the beam had more shear reinforcement in the critical regions. Each beam-to-column joint had five horizontal stirrups to prevent brittle shear failure. The diameter of the longitudinal reinforcement is Φ5.60 millimetre and the diameter of the stirrups is Φ3 millimetre, which corresponds to a 1:3 scale of Φ18 and Φ10 millimetre reinforcement diameters, respectively. The RC frame represents

a typical ductile concrete construction built according to the currently used codes and standards in Greece, which are like EC8 [84].

The brick shape is shown in Figure 4.4. The mortar joint dimensions were not scaled and the mortar mixture used for the infills contained proportions 1:1:6 (cement: lime: sand) which produced mechanical properties similar to type a M1 mortar according to (EN-998-2, 2001) [122].
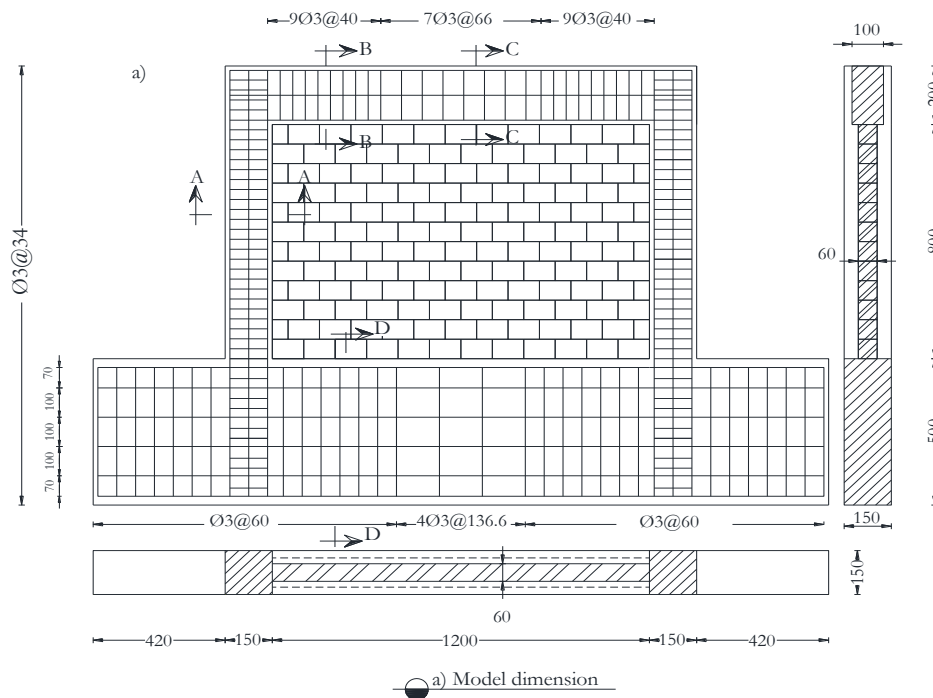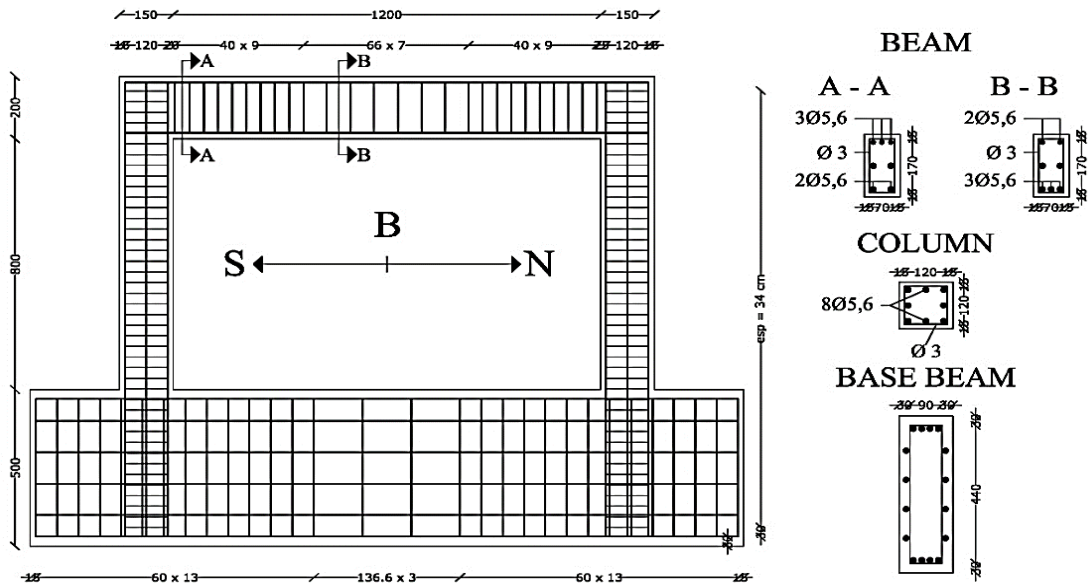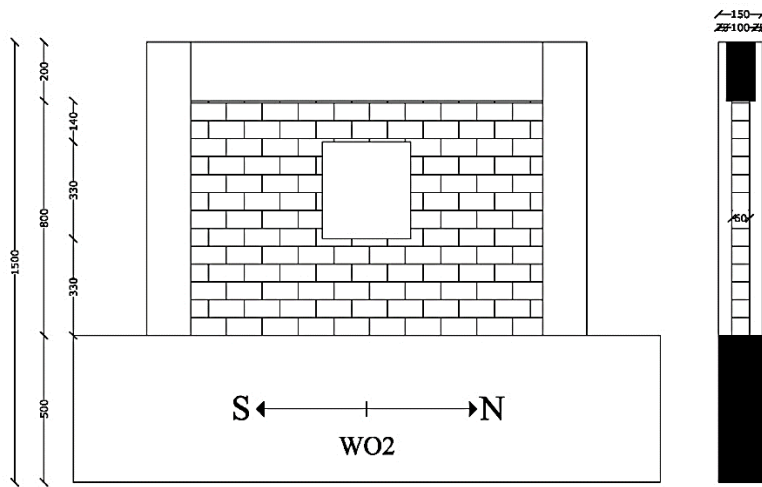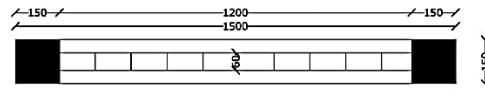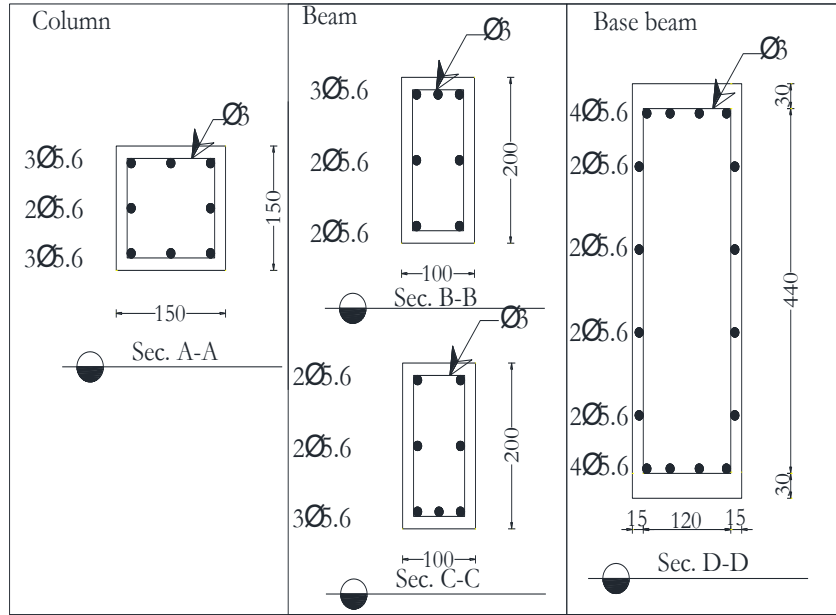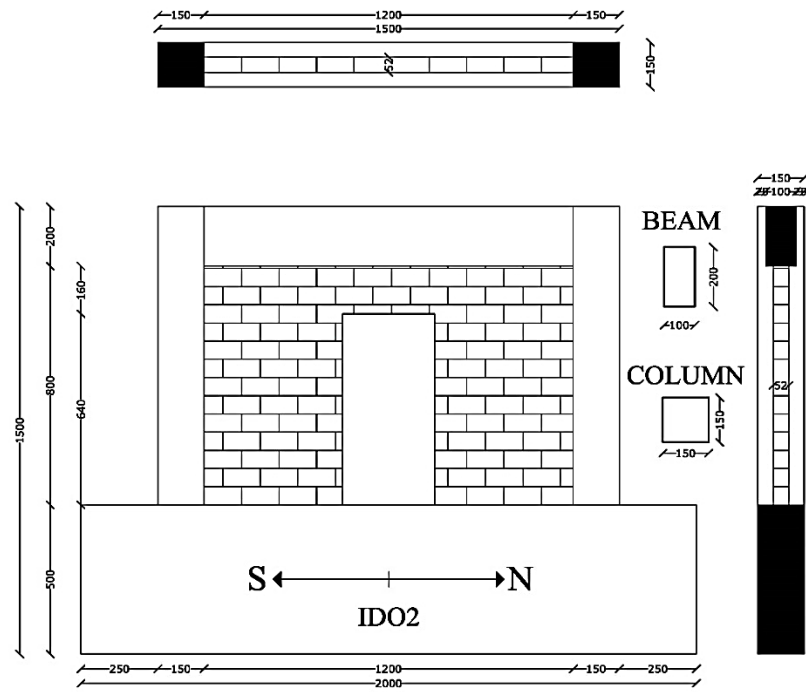
a) Model dimension

Figure 4.3: Reinforcement detailing of the RC frame model (All dimensions in millimetre)
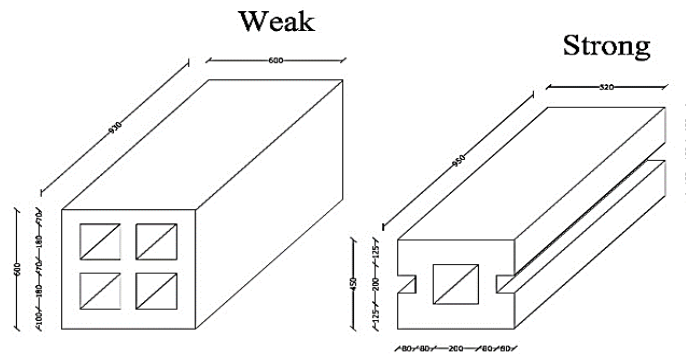
Figure 4.4: Brick unit dimensions (All dimensions in millimetre).

4.4.2. Material properties

In order to evaluate the mechanical properties of the materials used for construction of the infill panels, a set of supplementary tests were conducted. These tests include compression tests of mortar cubes, compression tests of masonry units, compression tests of masonry horizontal prisms (perpendicular to voids) and vertical prisms (parallel to voids), tests for the angle of internal

friction and shear strength (cohesion) at zero pre-compression tests. Table 4.2 summarizes the average values of the measured parameters for the infill panel materials.

To evaluate the RC frame materials, the compressive strength of the concrete was evaluated using standard compression tests and tensile tests were also conducted on steel bars to evaluate their tensile strength. The average results obtained from those tests are summarized in Table 4.3.

Table 4.2: Average values of the infill panels material parameters.

Mechanical properties	Values (unit)	
	Weak	*Strong*
Mortar		
Compressive strength f_m	1.53 (MPa)	1.75 (MPa)
Brick units		
Compressive strength f_{bc} (based on net cross section)	3.10 (MPa)	26.4 (MPa)
Masonry		
Compressive strength perpendicular to voids f_c	2.63 (MPa)	15.18 (MPa)
Elastic modulus perpendicular to voids E_c	660.66 (MPa)	2837.14 (MPa)
Compressive strength parallel to voids f_{c90}	5.11 (MPa)	17.68 (MPa)
Elastic modulus parallel to voids E_{c90}	670.30 (MPa)	540.19 (MPa)
Friction coefficient μ	0.770	0.957
Shear modulus G	259.39 (MPa)	351.37 (MPa)

Table 4.3: Average values of the RC frame material properties.

Mechanical properties	Values (unit)
Frame concrete	
Compressive strength $f_c^{'}$	*28.51 (MPa)*
Steel bars	
Yield tensile strength of longitudinal steel f_y	*390.47 (MPa)*
Ultimate tensile strength of longitudinal steel f_u	*516.27 (MPa)*
Yield tensile strength of transverse steel f_y	*212.20 (MPa)*
Ultimate tensile strength of transverse steel f_u	*321.07 (MPa)*

4.4.3. Test Setup and Instrumentation

The test setup is shown in Figure .(a). The lateral load was applied by means of a double action hydraulic actuator. The vertical loads were applied by hydraulic jacks that were tensioning four strands at the top of the column whose forces were maintained constant during each test. The level of this axial compressive load was set to 50 kN per column, which is equal to 10 % of the ultimate load. One Linear Variable Differential Transformer (LVDT) measured the lateral drift of the frame, and a load cell measured the lateral force of the hydraulic actuator.

After applying vertical loads, the hydraulic actuator started to introduce the lateral loading sequence. The horizontal loading sequence comprises full cycles of gradually increasing displacements. As shown in 4.5.(b), the full loading cycle was applied at each displacement level.
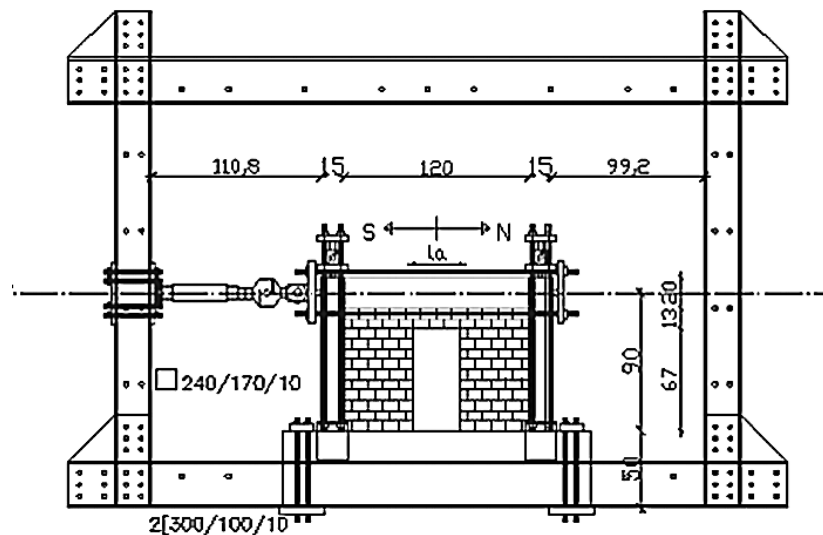
Figure 4.5.(a): Test setup
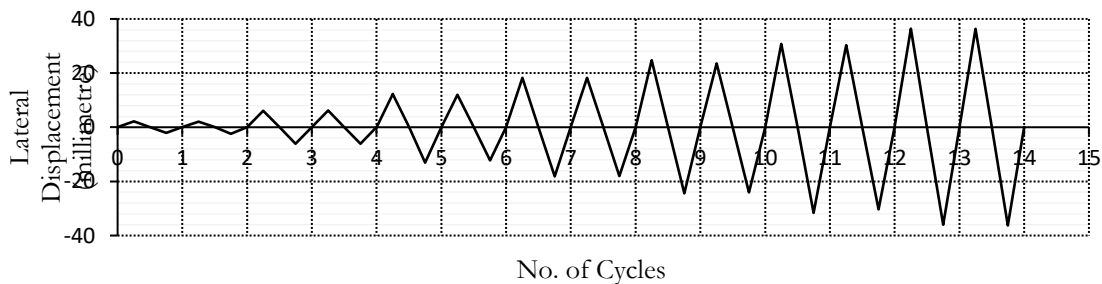
Figure 4.5.(b): Horizontal loading sequence.

75

4.4.4. Experimental and Numerical Results

4.4.4.1. Results obtained for the bare frames.

In order to verify the validity of the proposed modelling approaches for concrete and reinforcing steel, one bare frames specimen was analysed: Specimen B. The configurations and properties of these frames were presented in the explanation above. Where the behaviour of these frame was analysed for cyclic loading.

Figure 4.6 shows the load-displacement results obtained for specimen B, along with their corresponding experimental results in terms of shear-top displacement (Fig. 4.6.a), shear- top displacement envelopes (Fig. 4.6.b) and energy dissipated (Fig. 4.6.c) for the Specimen B. The obtained results with the numerical model (OpenSees) are in good agreement with the experimental response in terms of shear-top displacement response and energy dissipation.
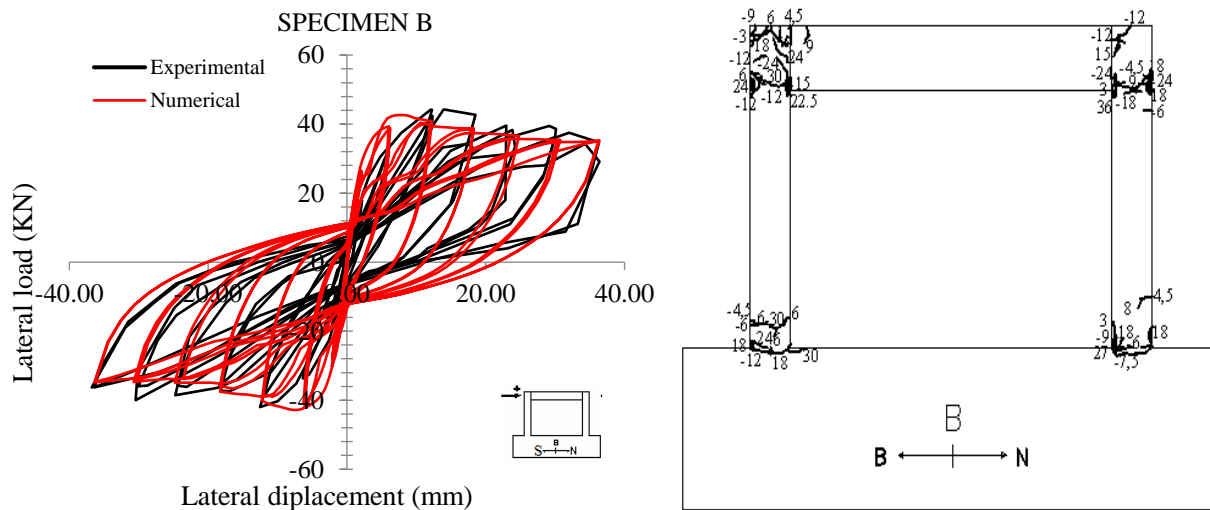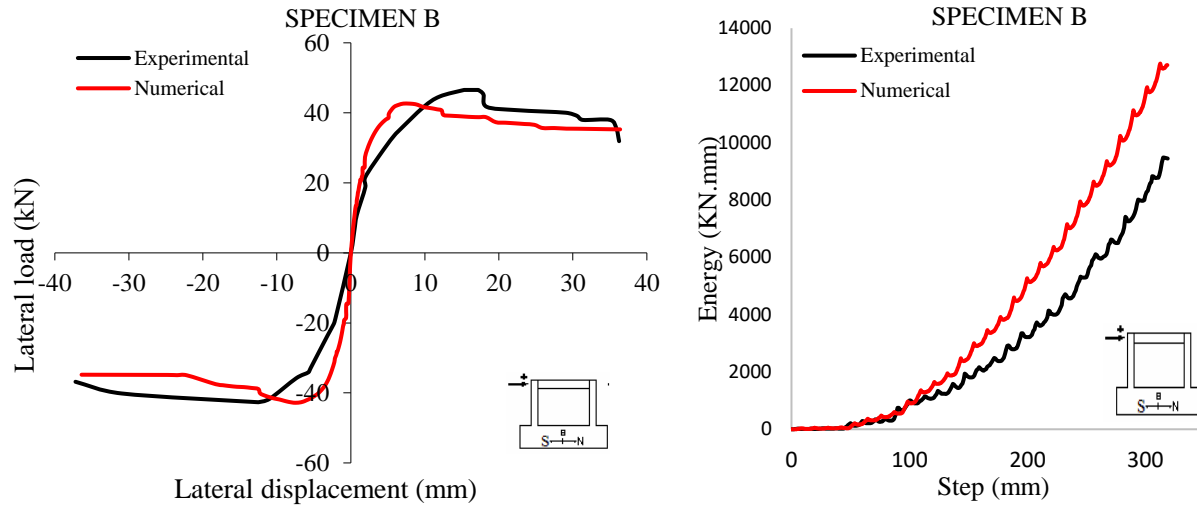
Figure 4.6: a. Hysteretic behaviour of the masonry infill wall, b. base shear–top displacement envelope, c. energy dissipated results of experimental test and the numerical model B specimens

In comparing the numerical results obtained from OpenSees with the experimental results of Kakaletsis, *et al.* [121], five parameters were analysed: the maximum lateral load, the initial secant stiffness, the secant stiffness, the end loading, and the maximum dissipative energy.

The base shear-top displacement hysteric curve of the numerical model is <4% higher in terms of the maximum lateral load than the experimental results. Also, the base shear-top displacement envelope of the numerical model is <2% lowest in terms of initial secant stiffness, <26% higher in terms of secant stiffness and <9% higher in terms of End loading for the same top displacement values compared to the experimental results. The dissipated energy was determined (Fig. 4.6.c), and the numerical model shows acceptable agreement with the experimental response, with <1 % of difference for the same step values (125 mm) and <25 % in the end of loading, which is acceptable because it is a simplified model to model the bare frame. In general, the OpenSees results are in good agreement with the experimental results in Specimen B's study case which demonstrates the ability of the proposed model to simulate the global hysteretic response of bare frames (Specimen B) In addition, the uncertainty regarding some of the properties of the materials used in the experimental tests can also be a factor, such as the loading rate which is not able to be represented numerically.

4.4.4.2. Results obtained for the fully infilled frames.

Figure 4.7 represents the calibration of numerical results with experimental results in terms of shear-top displacement (Fig. 4.7a), shear- top displacement envelopes (Fig. 4.7. b) and energy dissipated (Fig. 4.7.b) for the Specimens S and IS. The numerical results obtained are in excellent agreement with the experimental response in terms of shear-top displacement response and energy dissipation.
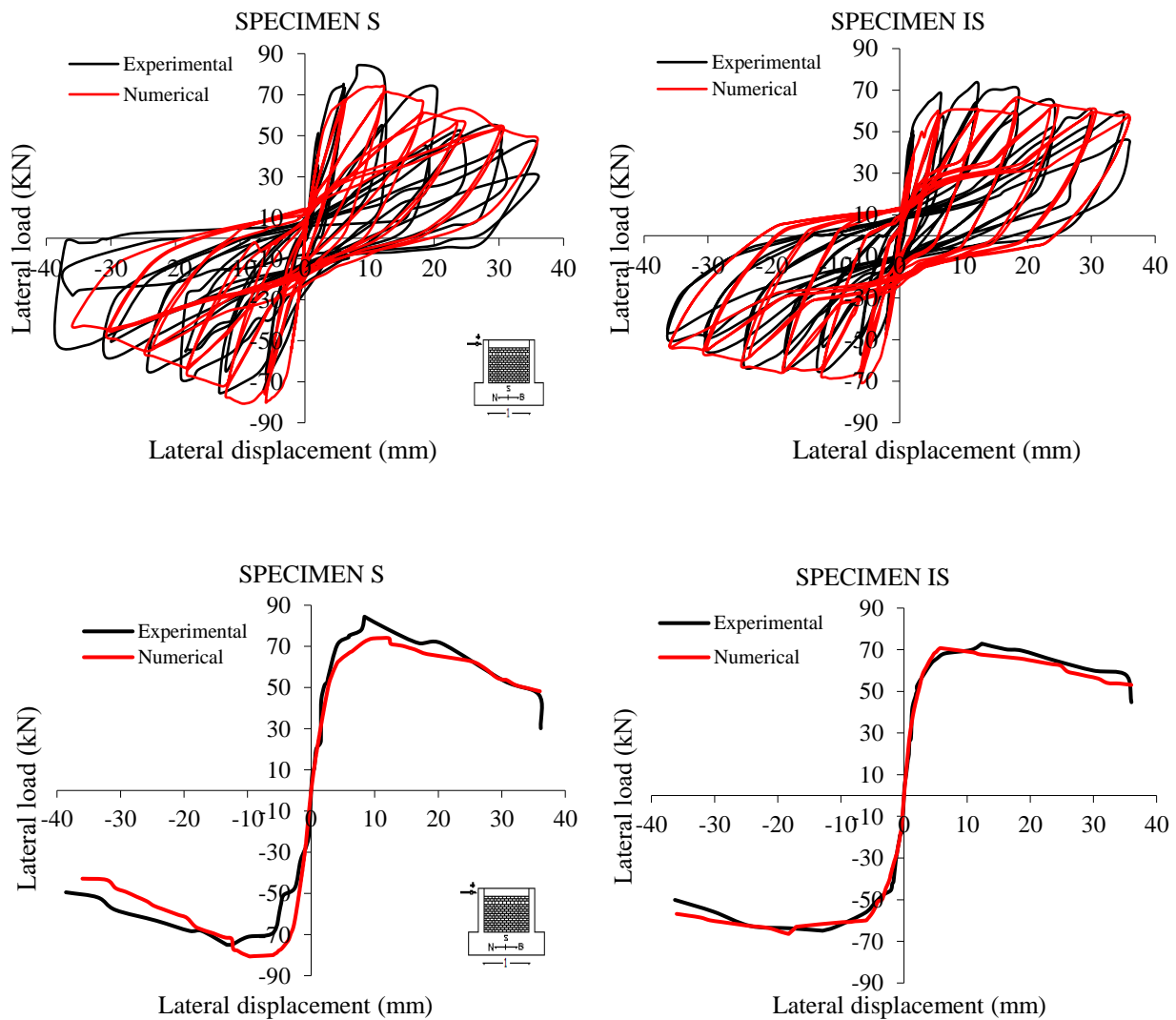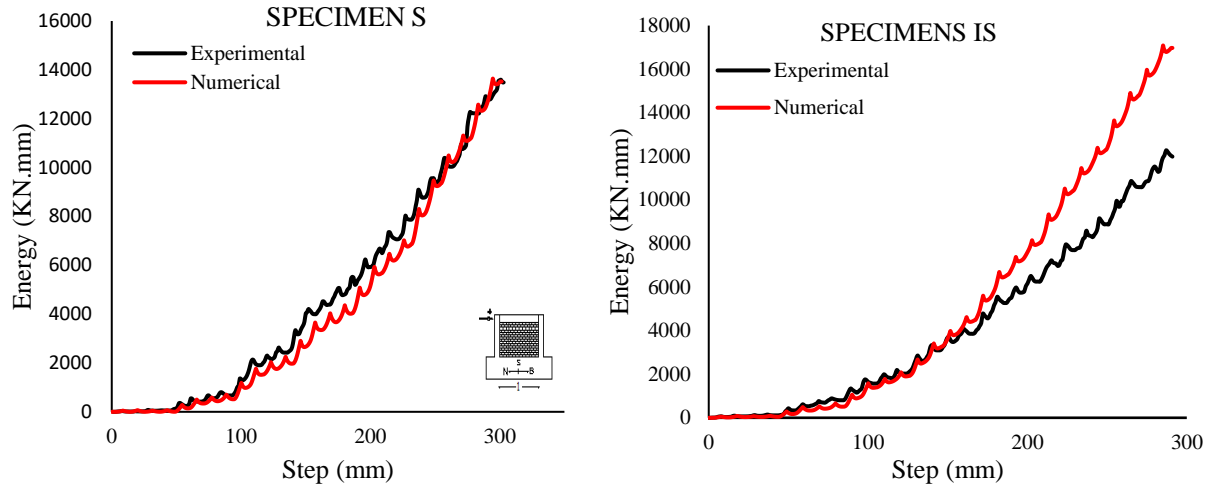
Figure 4.7: a. Hysteretic behaviour of the masonry infill wall, b. base shear–top displacement envelope, c. energy dissipated results of experimental test and the numerical model for S and IS specimens.

In comparing the numerical results of S and IS specimens obtained from OpenSees with the experimental results of Kakaletsis*, et al.* [121] for S and IS specimens, we relied on five parameters: the maximum lateral load, the initial secant stiffness, the secant stiffness, the end loading, and the maximum dissipative energy.

The base shear-top displacement hysteric curve of the numerical model is <9%, 8% higher in terms of the maximum lateral load than the experimental results for S and IS respectively. Also, the base shear-top displacement envelope of the numerical model is <2% higher in terms of initial secant stiffness for both specimens, <31 higher in terms of secant stiffness and <4%%, 15% higher in terms of End loading for the same top displacement values compared to the experimental results of S and IS specimens respectively. The dissipated energy was determined (Fig. 4.7.c), and the numerical model shows excellent agreement with the experimental response, with <1 % of difference for the same step values for specimen S, and acceptable agreement with the experimental response for IS specimen, with <1 % of difference for the same step values (180 mm) and <29 % in the end of loading.

In general, the results shown a good agreement between the numerical model and the experiment, especially in term of the global behaviour (stiffness and strength). And it can be concluded that this numerical modelling provides a useful alternative to experimental tests in terms

of defining the maximum strength and stiffness since the global behaviour envelope is seen to be adequately represented. Furthermore, this type of analysis also provides important information regarding the contact length between the infill panel and the RC frame which can be used to calibrate the structural parameters of equivalent diagonal strut models.

4.4.4.3. Results obtained for the partially infilled frames.

To emphasise the ability of the numerical approach to simulate the experimental test results in case of partially infilled panels, four numerical models with partially infilled panels with different configurations were constructed to match existing physical specimens. The findings of these numerical models will be discussed considering the existing experimental data in the following sections.

Specimens with window openings

Two specimens with window openings (WO2 and IWO) were modelled. The results of these analyses are presented in the following according to the window according to the type of masonry wall (weak and strong). The comparison between the load-displacement curves of each specimen obtained from the numerical analyses with those obtained from the experimental tests is presented in Figure 4.8.

Figure 4.8. represents the calibration of numerical results with experimental results in terms of shear-top displacement (Fig. 4.8. a), shear- top displacement envelopes (Fig. 4.8. b) and energy dissipated (Fig. 4.8.c) for the Specimens WO2 and IWO2. The obtained results with the numerical model (OpenSees) are in excellent agreement with the experimental response in terms of shear-top displacement response and energy dissipation.
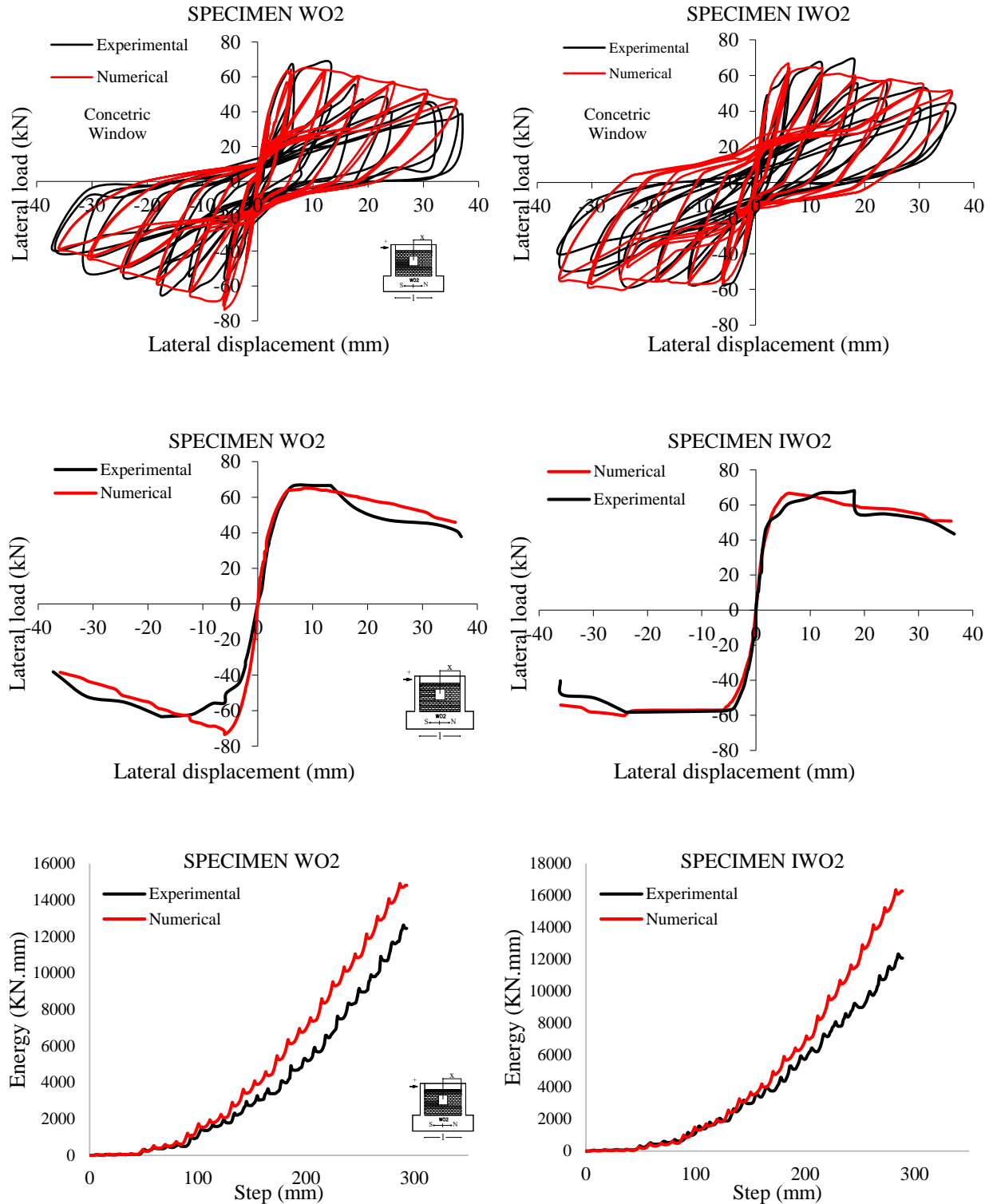
Figure 4.8: a. Hysteretic behaviour of the masonry infill wall, b. base shear–top displacement envelope, c. energy dissipated results of experimental test and the numerical model for WO2 specimens.

In comparing the numerical results obtained from OpenSees with the experimental results of Kakaletsis*, et al.* [121] for WO2 and IWO2 specimens, we relied on five parameters: the maximum lateral load, the initial secant stiffness, the secant stiffness, the end loading, and the maximum dissipative energy.

The base shear-top displacement hysteric curve of the numerical model is <2% higher in terms of the maximum lateral load than the experimental results for both specimen WO2 and IWO2. Also, the base shear-top displacement envelope of the numerical model is <2% higher in terms of initial secant stiffness, <14% higher in terms of secant stiffness and <8%, <14% higher in terms of End loading for the same top displacement values compared to the experimental results for both specimen WO2 and IWO2. The dissipated energy was determined (Fig.4.8.c), the numerical model shows acceptable agreement with the experimental response, with <1 % of difference for the same step values (160 mm and 200 mm for WO2 and IWO2 respectively, also <15 % and <25 % in the end of loading for both specimens respectively.

Specimens with door openings

Figure 4.9 represents the calibration of numerical results with experimental results in terms of shear-top displacement (Fig. 4.9. a), shear- top displacement envelopes (Fig. 4.9. b) and energy dissipated (Fig. 4.9.c) for the Specimens DO2 and IDO2. The obtained results with the numerical model (OpenSees) are in excellent agreement with the experimental response in terms of shear-top displacement response and energy dissipation.
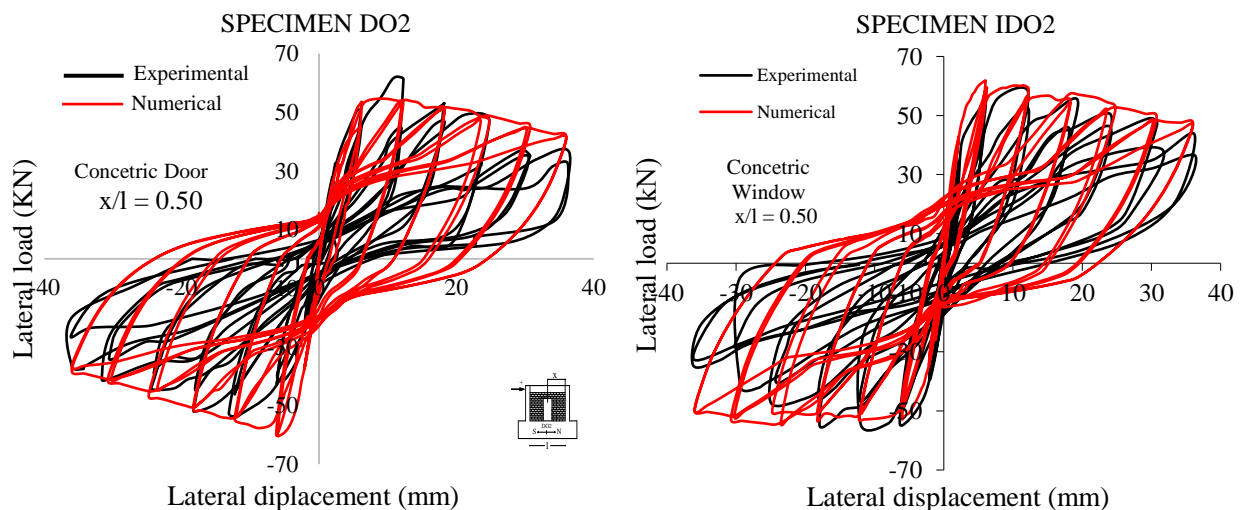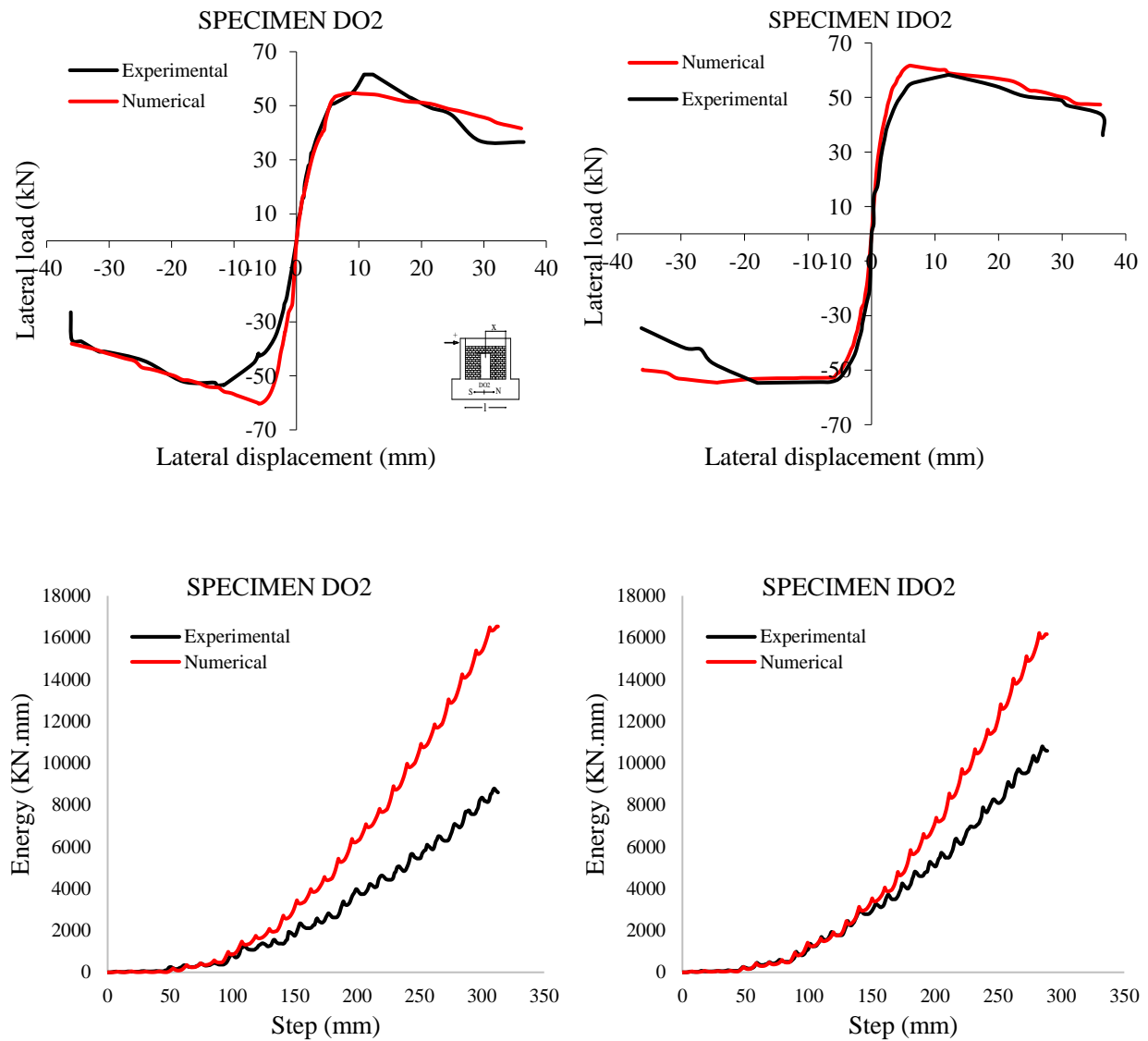
Figure 4.9: a. Hysteretic behaviour of the masonry infill wall, b. base shear–top displacement envelope, c. energy dissipated results of experimental test and the numerical model for DO2 and IDO2 specimens.

In comparing the numerical results obtained from OpenSees with the experimental results of Kakaletsis*, et al.* [121] , we relied on five parameters: the maximum lateral load, the initial secant stiffness, the secant stiffness, the end loading, and the maximum dissipative energy.

The base shear-top displacement hysteric curve of the numerical model is <12%, <4% higher in terms of the maximum lateral load than the experimental results for DO2 and IDO2

respectively. Also, the base shear-top displacement envelope of the numerical model is <1% higher in terms of initial secant stiffness, <5% higher in terms of secant stiffness for both specimens and <11%, <23% higher in terms of End loading for the same top displacement values compared to the experimental results for DO2 and IDO2 respectively. The dissipated energy was determined (Fig. 4.9.c), the numerical model shows acceptable agreement with the experimental response, with <1 % of difference for the same step values (180 mm and 1700 mm for DO2 and IDO2 respectively), also <40 % and <34 % in the end of loading for both specimens respectively.

In general, the OpenSees results are in good agreement with the experimental results in Specimens S and IS study case because it is a simplified model that is used to model the full infill panel and its surrounding frame elements, which demonstrating the ability of the proposed model to simulate the global hysteretic response of full frames considering the variation in mechanical properties (Specimen S and IS) and with openings (WO2,IWO2, DO2,IDO2 specimens).

Figure 10 and Figure 11 shows the envelope behaviour curves of the two specimens compared with those of the solid and bare frame specimens. From Figure 4.10 (a) and Figure 4.11 (a), it can be seen that the existence of the opening has a clear effect on the overall behaviour of the structure (namely in terms of its strength), also the type of masonry wall (weak and strong) appears to have a perceptible effect which is in agreement with the experimental data shown in Figure 4.10.(b) and Figure 4.11 (b).

a.1)

a.2)

b.1)   b.2)
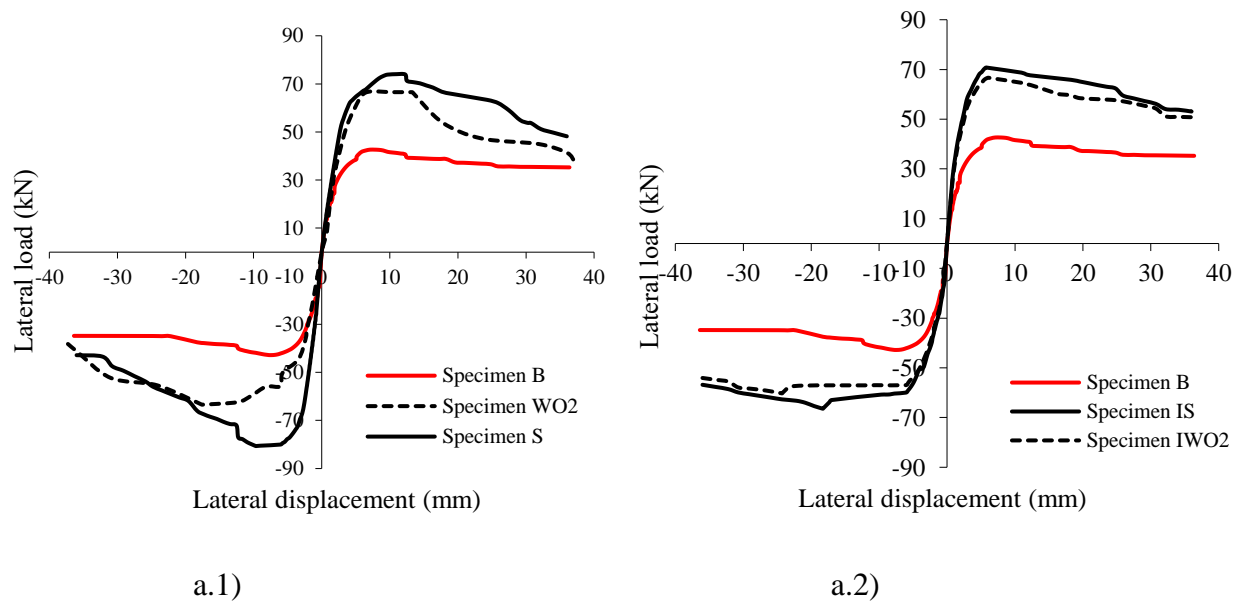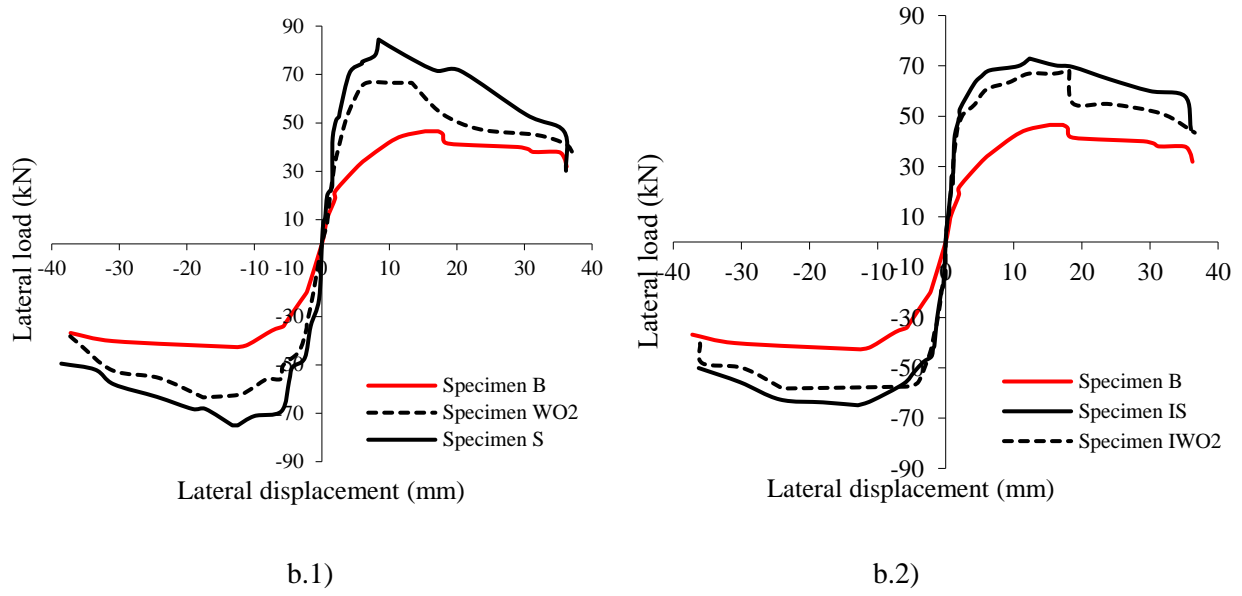
Figure 4.10: Numerical lateral load-displacement envelopes for specimens with window openings with different type of infill wall compared with those of the solid and bare frames : a) numerical model: a.1) weak unit a.2) strong units)   b) experimental data b.1) weak unit b.2) strong units) (Kakaletsis, 2008)

c.1)   c.2)

d.1)   d.2)
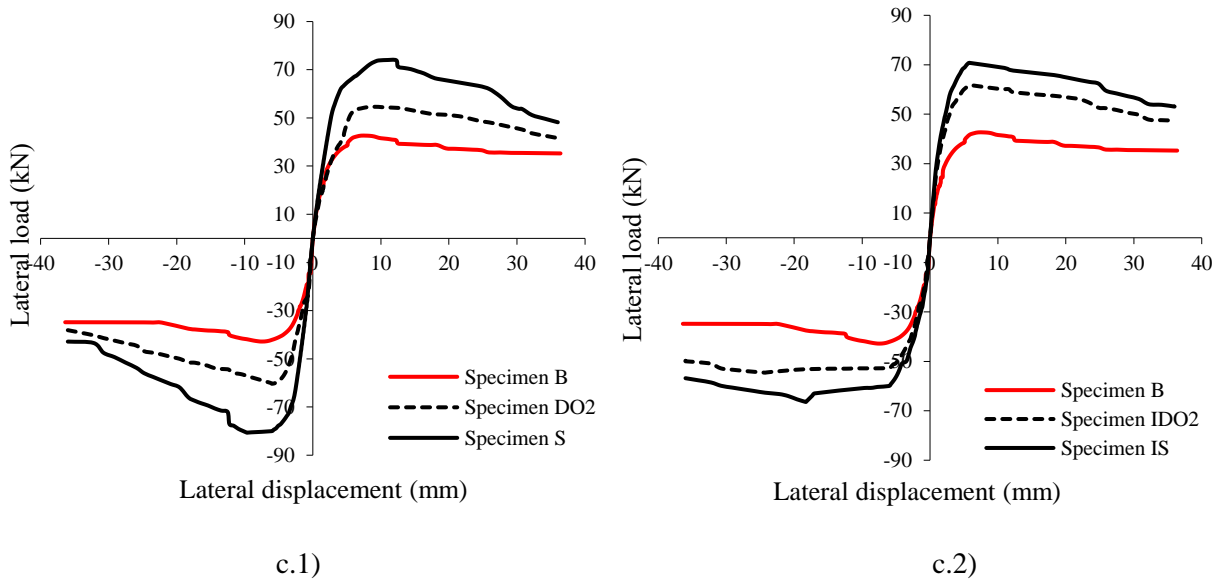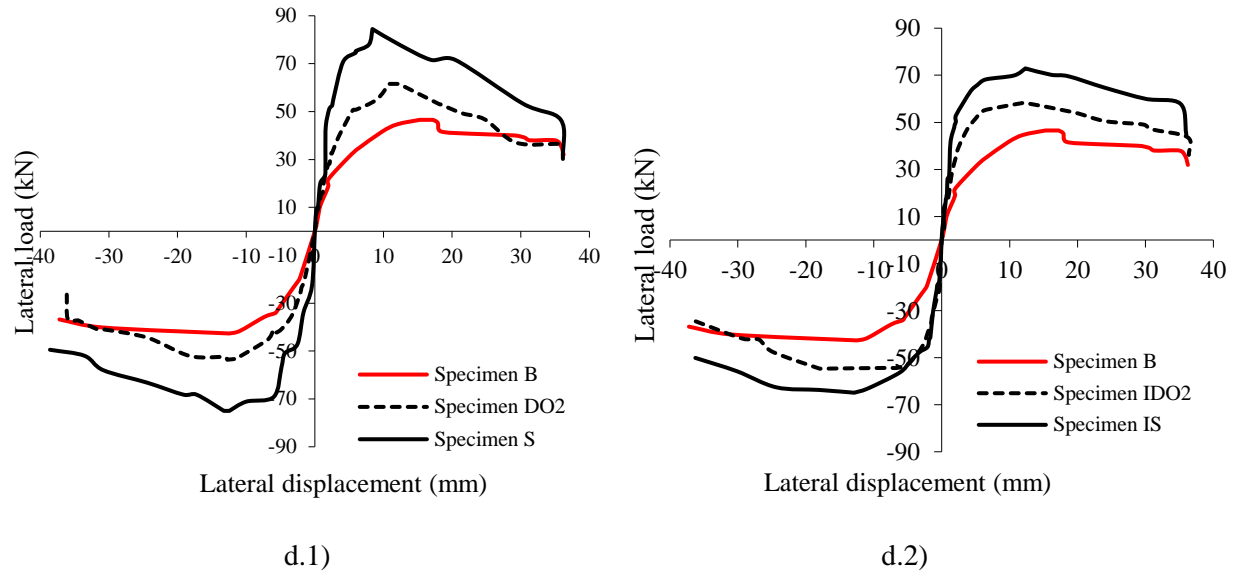
Figure 4.11 : Numerical lateral load-displacement envelopes for specimens with door openings with different type of infill wall compared with those of the solid and bare frames : c) numerical model: c.1) weak unit c.2) strong units)   d) experimental data d.1) weak unit d.2) strong units) (Kakaletsis, 2008).

4.5. André Furtado, et al. (2021) in-plane tests

4.5.1. Specimens' description

From the study developed by Furtado detailed in [123] , The geometric characteristics of the infill wall dimensions were set at 4.20x2.30 m (length and width, respectively, which are representative of those found in the Portuguese building stock. According to the study developed by Furtado, et al. [124], Figure 4.12 shows the schematic layout of the RC frame geometry with the corresponding columns and the dimensions of columns, beams, cross-sections, and reinforcement detailing. in-elevation dimensions, made of hollow clay horizontal brick units with 150 mm thickness as show in Figure 4.13. All the panels were built and aligned with the external side of the RC beam. 5 specimens total—2 reference specimens without strengthening and 3 strengthened panels make up the testing campaign.
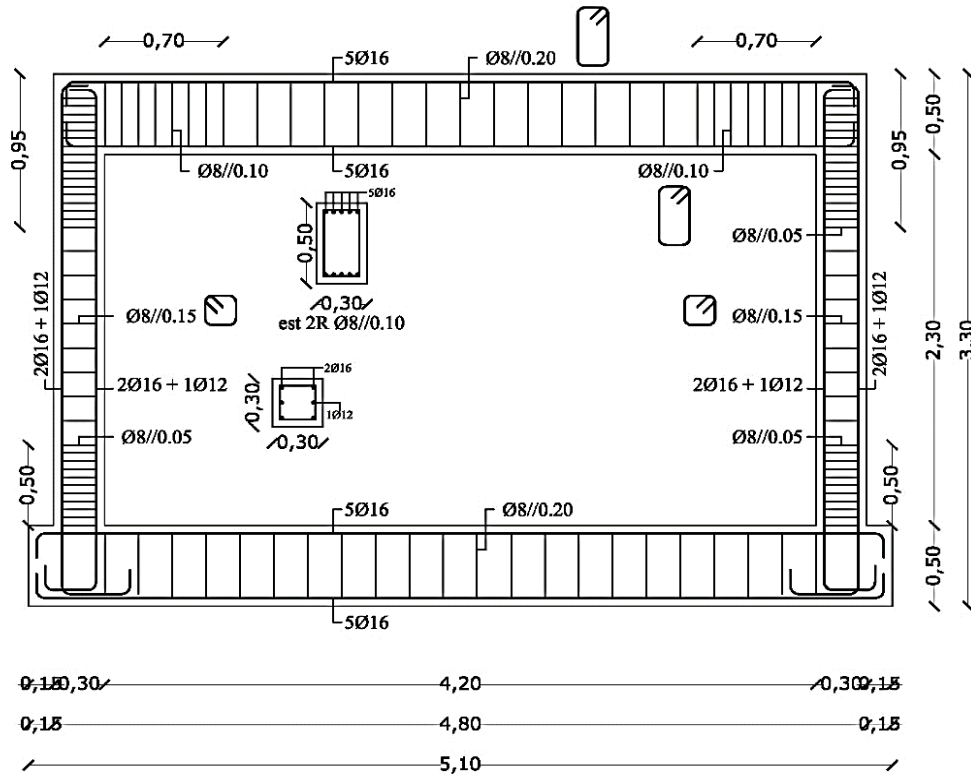
Figure 4.12: RC frame reinforcement detailing.
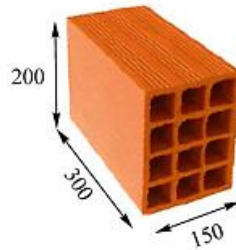
Figure 4.13: Detail of the masonry unit.

4.5.2. Material properties

The material used for the RC frame specimen construction consisted of regular C20/25-class concrete [125], with a coefficient of variation of 6.1% and a mean cubic compressive strength of $f_{cm,\ cyl}$ =21.4 MPa with a standard deviation of 1.35 MPa. With a mean elastic modulus of 24.3GPa, a standard deviation of 0.21GPa, and a coefficient of variation of 0.9%, the elastic modulus was on average reached. Concerning the steel reinforcement, three different bar diameters were used, from the same lot, namely 6 mm, 10 mm, and 16 mm. three samples of each were

obtained and evaluated in according to [128]. From the test results, the yield strength and the young modulus of the steel bars are 444 MPa and 204.2GPa regarding the φ6mm bars, 598.9 MPa and 209.7GPa regarding the φ10mm bars and 494.4 MPa and 209.4GPa regarding the φ16mm bars as show in the Table 4.4.

Table 4.4: Mechanical properties of the RC frame and walls components.

Component	Material Properties	Average value (MPa)	CoV (%)	SD (MPa)
Concrete	Compressive strength	22.85	6.1	0.88
	Elastic modulus	24 300	0.9	210
Steel rebars	Elastic Modulus			
	Φ8mm	198 000	5.4	10692
	φ12mm	192 000	6.2	11904
	φ16mm	187 000	2.1	3927
	Yielding stress			
	Φ8mm	535	2.2	11.8
	φ10mm	526	3.5	18.4
	φ16mm	532	3.2	17.1
Masonry wallets	Compressive strength parallel to the vertical hollows	0.806	12.81	0.14
	Elastic modulus parallel to the vertical hollows	1975	36.7	719
	Diagonal tensile strength	0.645	22,2	0.143
	Shear straining	996	8.91	88.7
	Flexural strength parallel to the bed-joints	0.139	12.63	0.018
	Flexural strength perpendicular to the bed joints	0.322	18.1	0.058
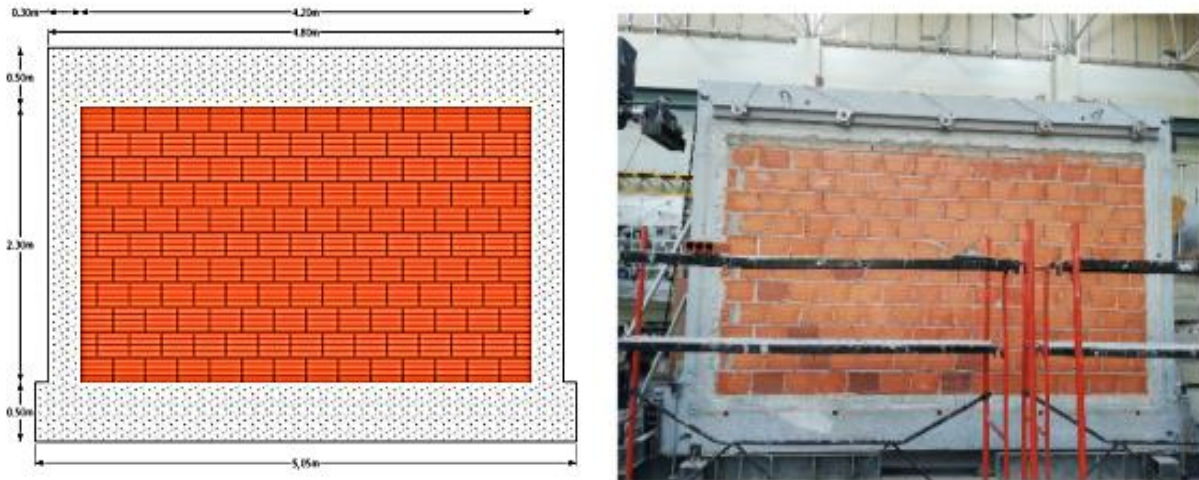
Figure 4.14: Infilled RC frame specimen dimensions (units in meters):
a) general dimensions; b) front view of the specimen.

4.5.3. Experimental and Numerical Results

Figure 4.15 show the numerical hysteresis, envelope curves and energy dissipated for 150mm bricks, along with the corresponding experimental results. The results show that there is an acceptable agreement between the numerical model (OpenSees) and the experiment at the early loading stage, especially in terms of the global behaviour (stiffness and strength). However, the unloading stiffness of specimens deviates slightly from the experimental result for large displacements (i.e., when it exceeds 7.5mm). It should be highlighted that the specimens were tested with a low-initial in-plan load to perform after an out-of-plane test, which was the main scope of this experiment.

For dissipated energy, numerical results are not so accurate and it is specially related with the low in-plane demand and the not so accurate unloading/reloading stiffness Still, this numerical modelling approach provides a useful alternative to experimental tests in terms of defining the maximum strength and stiffness since the global behaviour envelope is seen to be adequately represented.

SPECIMEN 150mm

SPECIMEN 150 mm
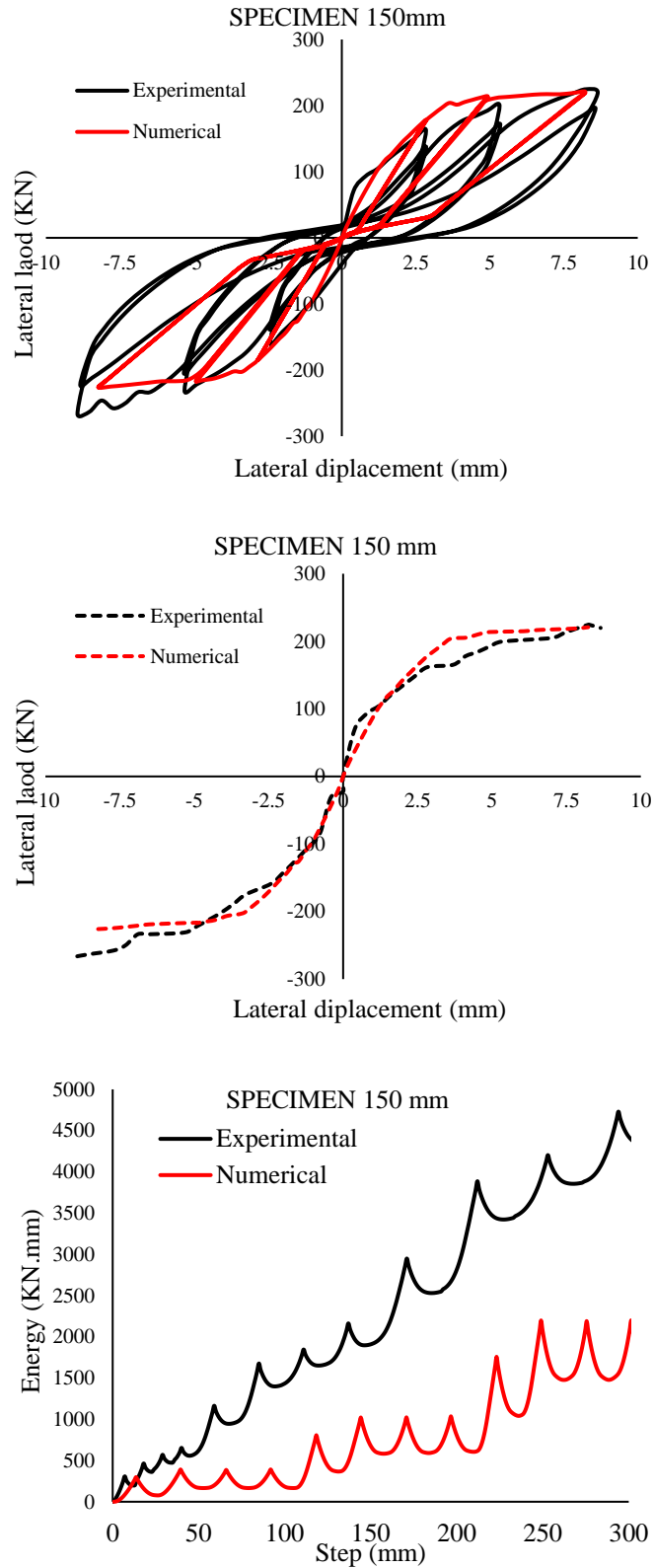
SPECIMEN 150 mm

Figure 4.15: Numerical and experimental hysteresis curves and their envelopes curves; Specimen 150mm: a) hysteresis curve b) envelope curve c) energy dissipated.

4.6. Marta Agante et al. (2021)

4.6.1. Specimens' description

From the study developed by Marta et al. detailed in [127] A full-scale RC frame was built in a laboratory, with the same frame geometry as presented before, designed according to Eurocode 8 – Part 1 [84]. The columns dimensions are 0.30×0.30 m2 with longitudinal reinforcement 4ø16 + 2ø12 and transversal reinforcement equal ø8//0.05 m along the plastic hinge regions and ø8// 0.15 m in the remaining extension of the column (see Figure 4.16). cross-section was defined to be 0.30×0.50 m2. This wall was first subjected to an IP test in which it was imposed a lateral drift of 0.3% to introduce slight/medium damage. After that, the wall was subjected to OOP distributed loadings until its failure.

Expanded light concrete bricks have the nominal dimensions of $400 \times 190 \times 315$ mm3. The thermal transmission coefficient (U) is 0.51 W/m2∘C and was specially designed for simple exterior walls or in contact with unheated areas. Vertical compressive strength tests were carried out in masonry units according to the standard EN 772-1 [128]. The result with symmetrical longitudinal reinforcement of 5ø16 + 5ø16 and transversal reinforcement of ø8//0.10 m along the plastic hinge length and ø8//0.20 m in the remaining beam extension. The dimensions and detailing of the frame are presented in Figure 4.16. The masonry infill walls were constructed with vertical hollow concrete blocks (see Figure 4.17).
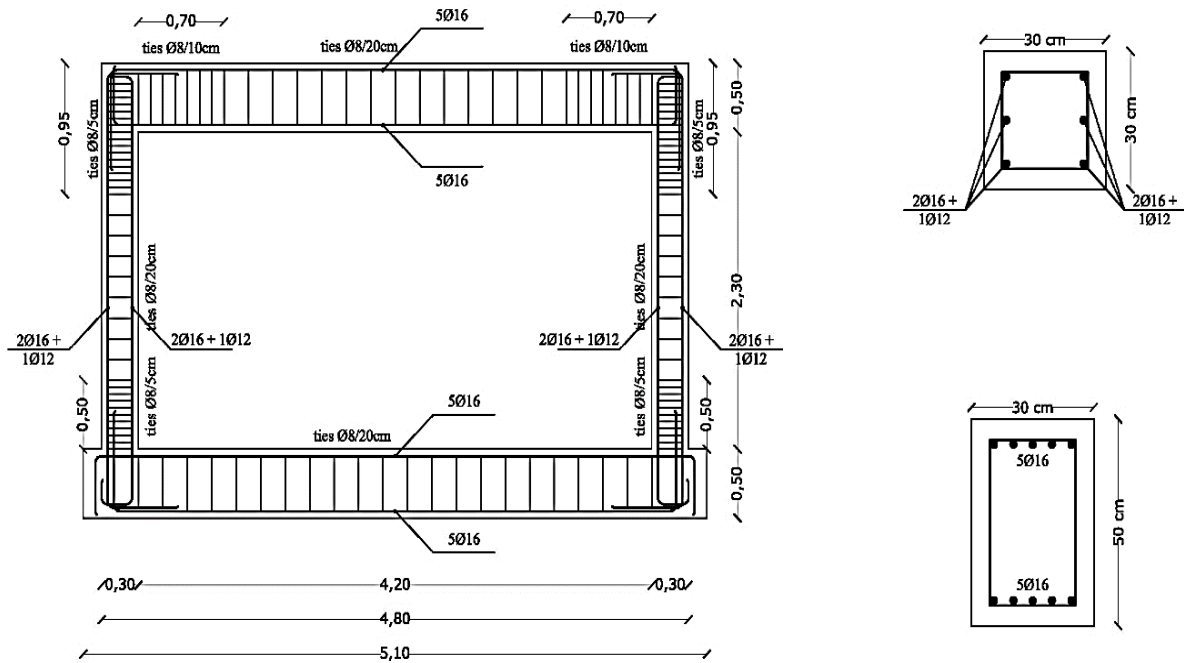
Figure 4.16: RC frame dimensions and detailing.
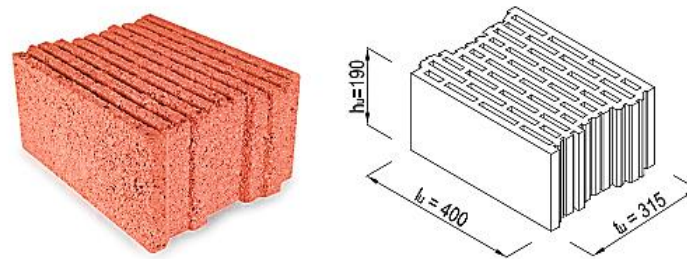
Figure 4.17: Detail of the masonry unit:

a) general overview; and b) geometric details (units in millimetres).

4.6.2. Material properties

Material characterization tests were performed to collect information about the RC frame's properties (concrete and steel samples), masonry units, small masonry wall and plaster. Starting from the RC frame properties, compressive strength tests were performed in six cylindrical specimens collected during the casting of the frame, which resulted in an obtained in the compressive strength and elastic modulus are summarised in Table 4.5. These masonry units are starting to become quite popular in the façades of new RC constructions in Portugal and other

Southern European Countries, as shown in Figure 4.18. The main advantage of these units is their thermal energy and acoustic properties compared to the ones of typical hollow clay horizontal brick units. It should be remarked that the specific properties of these vertical concrete blocks vary depending on the manufacturer. All the panels have the same geometrical dimensions, boundary conditions and materials.

Table 4.5: Mechanical properties of the RC frame and walls components.

Component	Material Properties	Average value (MPa)	CoV (%)	SD (MPa)
Concrete	Compressive strength	22.85	6.1	0.88
	Elastic modulus	24 300	0.9	210
Steel rebars	Elastic Modulus			
	Φ8mm	198 000	5.4	10692
	ϕ12mm	192 000	6.2	11904
	ϕ16mm	187 000	2.1	3927
	Yielding stress			
	Φ8mm	535	2.2	11.8
	ϕ10mm	526	3.5	18.4
	ϕ16mm	532	3.2	17.1
Masonry wallets	Compressive strength parallel to the vertical hollows	1.82	5.1	0.09
	Elastic modulus parallel to the vertical hollows	3251	10.9	355
	Diagonal tensile strength	0.204	5.7	0.01
	Shear straining	1389	36.1	501
	Flexural strength parallel to the bed-joints	0.08	14.2	0.01
	Flexural strength perpendicular to the bed joints	0.17	25.2	0.04
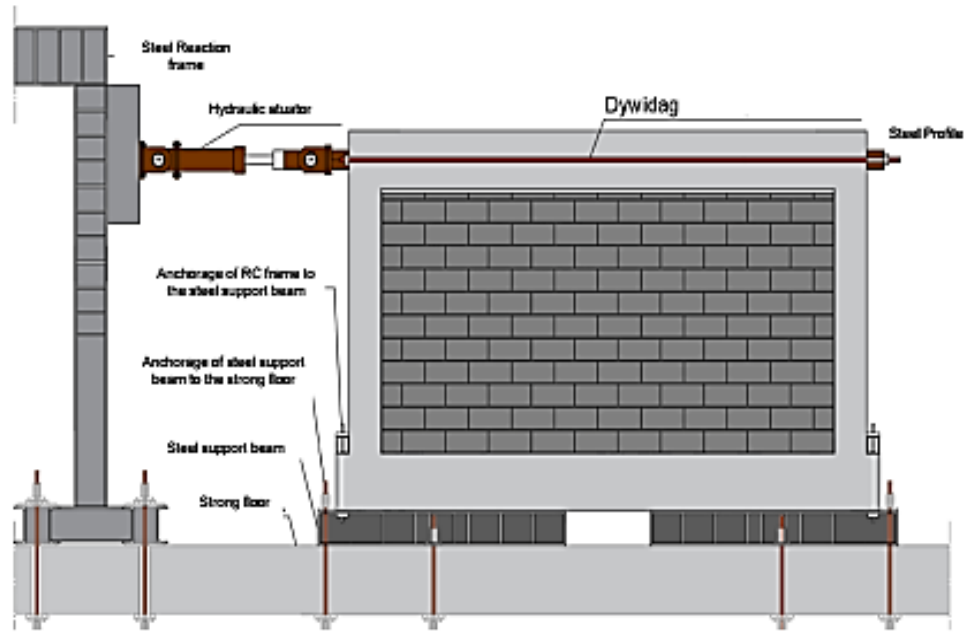
(a)
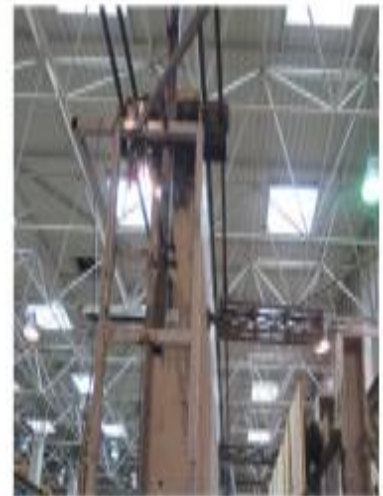
(b)   **(c)**

Figure 4.18: View of the IP test setup: a) Schematic layout; b) Front view; and c) Profile view

4.6.3. Experimental and Numerical Results

Figure 4.19 show the numerical hysteresis, envelope curves and energy dissipated for specimen 150mm, along with the corresponding experimental results.

SPECIMEN 310 mm
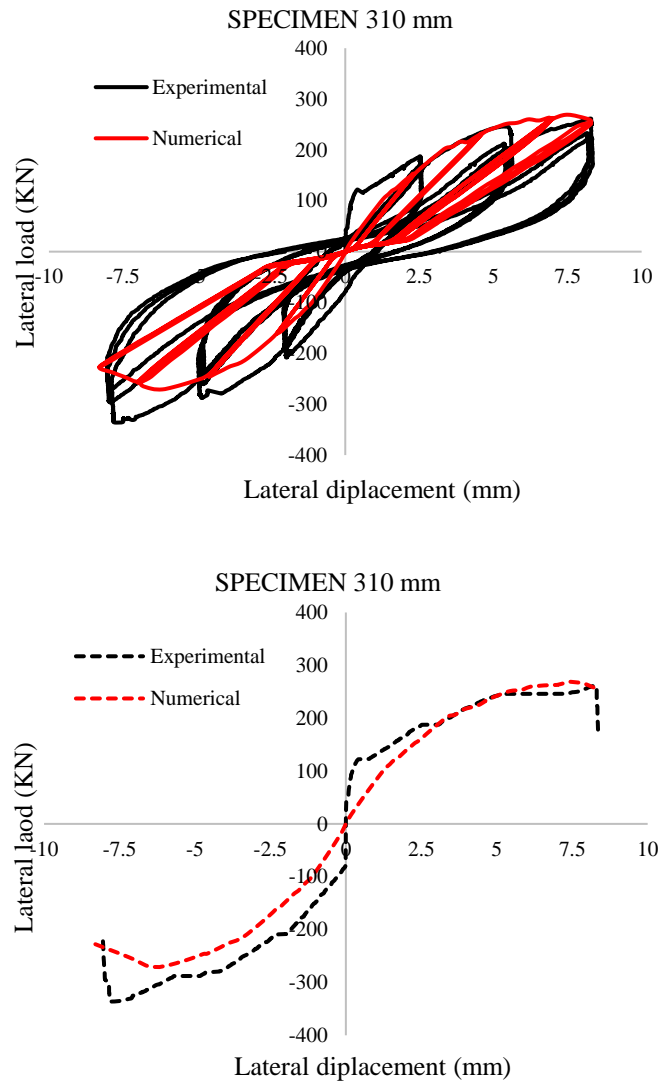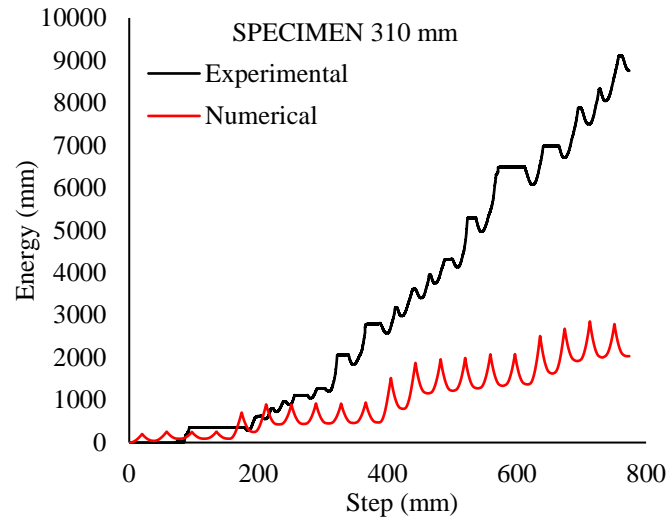
SPECIMEN 310 mm

Figure 4.19: Numerical and experimental hysteresis curves and their envelopes curves; Specimen 315mm: a) hysteresis curve b) envelope curve c) energy dissipated.

As shown, the numerical model presents the envelope of the experimental tests with a good accuracy, however it is clear that the initial stiffness is not clear captured in the numerical model, however the global envelope is captured. Like discussed in the previous section the unloading stiffness is not well captured and the cycles shapes does not reflect the observed experimental results and it is also reflected in the energy dissipated. The numerical model dissipates less energy when compared with the experimental result. However it should be highlighted that the differences in the type of bricks is well captured with the present model.

4.7. Maria Teresa, et al. (2022) tests

4.7.1. Specimens description

From the study developed by Maria et al. detailed in [129] In the continuity of the previous works, other two full-scale RC frames are built in the laboratory with the same geometry and detailing. The beam cross-section, symmetrical longitudinal reinforcement, transversal reinforcement is presented in Figure 4.20.

Figure 4.20: RC frame dimensions and detailing.

Figure 4.21: Detail of the masonry unit:

The masonry infill walls are constructed with hollow clay horizontal bricks 110 mm thick, 200 mm height and 300 mm wide as show Figure 4.21. According to the supplier, these brick units have an acoustic insulation of 40 dB, a unit weight of 3.9 kg, and a thermal resistance of 0.29m2K/W, Vertical compressive strength tests, perpendicular to the horizontal holes, were performed in brick units according to NP EN 771–1 [130] standard. According to the experimental testing (see Figure 4.22), the compressive strength had an average of 1.73 MPa and a coefficient of variation of 29.4%. The tested bricks' average void percentage is 74.9%. Boundary conditions

and materials. Each wall is built by first applying a continuous layer of mortar across the entire width of the previously humidified frame. In the weft and warp directions, the ultimate strain is 3.4% and 3.6%, respectively.

| (a) | (b) |
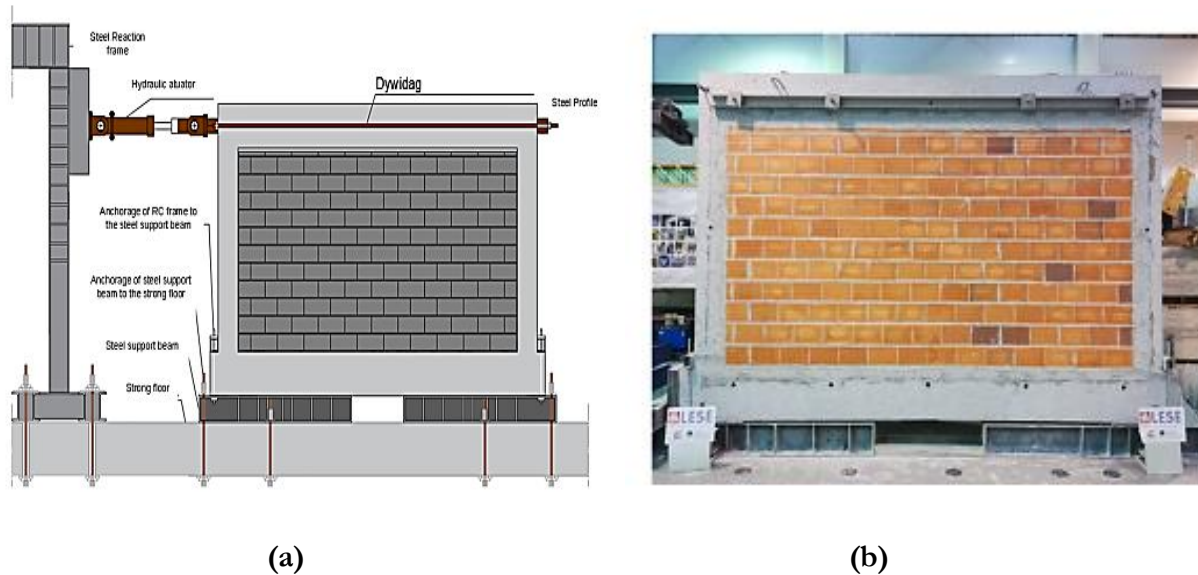
Figure 4.22: View of the IP test setup: a) schematic layout b) front view of the specimen.

4.7.2. Material properties

The purpose of the material characterisation tests is to gather information about the RC frames actual properties, masonry units, small masonry wallets, and plaster. Starting with the mechanical characteristics of the RC frame, compressive strength tests are carried out on six cylindrical specimens collected during the casting of the frame. A summary of the mechanical characteristics of the RC frame is shown in Table 4.6.

Table 4.6: Mechanical properties of the RC frame and walls components.

Component	Material Properties	Average value (MPa)	CoV (%)	SD (MPa)
Concrete	Compressive strength	22.85	6.1	0.88
	Elastic modulus	24 300	0.9	210
Steel rebars	Elastic Modulus			
	Φ8mm	198 000	5.4	10692
	ϕ12mm	192 000	6.2	11904

	ϕ16mm	187 000	2.1	3927
	Yielding stress			
	Φ8mm	535	2.2	11.8
	ϕ10mm	526	3.5	18.4
	ϕ16mm	532	3.2	17.1
Masonry wallets	Compressive strength parallel to the vertical hollows	0.66	19.68	0.131
	Elastic modulus parallel to the vertical hollows	1837	30.6	563
	Diagonal tensile strength	0.565	35.2	0.199
	Shear straining	1141	11.8	135
	Flexural strength parallel to the bed-joints	0.117	4.26	0.005
	Flexural strength perpendicular to the bed joints	0.271	30.3	0.083

4.7.3. Experimental and Numerical Results

Figure 4.23 show the numerical hysteresis, envelope curves and energy dissipated for specimen 110mm along with the corresponding experimental results. The results show an acceptable agreement between the numerical model (OpenSees) and the experiment, especially in term of the global behaviour (stiffness and strength). However, the unloading stiffness of specimens deviates slightly from the experimental result for large displacements (i.e., when it exceeds 7.5mm). This is a result of there were special configurations in this test. Where the specimens were tested with a low initial in-plan load before anticipation of the out of plan load which was the main scope of this test. It can also be caused by the unloading stiffness of the materials employed in OpenSees representing the compressive behaviour of concrete and masonry, which have an unloading stiffness with the same value of the initial stiffness.
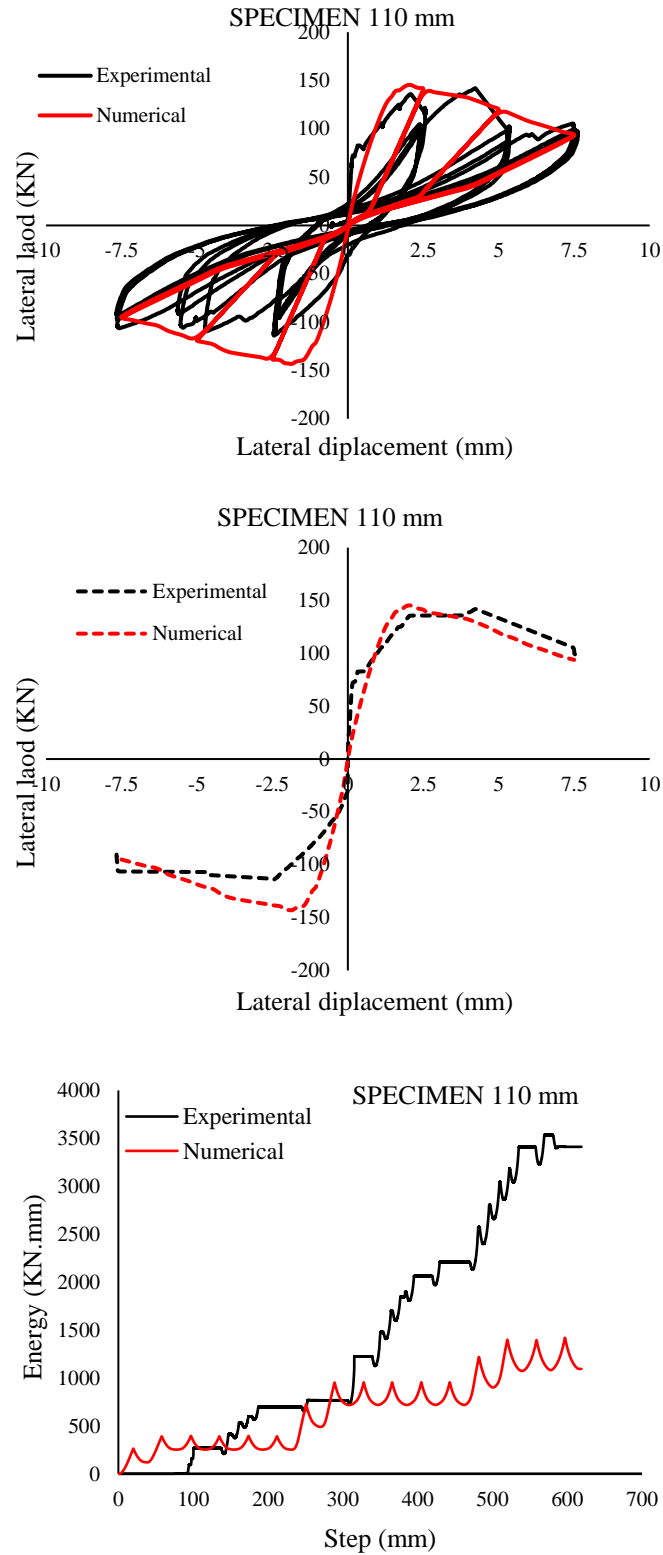
Figure 4.23: Numerical and experimental hysteresis curves and their envelopes curves; Specimen 110mm: a) hysteresis curve b) envelope curve c) energy dissipated.

In addition, the uncertainty regarding some of the properties of the materials used in the experimental tests may also be a factor. Still, this numerical modelling approach provides a useful alternative to experimental tests in terms of defining the maximum strength and stiffness since the global behaviour envelope is seen to be adequately represented. Furthermore, this type of analysis also provides important information regarding the contact length between the infill panel and the RC frame which can be used to calibrate the structural parameters of equivalent diagonal strut models.

4.8. Conclusions

To achieve realistic findings, the reliability of the adopted numerical modelling approach was examined against several experimental tests. The numerical simulation results presented in this chapter demonstrate that the adopted macro-modelling procedure can adequately represent the behaviour of masonry infilled frames and can be used to simulate this type of structural systems using only the essential mechanical properties of the material involved in the structures (i.e., without the need to test an entire specimen). This conclusion is reached based on the ability of the model to adequately capture the failure modes in the experiment, as well as the ultimate strength and stiffness with a reasonable match with experimental results. The adopted modelling approach can simulate different failure mechanisms in the infilled frame such as bed-joint sliding, tensile cracking, and compressive crushing failure of the masonry panel, as well as the flexural failure of the RC frame.

However, quantifying the main parameters of the single strut model using the existing model can lead to huge errors, therefore the mechanical properties shown in Table 4.7 were defined using the experimental data by tuning the mechanical properties of the strut to get the best fit. By comparing the obtained parameters with those found in the literature, it was found that there are significant differences between the obtained values and the conventional value which depend on the masonry configuration and geometric properties.

Table 4.7: Output the best parameters used in this calibration

Specimens	Area of Struct	f_m	ε_0	ε_u	f_{res}	$(f_{res}/f_m)\%$	Diagonal length	Wall thickness		factor to diagonal length
IS	1.89E-02	2248	0.0028	0.016	1420	63.16726	1.5	0.052	15600	2.42E-01
IDO2	1.29E-02	2248	0.0028	0.016	1420	63.16726	1.5	0.052	15600	1.66E-01
IWO2	1.50E-02	2248	0.0028	0.016	1420	63.16726	1.5	0.052	15600	1.92E-01
S	1.85E-02	2925	0.0046	0.016	732	25.02564	1.5	0.06	2600	2.05E-01
WO2	1.85E-02	2086.8	0.00375	0.016	411	19.69523	1.5	0.06	2600	2.05E-01
DO2	1.85E-02	1442	0.00317	0.016	107	7.42025	1.5	0.06	2600	2.05E-01
LESE 150	1.80E-01	1090	0.0007	0.006	272	24.95413	4.8	0.15	1090	2.49E-01
LESE 110	1.32E-01	1020	0.0003	0.0013	102	10	4.8	0.11	1020	2.49E-01
LESE 315	1.39E-01	1800	0.001	0.002	180	10	4.8	0.31	1800	9.33E-02
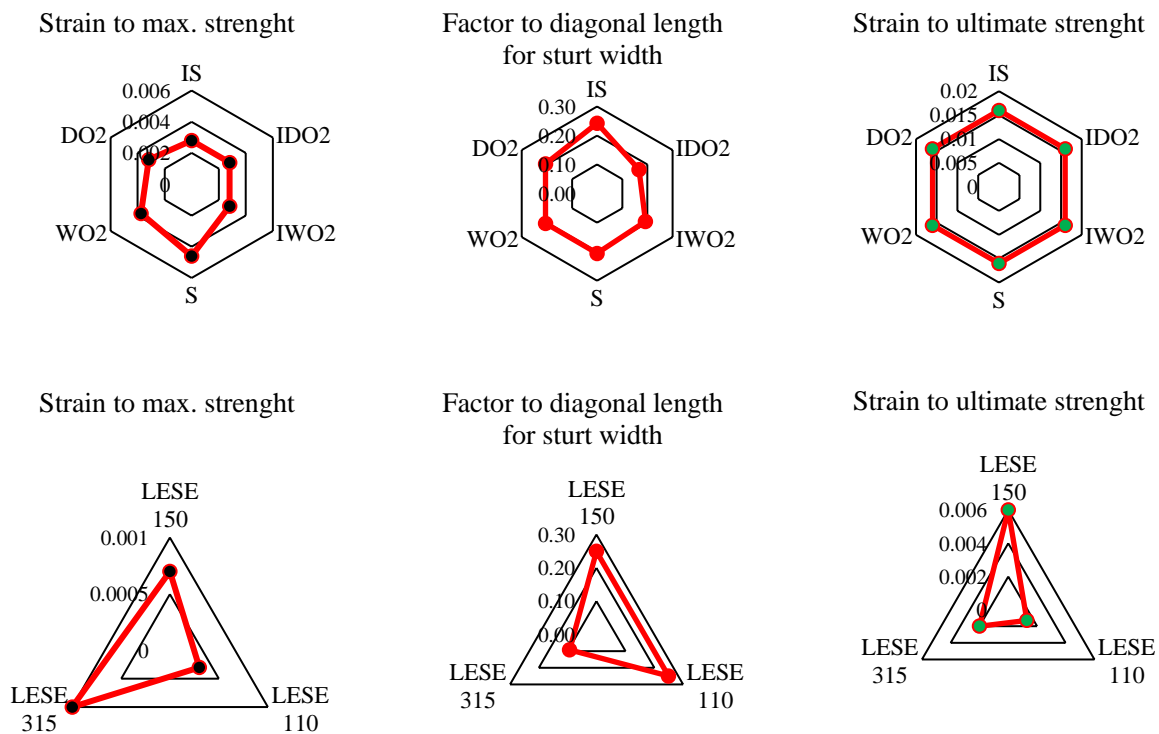
Figure 4.24: Radar plot of the best output parameters used in this calibration.

Chapter 5.

Static Non-Linear Analysis of Infilled RC Structures

5.1. Introduction

The masonry infill walls have an important influence on the characteristics of the structures; this practice consisting in neglecting the influence of the masonry was imposed by the use, mainly because of the absence of a practical method of calculation as well as of an appropriate regulatory tool. However, unfortunately, in Algeria, there are practically no standards concerning the behaviour of masonry. Masonry has a very complex behaviour due to the materials' heterogeneity and the almost artisanal techniques associated with its production, making it a very variable material that is difficult to standardize [131]. Most of the existing regulations simplify the behaviour of the masonry to provide practical criteria for the analysis and calculation of structures. This criterion involves, in general, the use of linear models that consider masonry as a homogeneous material. They are proposed based on mechanical properties determined using simple tests on small walls or prisms. However, the validity of these tests and these models to describe write the behaviour of an actual structure remains insufficient.

The present work aims to study the seismic behaviour of RC structures, considering the influence of the thickness and the compressive strength on the seismic behaviour of RC frame structures. For this, it was considered a six-story frame with three bays of the same length. This

frame is part of a building supposed to be in a zone of high seismicity (zone III according to RPA 99/2003 version), [5]. Two brick unit materials were considered the hollow concrete blocks and the hollow clay brick. These materials are based on their compressive strengths, respectively, low, average, and strong. To study the effect of the thickness of the infill walls, we considered a hollow clay brick wall with six different thicknesses (05 cm,10 cm, 15 cm, 20 cm,25cm, 30 cm) and six different thicknesses for a hollow concrete block they have the same thickness of a hollow clay brick wall. Another objective of this work is to study the effect of openings of different sizes on the seismic behaviour of RC frames (The reduction factor is from 10% to 90%).

The third objective is to study the variability of the presence of infill walls and its effect on the structural response, where we selected 15 models of the structure previously studied, considering the variation in the presence of building walls in each case. After designing the frame according to the RPA 99/2003 version [5], nonlinear static analyses (pushover) were carried out on the frame with different infill wall configurations. At the end of these post-elastic analyses, a discussion of the results is carried out, emphasizing the variation of the parameters, such as the base shear of the frame and the lateral displacements of floors.

5.2. Description of the building structure

To assess the effect of the infill panels on the vulnerability of RC buildings, a residential building was selected as a representative case study. The building has the plan dimensions of 17.4 m x 13.1 m, which consists of 4.3 x 4.3 m modules (longitudinal and transverse direction, respectively), with an inter-story height equal to 3m.

The chosen RC frames are defined as part of a residential structure, the architectural plan view of the typical floor, which is shown in Figure 5.1.a), and the structural system, which is shown in Figure 5.b). The frame of the vertical axis 5 between the horizontal axes AD, referred to herein as frame F5A-D, is the considered frame for the vulnerability analysis. The structures were designed for gravity loads to simulate a design situation where a global vertical load of 5.25kN/m^2 plus a variable load of 2 kN/m^2 was considered. Table 5.1 shows the mechanical parameters of the chosen materials, and Table 2 shows the cross-section data for frames F5A-D.
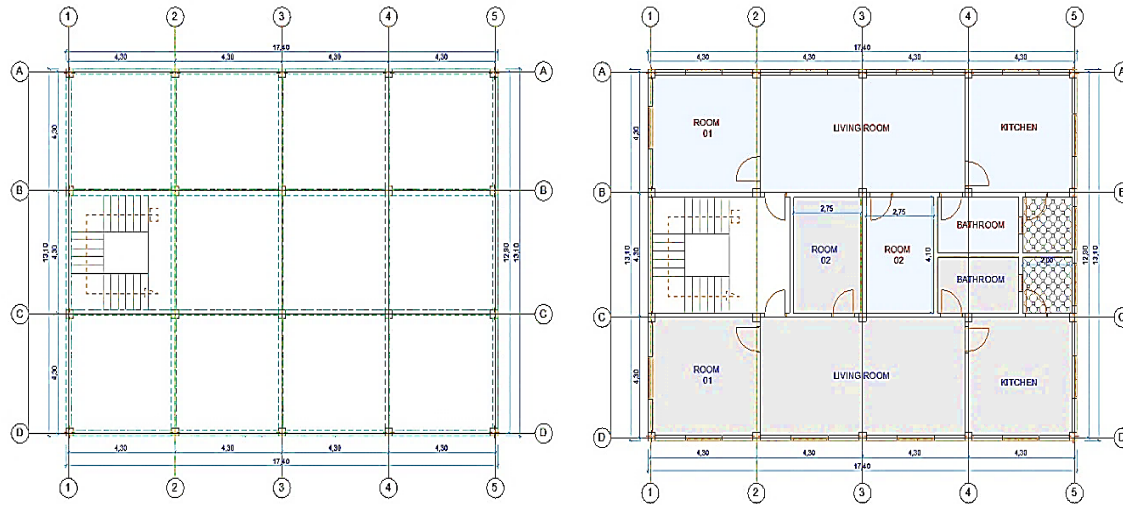
Figure 5.1. Typical plan view for the considered the building: a) architectural plan b) structural system showing the considered frame (all dimensions in m)

Table 5.1. Cross-section details for frame

Axis	Columns		Beams						
	Section (cm^2)	Reinfo-rcement	Section (cm^2)	Reinforcement					
				Start		Middle		End	
				Upper	Lower	Upper	Lower	Upper	Lower
A	30x30	8Ø15	25x40	4Ø12	4Ø12	4Ø12	4Ø12	4Ø12	4Ø12
B	30x30	8Ø15	25x40	4Ø12	4Ø12	4Ø12	4Ø12	4Ø12	4Ø12
C	30x30	8Ø15	25x40	4Ø12	4Ø12	4Ø12	4Ø12	4Ø12	4Ø12
D	30x30	8Ø15	25x40	4Ø12	4Ø12	4Ø12	4Ø12	4Ø12	4Ø12

5.3. Description of the numerical model

5.3.1. RC element modeling frame

The nonlinear static analyses were carried out by the software OpenSees (McKenn et al.) [105]. The RC frame elements were modelled using the beam with hinges that are represented by fibre sections (the nonlinear behaviour of the hinges) [19]. The Modified Radau Hinge Integration method [107,108]. was chosen to designate inelastic actions with a specified length at the end of the element.

The integration points are two for each hinge and two for the central part of the element, which is used in the element state determination. The value of the plastic hinge length lp suggested by Paulay and Priestley [109] was mentioned by the following expression:

$$lp = 0.08le + 0.022db\, fy \tag{5.1}$$

Where l_e Is the length of the element, d_b Is the diameter of the longitudinal steel rebar, and f_y is the yield strength of the used steel in MPa.

The concrete cover was modelled using the concrete model (Concrete01) for the fibre discretization of the RC cross-sections, this concrete model represents the uniaxial concrete material with no tensile strength and a degraded linear unloading/reloading stiffness in compression. Confined concrete was modelled using a confinement factor determined based on the proposed expression by Kent and Park [132] linked with the Concrete01 model. Steel reinforcement bars were modelled using the uniaxial Giuffre- Menegotto-Pinto model [110] with isotropic hardening, termed Steel02 in OpenSees, with the default parameters proposed by the software. For the beam-column joints, a rigid end-offset joint model was used [111]. The lengths of the rigid parts were considered to be half of the depth of the perpendicular element.

Figure 5.2 shows the general description of the model implemented in OpenSees for the RC frame and the infill panel with a detailed description of the RC element model.
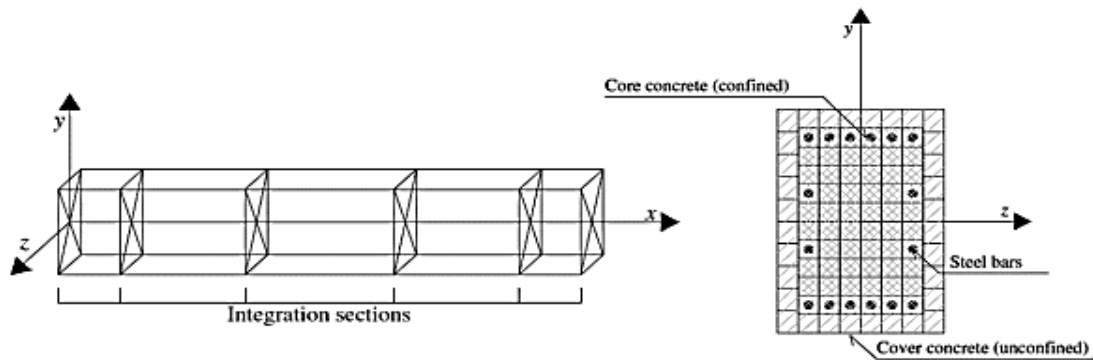
(a)
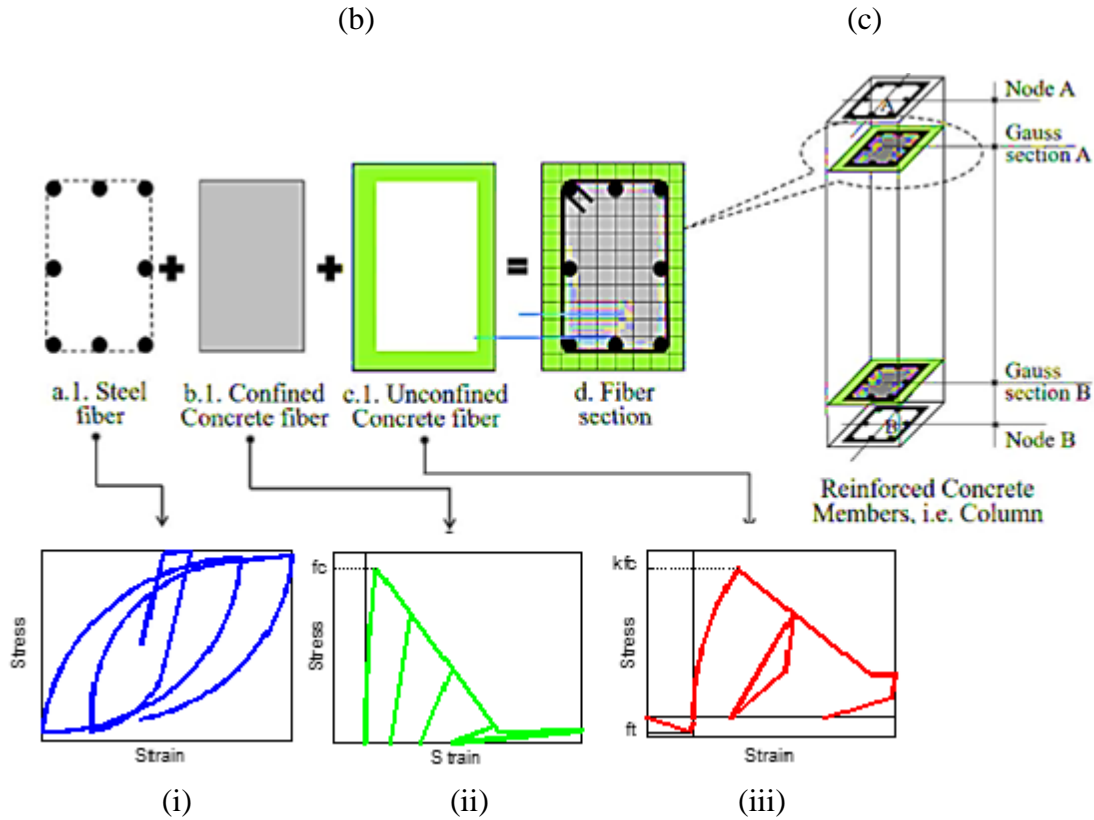
Figure 5.2: Adopted strategy for modelling RC elements. (a) Beam with hinge element general description (b) Fiber section discretization. (i). Steel material (steel02) (ii). unconfined concrete (Concrete01) (iii). confined concrete (concrete02). (c) column with hinge element general description.

5.3.2. Infill walls

The infills were modelled using a single compressive strut element with an area evaluated based on the expression that is proposed by Hendry [53] using the constitutive model for masonry, which matches the shape of the Concrete01 constitutive model. The following expression gives the constitutive model proposed by Hendry [53]:

$$\sigma_m = f_m' \left[2 \frac{\varepsilon_m}{\varepsilon_{crm}} - \left(\frac{\varepsilon_m}{\varepsilon_{crm}} \right)^2 \right]$$
(5.2)

Where ε_m and σ_m are the compressive strain and the corresponding compressive stress of the masonry, respectively, f_m' is the maximum compressive strength of the masonry and ε_{crm} is the

compressive strain at the onset of failure, which according to [112] ranges from 0.0015~0.002. In these analyses, the value of ε_{crm} was 0.002 in all models.

5.4. Influence mechanical properties of masonry infill wall.

The building was designed according to the Algerian code (RPA2003) [5]. After six 2D models were generated in the software OpenSees (Mckenna, Fenves, et al.) [105], one without infill walls herein designated "Bare Frame (BF) model" model and another one with infill panels distributed along the building's façades (Full Frame (FF) model, Also a model with openings (Partial Frame (PF) model) and another with a soft storey (Soft Storey Frame (SF) model) and taking two different types of bricks (hollow clay brick and hollow concrete block) in each case.

5.4.1. Methodology

The main aim of the present study is the study the effect of mechanical properties of building walls in the RC structure on the overall response of the building, which will provide interesting information concerning those values when it occurs the collapse of the buildings during a seismic event. For this, static non-linear analysis (Pushover analysis) was carried out to extract those results and assess the impact of mechanical properties of the infill masonry walls on the non-linear static behavior of the structure.

Table 5.2. Study summary.

No.	Acronym	Masonry Type	Fm (MPa)	Thickness (Cm)	Full Frame	Partial Frame (R_f=0.7)	Soft Storey
1	BF	/	/	/	/	/	/
2	FFHB05T	HB05	3.5	05	■		
3	FFHB10T	HB10	3.5	10	■		
4	FFHB15T	HB15	3.5	15	■		
5	FFHB20T	HB20	3.5	20	■		
6	FFHB25T	HB25	3.5	25	■		
7	FFHB30T	HB30	3.5	30	■		
8	FFHB05F	HB05	1.9	15	■		
9	FFHB10F	HB10	2.8	15	■		
10	FFHB15F	HB15	3.5	15	■		
11	FFHB20F	HB20	4.9	15	■		
12	FFHB25F	HB25	5.3	15	■		
13	FFHB30F	HB30	6.1	15	■		

14	FFHC05T	HC05	4.7	05	■
15	FFHC10T	HC10	4.7	10	■
16	FFHC15T	HC15	4.7	15	■
17	FFHC20T	HC20	4.7	20	■
18	FFHC25T	HC25	4.7	25	■
19	FFHC30T	HC30	4.7	30	■
20	FFHC05F	HC05	2.5	15	■
21	FFHC10F	HC10	3.5	15	■
22	FFHC15F	HC15	4.7	15	■
23	FFHC20F	HC20	5.9	15	■
24	FFHC25F	HC25	7.2	15	■
25	FFHC30F	HC30	8.1	15	■
26	PFHB05T	HB05	3.5	05	■
27	PFHB10T	HB10	3.5	10	■
28	PFHB15T	HB15	3.5	15	■
29	PFHB20T	HB20	3.5	20	■
30	PFHB25T	HB25	3.5	25	■
31	PFHB30T	HB30	3.5	30	■
32	PFHB05F	HB05	1.9	15	■
33	PFHB10F	HB10	2.8	15	■
34	PFHB15F	HB15	3.5	15	■
35	PFHB20F	HB20	4.9	15	■
36	PFHB25F	HB25	5.3	15	■
37	PFHB30F	HB30	6.1	15	■
38	SFHB05T	HB05	3.5	05	■
39	SFHB10T	HB10	3.5	10	■
40	SFHB15T	HB15	3.5	15	■
41	SFHB20T	HB20	3.5	20	■
42	SFHB25T	HB25	3.5	25	■
43	SFHB30T	HB30	3.5	30	■
44	SFHB05F	HB05	1.9	15	■
45	SFHB10F	HB10	2.8	15	■
46	SFHB15F	HB15	3.5	15	■
47	SFHB20F	HB20	4.9	15	■
48	SFHB25F	HB25	5.3	15	■
49	SFHB30F	HB30	6.1	15	■

To evaluate the effect of mechanical properties of building walls on the structural response of concrete buildings, one of the most important properties that we study is the change in thickness and compressive strength.

The thickness and compressive strength values of six samples for each type of brick were adopted from laboratory experiments obtained by the manufacturing companies in Algeria. This

frame was analyzed with different configurations (bare, fully infilled, soft-storey, and partially infilled frames) and with two different types of brick units (hollow bricks and hollow concrete), as shown in Figure 5.3 and Figure 5.4 respectively.

HB05   *HB10*   *HB15*   *HB20*   *HB25*   *HB30*

HC05   *HC10*   *HC15*   *HC20*   *HC25*   *HC30*
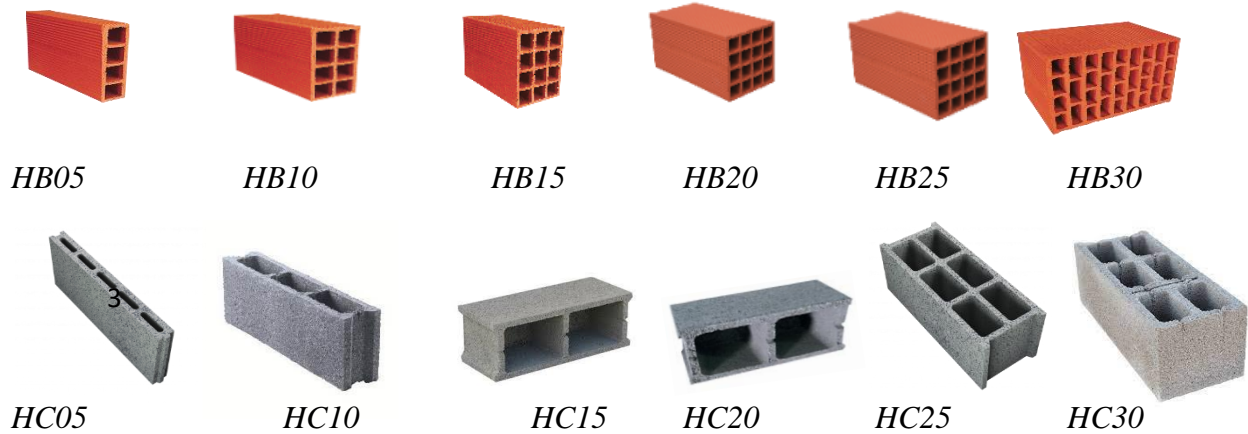
Figure. 5.3. Masonry units used in the study (HB, HC)

a) BareframeBF-6 (HB)   b) FullyinfilledFF-6 (HB)   c) Soft storeyframeSF-6(HB)   d) Partially infilledPF-6(HB)
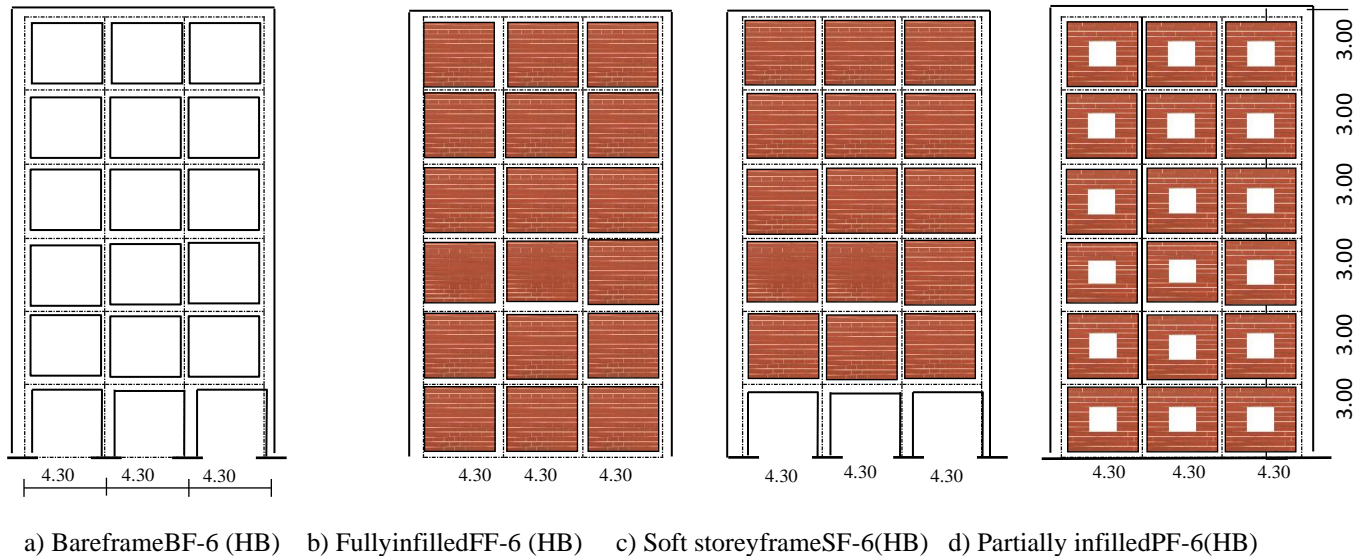
Figure 5.4.a: Different frame configurations for the Six-storey building (HB)

a) BareframeBF-6   b) FullyinfilledFF-6(HC)   c) Soft storeyframeSF-6(HC)   d) Partially infilledPF-6(HC)
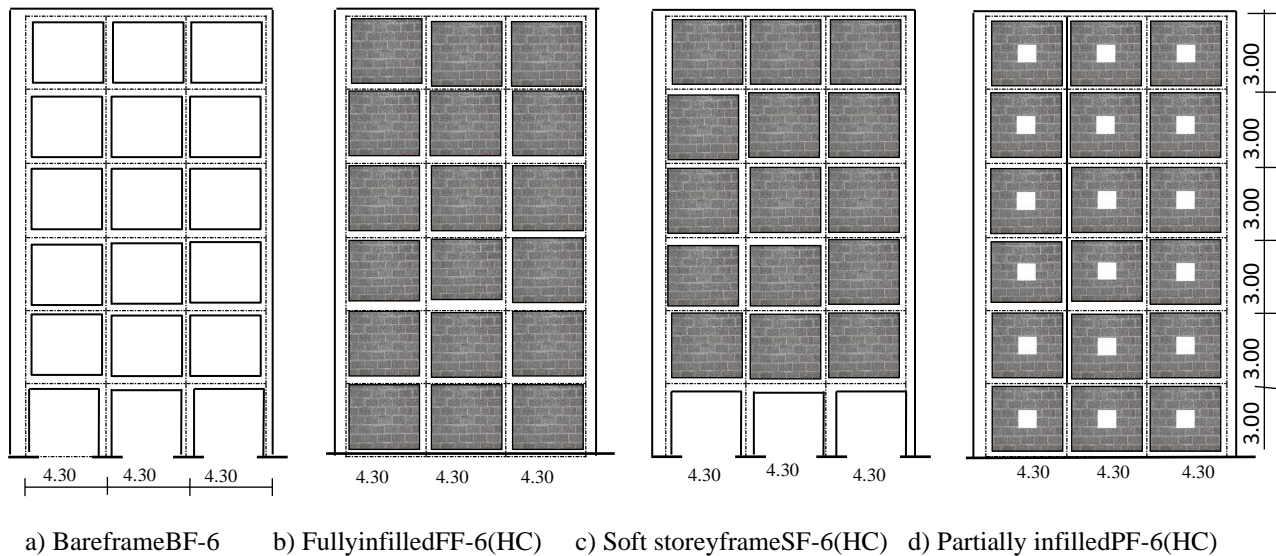
Figure 5.4: b. Different frame configurations for the Six-storey building (HC)

The mechanical properties of the selected materials are presented in Table 3, and the cross-section details for the frame are shown in Table 5.3. The characteristics of infills were defined according to the data from the experimental campaigns obtained from a National Center of Studies and Search Indegrees of Buildings (CNERIB).

Table 5.3. Mechanical properties of the materials

Concrete	Steel		*Mortar)*
$F_c(MPa)$	$\sigma_Y(MPa)$	$E(GPa)$	$Fm(MPa$
25.0	522.0	190.	10.0

Pushover analysis was used, once generally refers to non-linear static procedures applied to evaluate the seismic performance of existing structures and the design of new buildings [82], which is presented in several recent seismic regulations and guidelines [81,133]. Pushover analysis is performed by applying a series of inelastic static analyses on the building using a preselected lateral loading mode based on the first vibration mode of the structure or the equivalent static lateral loading modes in the seismic regulations.

111

5.4.1. Study of the effect of mechanical properties of infill walls

Cas 01: Full infill frame buildings

Effect of different wall thicknesses

Figure 5.5 presents the capacity curve base shear -Top displacement, base shear-global drift (%) values , inter storey drift ratio (ISD %), and the energy absorbed curve of the FFHB and FFHC buildings for both types of bricks (Bricks clay, hollow concrete), taking into account the change in thickness .The set of curves presented in Figure 5.5 shows the effect of the thickness difference on the overall response of the building, where a considerable increase in stiffness and maximum strength capacities was attained through the introduction of infilled walls for each the brick clay and hollow concrete building, where This increase is affected by the difference in thickness, as we notice an increase in the lateral stiffness, ISD %, and energy absorbed of both buildings with increasing thickness of infill.
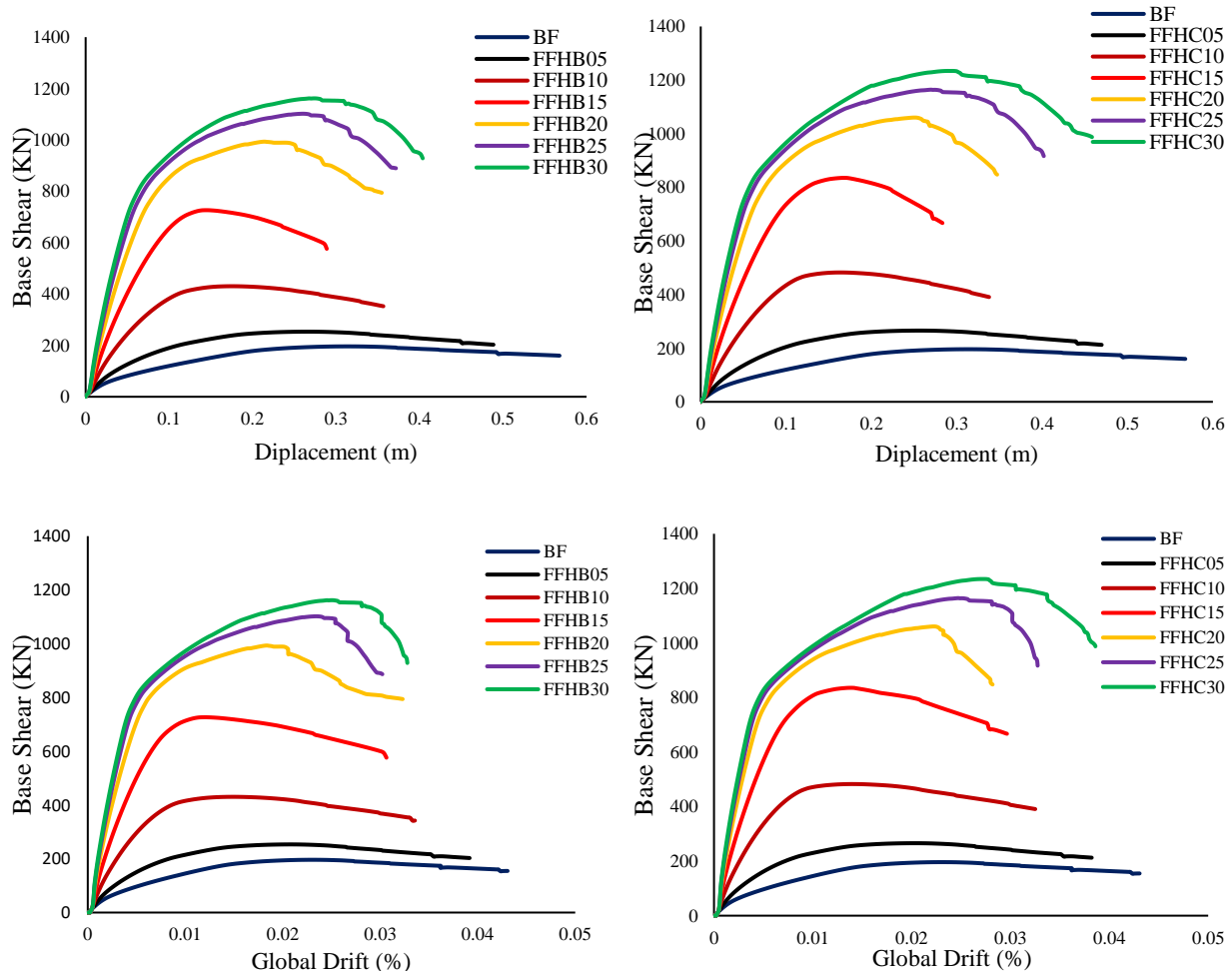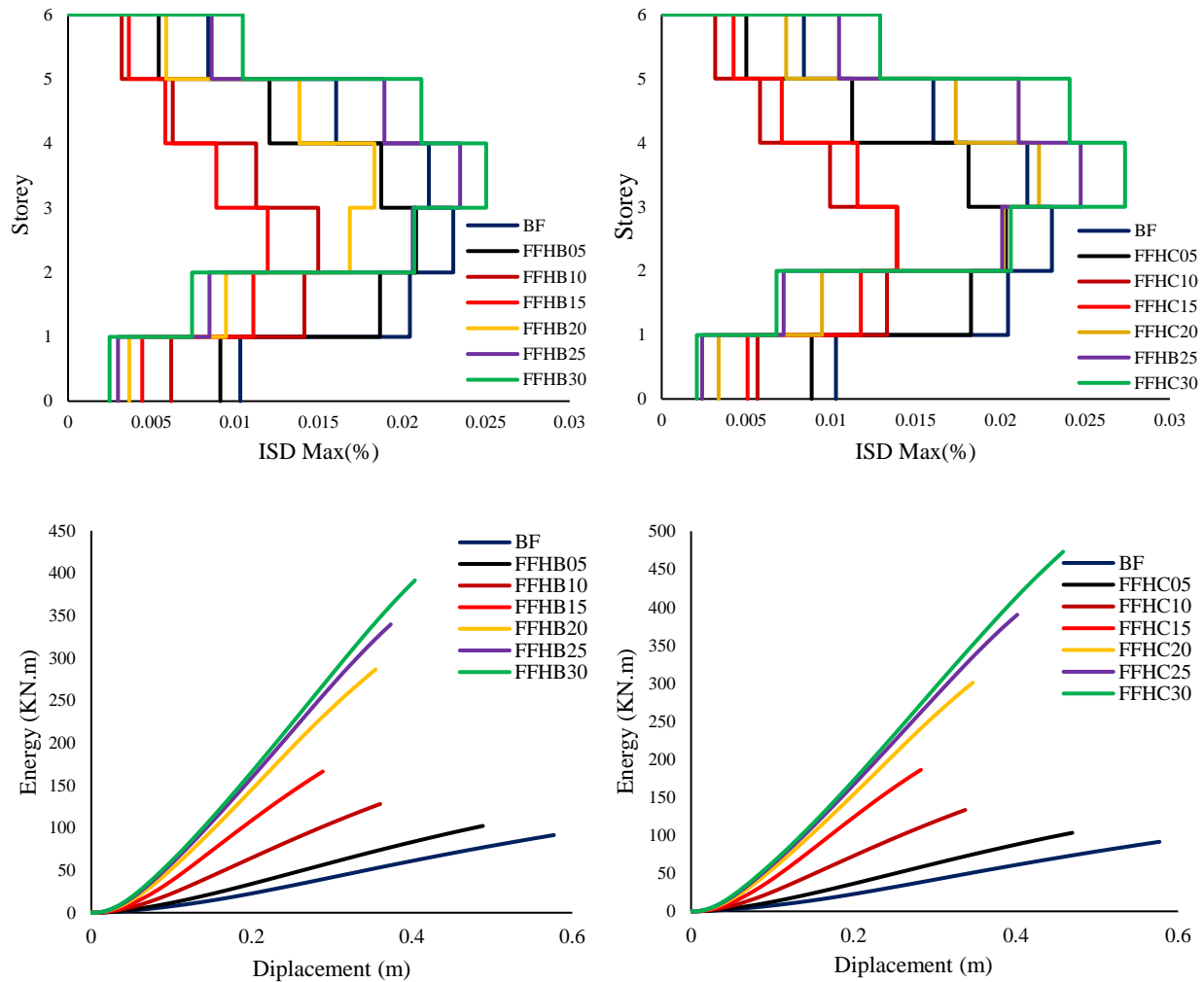
Figure 5.5: a) The capacity curve, b) the maxillary base shear values, c) the maximum ISD, d) the energy absorbed curve of the building.

Table 5.4. The values of maximum top displacement, maximum base shear, maximum inter-story drift, and the energy for all models are attributed to their corresponding in the Bare frame model. (Case of the thickness variation)

Models	Base Shear (KN)	Ratio (BF)	Max top displ (m)	Ratio (BF)	ISD Max (%)	Ratio (BF)	Energy (KN.m)	Ratio (BF)
BF	192.21	/	0.313	/	0. 0230	/	91.45	/
HB10	430.4	124%	0.175	-44%	0.0149	-35%	128.07	40.04%
HB15	726.34	278%	0.143	-54%	0.0119	-48%	166.39	81.95%
HB20	993.137	417%	0.213	-32%	0.0183	-21%	286.77	213.58%
HB25	1101.85	473%	0.26	-17%	0.0234	1%	339.7	271.46%
HB30	1161.69	504%	0.268	-14%	0.025	8%	391.55	328.16%
HC05	265.66	38%	0.256	-18%	0.0203	-12%	103.34	13.00%

HC10	482.5	151%	0.162	-48%	0.0139	-40%	133.38	45.85%
HC15	835.31	335%	0.168	-46%	0.0138	-40%	186.15	103.55%
HC20	1060.22	452%	0.2511	-20%	0.0222	-4%	300.84	228.97%
HC25	1164.15	506%	0.266	-15%	0.0247	7%	390.18	326.66%
HC30	1234.12	542%	0.299	-4%	0.0273	18%	473.1	417.33%

The rate increase in the stiffness was almost 32% - 504% and 38% - 542% for the bricks clay and hollow concrete, respectively approved of the thickness value: 5,10,15,20,25,30, as compared to the bare frame building, Fig 5.4. shows the variation of the thickness with maximum base shear. In addition, the infilled building shows a steep decline in the capacity curve after attaining the maximum capacity, potentially due to in-plane cracking and crushing and out-of-plane failure of the infilled panels.

Figure 5.5 also represents the global response represented by the base shear-Global drifts ratio curve, demonstrating that both the FFHB and FFHC. For FFHBC, the maximum base shear capacity attained at a global drift of 2.4% for the largest thickness value estimated at 0.3m and 2.7% for the FFHC building.

Also, looking at the energy compared to the bare frame, it can be observed a significant increase that varies according to the values of the thickness, where, for example, an increase in the energy absorbed concerning the thickness was 10, 15, 20 and 30% estimated at 40.04%, 81.95%, 213.58% and 328% respectively for hollow clay unit and 45.85%, 103.55%, 228.91% and 417.33 for the hollow concrete unit. This increase in energy is explained by the difference in the thickness values of the infill walls, which is directly affected by the value of thickness.

Effect of different Compressive Strength

Figure 5.6 and Table 5.5 presents capacity curves for the FFHB and FFHC buildings for both types of bricks (Bricks clay, hollow concrete), considering the variation of compressive strength where the base shear-top displacement curve represents the global response.

(a)   (b)

(c)   (d)

Figure 5.6: a) The capacity curve, b) the maximum ISD, c) the energy absorbed curve of the building.

The set of curves presented in figure 5.6 and Table 5.5 shows the effect of different values of compressive strength on the overall response of the building, where a considerable increase in stiffness and maximum strength capacities was attained through the introduction of infilled walls for each brick clay and hollow concrete building, where This increase is affected by the difference of Fm, as we notice an increase in the lateral stiffness, ISD % , and energy absorbed of both buildings with increasing the value of compressive strength of infill.

Table 5.5. The values of maximum top displacement, maximum base shear, maximum inter-story drift, and the energy for all models are attributed to their corresponding in the Bare frame model. (Cas of the Compressive Strength variation)

Models	Base Shear (KN)	Ratio (BF)	Dip at Max BS (m)	Ratio (BF)	ISD Max (%)	Ratio (BF)	Energy (KN.m)	Ratio (BF)
BF	192.21	/	0.313	/	0.0230	/	91.45	/
HB05	551	187%	0.1588	-49%	0.0137	-41%	150.14	64%
HB10	653.54	240%	0.143	-54%	0.0121	-48%	157.29	72%
HB15	726.34	278%	0.143	-54%	0.0119	-48%	166.39	82%
HB20	792.07	312%	0.151	-52%	0.0123	-47%	174	90%
HB25	874.37	355%	0.179	-43%	0.0145	-37%	207.95	127%
HB30	916.32	377%	0.198	-37%	0.0159	-31%	233.73	156%
HC05	620.6	223%	0.147	-53%	0.0126	-45%	154	68%
HC10	726.34	278%	0.143	-54%	0.0119	-48%	166.39	82%
HC15	835.31	335%	0.168	-46%	0.0138	-40%	186.15	104%
HC20	907.36	372%	0.194	-38%	0.0156	-32%	226.58	148%
HC25	956.6	398%	0.194	-38%	0.0162	-30%	254.8	179%
HC30	984.45	412%	0.211	-33%	0.018	-22%	261.29	186%

The rate increase in the stiffness Compared with the highest value taken for compressive strength with the lowest value was almost 187% - 377% and 223% - 412% for the bricks clay and hollow concrete, respectively approved of the compressive strength value, In addition, the infilled building shows a steep decline in the capacity curve after attaining the maximum capacity, which is directly proportional to the compressive strength values, And inversely with the bare frame, due to in-plane cracking and crushing out-of-plane failure of the infilled panels Compared with the blank wall.

Also, by looking at the recorded values of the maximum inter-storey drift, was noted that a significant increase in the ISD is 10% - 48% for buildings with a compressive strength value

2.5MPa,3.5MPa and 4.7MPa respectively. This increase is explained by the effect of the values of compressive strength of building walls in increasing buildings' rigidity.

Also, looking at the energy compared to the bare frame, it can be observed a significant increase that varies according to the values of compressive strength, where, for example, an increase in the energy absorbed concerning the compressive strength value 2.8MPa, 3.5MPa, 4.9MPa and 6.1MPa estimated at 72%, 82%, 127% and 156% respectively for hollow clay unit and 82%, 104%, 148% and 186% for the hollow concrete unit for 3.5MPa, 4.7MPa, 5.9MPa and 8.1MPa respectively. This increase in energy is explained by the difference in the compressive strength values of the infill walls, which are directly affected by these values.

Cas 2: Soft Storey frame buildings

Effect of different wall thicknesses

Figure 5.7 presents the capacity curve base shear -Top displacement, inter-storey drift ratio (ISD %), and the energy absorbed curve of the FFHB buildings considering the change in thickness.
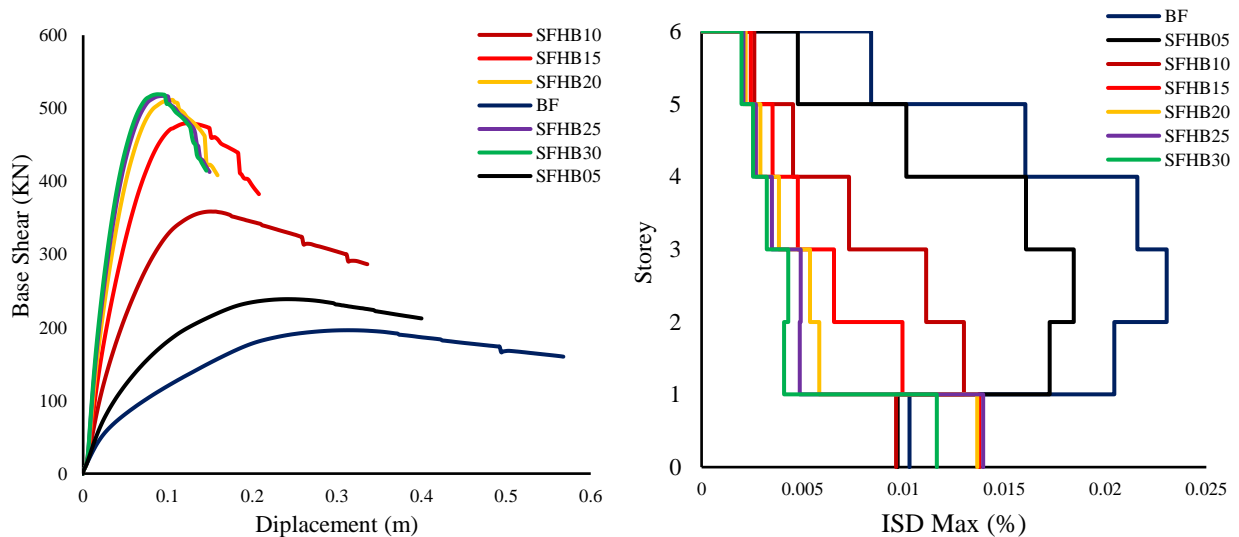
Figure 5.7: a) The capacity curve, b) the maximum ISD, c) the energy absorbed curve of the building.

Table 5.6. The values of maximum top displacement, maximum base shear, maximum inter-story drift, and the energy for all models are attributed to their corresponding in the Bare frame model. (Cas of the Thickness variation)

Models	Base Shear (KN)	Ratio (FF)	Dip at Max B.Sh (m)	Ratio (FF)	ISD Max (%)	Ratio (FF)	Energy (KN.m)	Ratio (FF)
HB05	238.72	-6%	0.242	-9%	0.018	-13%	96.06	-6%
HB10	358.64	-17%	0.151	-14%	0.013	-13%	97.81	-24%
HB15	480.36	-34%	0.129	-10%	0.014	-18%	77.62	-53%
HB20	511.33	-49%	0.106	-50%	0.014	-23%	62.29	-78%
HB25	516.88	-53%	0.097	-63%	0.014	-40%	59.8	-82%
HB30	519.144	-55%	0.087	-68%	0.012	-52%	58.84	-85%

The set of curves presented in figure 5.7 and Table 5.6 shows the effect of the thickness difference on the overall response of the building with a soft story, where a considerable decrease in stiffness and maximum strength capacities compared to the full infill frame. This decrease increases with the increasing value of the thickness corresponding to the full frame. This is explained by the total collapse of the building was most likely under the soft-storey mechanism and in some cases shear failure in the columns and short-columns. The rate decrease in the stiffness was almost 6% - 55% approved of the thickness value: 5cm-30cm compared to the full frame

building.

In addition, the soft storey building shows a steep decline in the capacity curve after attaining the maximum capacity at thickness values above 10 cm, potentially due to in-plane cracking and crushing and out-of-plane failure of the infilled panels. If such structures were subjected to increasing lateral forces, then the lateral forces would be expected to be resisted by the frames only. Ultimately, the total collapse of the building was most likely under the cases of shear failure in the columns and short columns.

Also, looking at the energy compared to the full frame, it can be observed a significant decrease increases with increasing thickness values corresponding to the full frame; for example, a decrease in the energy absorbed concerning the thickness was 10, 15, 20 and 30% estimated at 24%, 53%, 78% and 85% respectively. This is explained by the structural elements of the soft-storey building underwent an early hardening and the formation of plastic hinges was likely to be dominant, most likely due to higher seismic demand concentration in a single floor.

Also, by looking at the recorded values of the maximum inter-storey drift, it was noted that a Significant decrease in the ISD is 13% - 52% for buildings with a thickness value of 5cm to 30 cm, respectively. This decrease is explained by the effect of the thickness values of building walls on buildings' rigidity in the presence of the soft storey, where the larger variations in stiffness and strength capacities occurred between the ground floor and consecutive upper floors.

Effect of different Compressive Strength

Figure 5.8 presents capacity curves for the FFHB building for the types of bricks (Bricks clay, hollow concrete), considering the variation of compressive strength where the base shear-top displacement curve represents the global response.
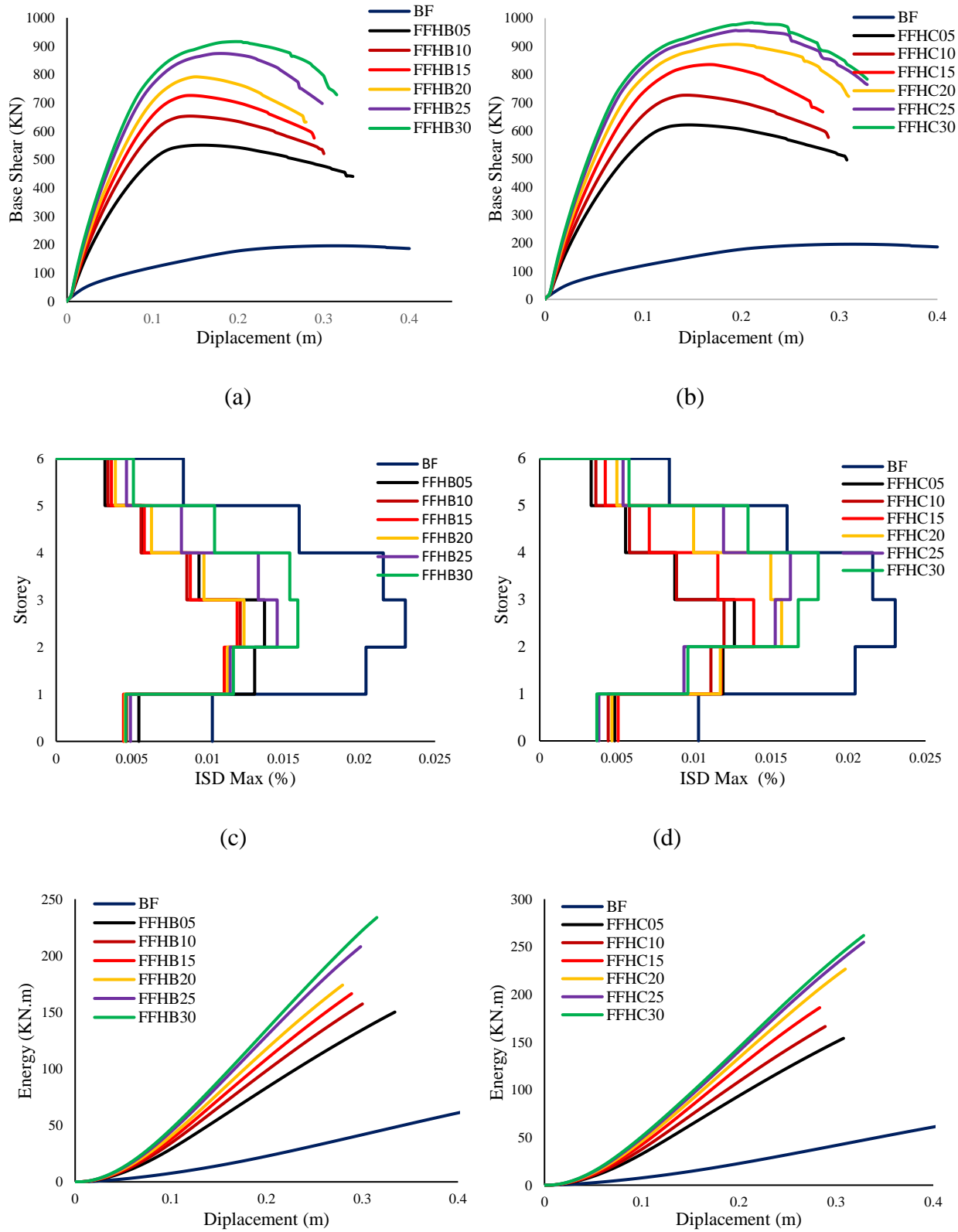
Figure 5.8: a) The capacity curve, b) the maximum ISD, c) the energy absorbed curve of the

building.

Table 5.7. The values of maximum top displacement, maximum base shear, maximum inter-story drift, and the energy for all models are attributed to their corresponding in the Full frame model. (Cas of the Compressive Strength variation)

Models	Base Shear (KN)	Ratio (FF)	Dipat Max BS (m))	Ratio (FF)	ISD Max (%)	Ratio (FF)	Energy (KN.m)	Ratio (FF)
HB05	420.266	-24%	0.13	-18%	0.0184	34%	103.01	-31%
HB10	459.22	-30%	0.121	-15%	0.013	7%	88.87	-43%
HB15	480.362	-34%	0.129	-10%	0.0138	16%	77.62	-53%
HB20	492.28	-38%	0.121	-20%	0.0137	11%	70.65	-59%
HB25	501.63	-43%	0.115	-36%	0.0137	-6%	66.61	-68%
HB30	505.451	-45%	0.112	-43%	0.0117	-26%	64.98	-72%

The set of curves presented in figure 5.8 shows the effect of the Compressive Strength values on the overall response of the building with a soft story, where a considerable decrease in stiffness and maximum strength capacities compared to the full infill frame. This decrease increases with the increasing value of the compressive strength corresponding to the full frame. This is explained by the soft-storey buildings being vulnerable, potentially due to the soft story frame's lower stiffness and strength capacities. Also, the total collapse of the building was most likely under the soft-story mechanism. The rate decrease in the stiffness was almost 24% - 45% approved of the compressive strength value: 2.5MPa - 8.1MPA, respectively, compared to the full frame building.

In addition, the soft-storey building shows a steep decline in the capacity curve after attaining the maximum capacity, potentially due to in-plane cracking and crushing and out-of-plane failure of the infilled panels. If such structures were subjected to increasing lateral forces, then the lateral forces would be expected to be resisted by the frames only. Ultimately, the total collapse of the building was most likely under the cases of shear failure in the columns and short columns.

Also, looking at the energy compared to the full frame, it can be observed Significant decrease increases with increasing compressive strength values corresponding to the full frame; for example, a decrease in the energy absorbed concerning the compressive strength was 10, 15, 20 and 30% estimated at 43%, 53%, 59% and 72% respectively. This is explained by the structural elements of the soft-storey building underwent an early hardening and the formation of plastic hinges was likely to be dominant, most likely due to higher seismic demand concentration in a single floor.
Also, by looking at the recorded values of the maximum inter-storey drift, it was noted that an increase in the ISD is 34% -11% for buildings with a compressive strength value of 2.5MPa-5.9MPa, respectively. Then a decrease that increases with an increase in the value of the compressive strength until it reaches a decrease from the corresponding value for the full frame by 6% - 26% for the compressive strength that exceeds 5.7MPa

This decrease is explained by the effect of the compressive strength values of building walls on buildings' rigidity in the presence of the soft storey, where the larger variations in stiffness and strength capacities occurred between the ground floor and consecutive upper floors.

Cas 03: Partial frame buildings

There is no doubt that the existence of an opening in the infill panel affects the structural behaviour and therefore, the failure mechanisms, as shown in Figure 5.9, are different than those illustrated in the previous section.

Effect of different wall thicknesses

Figure 5.9 presents the capacity curve base shear -Top displacement, inter-storey drift ratio (ISD %), and the energy absorbed curve of the FFHB buildings considering the change in thickness.
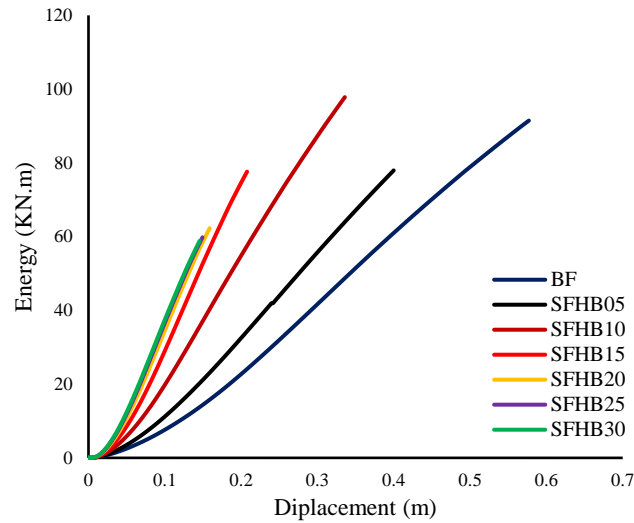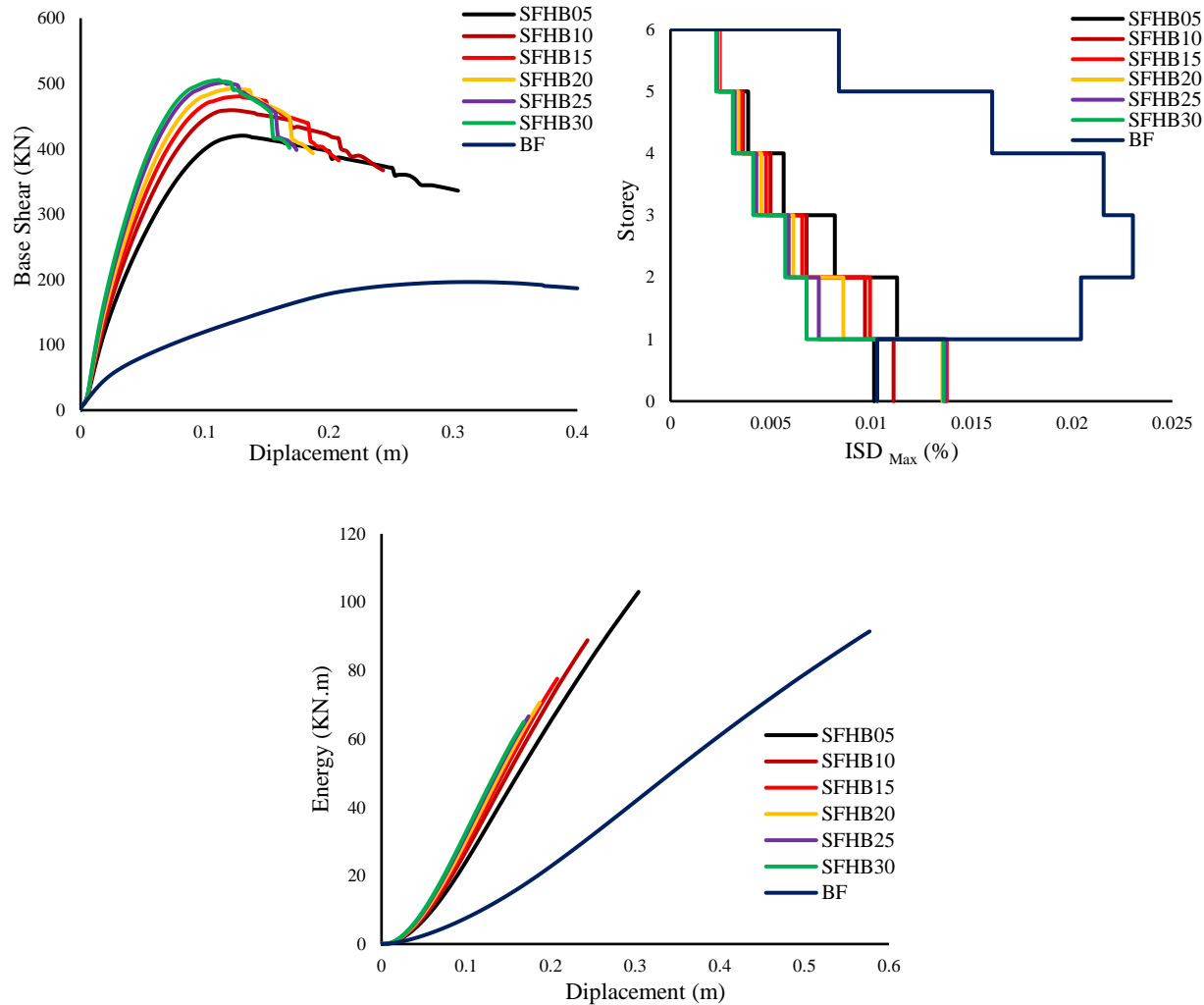

Figure 5.9: a) The capacity curve, b) the maximum ISD, c) the energy absorbed curve of the building.

Table 5.8. The values of maximum top displacement, maximum base shear, maximum inter-story drift, and the energy for all models are attributed to their corresponding in the Full frame model. (Cas of the Thickness variation)

Models	Base Shear (KN)	Ratio (FF)	Dip at Max BS (m)	Ratio (FF)	ISD Max (%)	Ratio (FF)	Energy (KN.m)	Ratio (FF)
HB05	236.23	-7%	0.277	4%	0.0213	2%	99.61	-3%
HB10	358.36	-17%	0.202	15%	0.017	14%	118.63	-7%
HB15	567.6	-22%	0.151	6%	0.013	9%	145.81	-12%
HB20	846.45	-15%	0.174	-18%	0.014	-23%	196.14	-32%
HB25	980.74	-11%	0.211	-19%	0.018	-23%	283.22	-17%
HB30	1045.256	-10%	0.243	-9%	0.021	-16%	304.41	-22%

The set of curves presented in figure 5.9 and Table 5.8 shows the effect of the thickness difference on the overall response of the building with openings, where a considerable slight decrease in stiffness and maximum strength capacities compared to the full infill frame. This is explained by the existence of openings in the infill panel affecting the structural behavior and therefore, the failure mechanisms are different than the full infill frame, where the rate decrease in the stiffness was almost 7% - 22% approved of the thickness value: 5cm-15cm and 15%,11% and 10% for the 20,25,30, thickness as compared to the full frame building. In addition, the partial infill frame slow decline in the capacity curve after attaining the maximum capacity is due to the internal crushing of the masonry segments between the columns and the window, and the sliding shear of the masonry zones above and below the window.

Also, looking at the energy compared to the full frame, it can be observed decrease that varies according to the values of the thickness, where, for example, a decrease in the energy absorbed concerning the thickness was 10, 15, 20 and 30% estimated at 7%, 12%, 32% and 22% respectively. where the existence of window opening in the infill leads to a plastic hinge failure mechanism at both ends of the columns. It can be also highlighted that there is an increase in varying proportions in the maximum Inter-storey drifts compared to the full frame, this is explained by the effect of the existence of the opening weakens the infill wall, Thus, an increase in the value of the maximum ISD values.

Also, it concluded that the behavior of the partial frame (infill with openings) is close to the behavior of the full infill frame in cases of strong bricks (thickness: 20,25. and 30).

Effect of different Compressive Strength

Figure 5.10 presents the capacity curve base shear -Top displacement, inter-story drift ratio (ISD %), and the energy absorbed curve for the FFHB buildings, considering the variation of compressive strength.
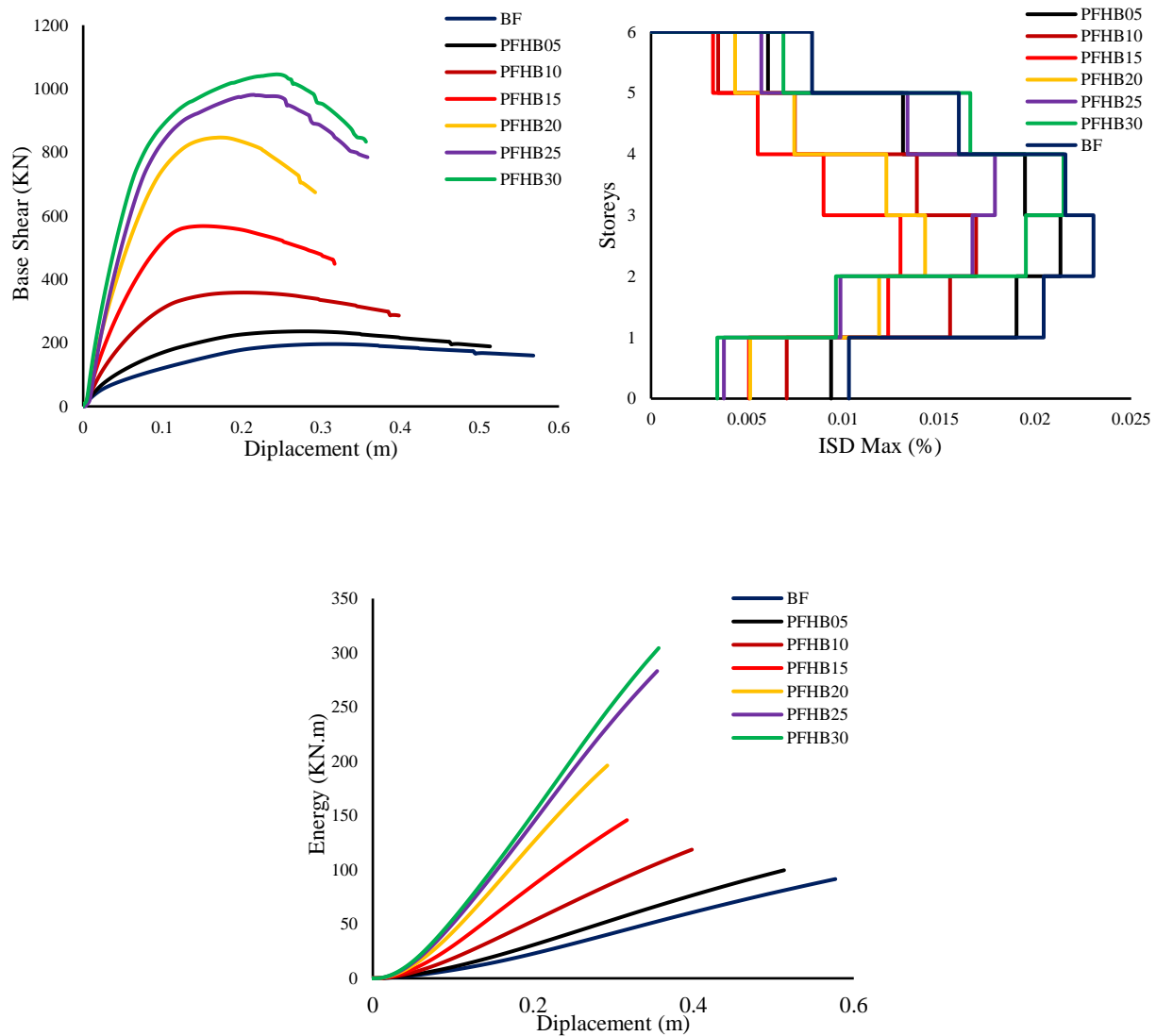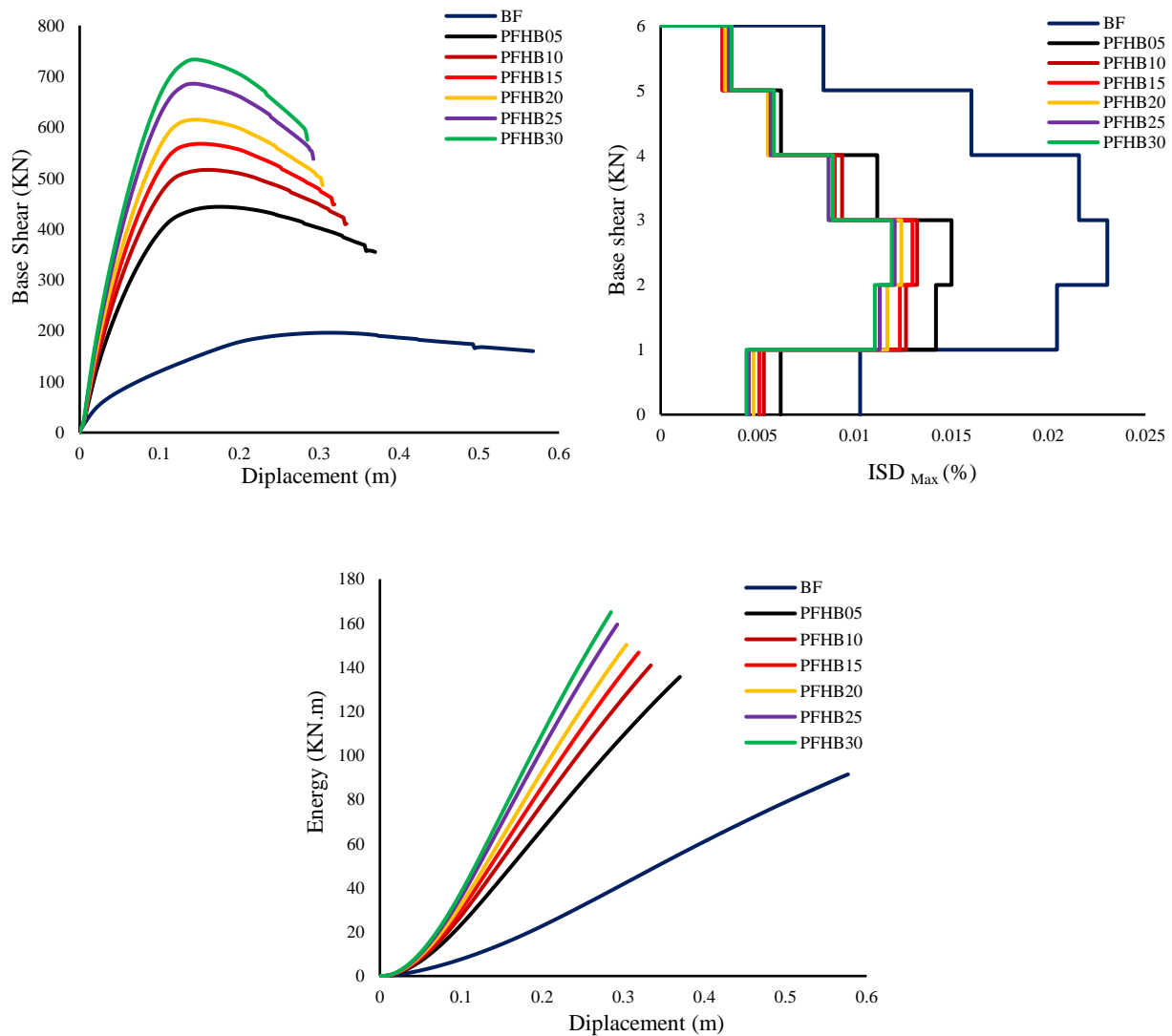

Figure 5.10: a) The capacity curve, b) the maximum ISD, c) the energy absorbed curve of the building.

Table 5.9. The values of maximum top displacement, maximum base shear, maximum inter-story drift, and the energy for all models are attributed to their corresponding in the Full frame model. (Cas of the Compressive Strength variation)

Models	Base Shear (KN)	Ratio (FF)	Dip at Max BS (m)	Ratio (FF)	ISD Max (%)	Ratio (FF)	Energy (KN.m)	Ratio (FF)
BF	192.21	/	0.313	/	0.0230	/	91.45	/
HB05	443.72	-19%	0.176	11%	0.015	9%	135.65	-10%
HB10	516.118	-21%	0.155	8%	0.013	7%	140.86	-10%
HB15	567.602	-22%	0.151	6%	0.013	9%	146.65	-12%
HB20	615.017	-22%	0.146	-3%	0.012	-2%	150.24	-14%
HB25	685.64	-22%	0.144	-20%	0.012	-17%	159.42	-23%
HB30	733.22	-20%	0.144	-27%	0.012	-25%	165.01	-29%

The set of curves presented in Figure 5.10 and Table 5.9shows the effect of the compressive strength values difference on the overall response of the building with openings, where there is a considerable decrease in stiffness and maximum strength capacities compared to the full infill frame. This is explained by the existence of the opening that weakens the infill and thus affects the structural behavior. Therefore, the failure mechanisms are different than the full infill frame, where the rate of decrease in the stiffness was almost 19% - 22% approved of the compressive strength value: 1.9MPa, -5.3MPa, respectively, as compared to the full frame building. In addition, the partial infill frame slow decline in the capacity curve after attaining the maximum capacity is due to the presence of an opening across the diagonal of the infill panel, which eliminates the well-known failure modes of Diagonal Compression (DC) and Diagonal Cracking (DK) (Asteris, et al., 2011d).

Also, looking at the energy compared to the full frame, it can be observed a decrease that varies according to the values of the thickness, where, for example, a decrease in the energy absorbed concerning the compressive strength values was 2,8MPa, 3.5MPa, 4.9MPa, and 6.1MPa estimated at 10%, 12%, 14%, and 29% respectively. Where does the presence of an opening across the diagonal of the infill panel lead to the elimination of the well-known failure modes of Diagonal Compression (DC) and Diagonal Cracking (DK) due to the fact that the main compressive strut is not formed, this causes the absorbed energy to decrease.

It can also be highlighted that there is an increase in varying proportions in the maximum

Inter Storey Drifts compared to the full frame. This is explained by the effect of the existence of the opening weakens the infill wall, Thus, an increase in the value of the maximum ISD values.

5.5. Influence of masonry infill wall position and openings

The present work aims to study the seismic behaviour of RC structures, considering the influence of the presence of openings, and the position of these infill walls on the seismic behaviour of RC frame structures. For this, it was considered a six-story frame with three bays of the same length. This frame is part of a building supposed to be in a zone of high seismicity (zone III according to RPA 99/2003 version) [5].

The secondary objective is to study the variability of the presence of infill walls and its effect on the structural response, where 15 models were selected from the structure previously studied, considering the variation in the presence of building walls in each case. After designing the frame according to the RPA 99/2003 version, non-linear static analyses (pushover) were carried out on the frame with different infill wall configurations. At the end of these post-elastic analyses, a discussion of the results is carried out, emphasizing the variation of the parameters, such as the base shear of the frame and the lateral displacements of floors.

Twenty-four 2D models were generated in the software OpenSees (Mckenna, Fenves, et al. 2000) [105], one without infill walls herein designated Bare Frame (BF) model and another one with infill panels distributed along the building's façades (Full Frame (FF) model. Also, eight different openings models (The reduction factor is from 10% to 90%). And thirteen models differ in the distribution of the infill walls. The masonry unit selected for the infill panels is hollow clay horizontal bricks 15cm thick, representing Algeria's most common masonry units. Once the main objective of the study was the assessment of the in plain influence of the infill masonry walls in the seismic response of RC frames, only a 2D frame was considered. Nevertheless, is recognized that the out-of-plane behaviour can change the structural response and an irregular distribution in plan could also develop a torsional response of the building.

The main aim of the present study is the study the effect of the openings of infill panels and to analyze the variation of the presence of infill walls in the RC structure on the overall response of the building, which will provide interesting information concerning those values when it occurs the collapse of the buildings during a seismic event. For this, static non-linear analysis

(Pushover analysis) was carried out to extract those results and assess the impact of the infill masonry walls on the non-linear static behaviour of the structure.

A set of 24 frames were defined. In a first stage, it was considered the effect of the openings. Then, it was considered a reduction factor from 0% to 100% in all the panels (0% representing BF, 10%, 20%, 30%, 40%, 50%, 60%, 70%, 80%, 90% and 100% representing FF) on the behaviour and capacity of the building by studying the capacitance curve, Maximum Inter Storey Drift (ISD max), and energy of each building.

The second stage the study is focused on different infill wall arrangements, consequently, the effect of the difference in the percentage of their contribution to the structural response of the studied buildings. From the infill walls, especially in the case of the soft story, to assess the levels of performance under the influence of lateral loads and to determine the effect of these distributions on seismic behavior. All studies discussed in this paper are summarized in table 5.10.

Table 5.10. Study summary

No.	Acronym	Masonry Type	Fm (MPa)	Thicknes (Cm)	Full Frame	Partial Frame	Variation Presence Of Infill
1	BF	/	/	/	/	/	/
2	FF	HB15	2.7	15	■		
3	FW10	HB15	2.7	15		■	
4	FW20	HB15	2.7	15		■	
5	FW30	HB15	2.7	15		■	
6	FW40	HB15	2.7	15		■	
7	F5W50	HB15	2.7	15		■	
8	FW60	HB15	2.7	15		■	
9	FW70	HB15	2.7	15		■	
10	FW80	HB15	2.7	15		■	
11	FW90	HB15	2.7	15		■	
12	SF	HB15	2.7	15			
13	2SF	HB15	2.7	15			
14	3SF	HB15	2.7	15			
15	RF	HB15	2.7	15			■
16	MF	HB15	2.7	15			■
17	UF	HB15	2.7	15			■
18	DF	HB15	2.7	15			■
19	MHF	HB15	2.7	15			■
20	MXF	HB15	2.7	15			■
21	RLF	HB15	2.7	15			■

22	2RF	HB15	2.7	15	■
23	2DF	HB15	2.7	15	■
24	SDF	HB15	2.7	15	■

5.5.1. Effect of infill openings on the global response

To study the effect of openings in the infill walls on the overall response of the building, the opening sizes were adjusted to get a range of reduction factors between 10% - 90%. The 6-story building models with a type of brick clay masonry with a thickness of 0.15 m and compressive strength value of 3500 KPa have been studied to evaluate the effect of opening on the determination and evaluation of base shear displacement, inter-story drift and energy absorption. The capacity curves, the maximum base shear, the inter-story drift profile for maximum strength and the energy until the convectional collapse are presented in Figure 5.11.

a)   b)

(c)   d)
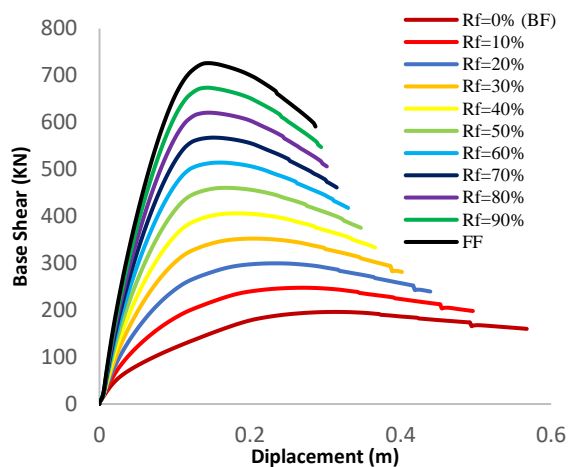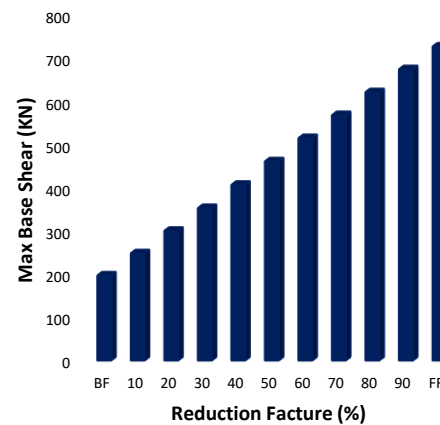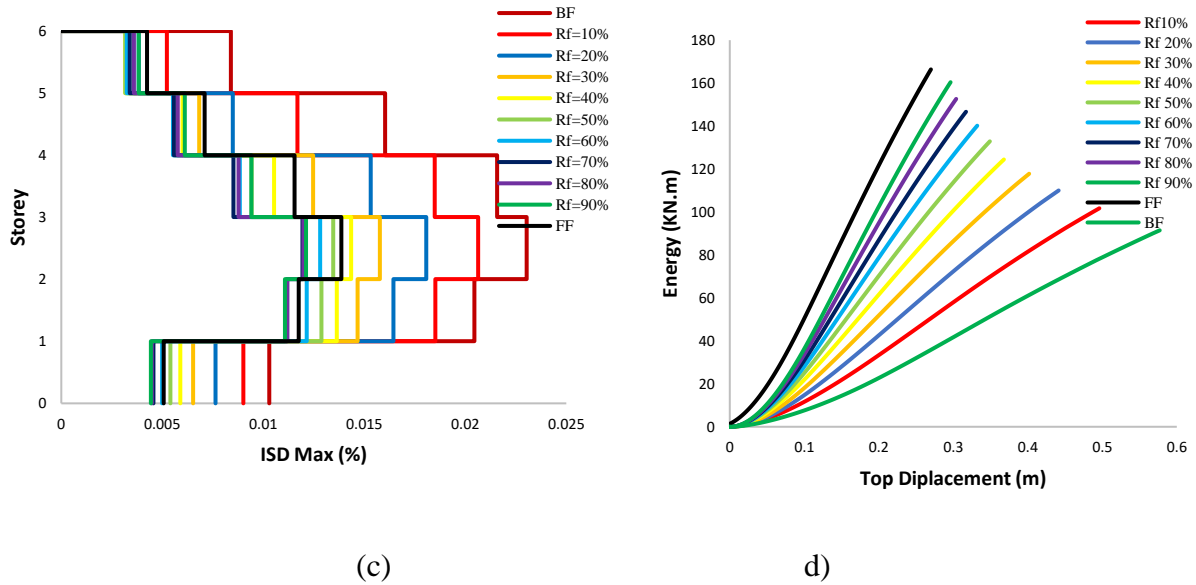
Figure 5.11: Represents a) the capacity curve, b) the maxillary base shear values c) the maximum

ISD, d) the energy absorbed curve of the building.

Table 5.11: Summarizing the results obtained: the values of maximum top displacement, maximum base shear, maximum inter-story drift, and the energy for all models are attributed to their corresponding in the Bare frame model.

Models	Base Shear (KN)	Ration (%)	Max top displacement (m)	Ratio (%)	ISD Max (%)	Ratio (%)	Energy (KN.m)	Ratio (%)
BF	196.21	/	0.313	/	0.023	/	91.45	/
Rf=10%	247.7	26.24%	0.2699	-13.77%	0.02098	-8.78%	101.72	11.23%
Rf=20%	299.72	52.75%	0.234	-25.24%	0.0188	-18.26%	110.01	20.30%
Rf=30%	352.45	79.63%	0.205	-34.50%	0.0172	-25.22%	117.8	28.81%
Rf=40%	406.17	107.01%	0.183	-41.53%	0.0155	-32.61%	124.44	36.07%
Rf=50%	460.63	134.76%	0.168	-46.33%	0.0141	-38.70%	132.89	45.31%
Rf=60%	514.44	162.19%	0.16	-48.88%	0.0136	-40.87%	140.17	53.28%
Rf=70%	567.75	189.36%	0.151	-51.76%	0.0129	-43.91%	146.565	60.27%
Rf=80%	620.75	216.37%	0.145	-53.67%	0.0124	-46.09%	152.63	66.90%
Rf=90%	673.99	243.50%	0.143	-54.31%	0.0121	-47.39%	160.43	75.43%
FF	726.34	270.19%	0.143	-54.31%	0.0119	-48.26%	166.45	82.01%

From the obtained results it can be observed that the stiffness increase, as shown in Table 5.11, compared to the bare frame. The, the high increase in the lateral building's stiffness was recorded between 247% - 26%, according to the difference in the value of the reduction factor

between 10% to 90%. Also, a decrease in the top displacement values was achieved by an estimated percentage of 54.31% - 13.77%, according to the difference in the reduction factor, and this is explained by the effect of the contribution ratio of the filling walls in increasing the lateral stiffness of the buildings and decreasing the displacement through the presence of walls.

The effect of the reduction ratio on the increase in the lateral stiffness is due to the difference in the percentage of the contribution of the infill walls, as the presence of openings in the filling walls negatively affects the contribution ratio and thus on the percentage of the increase in the lateral stiffness of the building.

Also, looking at the energy compared to the bare frame, it can be observed a significant increase that varies according to the values of the reduction factor, where, for example, an increase in the energy absorbed concerning the reduction factor was 20%, 40%, 60% and 80% estimated at 20.3%, 36.07%, 53.28% and 66.90 respectively. This discrepancy in the increase in energy is explained by the difference in the percentage of the contribution of the infill walls, which is directly affected by the value of the reduction factor.

Also, by looking at the recorded values of the maximum inter-storey drift, was noted that a significant decrease in the ISD is 11.2% - 47.39% for buildings with a reduction ratio between 10% to 90%. This discrepancy in the decrease is explained by the effect of the values of the reduction factor on the contribution ratio of building walls and thus the variance in increasing buildings' rigidity.

5.5.2. Influence of masonry infill wall position

The present part of the paper aims to study the effect of the reinforced concrete frame with infill walls with different distributions and to monitor the impact of the different distribution of these walls on the strength and ductility of the concrete frame, using a macro model to represent the infill wall in the analytical study, which facilitates the process of analysis and study of the effect. This can be related with the infill arrangement in new buildings or even due to the changes that occur during the building life.

The models developed as shown in figure 5.12 are: (1) frame without infill (BF); (2) building with masonry infill (FF); (3,4,5) building with masonry infill except for the ground,

second, third story (SF), (2SF), (3SF) (6) building completely infilled with except along the first bays (RF); (7) building fully infilled except along the middle bays (MF),(8) building infilled except along the first and third bay (RLF),(9) building fully infilled except along the first and second bay (2RF) (10) model of building filled in masonry without infill on the 4,5,6th storeys (UF), (11) building model filled masonry without infill on the 2,4,6th storeys (DF).12) building model filled masonry without infill on the 1,3,5th storeys (SDF), (13) model of building filled in masonry without infill on the 2,4,5,6th storeys (2DF), (14) model of building filled in masonry without infill on the 3,4,5th storeys (MHF), (15) buildings infilled randomly (MXFF).

BF-6   *FF-6*   *SF-6*   *RF-6*   *MF-6*

3SF-6   *UF-6*   *DF-6*   *MHF-6*   *MXF-6*

SDF-6   *2DF-6*   *RLF-6*   *2RF-6*   *2SF-6*
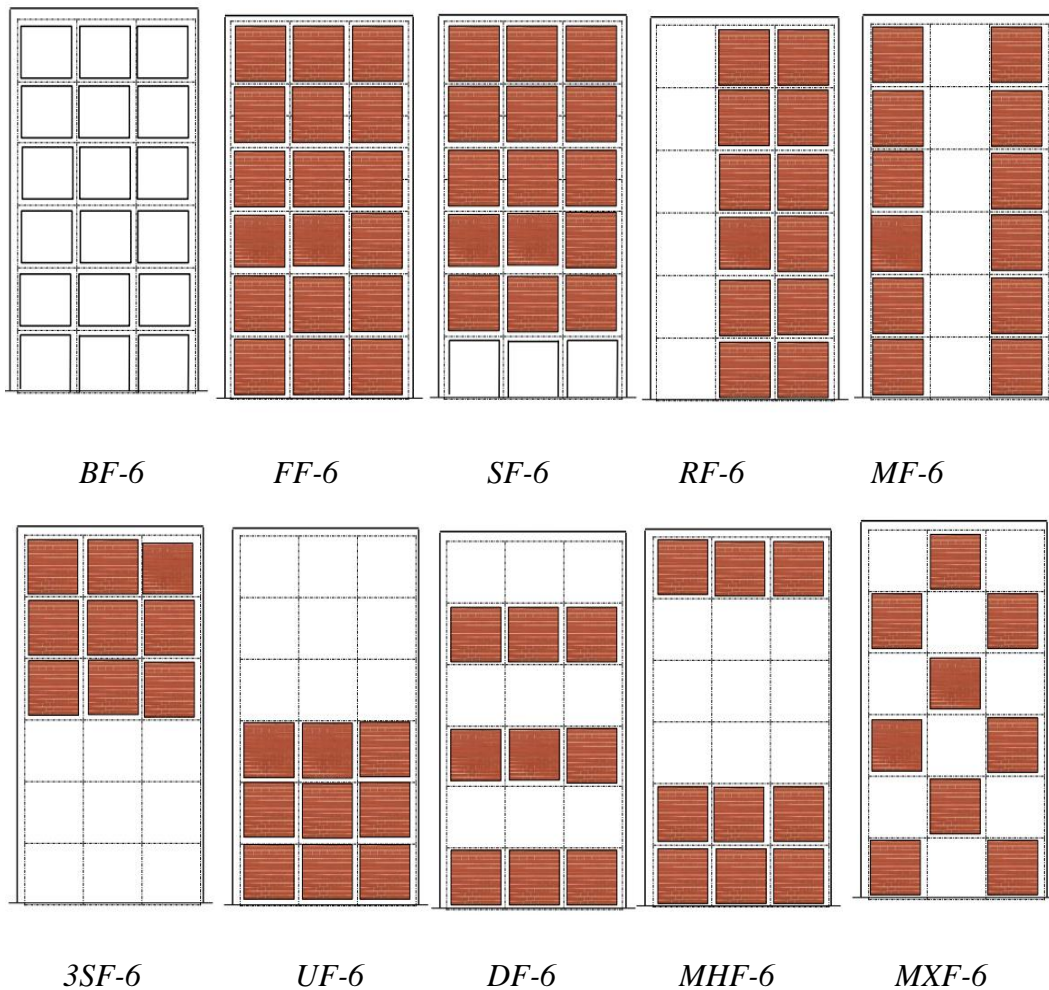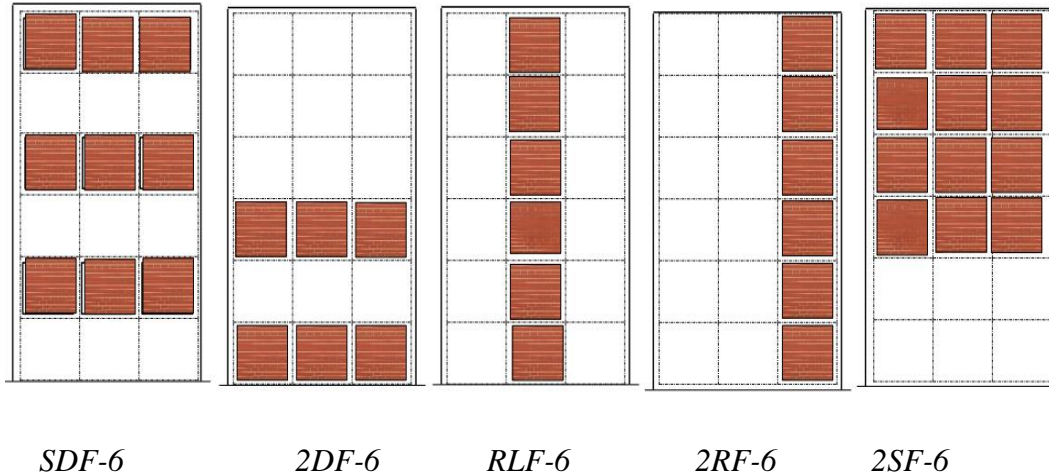
Figure 5.12: The models with the distribution of the different infill walls.

In the following, the results of the progressive pushover analyses performed, in the longitudinal X direction, on the 15 models presented in Figure 5.12 are presented and discussed. In addition, the evaluation of the effect of the presence of the infill and the flexible story and their height locations on the non-linear responses of reinforced concrete portal frame buildings is examined and compared below.

Figures 5.13 show the capacity curve of the studies' buildings; as a first observation, it can be noticed a fundamental difference directly in the structural response of the studied cases from the other cases that represent the bare frame and the infilled frame, as the lateral shift was accompanied by a deviation from centralization after the force subsides, which highlights the bad effect of the heterogeneous distribution of building walls.
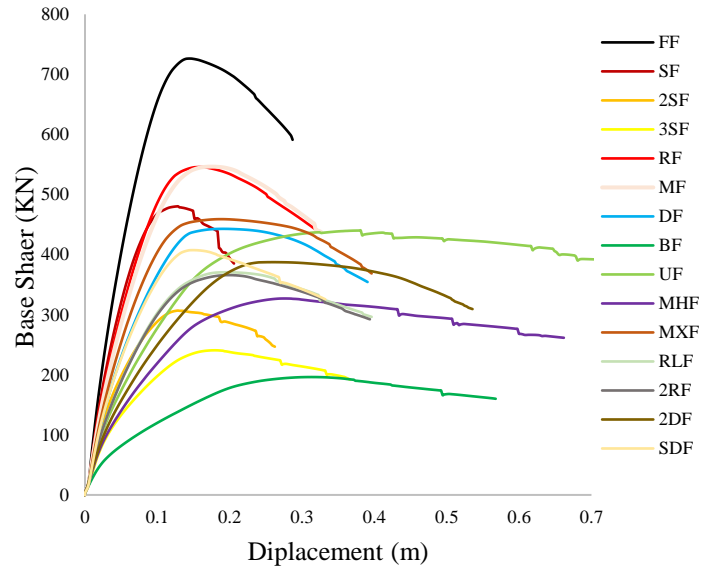
Figure 5.13: Pushover curves of the models studied.

Figure 5.14 shows the structural response of the maximum ISD for each storey for the cases studied, and Figure 5.14.b shows the damping plastic deformational energy in each model. It was observed that the infill walls' participation in the frame's energy damping in all models.

a)   b)
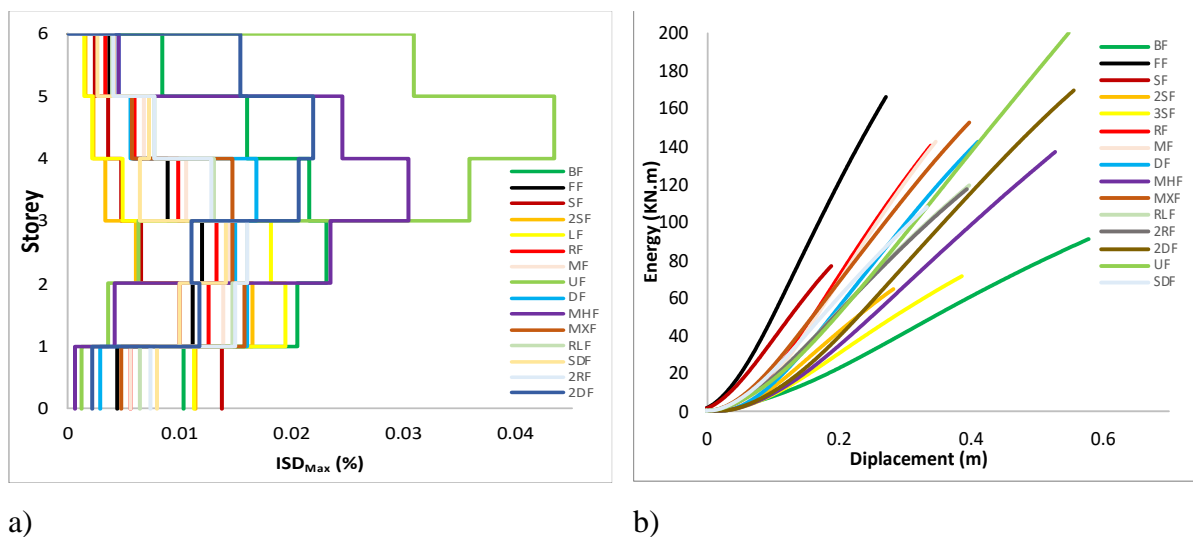
Figure 5.14: The structural response: a) maximum ISD for each storey for the cases studied; b) plastic deformational energy in each model.

A great disparity between the proportions of the ISD values in the studied models appears due to the heterogeneity of the distribution of the infill walls in the frame, as the maximum ISD values

in the infill frame model did not exceed 0.012 m, while none of the maximum ISD values in the rest of the models were less than 0. .015 m to 0.045 m, even the bare frame, which is considered the least rigid, in which the storeys displacements did not exceed the 0.023 m limit.

Table 5.12: The values of maximum top displacement, maximum base shear, maximum inter-story drift, and the energy of the plastic deformation damping for the models studied.

Models	Base Shear (KN)	Max top displacement (m)	ISD Max (%)	Energy (KN.m)
BF	192.21	0.313	0. 0230	91.45
FF	726.34	0.143	0.0119	166.45
SF	480.36	0.128	0.0138	64.92
2SF	306.85	0.128	0.0164	71.39
3SF	240.74	0.179	0.0194	76.89
RF	545.83	0.158	0.0132	140.57
MF	546.47	0.173	0.0144	142.45
UF	440.13	0.381	0.0434	199.52
DF	442.9	0.19	0.0168	142.47
MHF	326.95	0.275	0.0305	137.02
MXF	459.04	0.187	0.0158	152.76
RLF	370.61	0.194	0.016	119.5
2RF	365.88	0.197	0.016	117.34
2DF	387.45	0.26	0.022	169.79
SDF	407.45	0.149	0.0141	108.31

For the studied models, the approved output values (base shear, Top displacement, ISD$_{Max}$, Energy) were attributed to the corresponding values of the Bare frame model to obtain a direct comparison between each case with the case of the bare frame, in addition to the ability to compare between each of the cases of infill wall with the other cases of infill, as shown in Table 5.12).

Table 5.13: The values of maximum top displacement, maximum base shear, maximum inter-story drift, and the energy for all models are attributed to their corresponding in the Bare frame model.

Models	Base Shear (KN)	Max Top displacement (m)	ISD Max (%)	Energy (KN.m)
FF	3.78	0.46	0.52	1.82
SF	2.50	0.41	0.60	0.71
2SF	1.60	0.41	0.71	0.78
3SF	1.25	0.57	0.84	0.84
RF	2.84	0.50	0.57	1.54
MF	2.84	0.55	0.63	1.56

UF	2.29	1.22	1.89	2.18
DF	2.30	0.61	0.73	1.56
MHF	1.70	0.88	1.33	1.50
MXF	2.39	0.60	0.69	1.67
RLF	1.93	0.62	0.70	1.31
2RF	1.90	0.63	0.70	1.28
2DF	2.02	0.83	0.96	1.86
SDF	2.12	0.48	0.61	1.18

It is difficult to observe the differences between the infill models, so the comparison was made in a more effective way considering the base of the bare frame values, and the models were divided into groups that converge on the type of effect as shown in the following table 5.13.

Table 5.14: Summary of studies cases

Study Case No°:1	Study Case No°:2	Study Case No°:3	Study Case No°:4
BF	*BF*	*BF*	*BF*
FF	*FF*	*FF*	*FF*
SF	*RF*	*3SF*	*MXF*
2SF	*MF*	*UF*	*DF*
3SF	*RLFF*	*MHF*	*SDF*
	2RF		*2DF*

Case N°:1

From Figure 5.15, which represents the capacity curve Figure 5.15.a, the maximum base shear values Figure 5.15.b, the maximum ratio ISD Figure 5.15.c, and the energy absorbed curve of the building Figure 5.15.d, it can be noted that regarding the full frame, a significant increase in the base shear, reaching more than double 278 %, while the top displacement of the building decreased by 54%, and this indicates a significant increase in the lateral stiffness of the structure.

Also, looking at the percentage of energy absorbed by the full infill, a relative height of 82% was recorded. This indicates that the source of energy that the structure added is through the infill walls. Also, the ISD max is small, indicating homogeneity in the origin's behaviour. In the three SF, 2SF, and 3SF models and referring to the figures 5.15 and the Table 5.14, it is notice that the displacement ratio decreased by 59%, 59%, and 43%, while the percentage of the base shear increased by 150%, 60%, and 25% for SF, 2SF, 3SF, respectively, and the rate of energy absorbed by the origin decreased by 29%, 22%, 16%, and this is due to the absence of masonry walls in the soft storey and the low transmission, especially at the breaking point corresponding to 80% of the base shear, which explains the contribution of the infill walls to energy absorption was very little and the occurrence of collapse at a lower displacement.

It is also noted that the maximum ISD on the first storey is relatively large and increases with the increase of the soft storeys, where an increased rate of 15.97%, 37.82%, and 63.03% was achieved compared to the full frame.

a)   b)

c)

d)
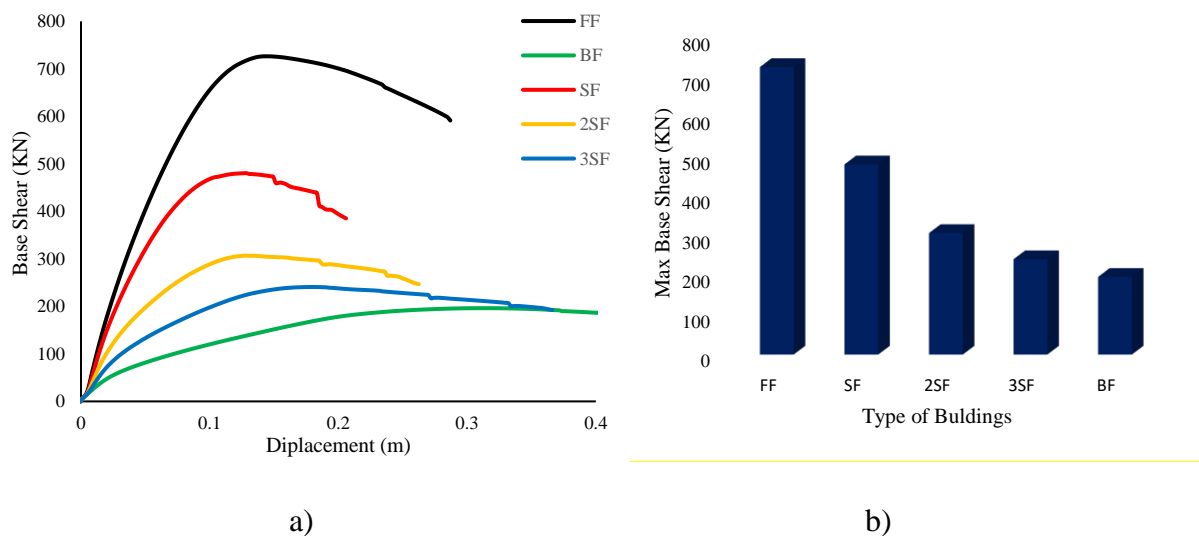
Figure 5.15: Case N°:1: a) the capacity curve, b) the maxillary base shear values, c) the maximum ISD, d) the energy absorbed curve of the building.

Case N° 2:

From Figure 5.16, which represents the capacity curve Figure 5.16.a, the maximum base shear Figure 5.16.b, the maximum ISD Figure 5.16.c, and the energy absorbed curve of the building Figure 5.16.d, it can be noticed that:

a)

b)

c)

d)

Figure 5.16: Case N°:2: a) the capacity curve, b) the maxillary base shear values, c) the maximum ISD, d) the energy absorbed curve of the building.

For the frame RF and MF, a significant increase in the lateral stiffness, around 184% was observed for each of the buildings when compared to the bare frame, and a decrease in the displacement for maximum strength ratio by 50% and 45%, respectively due to the presence of the infill walls in the first and second bays for structure RF and the first and third bays for building MF,

As well as for the RLF and 2RF buildings, it was recorded half the percentage increase in the global stiffness of the buildings RF and m MF compared to the bare frame estimated at 93% and 90% and a decrease in the transmission ratio by 38% and 37%, respectively, due to the low percentage of the contribution of the infill walls in the two buildings and their impact on the overall response of the building due to the presence of these walls at the level of the first bays in building RF, and the pedestal in the building MF. This is explained by the effect of the presence of infill walls in the building on the increase in the strength of buildings and displacement reduction.

Also, looking at the percentage of energy absorbed by the buildings compared to the bare frame, it was recorded a significant increase around 54% and 56% for the RF and MF buildings and 31%, 28% for the two buildings, RLF, 2RF, respectively, and this is due to the percentage of the infill walls' contribution to the increase in energy scattering.

It can be also highlighted that there is a significant decrease in the maximum Inter Storey Drifts in the RF and MF buildings compared to the bare frame by an estimated percentage of 43% and 37%, respectively, and an equal percentage estimated at 30% for the two buildings, RLF and 2RF. This is explained by the effect of the proportion of the contribution of the infill walls in reducing the maximum ISD values through the increase in the stiffness of the buildings.

Case N° 3:

From Figure 5.17, which represents the capacity curve Figure 5.17.a, the maximum base shear values Figure 5.17.b, the maximum ISD ratio Figure 5.17.c, and the energy absorbed curve of the building Figure 5.17.d, it can be observed that:
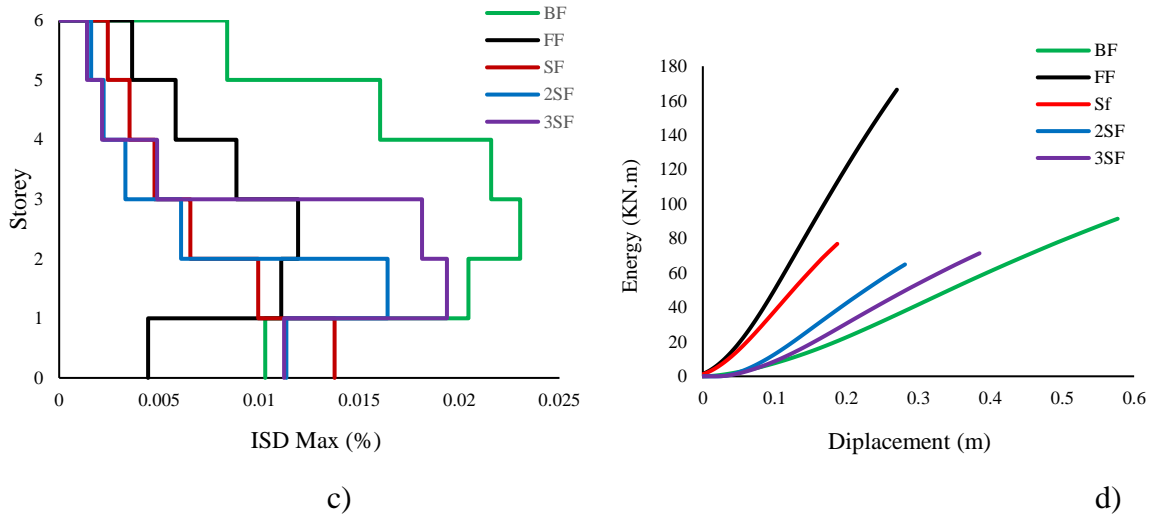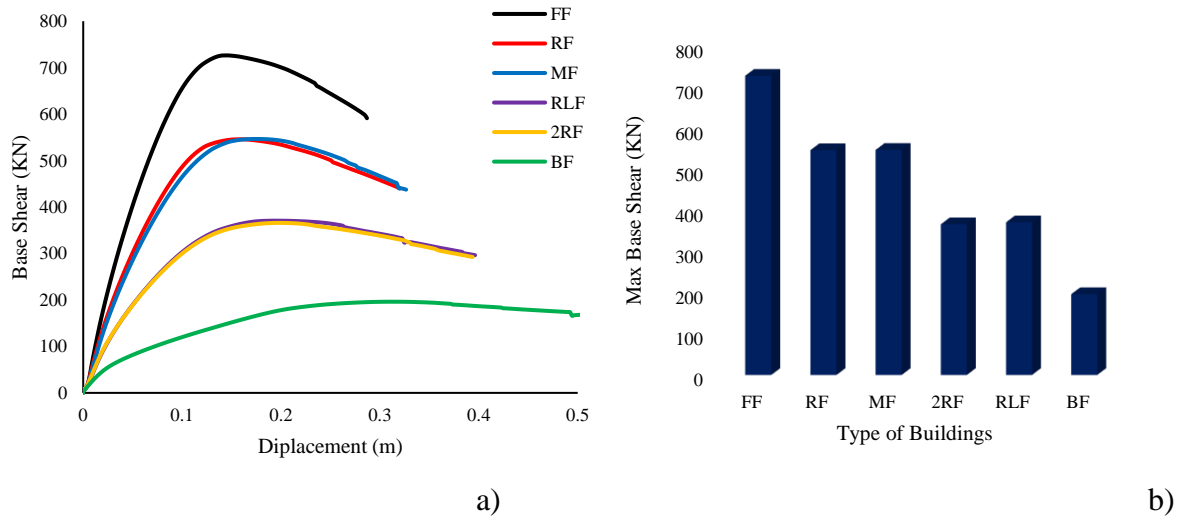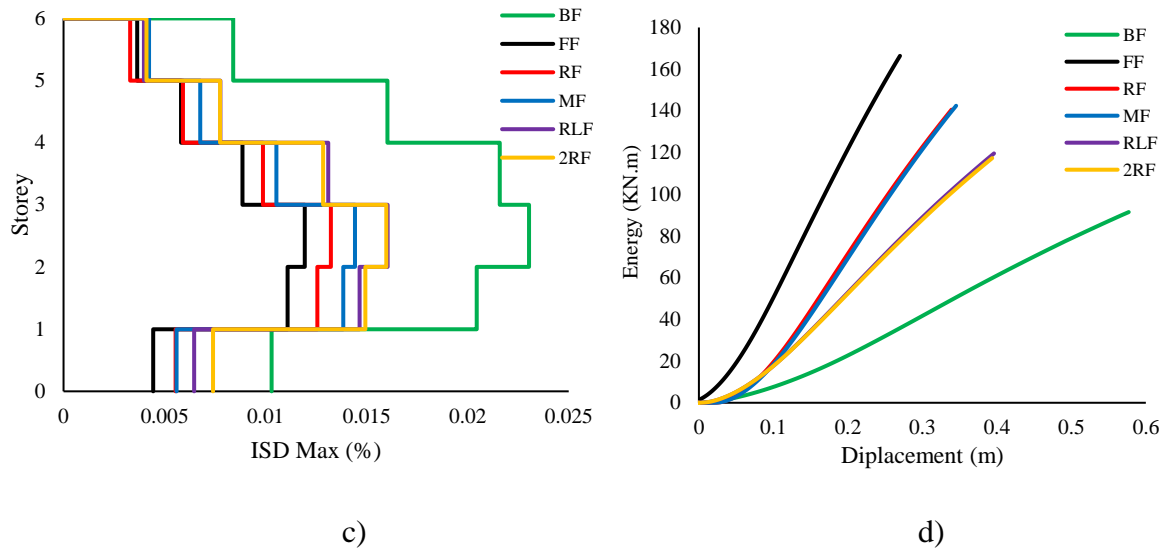

Figure 5.17: Case N°:3: a) the capacity curve, b) the maxillary base shear values, c) the maximum ISD, d) the energy absorbed curve of the building.

For the building 3SF, it was found a decrease in the base shear value of up to 66% compared to the infilled frame. In comparison, an increase in the upper displacement ratio by 25%, and this is due to the absence of infill walls in the first three storeys and the beginning of a mechanical collapse of the bare storeys, as well as for the UF frame was recorded a decrease in the base shear value by 39 due to the absence of infill walls in the last three storeys, which led to a decrease in the severity of the building. However, the effect of this is a significant increase of 166% in the top displacement of the building, and this is due to the building gaining softness at the level of the last three storeys that do not contain infill walls, as well as for the MHF frame A significant decrease in the maximum base shear estimated at 54% was observed. As for the top displacement, a significant increase was noticed estimated at 92% due to the absence of filling walls on the third, fourth and fifth storeys.

Also, considering the percentage of energy absorbed by the building compared to the bare frame, a large height of 118% was recorded for the UF building due to the presence of masonry walls in the first three storeys and a mechanical occurrence that forms plastic hinges in the last three stories, and this indicates that the source of damping energy is due to the infill walls in the first place and the plastic hinges that are formed before collapsing in the second.

As for the MHX building, a significant increase in energy absorbed was recorded, estimated at 50%. due to the infill walls on the first, second and last storeys. Its absence in the rest of the storeys gave the building ductility. It confirmed that the source of energy that is extinguished by the building is through the infill walls in the first storeys and Plastic hinges that are formed before the collapse of the building.

A big increase in the maximum ISD ratio in the UF and MH building compared to the filled frame by 264% and 156%, and this is explained by the absence of filling walls on the three floors of each building, which gave the building softness at the level of these storeys.

Case N° 4:

From Figure 5.18, which represents the capacity curve Figure 5.18.a, the maximum base shear values Figure 5.18.b, the maximum ratio ISD Figure 5.18.c, and the energy absorbed curve of the building Figure 5.18.d, it can be noted:
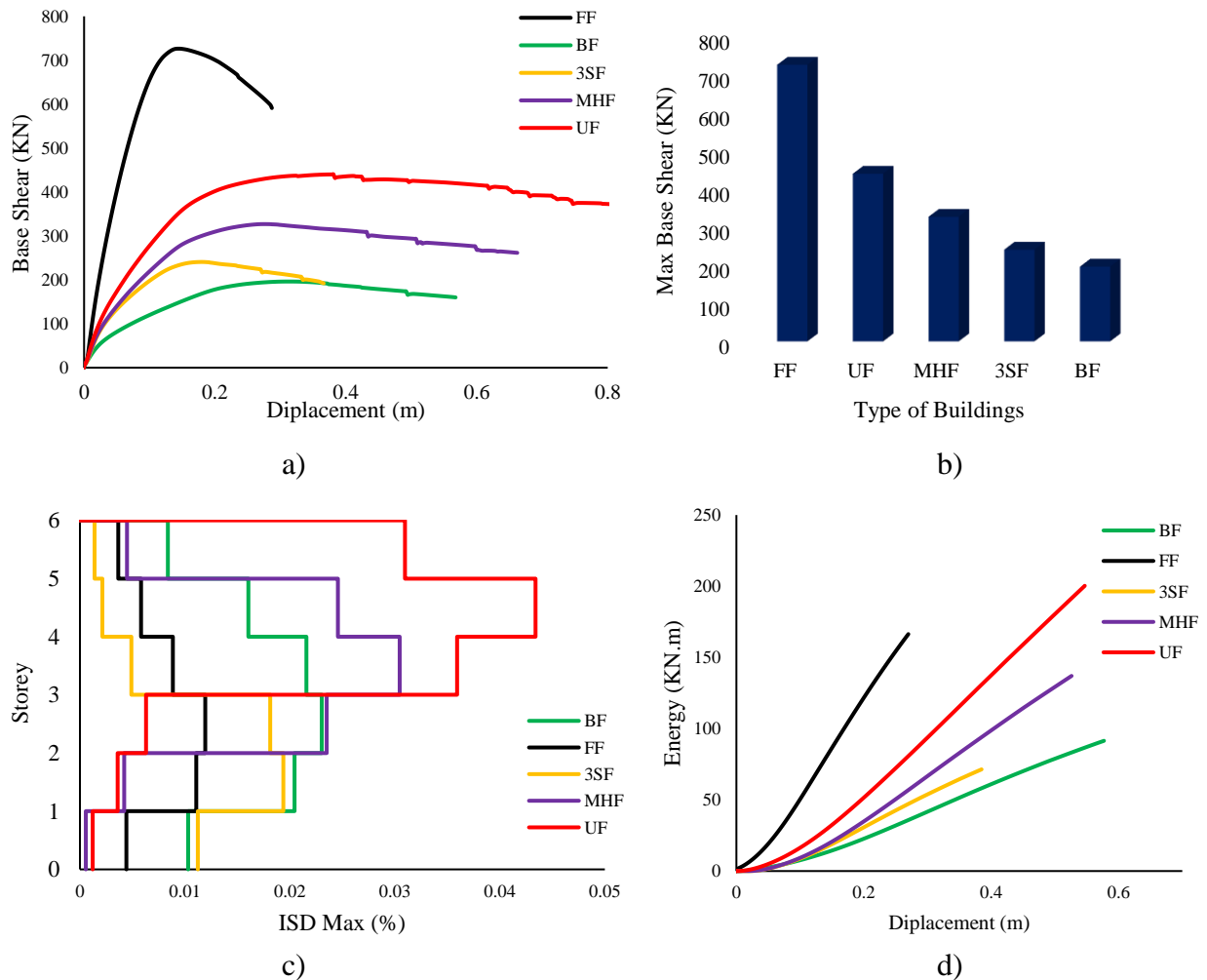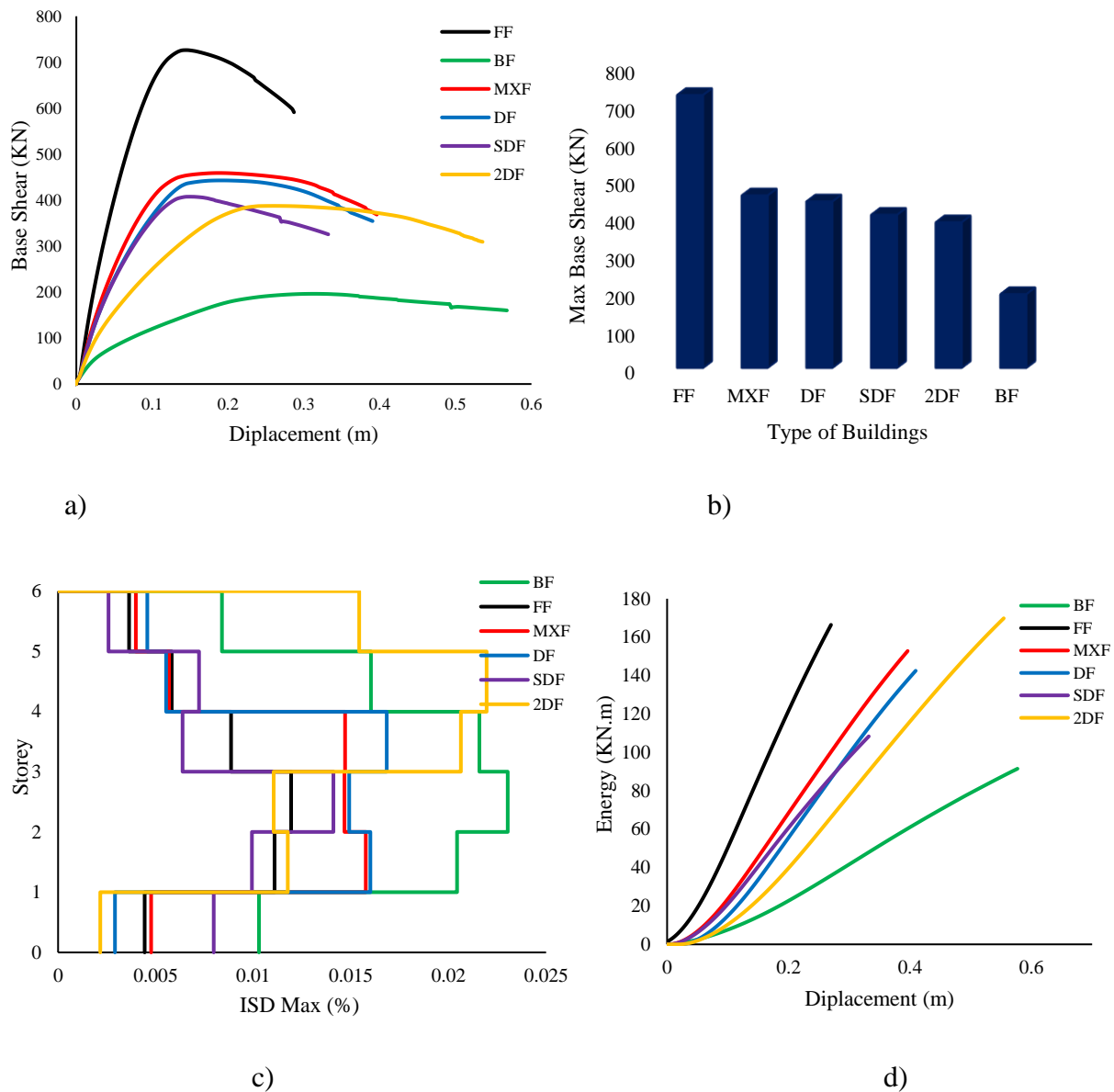

a)

b)

c)

d)

Figure 5.18: Case N°:4a) the capacity curve, b) the maxillary base shear values, c) the maximum ISD, d) the energy absorbed curve of the building.

For the building 3SF, it was found a decrease in the base shear value of up to 66% compared to the infilled frame. In comparison, it was recorded an increase in the upper displacement ratio by 25%, and this is due to the absence of infill walls in the first three storeys and the beginning of a mechanical collapse of the bare storeys, as well as for the UF frame, a decrease in the base shear value was recorded by 39% due to the absence of infill walls in the last three storeys, which led to a decrease in the severity of the building. However, the effect of this is a significant increase of 166% in the top displacement of the building, and this is due to the building gaining softness at the level of the last three storeys that do not contain infill walls, as well as for the MHF frame a significant increase in the maximum base shear was observed estimated at 54%.As for the top displacement, a significant increase was noticed estimated at 92% due to the absence of filling walls on the third, fourth and fifth storeys.

Also, considering the percentage of energy absorbed by the building compared to the bare frame, a large height of 118% was recorded for the UF building due to the presence of masonry walls in the first three storeys and a mechanical occurrence that forms plastic hinges in the last three stories, and this indicates that the source of damping energy is due to the infill walls in the first place and the plastic hinges that are formed before collapsing in the second.

As for the MHX building, a significant increase in the absorbed energy was recorded, estimated at 50%, due to the infill walls on the first, second and last storeys. Its absence in the rest of the storeys gave the building ductility. It confirmed that the source of energy that is extinguished by the building is through the infill walls in the first storeys and Plastic hinges that are formed before the collapse of the building.

A big increase was also observed in the maximum ISD ratio in the UF and MH building compared to the filled frame by 264% and 156%, and this is explained by the absence of filling walls on the three floors of each building, which gave the building softness at the level of these storeys, each line of Table 1 was represented with an axis on a diagram shown in the following Figure 5.19, where as long as the output values of these lines are relative to the output values of the bare frame, there will be no discrepancy that prevents us from noticing the resulting differences between all the outputs at once and in one table as shown in the figures.

(Study Case N°:1)

(Study Case N°:2)

(Study Case N°:3)   (Study Case N°:4)
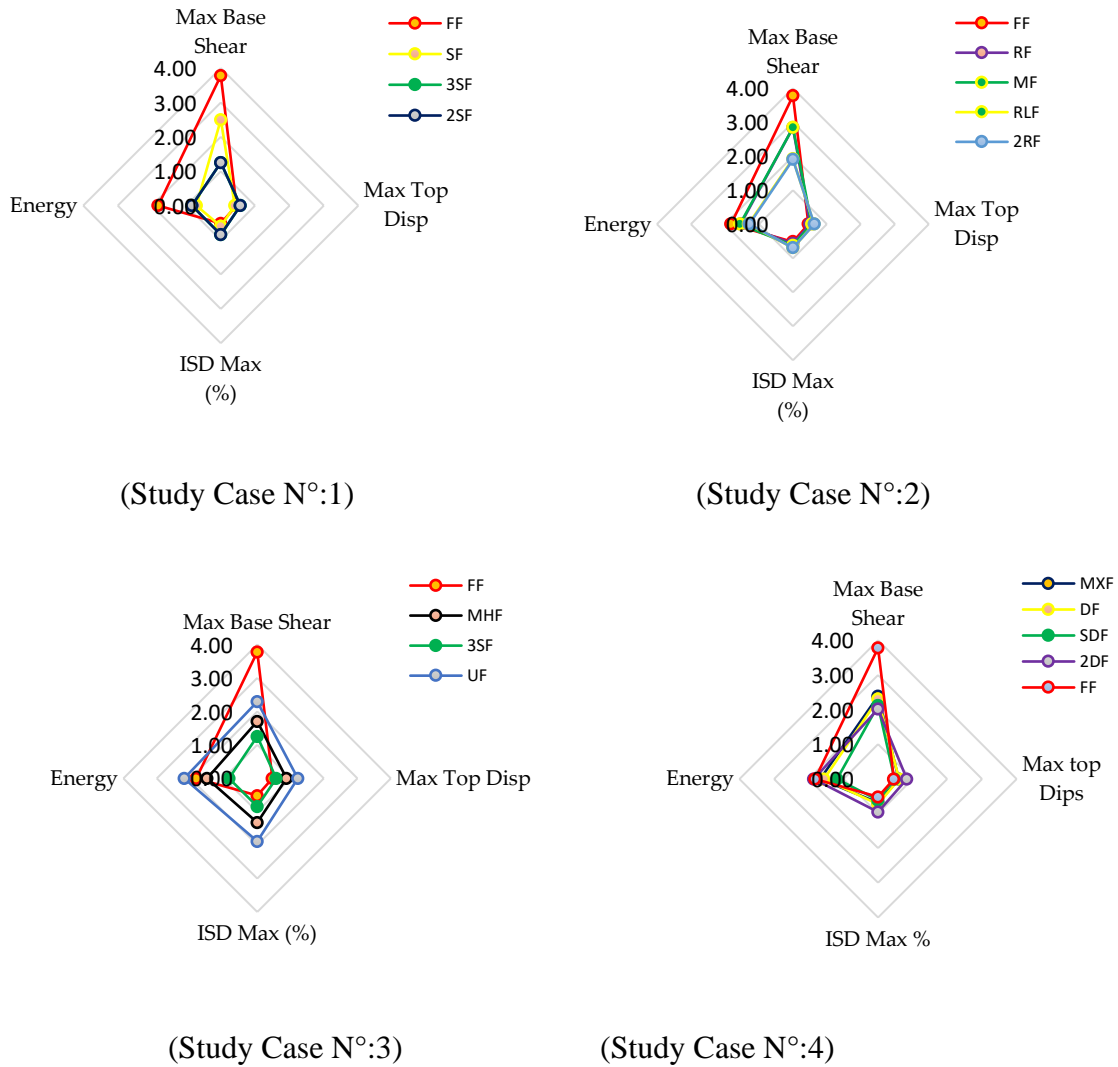
Figure 5.19: Radar diagrams to compare the studied results in the four cases.

5.6. Final Conclusions

This study aims to conduct an analytical study to verify the effect of the variability of the presence of infill walls on the behavior of these buildings on the lateral loads, and important results were drawn regarding the distribution of these walls in multi-storey buildings, which may be better taken into consideration in the future. The main conclusions that can be drawn from this study can be summarized as follows:

- The results of the pushover analysis show an increase in the initial stiffness and resistance capacity for the full infill frame compared by the bare frame despite the

brittle failure modes of the masonry wall. The presence of masonry walls has a significant effect on the observed collapse mechanism.

- From the failure mechanisms, it can be seen that, for the frames filled with thick bricks, the plasticization and the failure of the infill panels occur before the other reinforced concrete elements where the decrease in ductility is proportional to the thickness of the infill walls.

- The reduction of the overall ductility in portal frames with infills is caused by the masonry panels, which combine a high stiffness with a low capacity to undergo deformations.

- An increase in the ultimate strength due to the contribution of the masonry panels; since they have high compressive strength, this ultimate strength increases with the increase in the stiffness of the masonry panels.

- An increase in the initial lateral stiffness of the filled frames compared to the bare porticos is proportional to the increase in the stiffness of the masonry panels.

- The infill's presence brings about an increase in the resistance in the elastic state.

- A reduction in lateral displacements due to the presence of the infill walls that prevent the frames meshes from deforming freely.

- The size of the openings in the infill walls has a significant influence on the stiffness. Generally, it decreases as the size of the opening increases, indicating that the decrease in stiffness is more important than the decrease in mass.

- The infill panels increase the lateral stiffness of the frames, the presence of openings reduces the lateral stiffness of the frame, and with the increase in the size of the openings, the deformation capacity increases; in general, the bare frame shows better ductility than the infill walls frame; this can be attributed to the brittle behavior of masonry infill panels.

- It appears on the one hand that the masonry increases the lateral load-bearing capacity and reduces the deformation demand, which can reduce the damage in the structures; on the other hand, an irregular distribution of the masonry can result in a relatively fragile behavior of the structure. The failure modes of the bare frames are distributed over the height of the structures; in the case of the infilled frames, the failure modes are concentrated in the lower levels.

- The infill walls distributed homogeneously over the entire height of the building, such as FF, or the alternating distribution over the entire height of the building leads (as an example: RF, MF), to an increase in the stiffness of the structural system and thus a decrease in the desired ductility in the disposal of the structure before reaching the collapse.

- The ratio of the contribution of the infill walls affects the energy damping, as changing the distribution of the infill walls over the entire height of the building would increase the amount of energy absorbed by the buildings by controlling the collapse mechanism associated with the shape of this distribution (how plastic hinges are formed).

- The change in the distribution of infill walls while maintaining their number in the building has a major role in changing the percentage of building walls' contribution to bearing the base shear.

- The change in the number of masonry infill walls in the building plays a major role in changing the values of the contribution ratio, as the percentage of the building walls' contribution to bearing the base shear increases with the increase in the number of masonry walls in the building.

- The percentage of building walls' contribution to the bearing of the base shear is mainly related to the number and distribution of the filling walls.

Chapter 6.

Seismic vulnerability assessment of RC frames with masonry infills.

6.1. Introduction

As discussed in previous chapters, masonry walls are commonly used in RC buildings leading to a high level of rigidity and strength for the structures. Therefore, the lateral capacity of RC frames is different from bare frames. This can be mainly interpreted mostly as the effect of the masonry walls' configuration on the concrete buildings' general behaviour. on the other hand, the structural contribution of infill walls is discarded in many countries, including Algeria. The adopted practice which discarding the structural contribution of the masonry can be interpreted as the complex behaviour of infill walls. Thus, there is an urgent need to evaluate the seismic vulnerability of the RC frame considering the effect of the infill wall. Such studies, not only assess the effect of the infill wall on the overall behaviour but also determine their strengthening needs. In this context, this chapter presents a comprehensive numerical study that aims to assess the vulnerability of several 2D frames with different configurations of infill panels. To that end, it is necessary to conduct a study based on performance-based seismic engineering. Such studies

provide a comprehensive and detailed view of the behaviour of the building according to different degrees of damage.

To provide a comprehensive view regarding the effect of the infill and their configurations, the proposed study provides an extended parametric stud and assumptions regardingthe effect of the infill configuration and spatial distribution of the infill walls on final fragility curves. Numerical models of the structures were developed to obtain the fragility data, simulating the infill structures using single strut models. The models were analysed in the context of nonlinear dynamic analysis using incremental dynamic analysis (IDA) [101]. The intensity measure IM-based procedures were adopted to drive the fragility functions. The driven fragility functions were then used to compare the performance of the involved studied cases and assess the effect of the infill configuration on the overall performance.

6.2. Case studies

In order to study the effect of the infill spatial configurations along other infill configuration, the residential building shown in Figure 6.1 was selected as a representative case study. The building chosen has the plan dimensions of 13.1 m x 17.4 m, which consists of 4.3 x 4.3 m modules (i.e., in x and y direction, respectively). The floor heights were kept constant at (3) meters over the entire height of the building. The edge frame at vertical axis 5-5 between horizontal axes A and D was selected to generate the 2D models. The structures were designed for gravity loads to simulate a design situation where no seismic actions are included. A global vertical load of 5.25kN/m^2 plus a variable load of 2 kN/m^{2}were considered. Six storeys were chosen as a representative case for mid-rise buildings. Table 6.1 shows the mechanical parameters of the chosen materials, and Table 6.2 shows the cross-section data for the considered frame.

Different infill wall arrangements were selected to generate thirteen different configurations of infills frames in addition to the bare frame case. The selected frames represent different infill wall arrangements, in the vertical and horizonal direction. As shown in Figure 6.2, the considered cases represent cases with soft story at different level which can be subsequent or separated. Also, the considered cases present cases where infill have different vertical continuity in the horizonal directions. It is worth mentioning that all configurations can reflect buildings

configurations that exist not only in Algeria but also around the globe. These configurations were categorized into three main groups; fully infilled frame, partially infilled frame (i.e., infills have opening) and discontinuous infill panels as presented in Table 6.3. The case with discontinuous infill panel hasa large number of specimens in order to simulates several scenarios of infill presence.
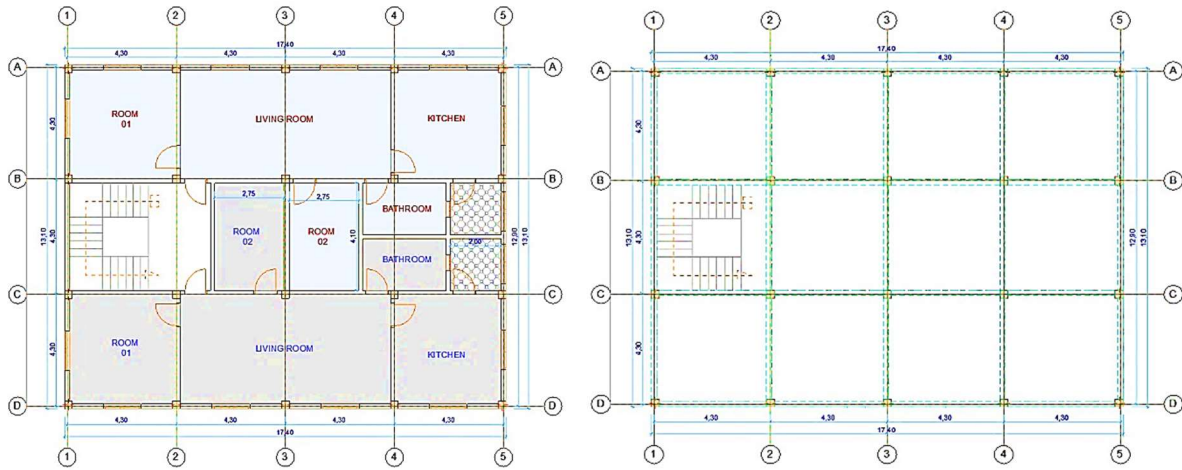
Figure 6.1: Typical plan view for the considered building: a) architectural plan b) structural system showing the considered frame (all dimensions in m)

Table 6.1: Mechanical properties of the materials

Concrete (MPa)F_c	Steel		Infill panel material	
	Yield stress $\sigma_Y (MPa)$	Elastic modulus $E(GPa)$	Brick unit compressive Strength $f_{masonry}$ (MPa)	Mortar compressive strength f_{mortat} (MPa)
25.0	522.0	190.0	2.7	10.0

Table 6.2: Cross-section details for frame

Axis	Columns		Beams						
	Section (cm²)	Reinfo-rcement	Section (cm²)	Reinforcement					
				Start		Middle		End	
				Upper	Lower	Upper	Lower	Upper	Lower
A	30x30	8Ø15	25x40	4Ø12	4Ø12	4Ø12	4Ø12	4Ø12	4Ø12
B	30x30	8Ø15	25x40	4Ø12	4Ø12	4Ø12	4Ø12	4Ø12	4Ø12
C	30x30	8Ø15	25x40	4Ø12	4Ø12	4Ø12	4Ø12	4Ø12	4Ø12
D	30x30	8Ø15	25x40	4Ø12	4Ø12	4Ø12	4Ø12	4Ø12	4Ø12

Table 6.3: Study summary

| No.	Description of the frame	Acronym	Masonry Type	Fm (MPa)	Thickness (Cm)	Full Frame	Partial Frame RF:0.7	Variation Presence Of Infill Vertical	Variation Presence Of Infill Horizontal
1	Bare frame (no infills)	BF	--	--	--	--	--		
2	Fully infilled	FF	HB15	2.7	15	X			
3	Infill wall with opening	PF	HB15	2.7	15		X		
4	no infill at ground floor	SF	HB15	2.7	15				
5	building with masonry infill except for the ground, second and third story	3SF	HB15	2.7	15				X
6	fully infilled except along the first and second bay	2RLF	HB15	2.7	15			X	
7	frame completely infilled with except along the first bays	RF	HB15	2.7	15			X	
8	frame fully infilled except along the middle bays	MF	HB15	2.7	15			X	
9	frame infilled except along the first and third bay	RLF	HB15	2.7	15			X	
10	frame fully infilled without 4th,5th,6th storeys (UF)	UF	HB15	2.7	15				X
11	frame fully infilled without 3rd,4th storeys	2MF	HB15	2.7	15				X
12	frame fully infilled without 3rd,4th and 5th storeys	MHF	HB15	2.7	15				X
13	frame model filled masonry without infill on the 2nd,4th,6th storeys (DF)	DF	HB15	2.7	15				X
14	frame model filled masonry without infill on the 1st,3rd,5th storeys	SDF	HB15	2.7	15				X
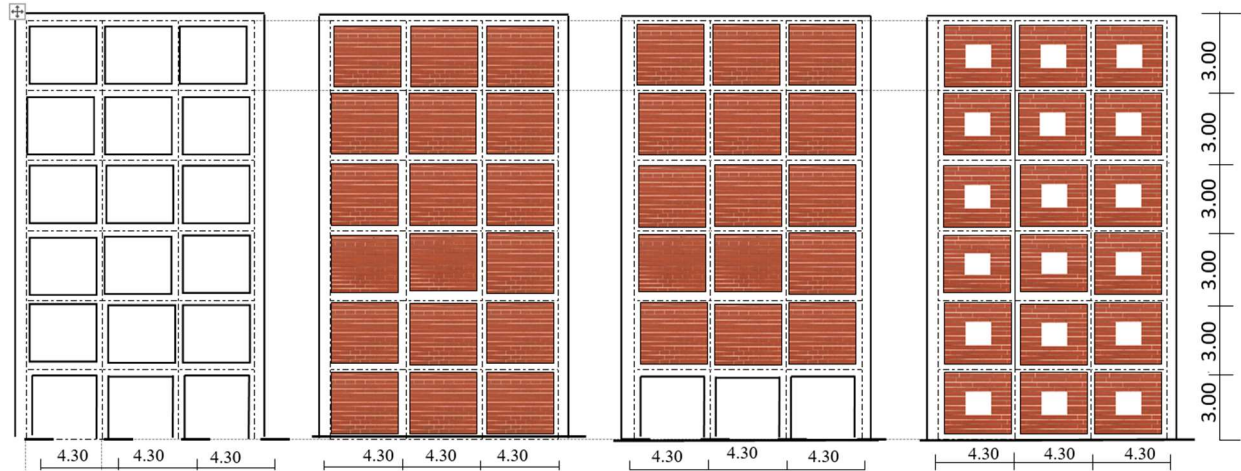
a) BF

b) FF

c) SF

d) PF
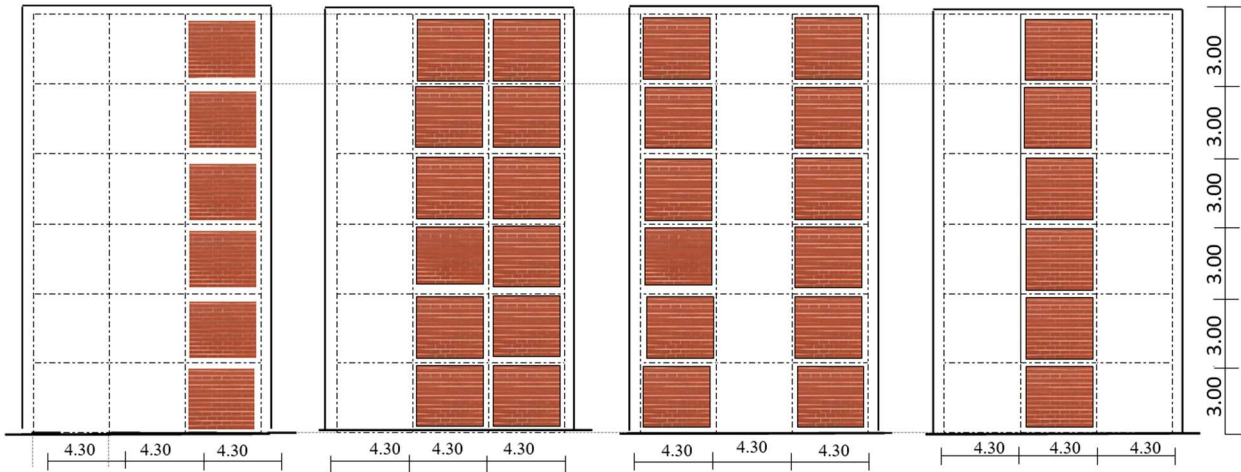
e) 2RLF

f) RF

g) MF

h) RLF

i) 3SF

j) UF
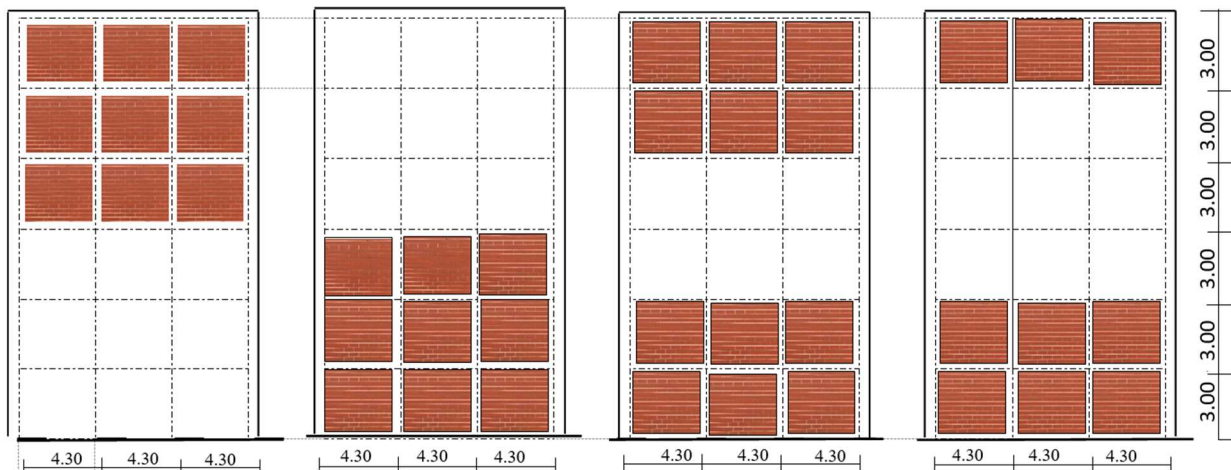
k) 2MF

l)MHF

m) DF   n) SDF
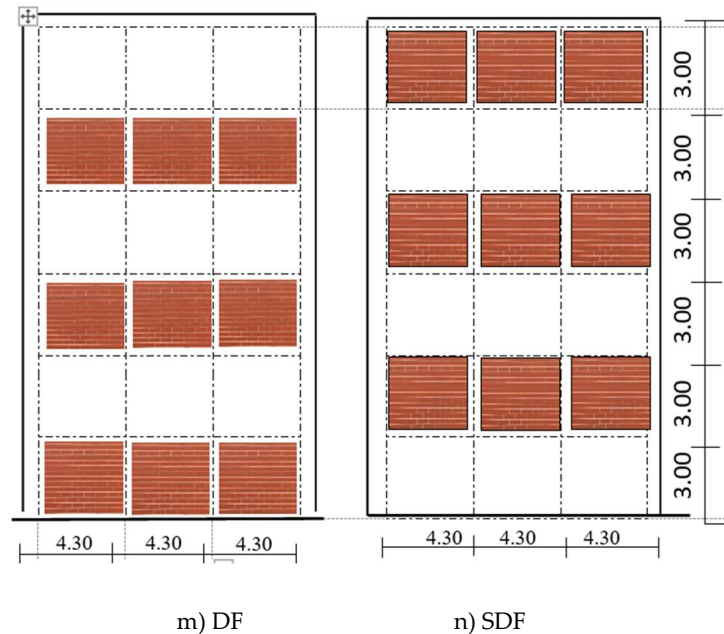
Figure 6.2: The considered frame configurations for the six-story building (all dimensions in m).

6.3. Description of the numerical model

6.3.1 Modelling of the RC frame

Due to its ability to carry out a series of analyses within affordable computational cost, the nonlinear dynamic studies were carried out by the software OpenSees software [105]. In addition, OpenSees provides a vast library of elements that can be adjusted to model different components of the structures. In this context and based on the verification that conducted previously in this thesis along with others from literature (e.g., see: [4], [113). Figure 6.3 shows the general description of the model implemented in OpenSees for the RC frame and the infill panel with a detailed description of the RC element model. As can be seen that the RC frame elements were modelled using the beam with hinges that are represented by fibre sections [19]. Using the Modified Radau hinge integration method [107,108] the RC elements (i.e., beam and columns were modelled using six integration points along each element. Figure 6.3 shows also that the distribution of these integration points along the RC element. The integration points are two for each hinge and two for the central part of the element, which is used in the element state

determination. The plastic hinge length (Lp) was computed according to the proposal of Paulay and Priestley as follows [109]:

$$L_p = 0.08l_e + 0.022d_b f_y \qquad (6.1)$$

Where d_b is the diameter of the longitudinal steel rebar, l_e is the length of the element, and f_y is the yield strength of the used steel in MPa.

The fibre-based section was adopted to discretize the RC sections into three main materials: unconfined concrete for cover, confined concrete for concrete inside the hoops and eventually steel material for steel reinforcements. The concrete cover was modelled using the concrete model (Concrete01) this concrete model represents the uniaxial concrete material with no tensile strength and a degraded linear unloading/reloading stiffness in compression. the confined concrete was modelled by incorporating the Concrete01 model with the confinement factor proposed by Kent and Park [132]. Steel reinforcement bars were modelled using the uniaxial Giuffre- Menegotto-Pinto model [110] with isotropic hardening, termed Steel02 in OpenSees, with the default parameters proposed by the software. For the beam-column joints, a rigid end-offset joint model was used [111]. The lengths of the rigid parts were half of the depth of the perpendicular element.
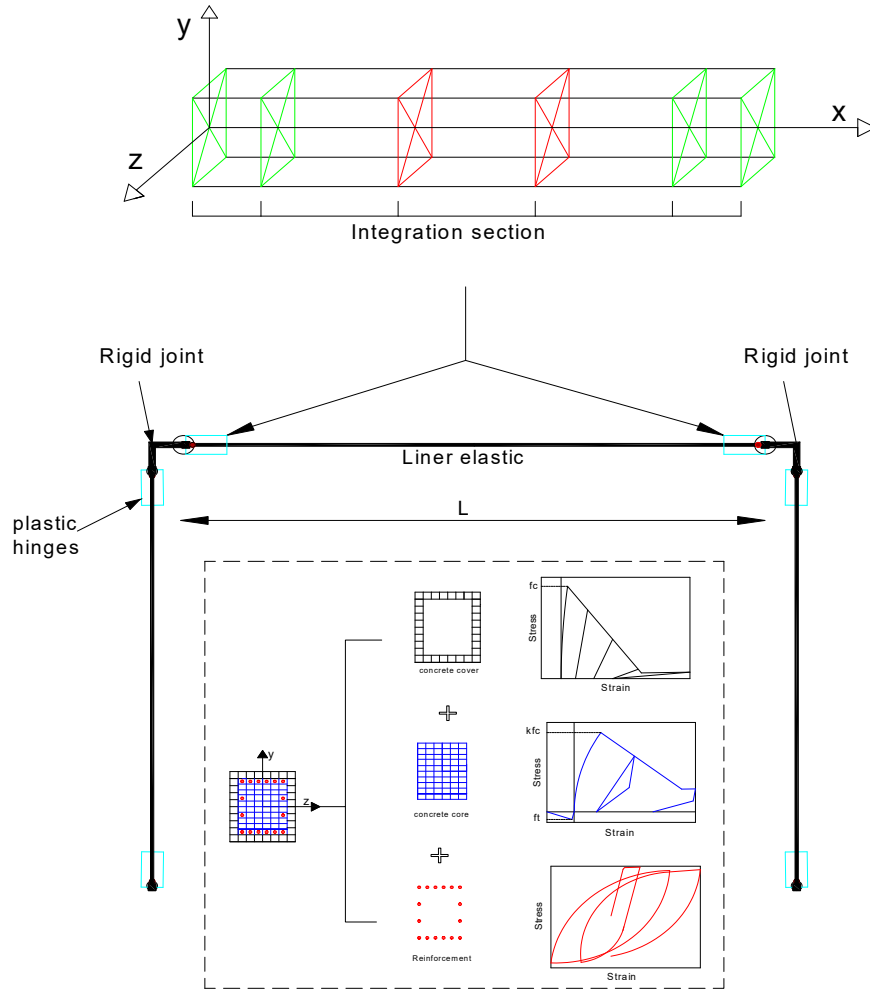
Figure 6.3: Adopted strategy for modelling RC elements.

6.3.2. Modelling of the masonry infills.

The strut model, which was proposed after the pioneered observations of Polyakov [21], is one of the most conventional models to consider the effect of the infill wall. The wide use of the strut model is promoted by its ability to consider the effect of the infill walls on global behaviour with an affordable computational effort. Thus, the infills were modelled using a single compressive strut element. The strut was defined as a compressive element with an equivalent area computed using the expression proposed by Hendry [53]. The constitutive model for masonry proposed by Hendry [53]. was used to define the input parameters for Concrete01 material in OpenSees. The model proposed is given as follows:

$$\sigma_m = f_m' \left[2 \frac{\varepsilon_m}{\varepsilon_{crm}} - \left(\frac{\varepsilon_m}{\varepsilon_{crm}} \right)^2 \right]$$ (6.2)

Where ε_m and σ_m are the compressive strain and the corresponding compressive stress of the masonry, respectively, f_m' is the maximum compressive strength of the masonry and ε_{crm} is the compressive strain at the onset of failure, which according to [112] ranges from 0.0015~0.002. In these analyses, the value of ε_{crm} was 0.002 in all models.

It is well established in literature (e.g., see:113,134-137 among others) that existing of an opening thought the infill wall change their behaviour. In this study, the reduction factor approach was adopted to count for the effect of the opening. Several proposals were found to count for the opening as a with reduced parameters of the fully infilled panels. These models account for different opening parameters, such as size, aspect ratio, type and position (e.g., see:113,134-137 among others). However, based on the assessment of the reliability of the existing models, Mohamed and Romão [113] presented a new model that showed adequacy performance compared to the other models. In this study, this model will be used to quantify the reduction factor. In this model two reduction factor for stiffness and strength were proposed these reduction factors are defined as follows:

$$R_s = 1 - 0.442\zeta_{area} - 0.554\zeta_l - 0.274\,\zeta_h$$ (6.3)

$$R_k = 1 - 0.543\zeta_{area} - 0.443\zeta_l - 0.041\,\zeta_h$$ (6.4)

Where R_s and R_k are the reduction factors for stiffness and strength respectively, ζ_{area} is the relative area of the opening to the wall's area, ζ_h is the opening height ratio to wall height, and similarly, ζ_l is the opening width ratio to the wall width.

6.4. Performance based procedures.

To assess the performance of the considered cases probabilistically, intensive nonlinear series of analyses were performed following the incremental dynamic procedures. Even though the outputs of the incremental dynamic analyses were then presented as IDA curves, several limit

states were defined to statistically analyse the performance of studied cases. The datasets were eventually used to develop the fragility functions. In the following sections, the description of each stage is briefly presented.

6.4.1. Incremental dynamic analysis

Incremental Dynamic Analysis (IDA) as a concept to subject a certain structure to substantial earthquakes that go for a different level of performance, was first proposed by Bertero [138] in 1977, and it is based on the dynamic elastoplastic time history analysis.. However, (Vamvatsikos, et al. [101]. presented IDA procedures in depth and comprehensiveness. They presented a detailed study that formulate the IDA, presented the main features of the procedures and the most convenient response curves of IDA. Given the computational effort behind running IDA procedures, an automated process was adopted to run the intended analyses which are presented in Figure 6.4. As can be seen, the process starts with the nonlinear model followed by gravity loads analysis. For the time history analysis, for each record i, several intensities I are considered to achieve all performance that is measured by engineering demand parameters EDP. As later will be mentioned that inter-storey drift (ISD max) is used as EPD. The intensity measure of each scaled record is recorded as the average spectral acceleration (Avg S_a) between 0.15 seconds to 1.5 seconds. The reason for using the average spectral acceleration (Avg SA) as an intensity measure IM on one hand is due to its compatibility with the range of fundamental periods of the considered cases (which have a wide range of variability in terms of periods). On the other hand, average spectral acceleration (Avg S_a) has been recommended in several research as a sufficient and efficient measure (e.g., see [139,140] among others).
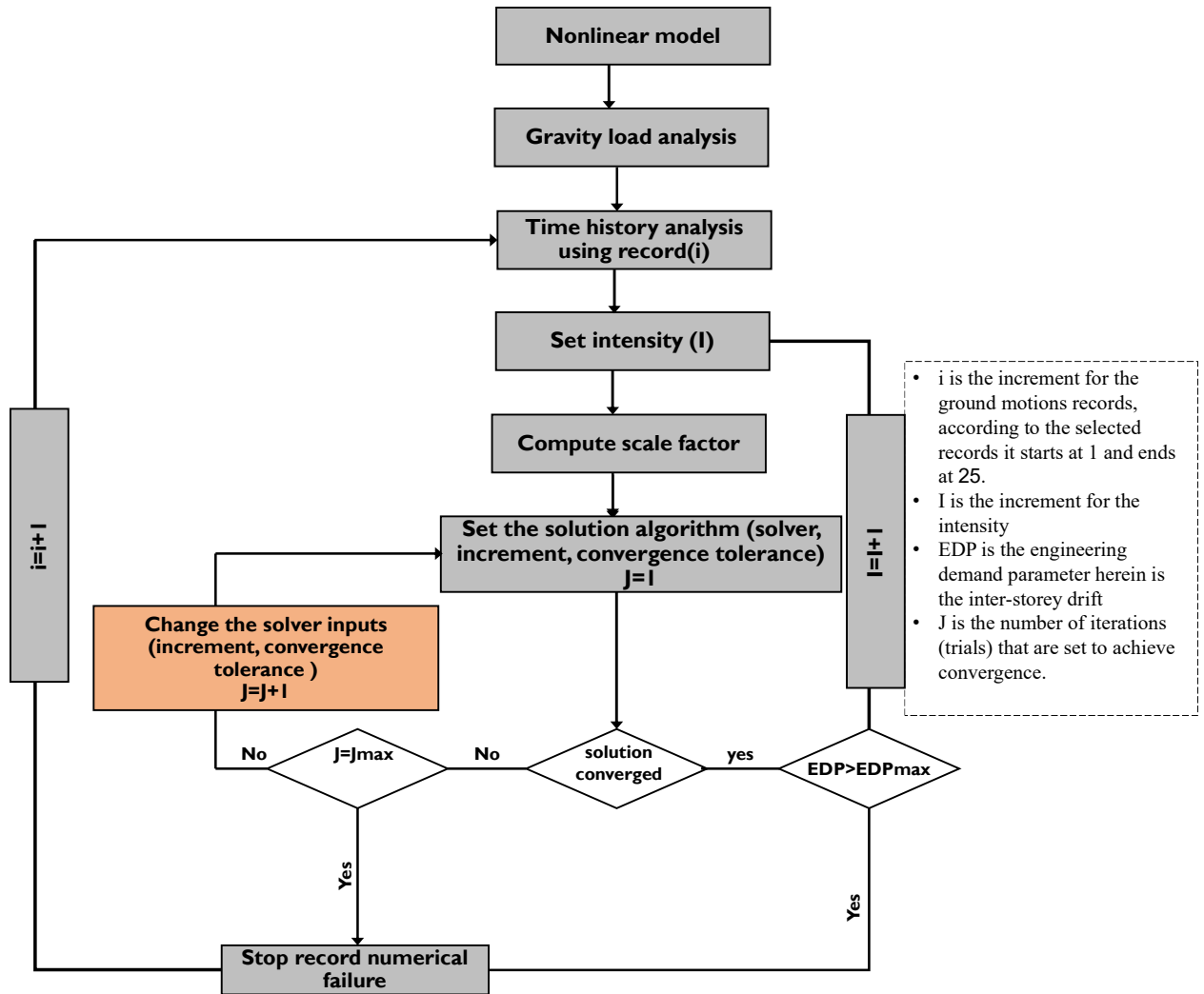
Figure 6.4: Adopted procedures to run IDA.

6.4.2. Ground motion record selection

As referred, the IDA procedures considera set of records that suite the seismic characteristics of the considered site, thus, 25 records have been selected from nearly 3500 records included in a database of ground motions recorded in the Mediterranean region. The selected records match target response spectrum defined in the Algerian Seismic Regulations RPA 99 corresponds to seismic Zone 3 of the Algerian territory and soil of type S3. The main input for the concerning design response spectrum is presented in Table 6.4. The selection criteria are like the strategy detailed in Eurocode 8. The following conditions are applied in the adapted selection procedures:

- The average spectrum of the selected ground motion should be higher than 90% of the code spectra along the period interval between 0.2 and 2 times the considered fundamental periods.

- The average spectrum of the selected ground motion should be higher than the code peak ground acceleration.

- The maximum scale for the selected records is defined to be equal or less than 2.5 or the original value to minimize the error in terms of maximum spectral accelerations.

For the visual representation, Figure 6.5 shows the response spectrum of the selected ground motions along with their mean value (thick dashed line) and the target response spectrum (dashed red line).

Table 6.4: the main site characteristics for the considered region according to Algerian Seismic Regulations RPA 99 [5]

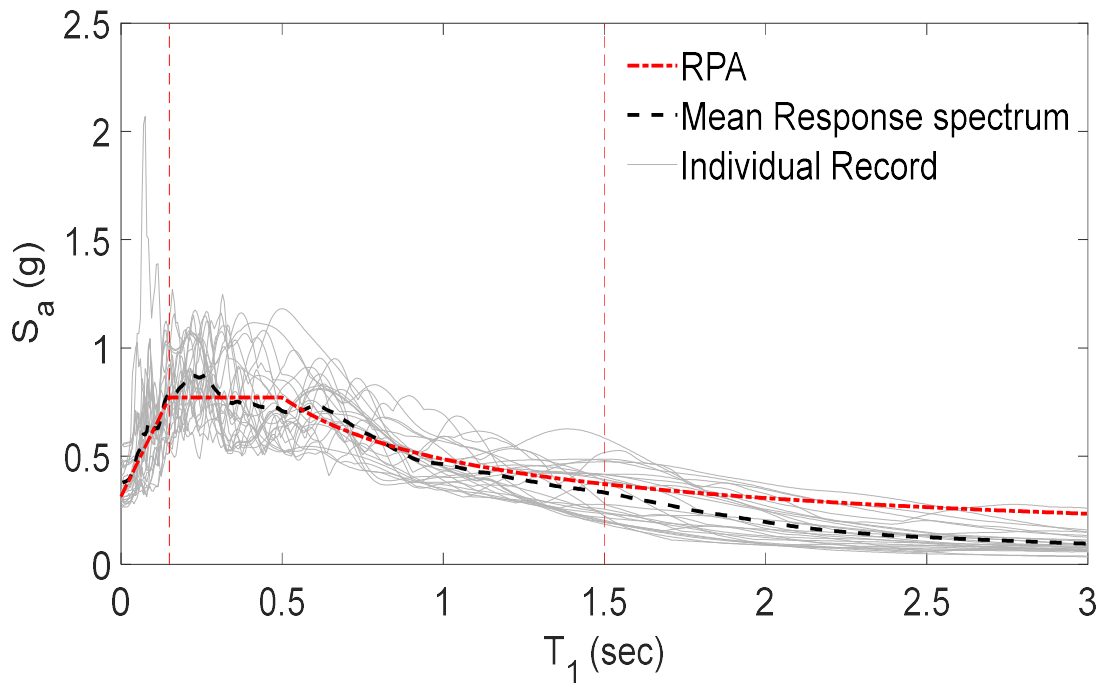| Seismic zones	Zone III: High Seismicity
The Constructions According of Their Importance	Groupe 2: Current constructions or those of moderate importance
Sites	Category S3: Soft Site
Coefficient of zone acceleration	A= 0.25
Quality factor	Q = 1.05
Damping correction factor	η= 0.94
Damping coefficient	ξ = 6 %

Figure 6.5: Scaled response spectra for the twenty-five ground motions with their mean response spectrum and the target elastic response spectrum for Zone III according to the Algerian Seismic Regulations RPA 99/2003.

6.4.3. Definition of the limit states

Limit states are a measure used to describe the state of the structure according to predefined levels of damage, e.g., the onset of cracking, yielding, collapse. Avast body of have been conducted! to define limit states for the performance of RC buildings (see, for example, (FEMA-273 [85], 1997, FEMA-356, 2000 [81], Rossetto, et al., 2003 [141], Ghobarah, 2004 [103], Rossetto, et al., 2005 [102]) and several others). In the present study, the limit states listed in Table 6.5 were used, which correspond to the limit states proposed by Rossetto, et al. [102], since the structural requirements and the performance in terms of maximum displacements between floors are defined by the height of the structure (ISD max). The performance of the structures was evaluated considering the deterministic limit states. The performance is determined for each ground motion by determining the value IM at which the deterministic value of a given limit state is reached, as shown in Figure 6.6. Later in this chapter, the extracted datasets are used to quantify the fragility corresponding to each limit state.

Table 6.5: The adapted threshold values for the considered limit state of damaged given by the value of inter-storey drift in percentage.

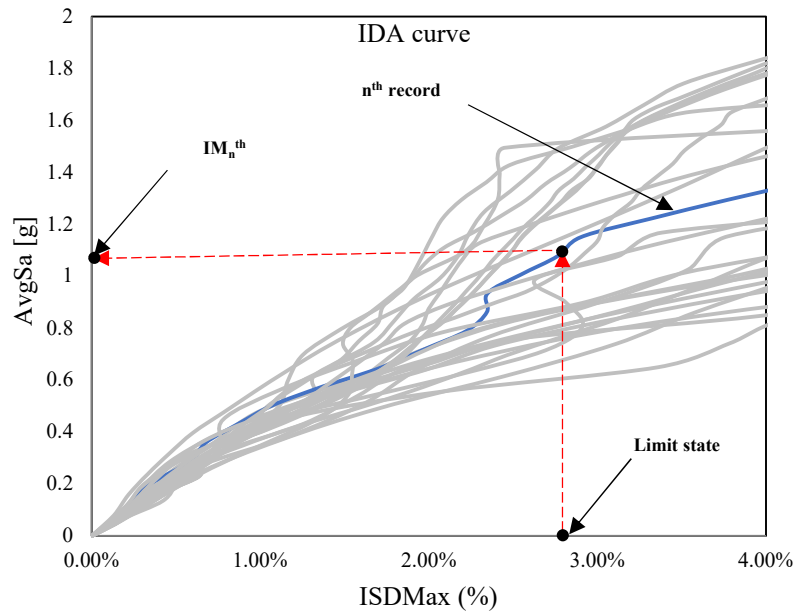| Damage State	Slight damage	Light damage	Moderate damage	Extensive damage	Partial collapse	Collapse
IDR(%)	0.05	0.08	0.30	1.15	2.80	> 4.36

Figure 6.6: Performance analysis based on the IDA curves for a deterministic limit state.

6.4.4. Fragility curves

The seismic vulnerability of RC buildings can be assessed by developing fragility curves which then can be integrated with a consequences model to develop the final fragility function. These functions are given by the probability that a certain damage state of the structure or one of its components exceeds a given seismic intensity expressed by intensity measure (IM). Thus, the key parameters for the fragility function are the engineering demand parameter, the threshold of onset of the damage state and the intensity measure for the seismic action. A damage state may correspond, for example, to the spalling of the concrete cover of the columns, infill walls cracking or, even worse, losing an element due to severe damage which eventually leads to the collapse of the structure. These states can generally be related to a structural seismic Engineering Demand

Parameter (EDP), such as the global drift of the building (which defines as the ratio between the top displacement to the total hieght of the building). Examples of seismic intensity measures are the earthquake's maximum horizontal acceleration or the spectral acceleration magnitude and the structure's fundamental period (T_1).

In literature, three approaches can be used to drive a fragility curve [142];

- ❖ Empirical fragility function using the recorded data from pervious earthquake.
- ❖ Experimental fragility curves
- ❖ Expert-based/ judgmental fragility funciton curves.
- ❖ Theortical fragility function

However, the first two approaches require the availability of a considerable amount of observations and resources, respectively which are not affordable, particularly for developing countries such as Algeria. In addition, the third approach is smeared with manifold uncertainties. In this context, fragility curves herein are determined using analytical procedures based on the study of the nonlinear seismic response of a numerical model of the building. The obtained responses from time history nonlinear analyses are associated with a set of damage states to drive the level of performance at a given level of the seismic intensity measure (Vamvatsikos & Cornell, 2002). It is worth noting that to assure compatibility with the seismic scenario provided by the Algerian seismic regulation RPA99/version 2003 the used seismic records were selected as referred to match the target response spectrum and the studied area.

6.4.5. Seismic vulnerability assessment: influence of the limit state definition

Figure 6.7 represents the fragility curves of a building corresponding to six different damage states: slight damage, light damage, moderate damage, extensive damage, partial collapse and total collapse according to the referred reference. For example, for AvgSa=2.0g, there is a probability of 95% to reach the state of partial collapse damage and 80% to reach the state of total collapse damage. It is clear from this illustrative example that the fragility curves provide an essential information regarding the performance or capacity limits of the resistance of a structure under different earthquakes.
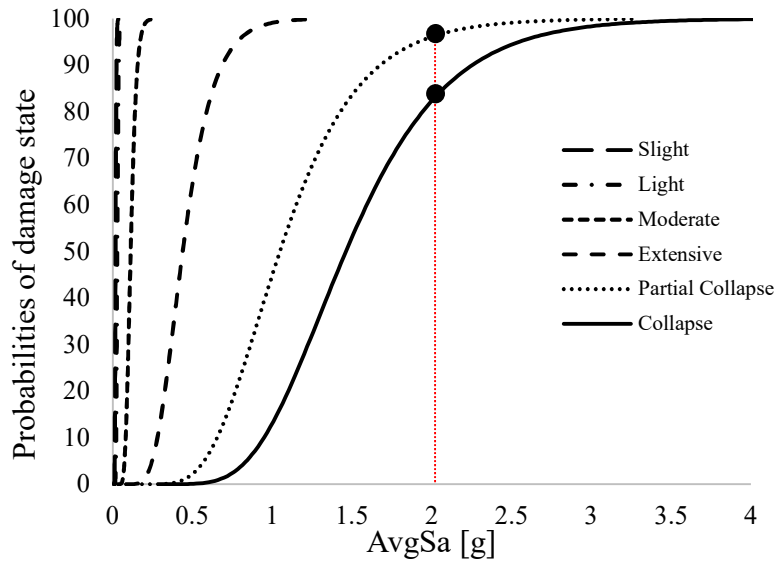
Figure 6.7: illustrative example of the building fragility curves at different performance limits.

Given that the comparison between the building performance was held using the fragility function, Figure 6.8 illustrates an example of two fragility curves for two types of buildings with different characteristics (e.g., differences in geometry, length, and the number of bays) that correspond to the same damage state as a function of maximum earthquake acceleration. As can be seen, building 1 shows a better performance where if the two buildings experience an earthquake of AvgSa=1.0g, there is a probability of 95% for building 1 to exceed this state, while this probability for building 2 is only 15%. This result shows us that building 1 is more vulnerable to damage from an earthquake of a particular intensity than building 2.
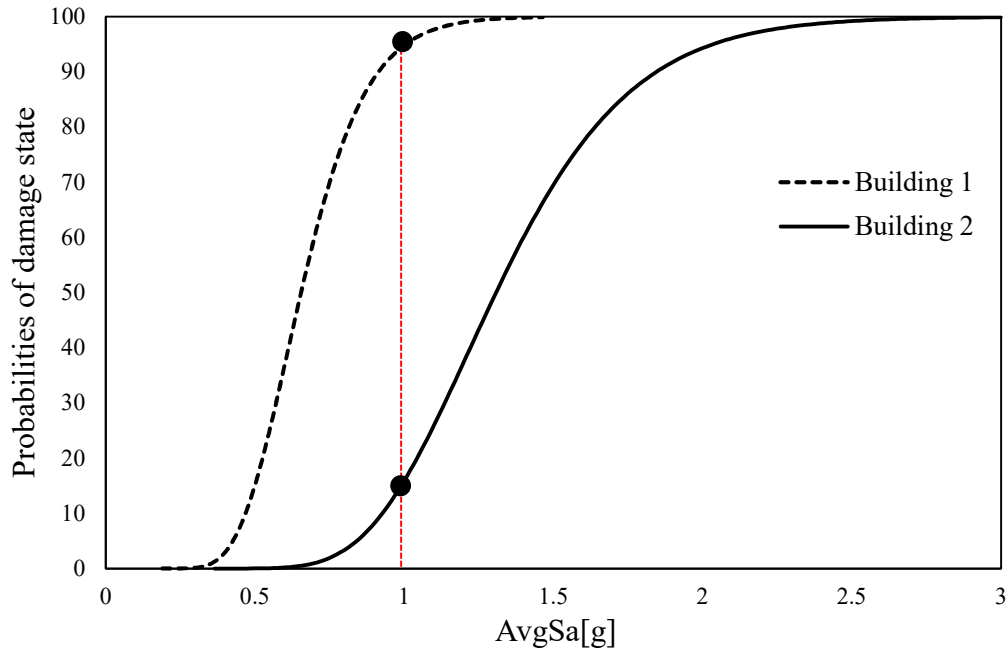
Figure 6.8: Fragility curves for two differents buildings.

6.5. Results and discussion

6.5.1 Results of the IDAs

The incremental dynamic analyses were performed for all models using the selected ground motions records. The results in Figure 6.9 illustrate the IDA curves obtained for the different structures. Each curve represents the response of structure given by the maximum inter-storey drift ISD $_{max}$ and the correspond IM of the used record expressed as AvgSa. To assess quantitatively the effect of infill configurations on the global behaviour of the RC frames, several comparisons of the IDA curves were held based on a set of variables, for example, the effect of openings compared to the bare frame and full frame (PF), the horizontal continuity of the infill walls (RF and MF models). In addition, the difference is in the horizontal presence of the filled walls (2RLF and RLF models), and the presence of the soft floor with the different concentration: On the first three floors (3SF), on the middle three floors (MHF), and the upper three floors (UF). Eventually, the homogeneity in the variation in the presence and absence of the fill walls (SDF and DF models).

In the referred context for all models, the SF, SDF, and DF structures always exhibit higher values of ISD $_{max}$ for low IMs (IM: 0.02-1.3 ,0.45- 1.7 ,0.45- 1.7) respectively, even when compared to those of the bare frame and full frame. This is due to the soft-story failure mechanism that occurs very early as a result of the structural configuration that is considered for these structures, especially for model SF (IM: 0.02-1.3), which is considered the worst behaviour due to the concentration of the soft floor at the first floor only, which leads to premature soft storey behaviour at the weak floor (i.e., the ones without infill).

On the other hand, for a given IM level, the fully infilled structure (FF), followed by the partially infilled structure (PF), generally exhibits lower ISD $_{max}$ values than the corresponding bare frame structure. As for each of the two RLF and 2RLF models, they were found similar in their response seismic with an estimated value of IM: 2.7 for both models. Thus, it can be concluded that the position of the walls with a regular distribution over the building height has a minor effect compared to those with irregular distribution over the height of the building. In contrast, RF and MF models showed a higher difference in the value of IM at the point of collapse estimated at 2.3 and 2.8 for MF and RF, respectively. This is due to the effect of the horizontal discontinuity of the masonry walls which affects the horizontal continuity formed for the infill walls in the model and, thus, affects the general behaviour of the building.

For models 3SF, MHF, and UF, which show the impact of the development of the soft floors at the total response of the concrete buildings, where it is clear that the building with three different soft floors, the location of the three first floors, three middle floors, and three upper floors have significant differences in their responses expressed in term of IM which it was recorded that (0.5 -2.8), (0,6 -2.3) and (0,45-1,6) for 3SF, MHF, UF respectively. This can be interpreted as the effect of the vertical presence of the soft floor along the height of the building, where it is noticed that the behaviour of the model that has soft floors at the bottom developed a better performance compared to those with soft floors at the middle. The model that has soft floors at the top of the building is considered the worst model in terms of behaviour and in terms of performance.

For the two models SDF and DF, which shows the effect of homogeneous vertical discontinuity in RCbuildings, consideringthat the soft storeyon the first floor, asimilar behaviourwas observed for both models due to the homogeneity in the presence of the soft storeyat the level of the floors of the building, with no effect of the presence of the soft storeyat the ground

floor.Therefore, the differences in the strut parameters have a minor effect on the mean IDA curve. However, the effect of these different modelling parameters will also be analysed in further steps of the performance assessment of the structures, namely on the fragility curves obtained for different limit states. Even though the IDA curves give qualitative information on the behaviour of the building, fragility curves provide a more comprehensive and quantitative representation to facilitate the comparison between the different structures and to identify the most vulnerable cases.
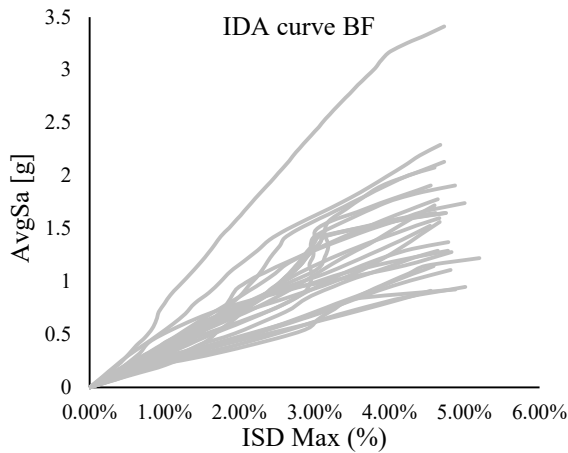
BF-6
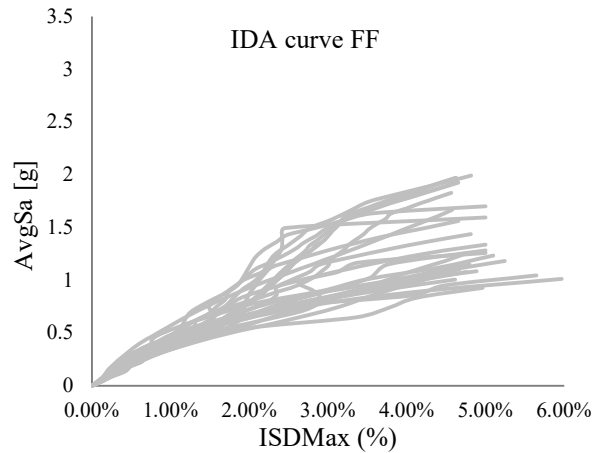
FF-6
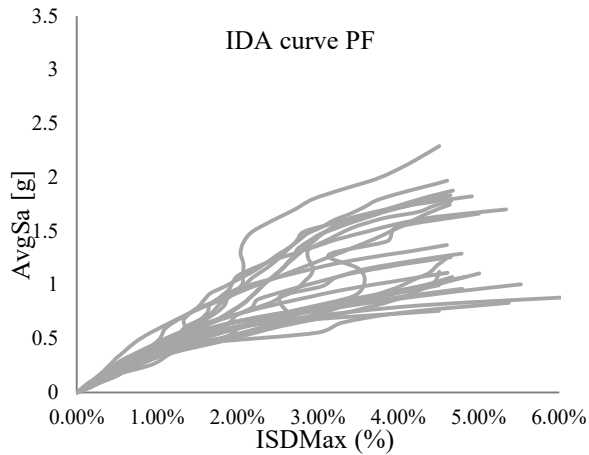
PF-6

SF-6
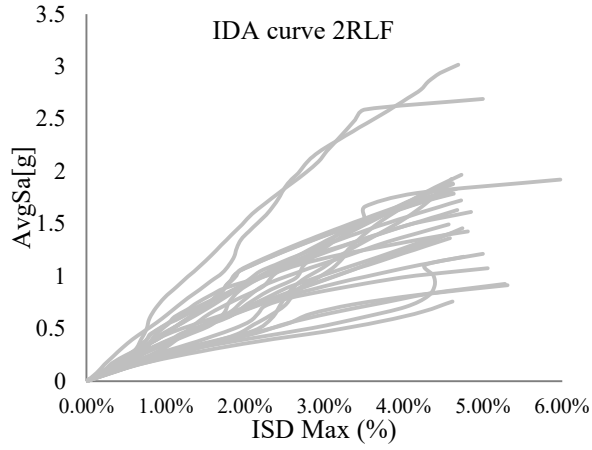
2RLF-6
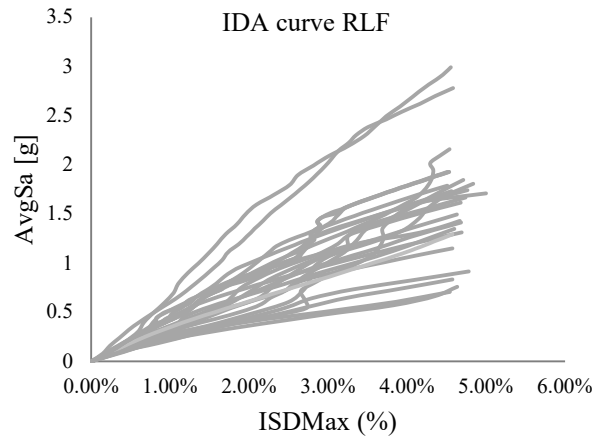
RLF-6

RF-6

MF-6

3SF-6

MHF-6

UF-6   2MHF-6
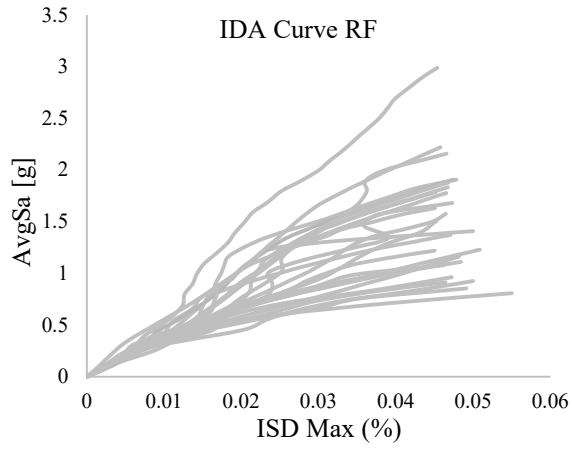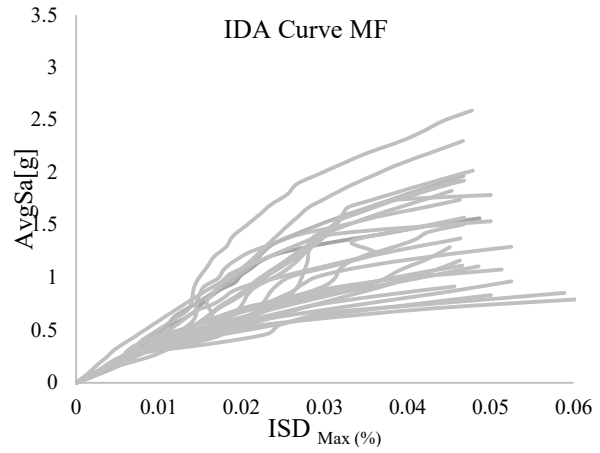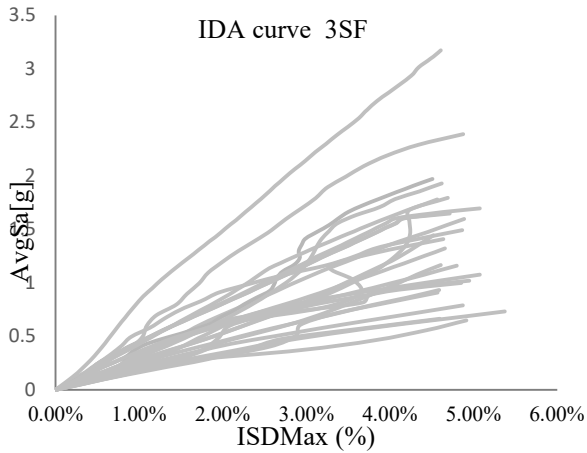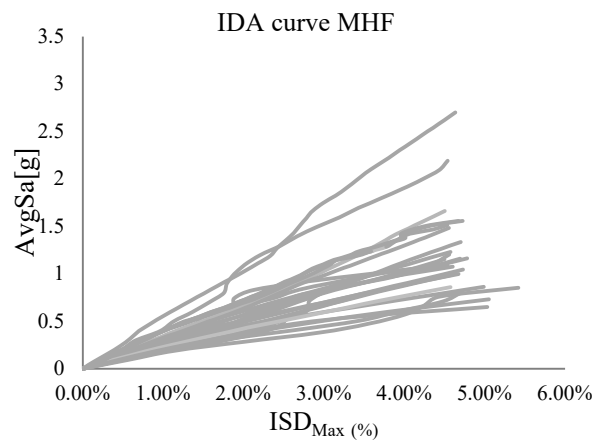
SDF-6   DF-6

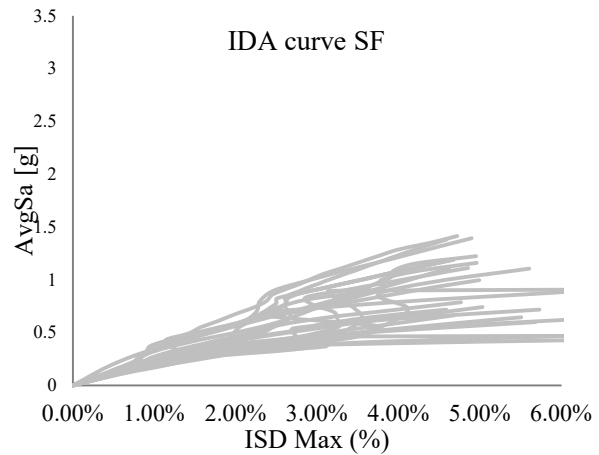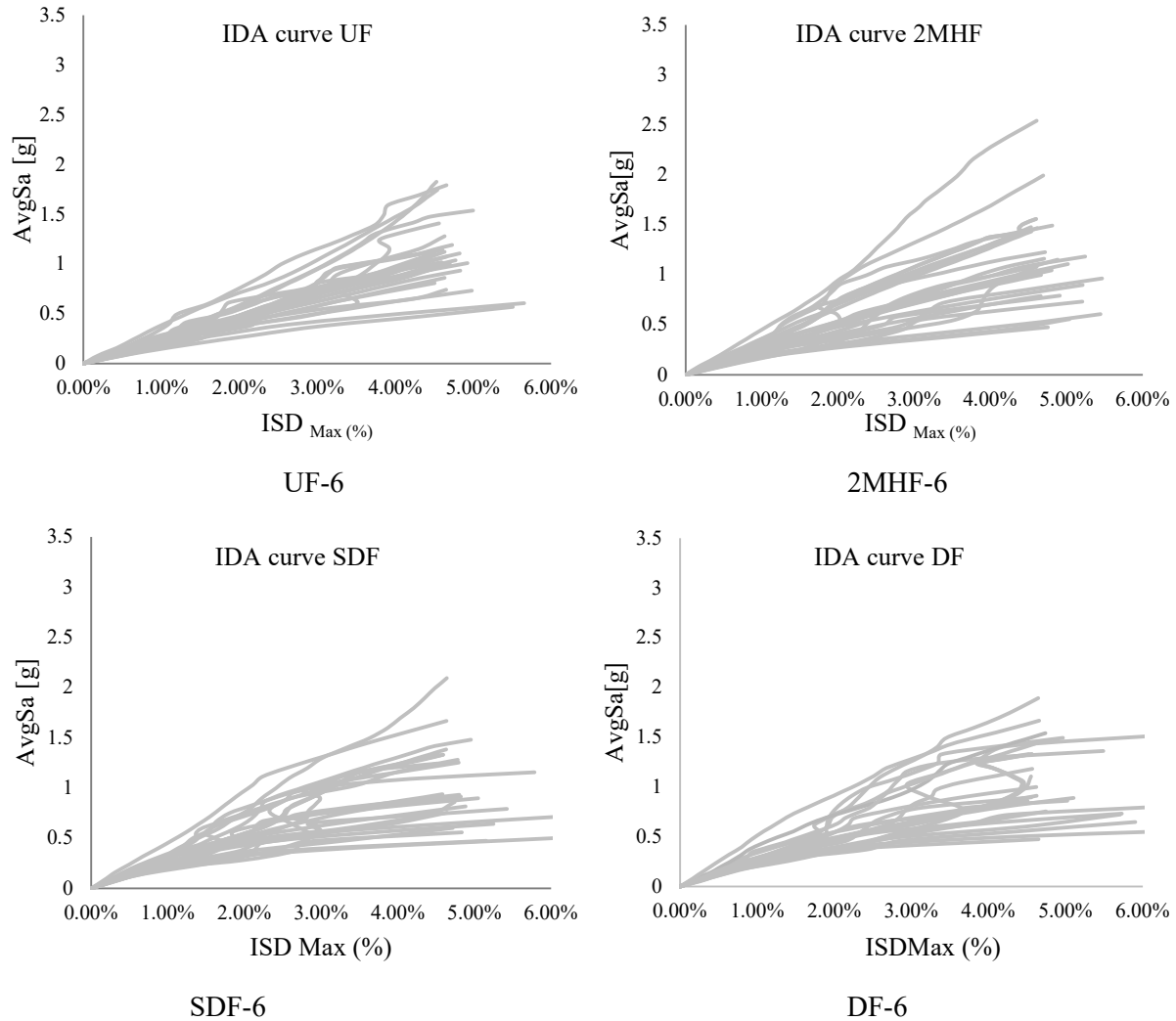Figure 6.9: The IDA curves obtained for the cases of study.

6.5.2 Fragility fucntion curves

Using the described procedures in the previous sections, the dataset that corresponds to each threshold of the damage state has been obtained. Several proposals were found to fit the empirical dataset and therefore define the theoretical fragility function such as Gamma distribution, normal distribution and etc. However, the use of the lognormal cumulative was found to provide adequate results [143]. The lognormal cumulative function parameters were obtained for the six limit states for all considered buildings. Figure 6.10 presents the obtained fragility functions for all considered cases.

BF

FF

PF

SF

RLF

2RLF

RF

MF

3SF

MHF

UF
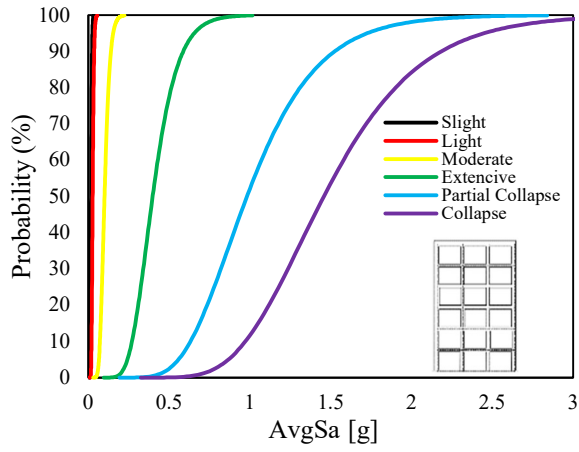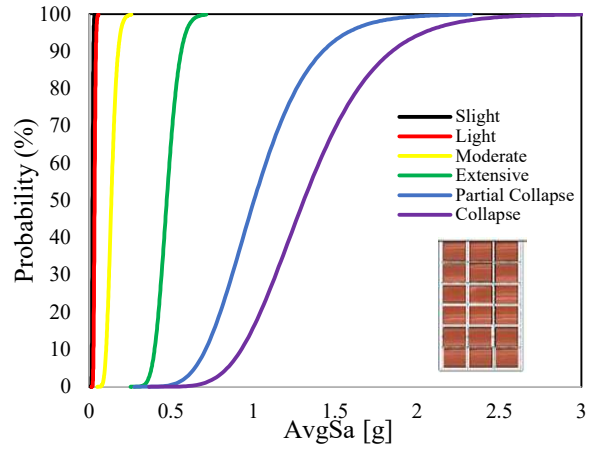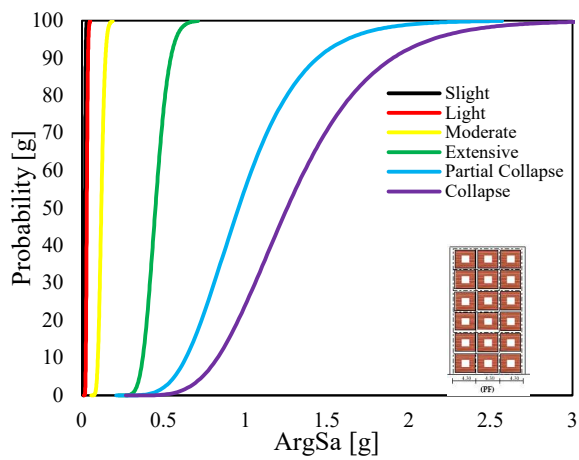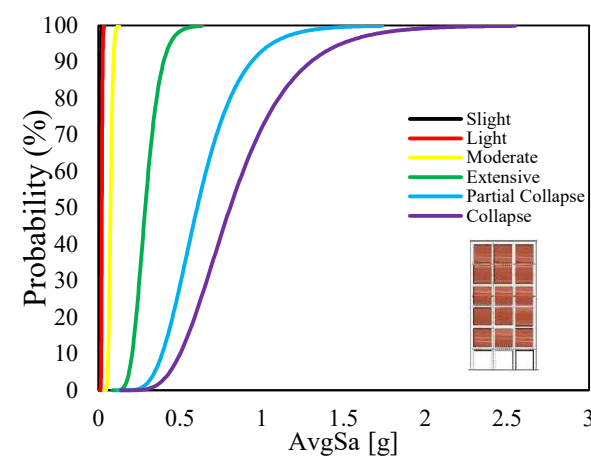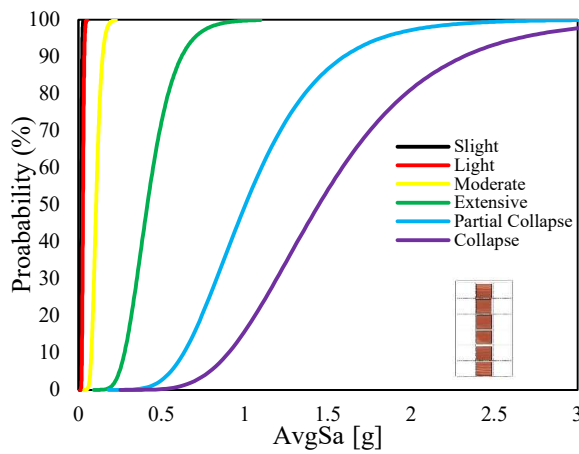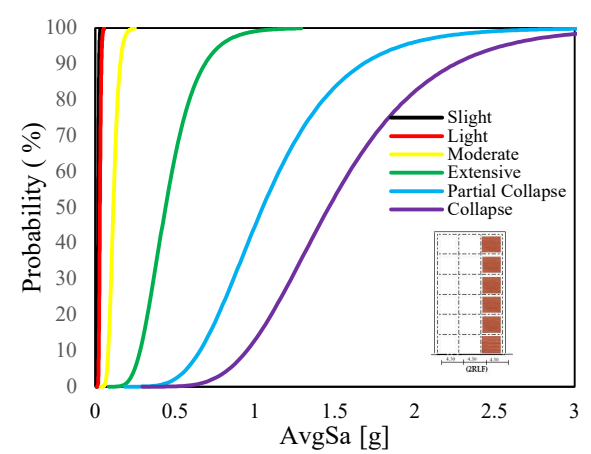
2MHF
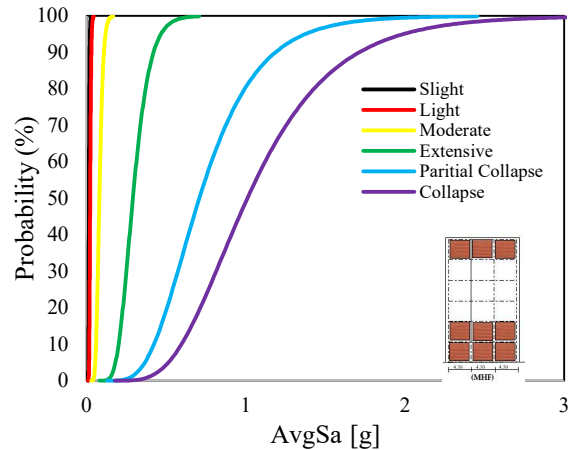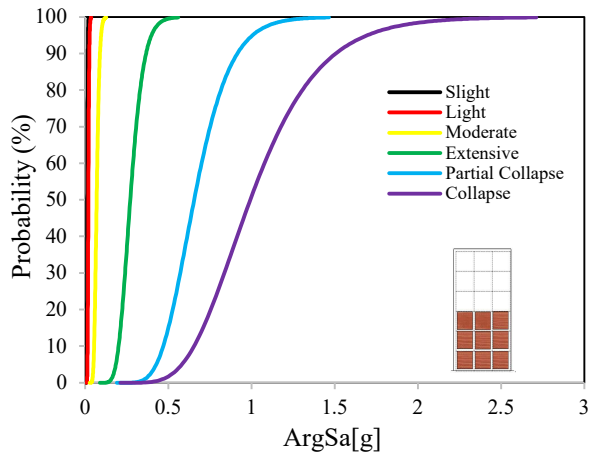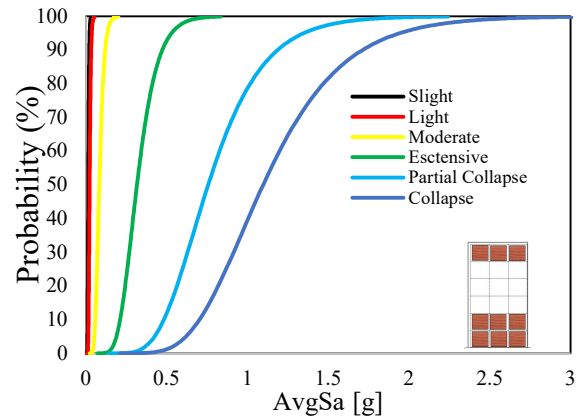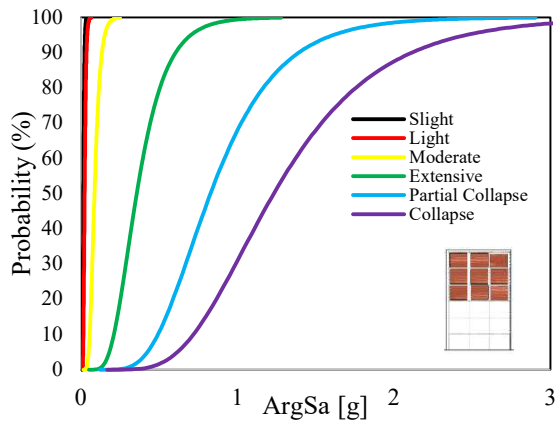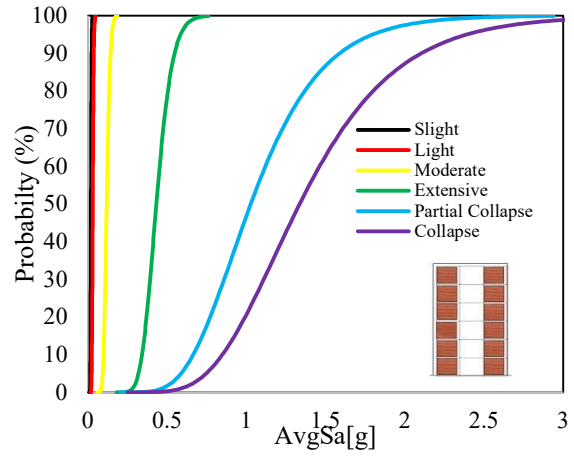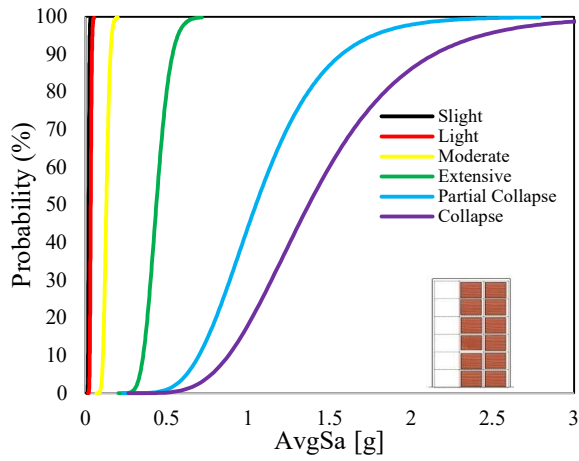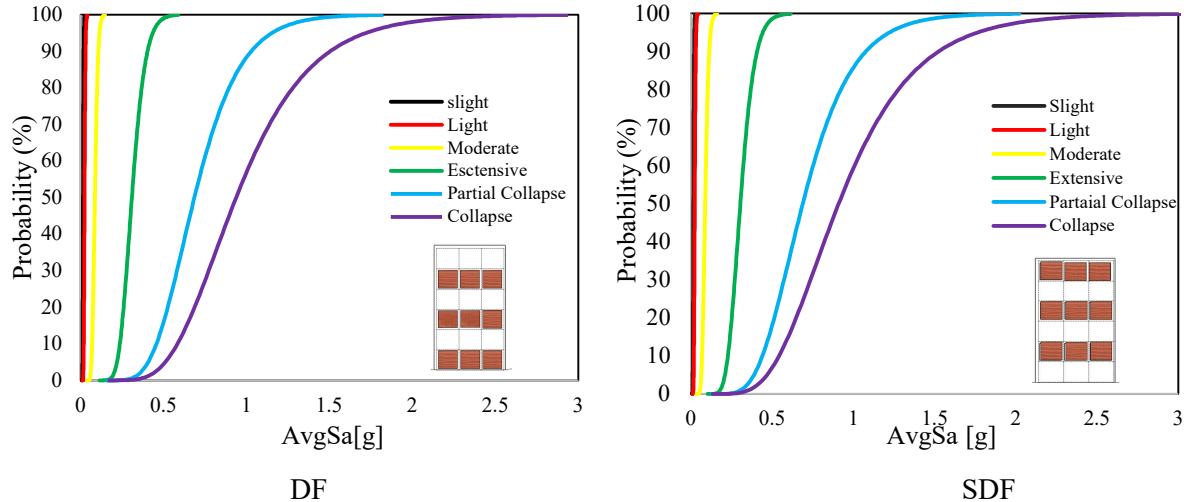
Figure 6.10: The obtained fragility functions for the considered case of studies

As a general comparison, all cases that involve one or more soft-storey exhibited fragile behaviour due to their inherited fragility for forming the weak storey mechanism. Another aspect that is worth noting, cases that involve a continuous infill over the height (e.g. RF, Mf, 2RLF and RLF) show better performance compared to those with discontinued infill wall at a certain level. In addition, the existing two subsequent bare floors enhance the performance compared to the cases with one bare between to floor with infills. The latter remark can be interpreted that having two or more bare frame provide a higher level of flexibility for the structure to absorb the vibration without causing damage.

6.5.3. Fragility curves result for all model in each cases of state limites

As a quantitive comparison, Figure 6.11 compares between all involved cases for each level of performance (i.e. the six damage limit states). Recalling what was reported in the previous comparison, the SF, UF, DF, and SDF model exhibited vulnerable performance among all studied cases not only for the higher damage state but for all considered damage limit states. Thus, these configurations are not recommended for the newly constructed building. Also, it is clear that cases involving continuous infill in vertical and horizontal directions exhibited a better performance closer to those recorded for reference case i.e. FF. in order to have a more clear comparsion between all involved cases, the comparison was made in a more effective way considering bare frame and full frame result as a reference cases. For that end, the models were divided into groups

that converge on the type of effect as shown in Table6.6. The upcoming sections discuss the comparison of each groups along with the main conclusions.

Table 6.6: The considered cases of study and their main comparison features.

Study Cases	Comparison principle	Comparison cases	Limit State for Comparison
Case N° 1 BF, FF, PF	Effect of openings in the walls of the building		
Case N° 2 BF, FF, SF, 3SF	Effect of a soft floor on the ground floor		Slight Light
Case N° 3 BF, FF,3SF UF, MHF, 2MHF	Influence of the location of the soft storey		Moderate Extensive
Case N° 4 BF, FF, 3SF, SDF, DF	Effect of vertical discontinuity of infill walls		P. Collapse Collapse
Case N° 5 BF, FF, RF MF	Effect of horizontal discontinuity of building walls		
Case N° 6 BF, FF, 2RLF, RLF	Effect of the positioning of the vertical distribution of the infill walls.		
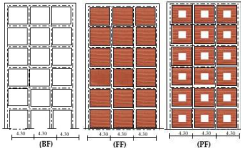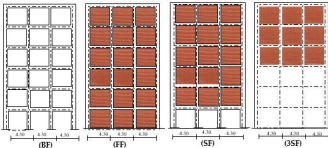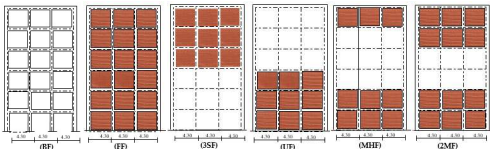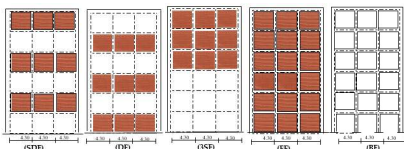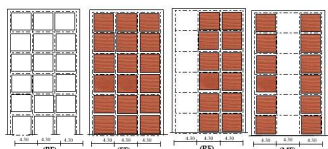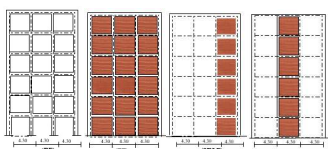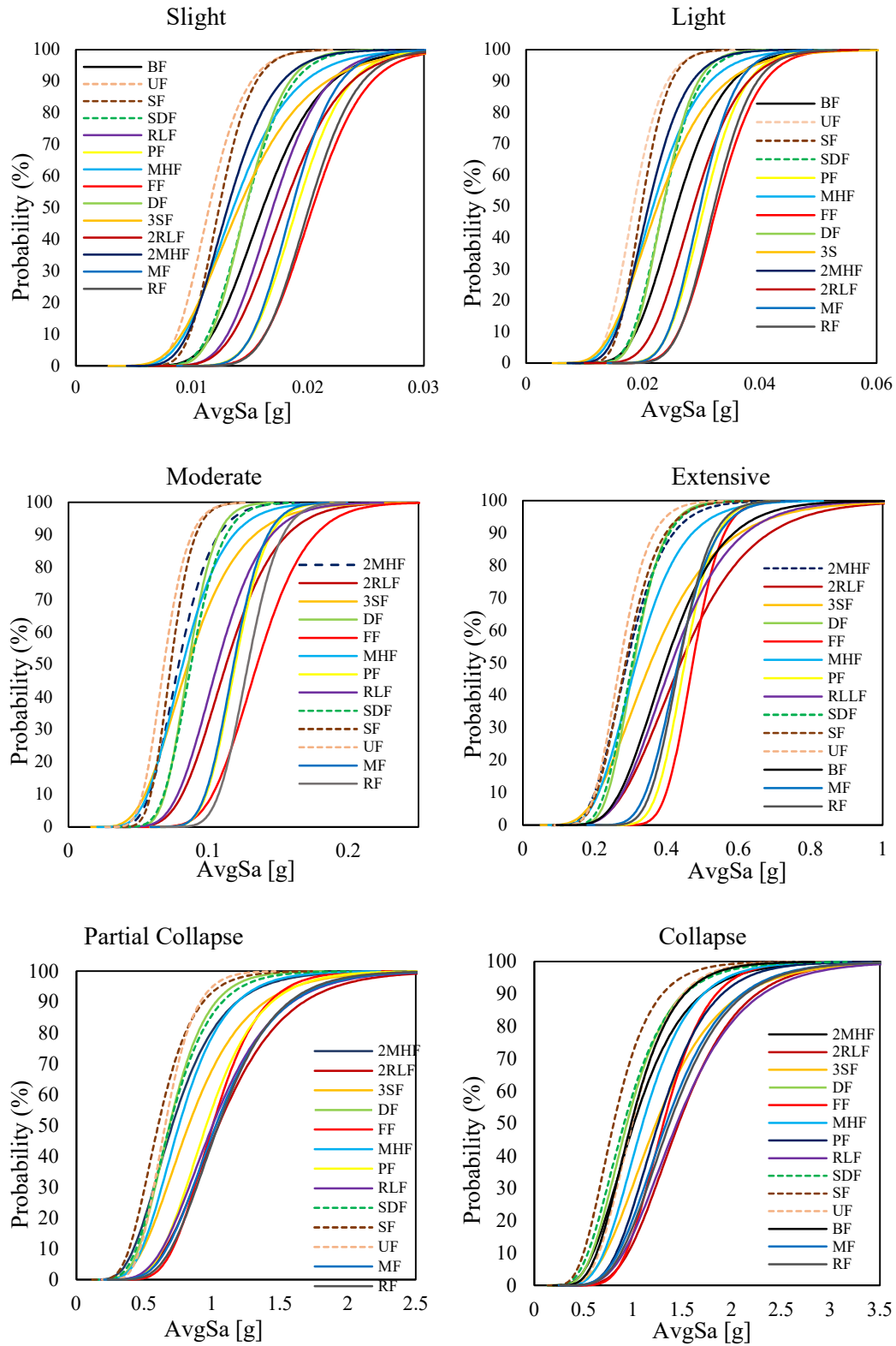
Figure 6.11: The obtained fragility functions plotted for each limit states for all considered buildings.

Case Study No 1 effect of openings in the infill walls

Figure 6.12 shows the comparison between the fragility functions obtained for PF compared with the FF and BF as reference cases for the considered six damage states. As can be seen from the PF and FF structures show better performance than the BF structure for all cases of limit states (slight, light, moderate, extensive, partial collapse, collapse), due to the contribution of infill walls in increasing the rigidity of the buildings, and thus better behavior and performance. It is worth noting that the latter conclusion is drawn for the cases that infill loaded along their in plane. Another aspect that can be seen that the fragility curve for partially infilled wall i.e. PF, for most cases, locates at a middle between the other two curves. Therefore, it is can be interpreted due to the reduction in strength and stiffness of the wall but with the same uniformity of loading paths. Also, by looking at the first limit states cases (slight, light, moderate and extensive), it is clear that each of the structure's FF and PF curves start latter (the lower tail of the fragility function), which is not the case for the BF which shows a sooner trigger of the damage state. This aspect important when assessing the losses based on the fragility function.

In a more quantitive way, the BF structure can be seen to reach the slight and light limit states for AvgSa values lower than 0.015 g for the slight limit state and 0.02g for the light limit states, respectively. In comparison, the FF and PF structures require excitation levels higher than 0 .015 g for the slight limit state and 0.025g for the light limit state.In other words, and by quantitative analysis, the probability of exceeding the slight and light limit states for structure BF at 0.02 g was about 80% and 55%, respectively. In contrast, structure FF was 35% and 10%, as well as for PF, it was 55% and 15%, respectively.Likewise, for the case of moderate limit state at 0.1g, the probability of exceeding these cases for the structure BF was 55%, while FF and PF structures were 10% and 15%, respectively.For extensive damage limit state cases, the collapse probability for structure BF at 0.1g was 65%, while we recorded a probability of 25% and 30% for both the FF and PF frames. For the partial collapse limit state, each of the structures BF, FF, and PF now have similar behaviour and performance and are closer as well as their capacities. In this case, the capacities of the limit state condition of BF, FF and PF frames can go up to 2.5 g.
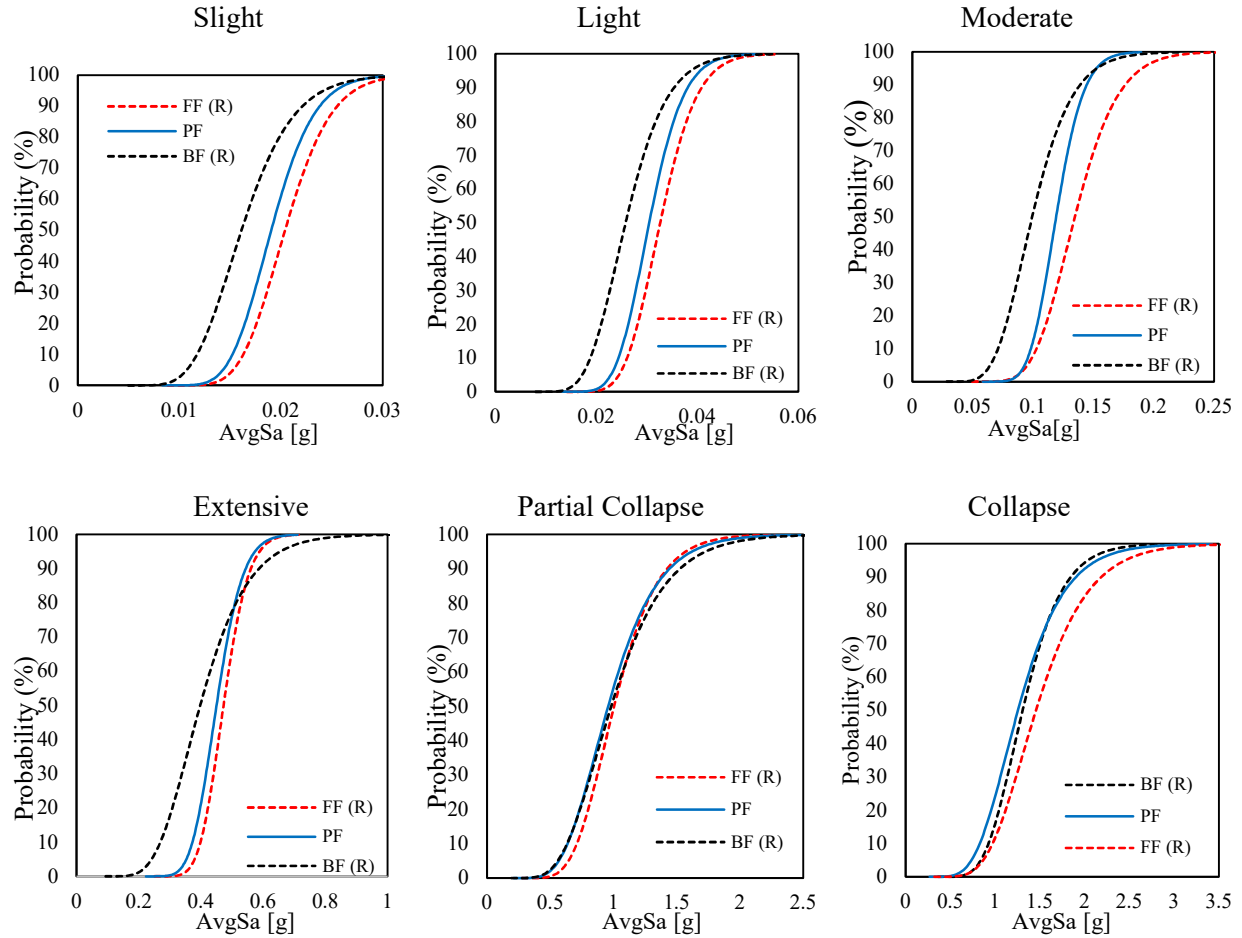
Figure 6.12: Comparison between the fragility functions obtained for PF compared with the FF and BF as reference cases.

Finally, for the collapse limit state, the capacities of the limit states of the BF, PF and FF structures can be increased by 2.7 g,2.7 g and 3 g, respectively. In these, the BF structure seems to be able to represent and resemble the behavior of the PF structure, but on the other hand, the FF structure stay has the best performance behavior when seismic impact. Figure 6.13 shows the values of AvgSa reached by each of the models FF, BF and PF, corresponding to the probability of exceeding an estimated 50% corresponding to the buildings reaching a state of collapse.

Figure 6.13: Radar plot of AvgSa at a probability of 50% for BF, PF and FF at different damage limit state.

Case Study N° 2: Effect of a soft floor on the ground floor:

Figure 6.14 shows the comparison between the fragility functions obtained for SF and 3SF compared with the FF and BF as reference cases for the six considered damage states. As can be seen from the SF structure can be considered as the worst performing among all the studied configurations, especially in severe damage cases, while the 3SF structure shows better performance compared to SF for all the limit states cases (slight, light, moderate, extensive, partial collapse and collapse). The latter remark can be interpreted as the weak floor failure mechanism for the SF which is also the case for 3SF. However, the flexibility that is found in 3SF, due to the three-storey consequent bare frame, compromises this effect for that case.

As a numeral analysis of the obtained data, the SF structure can be seen to reach the limit states for AvgSa values lower than 0.02 g for the slight limit state and 0.03 g for the light limit state, respectively. On another hand, the FF, 3SF and BF structures achieve a higher level of IMswhich are higher than 0.03 g for the slight limit state and 0.05g for the light limit state, respectively. In other words, the probability of exceeding the slight limit state at 0.015 g and light limit states at 0.02 grecorded 85% and 55% probability of exceedance, respectively. In contrast, structure FF was 5% and <1%, as well as for 3SF, it was 55% and 30%, and for BF, it was 40% and 10%, respectively. Likewise, for the case of moderate limit state at 0.1g, the probability of

exceeding these cases for the structure SF was 95%, while 3SF, BF and FF structures were 75%, 50% and 05%, respectively. For extensive damage limit state cases, the probability for structure SF at 0.40g was 90%, while it was recorded a probability of 60%, 50% and 05% for 3SF, BF and FF, respectively. for the partial collapse limit state, the probability of exceeding of this limit for SF at 1 g was about 95% while these values were recorded 68%, 53% and 50%, for 3SF, BF and FF, respectively. Eventually, probability of exceeding for the collapse limit states of structures SF, BF, 3SF and FF at 2 g were about 99%, 95%, 88% and 85%, respectively. Figure 6.15 shows the values of AvgSa reached that recorded for the models FF, BF,3SF and SF, corresponding to the probability of exceeding of 50% corresponding to the buildings for the considered limit states. It is clear that this plot confirms the previous remarks regarding the fragile behaviour of the SF and 3SF compared to the reference cases.

Figure 6.14: Comparison between the fragility functions obtained for 3SF and SF along with the FF and BF as reference cases.
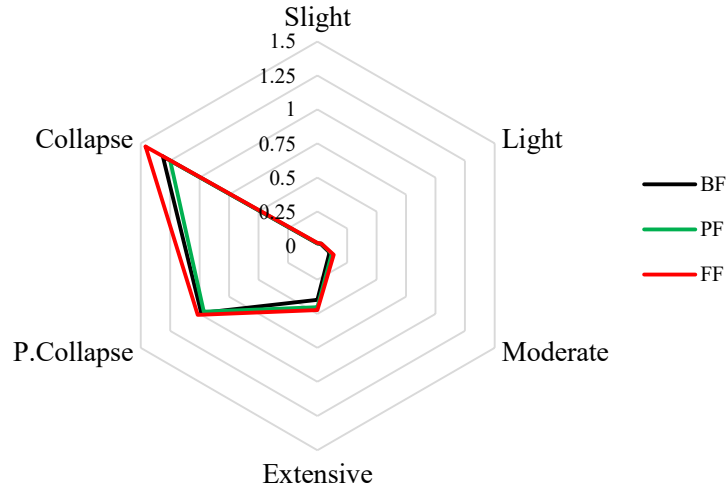
Figure 6.15: Radar plot of AvgSa at a probability of 50% for BF, SF,3SF and FF at different damage limit state.

Case Study N° 3: Influence of the location of the soft floor

From the fragility curves shown in Figure 6.16, it can be seen that for models UF, MHF and 3SF. UF structure shows the inadequate performance among all configurations for all limit states. Moreover, structure 3SF shows better performance than MHF which can be interpreted as as aforementioned to the added flexibility for this configuration. On the other hand, by comapring 2MHF with MHF to trace the effect of the number of soft storeys centered in the middle of the building, the results showed that the model MHF with three soft floors in the middle shows better performance than model 2MHF for the low and mild damage states (i.e. Slight, light and moderate damage limit states cases) due to the occurrence of the soft story failure mechanism occurring earlier than the MHF form. Also, the mechanism of the short floor compared to the structure MHF. After reaching the comprehensive moderate and partial collapse limit states, the structure 3SF shows a performance closer to the FF and BF structure due to the structural flexability of this model.

As a numerical analysis, the UF structure can be observed to reach the slight and light limit states for AvgSa values less than 0.08 g, while the 2MHF, MHF and 3SF structures require IM levels higher than 0.023 g. Alternatively, the probability of exceeding the slight limit state at 0.015 g and light limit states at 0.02 g for structure UF was about 90% and 65%, respectively. In contrast,

structure FF was 4% and <1%, as well as for 3SF, it was 60% and 35%, for BF, it was 40% and 15%, for MHF, it was 65% and 38% and for 2MHF, it was 75% and 45% respectively. Likewise, for the case of moderate limit state at 0.1g, the probability of exceeding these cases for the structure UF was 97%, while 3SF, MHF, 2MHF, BF and FF structures were 65%, 75%, 85%, 50% and 05%, respectively. For extensive damage limit state cases, the collapse probability for structure UF at 0.4 g was 95%, while we recorded a probability of 85%, 77%, 60%, 50% and 10 % for 2MHF, MHF, 3SF, BF and FF, respectively. On the other hand, for the partial collapse limit state, the structures with distinct behaviour are now closer to the side of their capabilities, where in this case, the capacitances of the limit states of the UF, 2MHF and MHF structures can be increased to 1.25 g, 1.75 g and 1 g, respectively. Finally, for the collapse limit state, the capabilities of the limit states of the UF structure can be increased to 2.2 g and 2.5 g for both 2MHF and MHF structures. While the 3SF structure can support higher excitation levels, the limit state's capabilities can go up to 3.5 g, similar to the same behaviour of FF

Figure 6.16: Comparison between the fragility functions obtained for 2MHF, MHF, 3SF and UF along with the FF and BF as reference cases.

Figure 6.17 shows the values of AvgSa that are recorded at the probability of exceeding of 50% which corresponds to the considered limit states for FF, BF,3SF, UF, and MHF. It is clear that this plot confirms the previous remarks regarding the fragile behaviour of the UF and 3SF compared to the other cases.

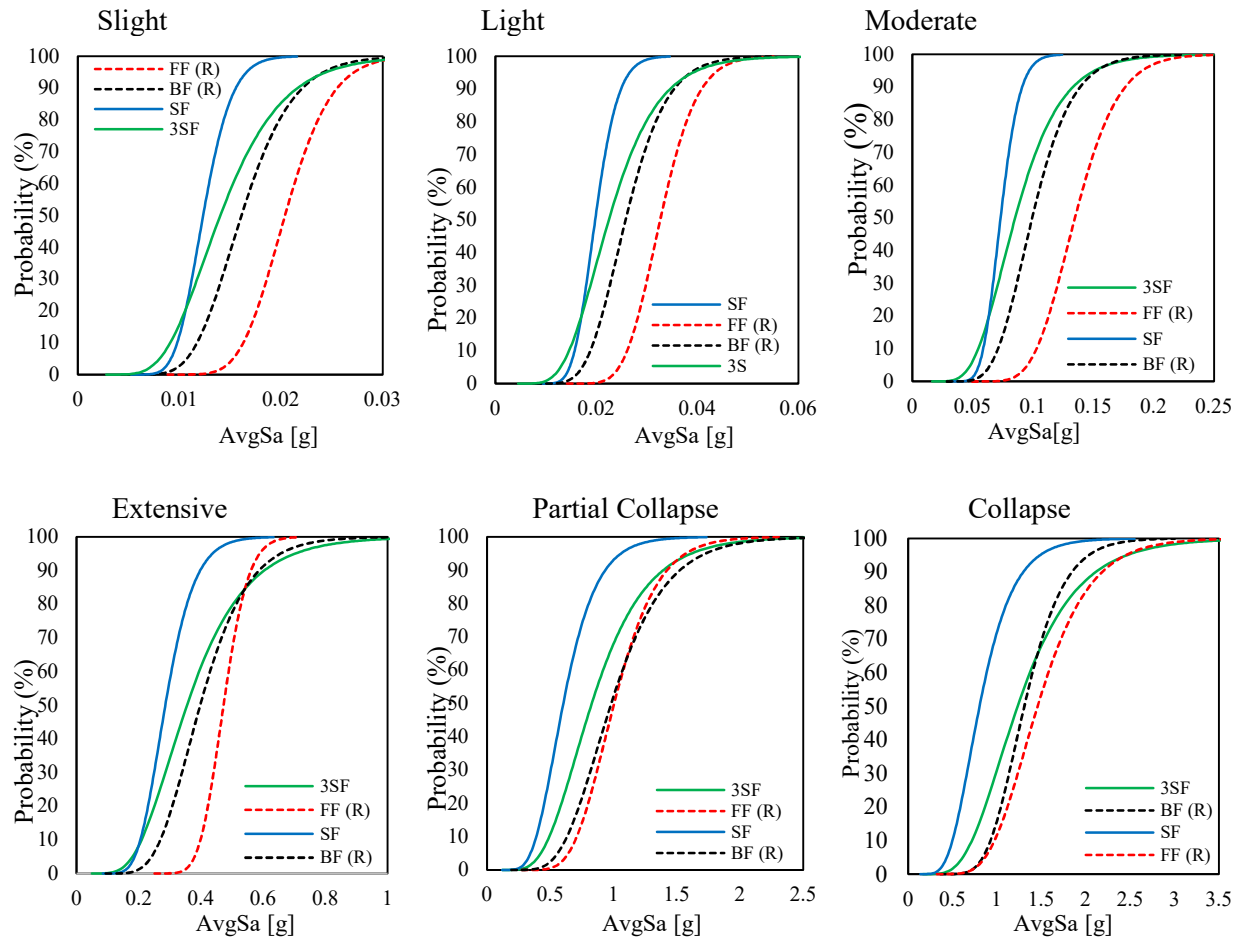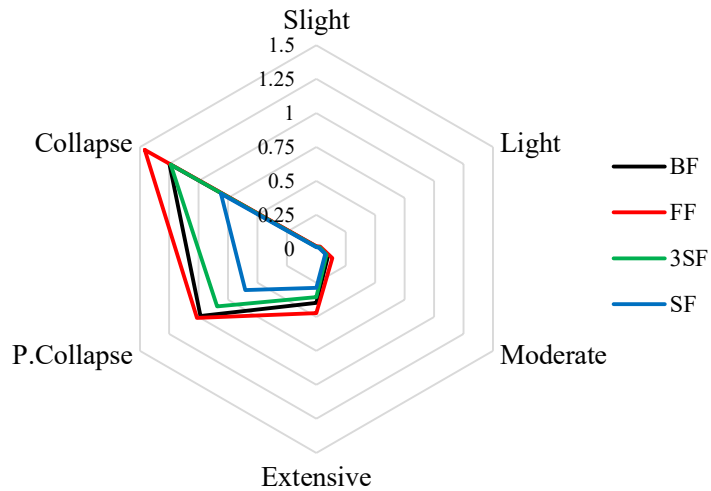Figure 6.17:Radar plot of AvgSa at a probability of 50% for BF, UF, 3SF, MHF and FF at different damage limit state.

Case Study N° 4: Effect of horizontal discontinuity of infill walls

Figure 6.18 shows the comparison between the fragility functions obtained for the models SDF and DF compared with FF, BF and 3SF as reference cases for the six considered damage cases. The main purpose of this comparison is to study and clarify the effect of horizontal discontinuity of infill walls on the general behaviour of buildings when an earthquake occurs.

Due to the inherited vulnerability of the involved cases (i.e. the forced weak floors along their height), FF and BF structures show better performance in most cases of limitation (slight, light, moderate, extensive and partial collapse). In a closer look, the SDF and DF structures show the worst performance among all configurations. This remark as referred to before can be explained in light of forming the weak floor failure mechanism over the higher of these buildings at floors without infills. This highlights how crucial the effect of the horizontal discontinuity and the distribution of infill walls along the height of the buildings is for infilled RC frames.

Furthermore, it is also noted that for the severe limit states (i.e. partial collapse and collapse), the behaviour of structure 3SF shows a better performance compared to SDF and DF which is again due to the margin of flexibility added in this configuration by having more vertical bare frames. By comparing the performance of SDF and DF, which show the effect of vertical discontinuity in RC infilled RC frames, it is clear that both behaviours resemble, reflecting that the behaviour of the building is not sensitive to the location of the soft storey. Also, by looking at the first limit states cases (slight, light, moderate and extensive), it is clear that each of the structure's FF curve start later (the lower tail of the fragility function), which is not the case for the BF, SDF, DF and 3SF which shows a sooner trigger of the damage state. This aspect is important when assessing the losses based on the fragility function.
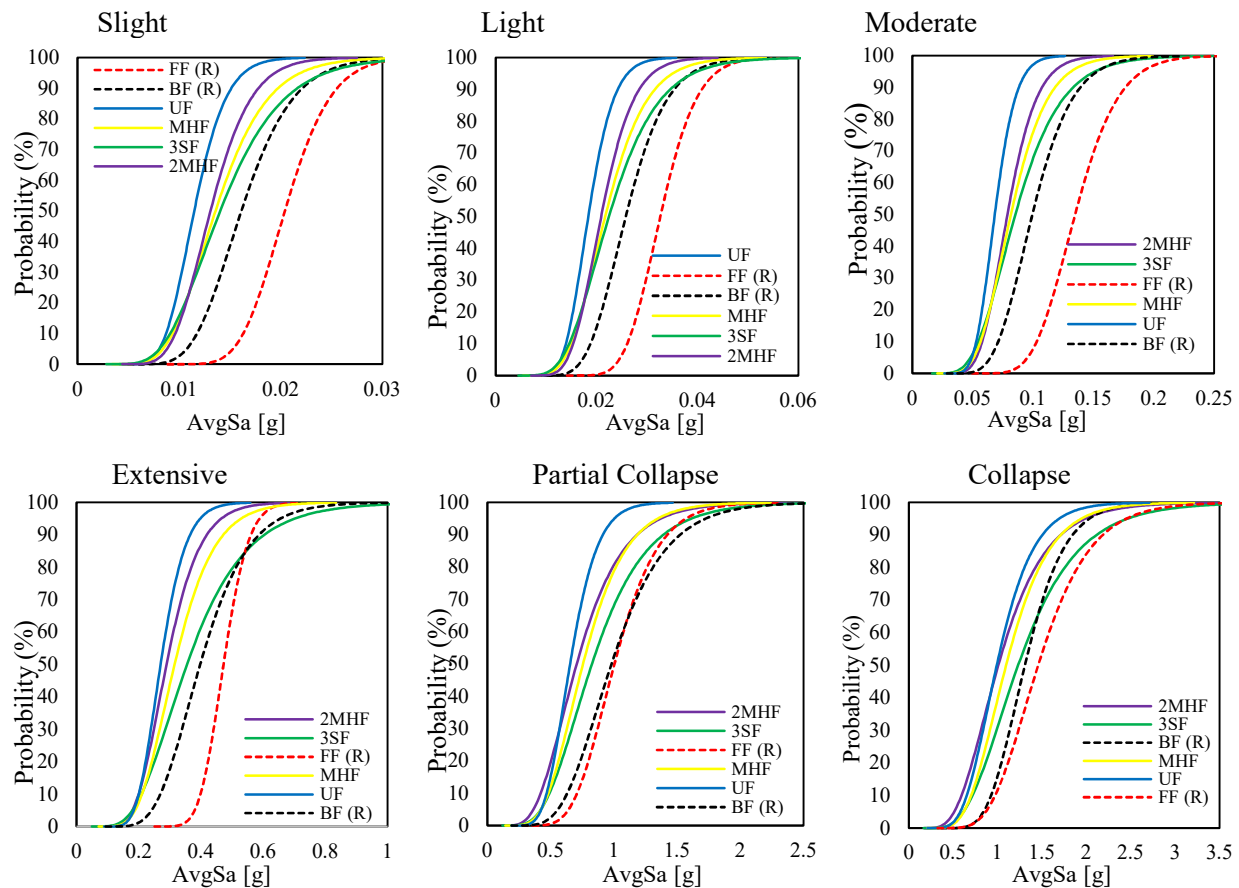

Figure 6.18: Comparison between the fragility functions obtained for 3SF, DF and SDF along with the FF and BF as reference cases.

In term of numbers, the SDF and DF structures reach the slight and light limit states for AvgSa values lower than 0.025 g, 0.03, respectively. For the rest of the models required excitation levels higher than 0.03 g for the slight limit state and 0.04 g for the light limit state. More quantitatively, the probability of exceeding the case of a slight limit state at 0.015 g and the case of a light limit state at 0.025 g for structures SDF and DF was about 55% and 60% for both structures, respectively. In contrast, structure FF was 4% and 5%, and for BF, it was 40% and 45%, and for 3SF, it was 55% and 60%, respectively. Likewise, for the case of moderate limit state at 0.1 g, the probability of exceeding these cases for the structure FF and BF were 10% and 50%, respectively, while structures SDF and DF were 75% and 80%, respectively, while structure 3SF was 65%.For extensive damage limit state cases, the collapse probability for structures SDF and DF at 0.4 g was 90% for both, while we recorded a probability of 10%, 50% and 60% for FF, BF and 3SF, respectively.Also, the probability of exceeding the partial collapse limit states of structures SDF and DF at 1 g was about 87% and 90 %, respectively. For FF, BF and 3SF, the probability of exceedence of the partial collapse limits state are 50%, 55% and 88%, respectively. Similary, the probability of exceedence of the collapse limit states for SDF and DF at IM equals to 2 g were found to be around 98% for both. For structure FF, BF and 3SF were about 85%, 95% and 88%, respectively.

Figure 6.19 shows the values of AvgSa reached by each of the models FF, BF,SF, DF, SDF and 3SF, corresponding to the probability of exceeding an estimated 50%, corresponding to the buildings reaching a state of collapse. This figure reflects a similar conclusion but in a more readable representation. As such DF shows the lowest IM values for all limit states relecting their inhirited vulnerability. In contrast, FF shows adequate behaviour in all the limit states in comparsion with other frames.
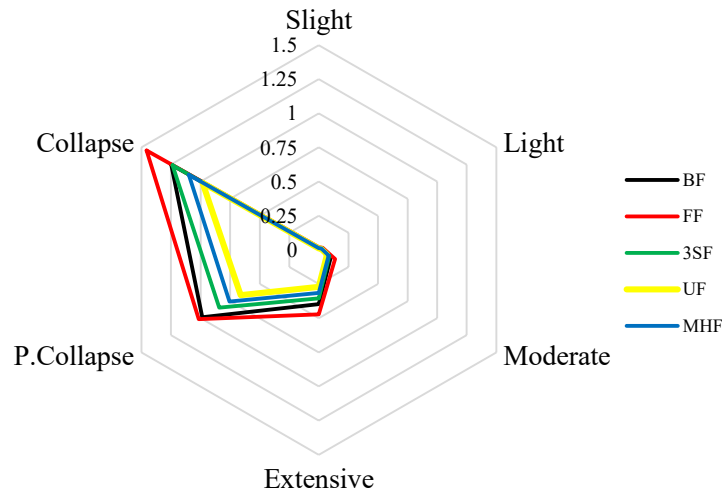
Figure 6.19: Radar plot of AvgSa at a probability of 50% for BF, 3SF, SDF, DF and FF at different damage limit state.

Case Study N° 5 : Effect of vertical discontinuity of infill walls distribution

From Figure 6.20, which shows the comparison of the fragility functions obtained for the models MF and RF compared with FF and BF as reference cases I for the six considered damage states. As can be seen from FF, RF and MF structures, they show an adequate performance than the BF structure for all cases of limit states (slight, light, moderate, extensive, partial collapse, and collapse). This can be interpreted as the contribution of the infill walls that leads to an increase in the structural stiffness and thus better behaviour and performance. It should be noted that the last conclusion can be drawn for the cases that infill loaded along their in-plan direction i.e.,not out of plan load is considered which might be relevant. Another aspect that can be noticed, that the fragility curves of the two structures RF and MF are located in most cases in the middle between the other two curves (FF and BF), this can be explained by the decrease in the contribution of the infill walls due to the absence of these walls in the first bays in the structure RF and the middle in bays to the structure MF, which decreasing to low strength and stiffness of the building. However, the uniformity in load paths in these cases didn't introduce unexpected deviation from the reference cases. Also, by looking at the first limit states cases (slight, light, moderate and extensive), each of the structure's FF, RF and MF curves start latter (the lower tail of the fragility function), which

is not the case for the BF which shows a sooner trigger of the damage state. This aspect important when assessing the losses based on the fragility function.

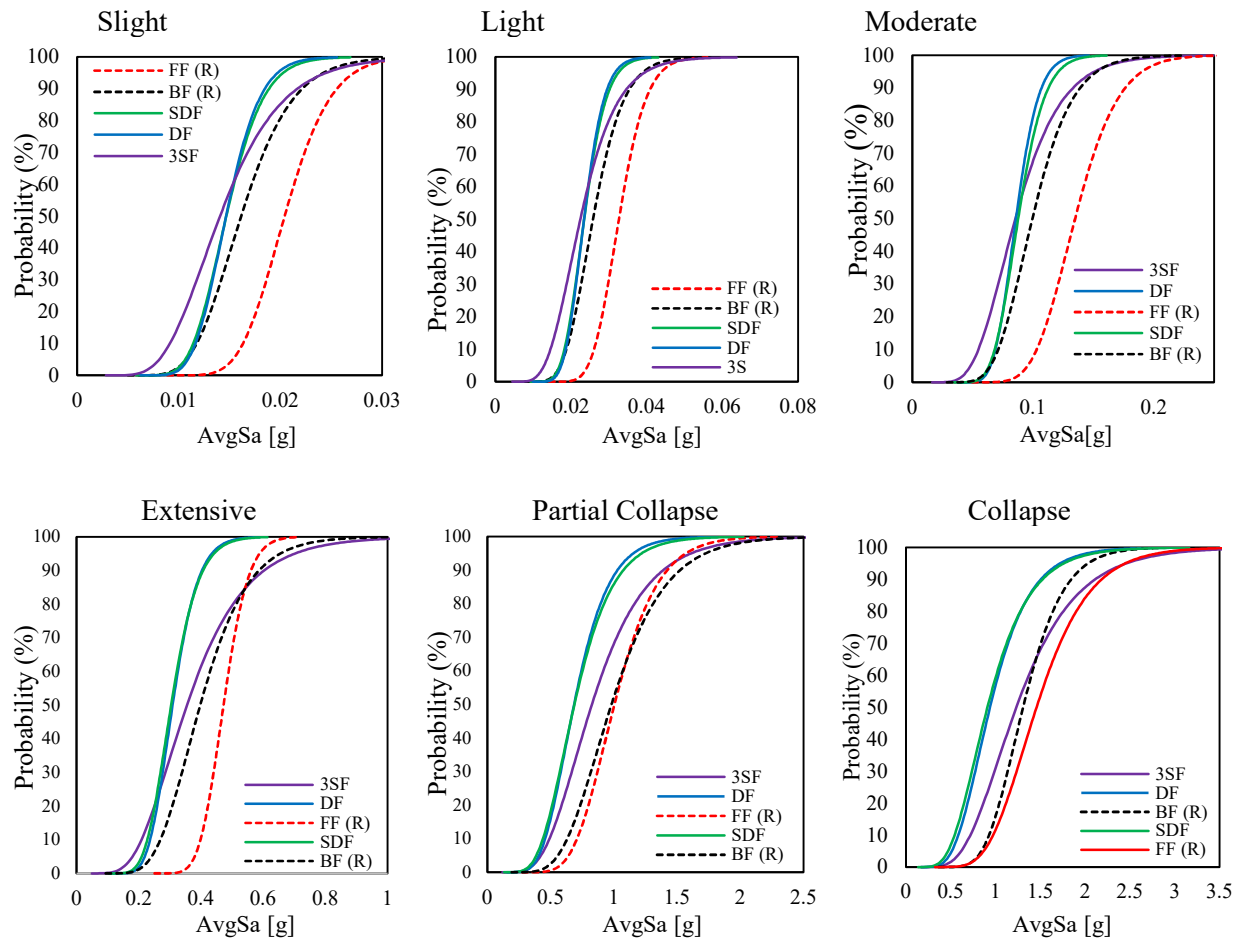Figure 6.20: Comparison between the fragility functions obtained for MF and RF along with the FF and BF as reference cases.

More quantitatively, the probability of exceeding the case of a slight limit state at 0.02 g and the case of a light limit state at 0.03 g for structure BF was about 80% and 75%, respectively. In contrast, structure FF was 45% and 32%, as well as for RF, it was 50% and 35%, for MF, it was 65% and 50%, respectively.Likewise, for the case of moderate limit state at 0.12 g, the probability of exceeding these cases for the structure FF and RF were 30%, while structures MF and BF were 55% and 75%, respectively.For extensive damage limit state cases, the collapse probability for structure BF at 0.4 g was 50%, while we recorded a probability of 10%, 30% and 35% for FF, RF, and MF, respectively.For the partial collapse limit state, each of the structures BF, FF, RF and MF now have similar behaviour and performance and are closer as well as their capacities. In this case,

the capacities of the limit state condition to these structures can go up to 2 g.Finally, for the collapse limit state, the capacities of the limit state of the BF structure can be increased by 2.5 g. In these, the MF and RF structures seem to be able to represent and resemble the behaviour of the FF structure, where the FF, RF and MF structures require excitation levels higher than 3 g, It may reach more than 4 g, but on the other hand, the FF structure stay has the best performance behaviour when strong seismic impact. Figure 6.21 shows the values of AvgSa reached by each of the models FF, BF,RF and MF, corresponding to the probability of exceeding an estimated 50%, corresponding to the buildings reaching a state of collapse.

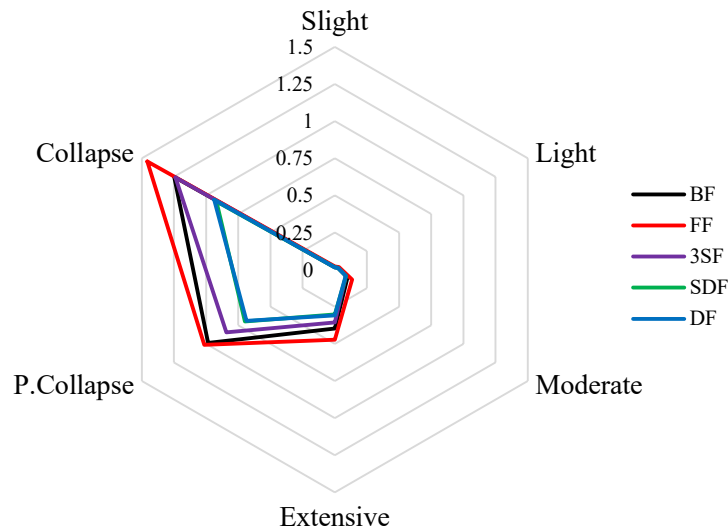
Figure 6.21: Radar plot of AvgSa at a probability of 50% for BF, RF, MF and FF atdifferent damage limit state.

Case Study N° 6: Effect of the positioning of the vertical distribution of infill walls.

Based on Figure 6.22, which shows the comparison between the fragility functions obtained for the models RLF and 2RLF compared with FF and BF as reference cases (R) for the six considered damage cases, to study and clarify the effect of vertical positioning of infill walls on the general behaviour of buildings following the occurrence of a seismic hazard.As evidenced by the FF, 2RLF, and RLF structures, they show better performance than the BF structure for all

cases of limit states (slight, light, moderate, extensive, partial collapse, and collapse); this is due to the configurations of the infill walls and their contribution to increasing the rigidity of the buildings. It should be noted that the last conclusion can be drawn for the cases loaded along their level. Another aspect that can be noticed is that the fragility curves of the two structures, 2RLF and RLF are located in most cases in the middle between the other two curves (FF and BF), this can be explained due to the low strength and rigidity of the structures, and that is a result of the absence of infill walls in the first and second bays concerning the structure 2RLF, the first and the third For the structure RLF, which led to a change in the percentage of the contribution of the infill walls. Another aspect the structure 2RLF shows a better performance than the RLF structure in all cases of limit states due to the effect of the position of the walls with the distribution of the building height on the general behaviour of the buildings.

Also, by considering the cases of the first limiting states (slight, light, moderate and extensive), it is clear that each of the structure's FF, 2RLF and RLF curves start later (the lower tail of the fragility function), which is not the case for BF which a sooner trigger of the damage state. This aspect is important when assessing the losses based on the fragility function. Moreover, it is noted that for the cases of the most severe limits (i.e., partial collapse and collapse), the two structures, 2RLF and RLF are similar and similar in behaviour, and their performance is closer to that of the structure FF. It can be concluded that the position of the infill walls with regular distribution over the height has a minor effect on the general performance of buildings.
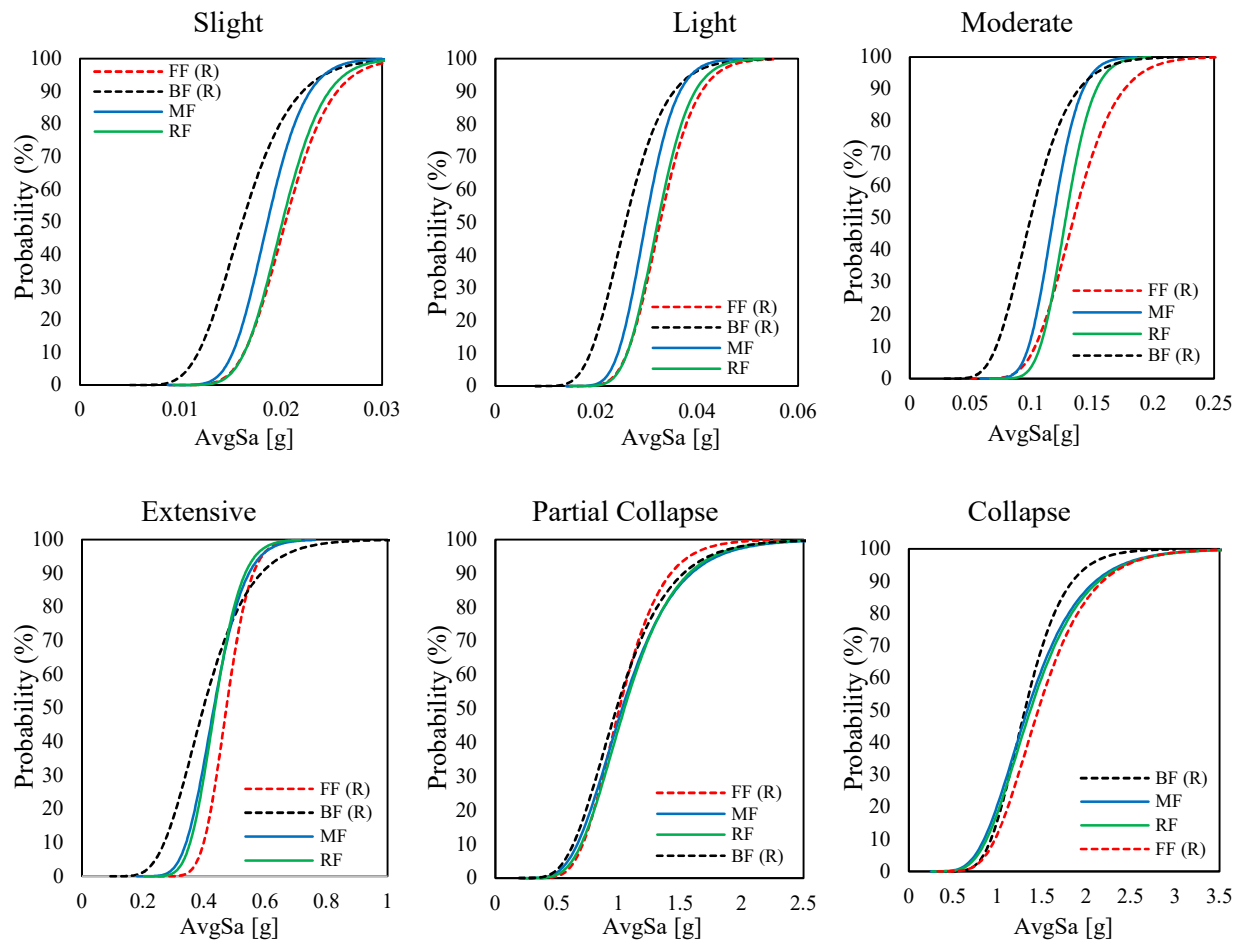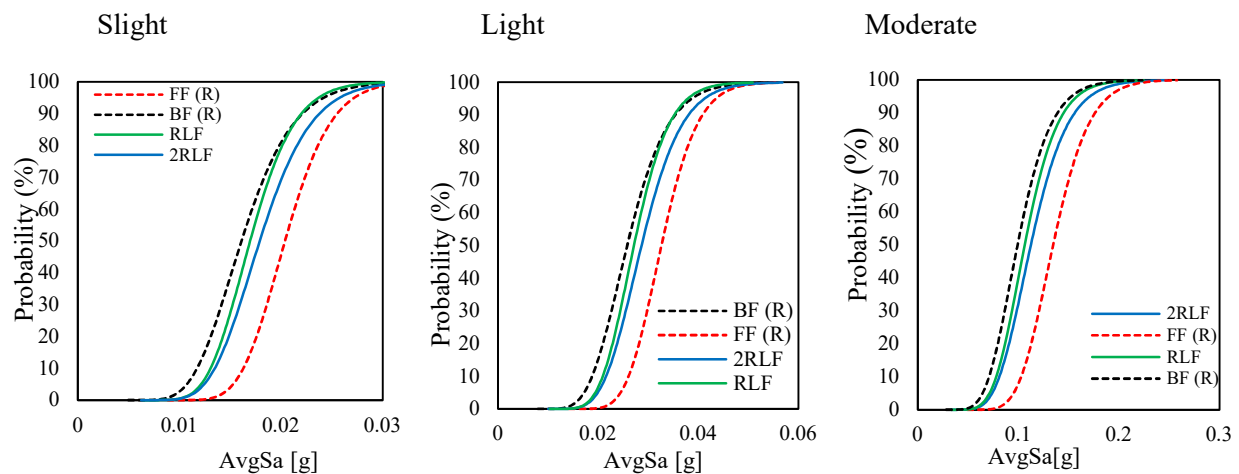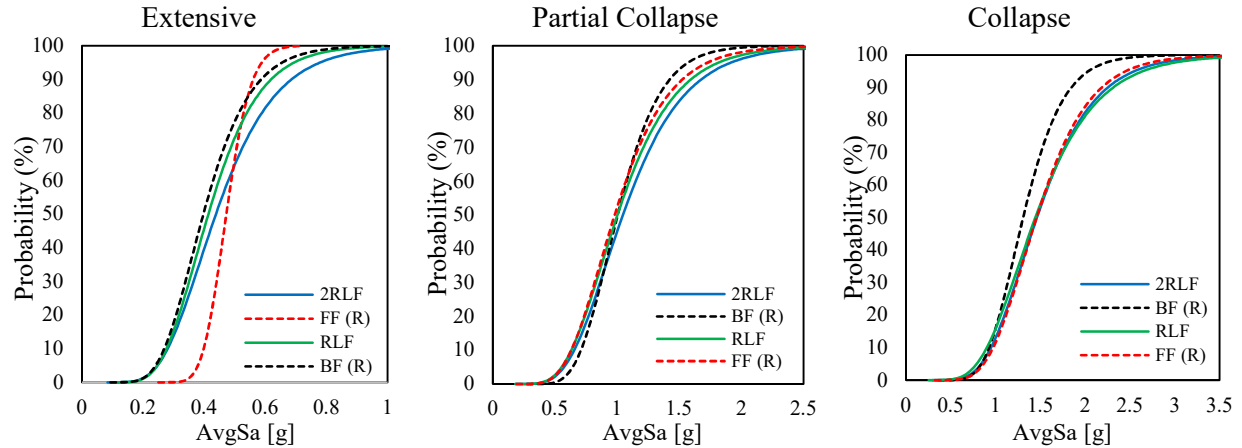
Figure 6.22: Comparison between the fragility functions obtained for 2RLF and RLF along with the FF and BF as reference cases.

More quantitatively, the probability of exceeding the case of a slight limit state at 0.02 g and the case of a light limit state at 0.03 g for structure BF was about 85% and 75%, respectively. In contrast, structure FF was 45% and 30%, and for 2RLF, it was 70% and 55%, and for RLF, it was 78% and 68%, respectively. Likewise, for the case of moderate limit state at 0.12 g, the probability of exceeding these cases for the structures FF and 2RLF were 30% and 60%, respectively, while structures 2RLF and BF were 70% and 75%, respectively. For extensive damage limit state cases, the collapse probability for structure BF at 0.4 g was 53%, while we recorded a probability of 10%, 40% and 45% for FF, 2RLF, and RLF, respectively. For the partial collapse limit state, each of the structures BF, FF, 2RLF and RLF now have similar behaviour and performance and are closer as well as their capacities. In this case, the capacities of the limit state condition to these structures can go up to 2g. Finally, for the collapse limit state, the capacities of the limit state of the BF structure can be increased by 2.7 g. In these, the 2RLF and RLF structures represent and resemble the behaviour of the FF structure, where the FF, RF and MF structures require excitation levels higher than 3 g; it may reach more than 4 g when strong seismic impact. Figure 6.23 shows the values of AvgSa reached by each of the models FF, BF, 2RLF and RLF, corresponding to the probability of exceeding an estimated 50% corresponding to the buildings reaching a state of collapse.
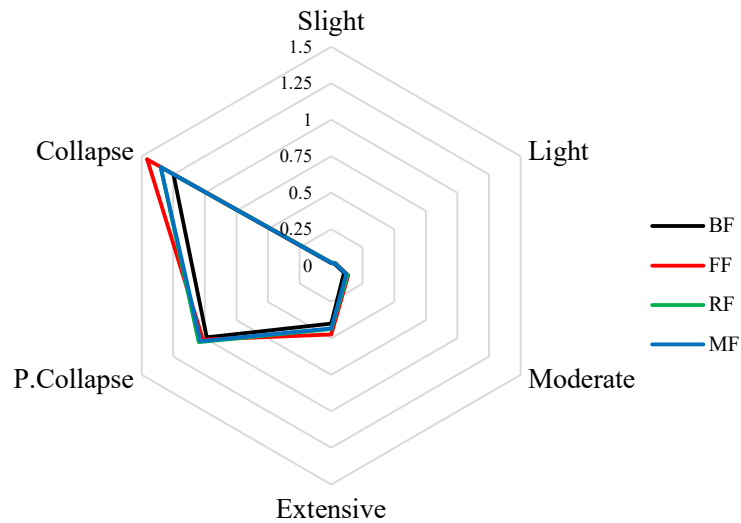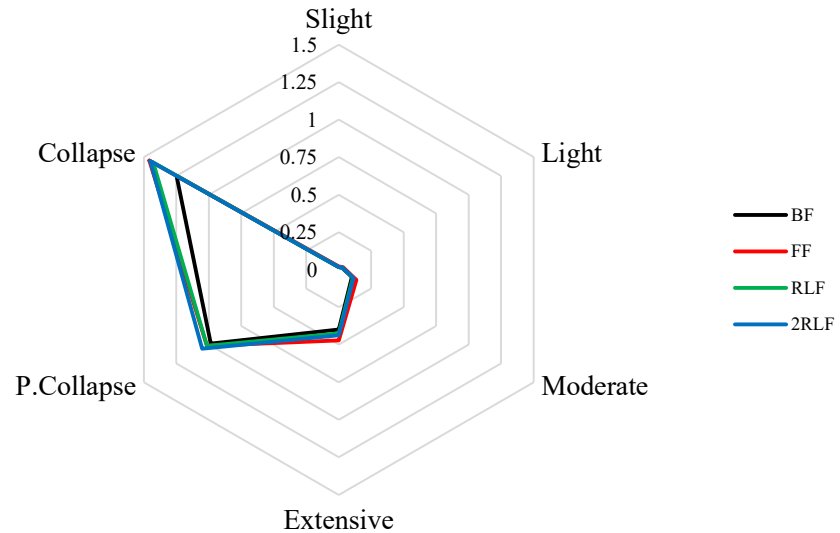
Figure 6.23: Radar plot of AvgSa at a probability of 50% for BF, RLF, 2RLF and FF at different damage limit state.

6.6. Final comments

This chapter investigates the effect of infill walls on the global performance of RC frames using time history analysis. Several configurations were included to identify the effect of infill configurations on global performance. The incremental dynamics analysis IDA was adopted to drive the data for fragility curves. The IM-based fragility curves were then developed using six limit states expressed in terms of maximum inter-storey drift. The comparison between the studied cases was held using the developed fragility curves .

One of the main remarks of this study that all cases that involve one or more soft-storey exhibited fragile behaviour due to their inherited fragility for forming the weak storey mechanism. Another aspect that is worth noting, cases that involve a continuous infill over the height (e.g. RF, Mf, 2RLF and RLF) show better performance compared to those with discontinued infill walls at a certain level. In addition, the existing two subsequent bare floors enhance the performance compared to the cases with one bare between to floor with infills. The latter remark can be interpreted that having two or more bare frame provide a higher level of flexibility for the structure to absorb the vibration without causing damage. In addition, the vertical continuity of the infill over the height of the buildings leads to better performance compared to those cases with discontinuous. Based on the referred conclusions, the vertical continuity of the infill should be

preserved over the height of the building. In case of discontinuous infill over the height, strengthening interference should be conducted in order to enhance their ability to withstand the seismic loads.

Chapter 7.

Final conclusions and future works

7.1 Final Conclusions

The current thesis provided a comprehensive numerical study of RC frames with masonry infills in order to assess the effect of infill walls on the global performance of these structures. Several parameters have been studied including the mechanical properties of the infill, configurations of the infills and percentage of opening. These cases were analysed using static pushover analysis and nonlinear time history analysis. The main conclusion of each part of this thesis was introduced in each chapter, nevertheless, this chapter presents the most relevant remarks as will be presented in the following paragraphs.

In order to achieve representative conclusions, the reliability of the adopted numerical modelling approach was examined against several experimental tests. The main findings of this calibration demonstrates that the adopted macro-modelling procedure is able to adequately represent the behaviour of masonry infilled frames and can be used to simulate this type of structural system using a single strut element. However, quantifying the main parameters of the single strut model using the existing model can lead to huge errors therefore the mechanical properties were defined using the experimental data by tuning the mechanical properties of the strut to get the best fit. By comparing the obtained parameters with those found in the literature, it

was found that there are significant differences between the obtained values and the conventional value which depend on the masonry configuration and geometric properties. Using the calibarted model, the variability of the presence of infill walls on the behavior of these buildings on the lateral loads is exmined using nonlinear static pushover analysis. From this study the following conclsion were drawn:

✓ The results of the pushover analysis show an increase in the initial stiffness and resistance capacity for the full infill frame compared by the bare frame despite the brittle failure modes of the masonry wall. The presence of masonry walls has a significant effect on the observed collapse mechanism.

✓ The size of the openings in the infill walls has a significant influence on the stiffness. Generally, it decreases as the size of the opening increases, indicating that the decrease in stiffness is more important than the decrease in mass.

✓ The infill panels increase the lateral stiffness of the frames, the presence of openings reduces the lateral stiffness of the frame, and with the increase in the size of the openings, the deformation capacity increases; in general, the bare frame shows better ductility than the infill walls frame; this can be attributed to the brittle behavior of masonry infill panels.

✓ It appears on the one hand that the masonry increases the lateral load-bearing capacity and reduces the deformation demand, which can reduce the damage in the structures; on the other hand, an irregular distribution of the masonry can result in a relatively fragile behavior of the structure. The failure modes of the bare frames are distributed over the height of the structures; in the case of the infilled frames, the failure modes are concentrated in the lower levels.

✓ The infill walls distributed homogeneously over the entire height of the building, such as FF, or the alternating distribution over the entire height of the building leads (as an example: RF, MF), to an increase in the stiffness of the structural system and thus a decrease in the desired ductility of the structure before reaching the collapse.

✓ The ratio of the contribution of the infill walls affects the energy damping, as changing the distribution of the infill walls over the entire height of the building would increase the amount of energy absorbed by the buildings by controlling the collapse mechanism

associated with the shape of this distribution (where changing the distribution of the infill walls affects the rigidity of the structure, which which leads to changes how the plastic hing is formed.).

✓ The change in the distribution of infill walls while maintaining their number in the building has a major role in changing the percentage of building walls' contribution to bearing the base shear.

✓ The changes in the number of masonry infill walls in the building plays a major role in changing the values of the contribution ratio, as the percentage of the building walls' contribution to bearing the base shear increases with the increase in the number of masonry walls in the building.

✓ The percentage of building walls' contribution to the bearing of the base shear is mainly related to the number and distribution of the filling walls.

As a general conclusion of this part, it is highly recommended to consider the effect of masonry infill due to the fact that it tends to drastically modify the seismic response of structures, and it is desirable that in future versions of the RPA, specific provisions be dedicated to the effects of infill. Future research work should be done to consider the irregular distributions of the infill masonry walls in the plan, with 3D models, to understand the influence of the irregular distribution of infill masonry walls in the torsional behaviour of the buildings.

In the context of perforamnce assessment of the cosidered cases, chapter 6 investigates the effect of infill walls on the global performance of RC frames using time history analysis. Several configurations were included to identify the effect of infill configurations on global performance. The incremental dynamics analysis IDA was adopted to drive the data for fragility curves. The IM-based fragility curves were then developed using six limit states expressed in terms of maximum inter-storey drift. The comparison between the studied cases was held using the developed fragility curves

One of the main remarks of this study that all cases that involve one or more soft-storey exhibited fragile behaviour due to their inherited fragility for forming the weak storey mechanism.

Another aspect that is worth noting, cases that involve a continuous infill over the height (e.g. RF, Mf, 2RLF and RLF) show better performance compared to those with discontinued infill walls at a certain level. In addition, the existing two subsequent bare floors enhance the performance compared to the cases with one bare between two floor with infills. The latter remark can be interpreted that having two or more bare frame provide a higher level of flexibility for the structure to absorb the vibration without causing damage. In addition, the vertical continuity of the infill over the height of the buildings leads to better performance compared to those cases with discontinuous. Based on the referred conclusions, the vertical continuity of the infill should be preserved over the height of the building. In case of discontinuous infill over the height, strengthening interference should be conducted in order to enhance their ability to withstand the seismic loads.

7.2 Recommendations for future research work

This thesis studied the infills walls using two approaches static and dynamic analysis with different configurations and properties, nevertheless, some points are not fully covered. Therefore, these points are identified for further investigation to carry out:

- For the mechanical properties of a single strut element, a database for all available experimental data need to be compiled and using the described methodology, the properties of the strut element can be identified and perhaps a generalized model can be identified.

- The effect of the design level for RC frame should be studied closely to identify its effect on the findings of this study since this study used only non-seismically designed frames.

- Further research should address effect of the out-of-plane behaviour of masonry infill on the global behaviour of RC frames.

- Deepen the 3D analysis to consider better the influence of the distribution of the panels on the torsional behavior of the structures.

- Conducting experimental studies to validate the numerical results.

Finaly, from the results obtained, it appears that the infill masonry walls must be considered in a non-linear analysis because they tend to drastically modify the seismic response of structures, and it is desirable that in future versions of the RPA, specific provisions be dedicated to the effects of infill.

References

1. G. Uva, F. Porco, and A. Fiore (2012) Appraisal of masonry infill walls effect in the seismic response of RC framed buildings: A case study, Engineering Structures, vol. 34, pp. 514–526.

2. G. Uva, D. Raffaele, F. Porco, and A. Fiore (2012) On the role of equivalent strut models in the seismic assessment of infilled RC buildings," Engineering Structures, vol. 42, pp. 83–94.

3. X. Romão (2013) Field observations and interpretation of the structural performance of constructions after the 11 May 2011 Lorca earthquake, Engineering Failure Analysis, vol. 34, pp. 670–692.

4. Mohamed, Hossameldeen, and Xavier Romão (2021) Robust calibration of macro-models for the in-plane behavior of masonry infilled RC frames. Journal of Earthquake Engineering 25.3, 407-433.

5. C. de National de Recherche Appliquée En Génie-parasismique (2003) Règles parasismique Algériennes RPA 99/version 2003".

6. Pradhan, P. M., P. L. Pradhan and R. K. Maskey (2012) A review on partial infilled frames under lateral loads. Kathmandu university journal of science, engineering and technology 8(1), 142-152.

7. Li, B., Z. Wang, K. M. Mosalam and H. Xie (2008) Wenchuan Earthquake Field Reconnaissance on Reinforced Concrete Framed Buildings With and Without

Masonry Infill Walls. The 14th World Conference on Earthquake Engineering October 12-17, 2008, Beijing, China.

8. Asteris, P. G., K. D.J., C. Z. Chrysostomou and S. E.E. (2011b) Failure Modes of In-filled Frames Electronic Journal of Structural Engineering 11(1), 11-20.

9. Sattar, S. (2013) Influence of masonry infill walls and other building characteristics on seismic collapse of concrete frame buildings. PhD Thesis University of Colorado Boulder,Colorado,USA Colorado,USA.

10. Mehrabi, A. B. (1994) Behavior of masonry-infilled reinforced concrete frames subjected to lateral loadings. PhD Thesis,University of Colorado,Colorado,USA.

11. Stavridis, A. (2009) Analytical and experimental study of seismic performance of reinforced concrete frames infilled with masonry walls. PhD Thesis,University of California San Diego.

12. LNEC (1995) Earthquake behaviour study of masonry infilled concrete frame test of model MD4. Laboratório Nacional de Engenharia Civil (LNEC), report no. 70/95-C3ES Lisbon, Portugal.

13. Blackard, B., K. Willam and S. Mettupalayam (2009) Experimental observations of masonry infilled RC frames with openings. ACI Special Publication 265, 199–222.

14. Armin B. Mehrabi and z. P.Benson Shing (1996) Experimental evaluation of masonry infilled RC. frames. journal of structural engineering 122, 228-237.

15. Al-Chaar, G. (2002) Evaluating strength and stiffness of unreinforced masonry infill structures. Construction Engineering Research Laboratory, US Army Corps of Engineers, Washington, USA.

16. El-Dakhakhni, W. W., M.Elgaaly and A. A. Hamid (2003) Three-Strut Model for Concrete Masonry-Infilled Steel Frames. Journal of Structural Engineering 129(2), 69-77.

17. Ghosh, A. and A. Amde (2002) Finite Element Analysis of Infilled Frames. Journal of Structural Engineering 128(7), 881-889.

18. CEB (1996) RC frames under earthquake loading. Comité Euro-International du Béton (CEB), Thomas Telford, London, England, UK.

19. H. M. A. Mohamed. (2017) "Seismic risk assessment of reinforced concrete frames with masonry infill," PhD, Department of Civil Engineering, Universidade do Porto.

20. Asteris, P. G., K. D.J., C. Z. Chrysostomou and S. E.E. (2011b) Failure Modes of In-filled Frames Electronic Journal of Structural Engineering 11(1), 11-20.

21. Polyakov, S. V. (1956) Masonry in Framed Buildings : An Investigation into the Strength and Stiffness of Masonry Infilling. "Gosudarstvennoe izdatel'stvo Literatury po stroitel'stvu i arkhitekture", Moscow Russia. (English translation by G. L. Cairns, National Lending Library for Science and Technology, Boston, Yorkshire, England, 1963).

22. Sachanski, S. (1960) nalysis of the earthquake resistance of frame buildings taking into consideration the carrying capacity of the filling maosnry. Proc. 2nd World Conference on Earthquake Engineering & Structural Dynamics, 2127-2141.

23. Holmes, M. (1961) Steel frames with brickwork and concrete infilling. ICE Proceedings 19(4), 473-478.

24. Mainstone, R. J. (1971) On The stiffness and strengths of infilled frames. ICE Proceedings 49(2), 230.

25. Mainstone, R. J., G. A. Weeks and S. Building Research (1972) The influence of a bounding frame on the racking stiffness and strengths of brick walls. Building Research Station,Garston, Eng.

26. Fiorato, A. E., M. A. Sozen and W. L. Gamble (1970) An Investigation of the Interaction of Reinforced Concrete Frames with Masonry Filler Walls. Department of civil engineering, Illinois university Urbana, Illinois, USA.

27. Klingner, R. E. and V. V. Bertero (1978) Earthquake resistance of infilled frames. Journal of the structural division 104(6), 973-989.

28. Zarnic, R. and M. Tomazevic (1984) An experimentally obtained method for evaluation of the behaviour of masonry infilled RC frames. 9th World Conference on Earthquake Engineering, San Francisco, USA, 863-870.

29. Pires, F. M. G. (1990) Influence of masonry walls over the behavior of reinforced concrete frames under horizontal actions. Thesis (in Portuguese) National Laboratory for Civil Engineering.

30. Mosalam, K. M., R. N. White and G. Ayala (1998) Response of infilled frames using pseudo-dynamic experimentation. Earthquake engineering & structural dynamics 27(6), 589-608.

31. Buonopane, S. and R. White (1999) Pseudodynamic testing of masonry infilled reinforced concrete frame. Journal of structural engineering 125(6), 578-589.

32. Lee, H. S. and S. W. Woo (2002) Effect of masonry infills on seismic performance of a 3-storey R/C frame with non-seismic detailing. Earthquake engineering & structural dynamics 31(2), 353-378.

33. Hashemi, A. and K. M. Mosalam (2006) Shake-table experiment on reinforced concrete structure containing masonry infill wall. Earthquake engineering & structural dynamics 35(14), 1827-1852.

34. Anil, Ö. and S. Altin (2007) An experimental study on reinforced concrete partially infilled frames. Engineering Structures 29(3), 449-460.

35. Blackard, B., K. Willam and S. Mettupalayam (2009) Experimental observations of masonry infilled RC frames with openings. ACI Special Publication 265, 199–222.

36. Stavridis, A., I. Koutromanos and P. B. Shing (2012) Shake-table tests of a three-story reinforced concrete frame with masonry infill walls. Earthquake Engineering & Structural Dynamics 41(6), 1089-1108.

37. Sigmund, V. and D. Penava (2013) Assessment of masonry infilled reinforced-concrete frames with openings. Tehnički vjesnik 20(3), 459-466.

38. Mansouri, A., M. S. Marefat and M. Khanmohammadi (2014) Experimental evaluation of seismic performance of low-shear strength masonry infills with openings in reinforced concrete frames with deficient seismic details. The Structural Design of Tall and Special Buildings 23(15), 1190-1210.

39. Mallick, D. and R. Severn (1967) The behaviour of infilled frames under static loading. ICE Proceedings 38(4), 639-656.

40. Mallick DV, Garg RP. (1971) Effect of openings on the lateral stiffness of infilled frames. Proc Inst Civil Engrs; 49:193–209.

41. Dhanasekhar, M. and A. Page (1986) The influence of brick masonry infill properties on the behaviour of i nfilled frames. ICE Proceedings 81(4), 593-605.

42. Lotfi, H.R., Shing, P.B. (1991) An appraisal of smeared crack models for masonry shear wall analysis. Computers & Structures 41, 413–425.

43. Lotfi, H. R. and P. B. Shing (1994) Interface model applied to fracture of masonry structures. Journal of structural engineering 120(1), 63-80.

44. Lourenço, P. and J. Rots (1997) Multisurface Interface Model for Analysis of Masonry Structures. Journal of Engineering Mechanics 123(7), 660-668.

45. Mehrabi, A. and P. Shing (1997) Finite Element Modeling of Masonry-Infilled RC Frames. Journal of Structural Engineering 123(5), 604-613.

46. Oliveira, D.V., Lourenco, P.B (2004) Implementation and validation of a constitutive model for the cyclic behaviour of interface elements. Computers & structures 82, 1451–1461

47.   Stavridis, A. and P. Shing (2010) Finite-element modeling of nonlinear behavior of masonry-infilled RC frames. Journal of structural engineering 136(3), 285-296.

48.   Koutromanos, I., A. Stavridis, P. B. Shing and K. Willam (2011) Numerical modeling of masonry-infilled RC frames subjected to seismic loads. Computers & Structures 89(11), 1026-1037.

49.   Smith, B. S. and C. Carter (1969) A method of analysis for infilled frames. ICE Proceedings 44(1), 31-48.

50.   Mainstone, R. J. (1974) Supplementary note on the stiffness and strengths of infilled frames. Building Research Station, .

51.   Decanini, L. D. and G. E. Fantin (1987) Modelos simplificados de la mampostería incluida en porticos. Características de rigidez y resistencia lateral en astado límite. Jornadas Argentinas de Ingeniería Estructural III Asociacion de Ingenieros Estructurales 2, 817-836.

52.   Moghaddam, H. and P. Dowling (1988) Earthquake resistant design of brick infilled frame. Proceedings of the Eighth international brick and block masonry conference, 774-784.

53.   Hendry, A. (1990) Structural masonry. MacMillan Education, Ltd.,London, UK.

54.   Paulay, T. and M. J. N. Priestley (1992) Seismic design of reinforced concrete and masonry buildings. John Wiley & Sons, Inc.,Toronto, Ontario, Canada.

55.   Durrani, A. J. and Y. H. Luo (1994) Seismic retrofit of flat-slab buildings with masonry infills. Proceedings NCEER Workshop on Seismic Response of Masonry Infills.

56.   NZS 4230 (2004) The New Zealand masonry Code: Design of Reinforced Concrete Masonry Structures Authority, Building Industry New Zealand.

57.   Chethan, K., R. Babu, K. Venkataramana and A. Sharma (2009) Study on Dynamic Characteristics of 3D Reinforced Concrete Frame with Masonry Infill. Journal of CPRI 5(2), 11-18.

58.   Md.Khaja.M, Chethan.K and R. Babu (2013) Earthquake analysis on 2d RC frames with different aspect ratios of masonry infill and monolithic panel. International Journal of Research in Engineering and Technology, 18-23.

59.   CCMPA (2009) Seismic design guide for masonry buildings. Canadian Concrete Masonry Producers Association (CCMPA) Toronto,Ontario, Canada.

60.   ACI 530/530.1-08 (2011) Building code requirements and specification for masonry structures and related commentaries. . American Concrete Institute, Masonry Standards Joint Committee Farmington Hills, Michgan,USA.

61.   Turgay, T., M. C. Durmus, B. Binici and G. Ozcebe (2014) Evaluation of the Predictive Models for Stiffness, Strength, and Deformation Capacity of RC Frames with Masonry Infill Walls. Journal of Structural Engineering 140(10).

62.   Buonopane, S. and R. White (1999) Pseudodynamic testing of masonry infilled reinforced concrete frame. Journal of structural engineering 125(6), 578-589.

63.   Reflak, J. and P. Fajfar (1991) Elastic analysis of infilled frames using substructures. Proceeding of the sixth Canadian Conference on Earthquake Engineering, Ontario, Canada, 285-292.

64.   Saneinejad, A. and B. Hobbs (1995) Inelastic design of infilled frames. Journal of Structural Engineering 121(4), 634-650.

65.   Leuchars, J. M. and J. C. Scrivener (1976) Masonry infill panels subjected to cyclic in-plane loading. Bulletin of the New Zealand National Society for Earthquake Engineering 9 n 2 122-131.

66.   Zarnic, R. and M. Tomazevic (1988) An experimentally obtained method for evaluation of the behavior of masonry infilled RC frames. Proceedings of the 9th World Conference on Earthquake Engineering. , Tokyo-Kyoto, Japan, 163–168.

67.   Schmid, B., J. Kariotis and E. Schwartz (1973) Tentative Los Angeles ordinance and testing program for unreinforced masonry buildings. Department of Building and Safety, City of Los Angeles, Los Angeles,California, USA.

68.   Syrmakezis, C. A. and V. Y. Vratsanou (1986) Influence of infill walls to RC frames Response. Proc., 8th European Conf. on Earthquake Engineering, European Association for Earthquake Engineering (EAEE). Istanbul, Turkey, 47-53.

69.   Andreaus, U., M. Cerone, P. D'Asdia and F. Iannozzi (1985) A finite element model for the analysis of masonry structures under cyclic actions. Proceeding of the seventh internacional brick and masonry conference, Melbourne, Australia, 479-88.

70.   Chrysostomou, C. Z. (1991) Effects of degrading infill walls on the nonlinear seismic response of two-dimensional steel frames. PhD Thesis,Cornell University, New York, USA.

71.   Chrysostomou, C. Z., P. Gergely and J. F. Abel (1992) Non-linear seismic response of infilled steel frames. Proceedings Tenth World Conference on Earthquake Enginerring, Madrid, Spain, 4435-4437.

72.   Te-Chang, L. and K. Kwok-Hung (1984) Nonlinear behaviour of non-integral infilled frames. Computers & structures 18(3), 551-560.

73.   Crisafulli, F. G. (1997) Seismic behaviour of reinforced concrete structures with masonry infills. PhD Thesis,University of Canterbury, Christchurch, New Zealand.

74.   Rodrigues, H., H. Varum and A. Costa (2010) Simplified Macro-Model for Infill Masonry Panels. Journal of Earthquake Engineering 14(3), 390-416.

75.   Pinto, A. V. and F. Taucer (2006) Book section title "Assessment and retrofit of full-scale models of existing RC frames" book title "Advances in earthquake engineering for urban risk reduction".Springer,Netherlands.

76.   ASCE ASCE/SEI 41-06 (2007) Seismic rehabilitation of existing buildings American Society of Civil Engineers, Reston, Virginia, USA.

77.   TEC (2007) Turkish Code for Buildings in Seismic Zones The ministry of public works and settlement Cengelkoy, Istanbul, Turkey.

78.   Abdesslam, Issam (2018) Analyse Pushover des structures en béton armé tridimensionnelle à étage souple. PhD Thesis University of Biskra. Biskra, Algeria.

79.   Abdesslam Issam (2010) Analyse sismique des structures en béton arme par la méthode Pushover. Magister Thesis, Université Mohamed Khider-Biskra, Algeria.

80.   Gupta B (1998) Enhanced Pushover Procedure and Inelastic Demand Estimation for Performance-based Seismic Evaluation of Buildings, Ph.D. Dissertation, Orlando, Florida, University of Central Florida, USA.

81.   FEMA-356 (2000) Prestandard and commentary for seismic rehabilitation of buildings. Federa l Emergency Management Agency Washigton D.C., Maryland, USA.

82.   Chopra A.K. and Goel, R.K (1999) Capacity-Demand-Diagram Methods for Estimating Seismic Deformation of Inelastic Structures: SDF Systems, PEER Report 1999/02, University of California, Berkeley, USA.

83.   Applied Technology Council, ATC 40 (1996) Seismic Evaluation and Retrofit of Concrete Buildings, Volume 1-2, California.

84.   Eurocode 8 (2003), Design of Structures for Earthquake Resistance: General Rules, Seismic Actions and Rules for Buildings, EN1998-1:2003, British Standards Institution, London.

85.   Federal Emergency Management Agency, FEMA-273, NEHRP (1997) Guidelines for the Seismic Rehabilitation of Buildings.

86.   Spacone, E. (2000). Nonlinear Pushover Analysis of Reinforced Concrete Structures, Colorado Advanced Software Institute, FINAL REPORT Spacone, E., Ciampi, V. and Filippou, FC (1996), Mixed Formulation of Nonlinear Beam Finite Element. Computer and Structure, 58, 71-83.

87.   Krawinkler, H., & Seneviratna, G. D. P. K. (1998). Pros and cons of a pushover analysis of seismic performance evaluation. Engineering structures, 20(4-6), 452-464.

88.   Fajfar, P., & Fischinger, M. (1988, August) N2-A method for non-linear seismic analysis of regular buildings. In Proceedings of the ninth world conference in earthquake engineering (Vol. 5, pp. 111-116).

89.   Fajfar P (2002) Structural Analysis in Earthquake Engineering – A Breakthrough of Simplified Non-linear Methods, Proceedings of 12th European Conference on Earthquake Engineering, London, Paper No. 843, (1-20).

90.   Li Gang. Liu Yong (2004) Target Displacement in Pushover Analysis for Eccentric Building Structures Considering Torsion Effect, The Sixth World Congress on Computational Mechanics, Beijing.

91.   Fajfar, P. (1999). Capacity spectrum method based on inelastic demand spectra. Earthquake Engineering & Structural Dynamics, 28(9), 979-993.

92.   Miranda, E. (1993). Evaluation of site-dependent inelastic seismic design spectra. Journal of Structural Engineering, 119(5), 1319-1338.

93.   Kalkan, E., 2006, Prediction of Seismic Demands in Building Structures, PhD dissertation in Civil and Environmental Engineering, University of California, Davis.

94.   Chopra, A. K., & Goel, R. K. (2002). A modal pushover analysis procedure for estimating seismic demands for buildings. Earthquake engineering & structural dynamics, 31(3), 561-582.

95.   A S. Elnashai and L. Di Sarno, Fundamentals of earthquake engineering: Wiley New York, 2008.

96.   Gupta, B., and Kunnath, S. K. 2000. "Adaptive spectra-based pushover procedure for seismic evaluation of structures." Earthquake Spectra,162, 367–391

97.   FEMA-440 (2005). Improvement of nonlinear static seismic analysis procedures. Federal Emergency Management Agency. Washington D. C.

98.   Mezgeen, R. (2014). Seismic Performance Assessment and Strengthening of a Multi-Story RC Building through a Case Study of Seaside Hotel. Gazimağusa, North Cyprus: Eastern Mediterranean University.

99.   Vamvatsikos, D., & Cornell, C. (2002). Incremental dynamic analysis. Submitted to Earthquake Engineering and Structural Dynamics, John Wiley & Sons, Ltd.

100.   Rossetto, T. and Elnashai, A. (2005) A new analytical procedure for the derivation of displacement based vulnerability curves for populations of RC structures. Engineering Structures 27(3), 397-409.

101.   A. Papaila (2011) Seismic fragility curves for reinforced concrete buildings. M. Tech Dissertation, University of Patrax, Greece.

102.   Ay, B. Ö., Erberik, M. A., & Akkar, S. (2006, September). Fragility based assessment of the structural deficiencies in turkish RC frames structures. In First European Conference on Earthquake Engineering and Seismology (No. 593).

103.   Ghobarah, A. (2004). "On drift limits associated with different damage levels". Proceedings of the international workshop, BLED, Slovenia, 28 JUNE – 1 July 2004.

104.   SEAOC (1995). Vision 2000, Performance based seismic engineering of buildings, vols. I and II: Conceptual framework. Sacramento (CA): Structural Engineers Association of California.

105.   McKenna, F. OpenSees (2011) A Framework for Earthquake Engineering Simulation. Comput. Sci. Eng 13, 58–66.

106.   O'Reilly, G.J.; Sullivan, T.J. (2017) Modeling Techniques for the Seismic Assessment of the Existing Italian RC Frame Structures. J. Earthq. Eng, 23, 1262–1296.

107.   Scott, M.H.; Ryan, K.L. Moment-Rotation (2013) Behavior of Force-Based Plastic Hinge Elements. Earthq. Spectra 29, 597–607.

108.   Scott, M.H.; Fenves, G.L. (2006) Plastic Hinge Integration Methods for Force-Based Beam–Column Elements. J. Struct. Eng. 132, 244–252.

109. Paulay, T.; Priestly, M.J.N.(1992) Seismic Design of Reinforced Concrete and Masonry Buildings, 1st ed.; John Wiley & Sons, Inc.: New York, NY, USA, 1992; p. 744.

110. Menegotto, M.; Pinto, P.E.(2022) Method of analysis for cyclically loaded R.C. plane frames including changes in geometry and non-elastic behaviour of elements under combined normal force and bending. IABSE reports. Available online: https://www.eperiodica.ch/digbib/view?pid=bse-re-001:1973:13::9#90 .

111. Mondal, G.; Jain, S.K.(2008) Lateral Stiffness of Masonry Infilled Reinforced Concrete (RC) Frames with Central Opening. Earthq. Spectra 2008, 24, 701–723.

112. Dolšek, M.; Fajfar, P. (2008) The effect of masonry infills on the seismic response of a four-storey reinforced concrete frame—A deterministic assessment. Eng. Struct, 30, 1991–2001.

113. Mohamed, H.; Romão, X. (2020) Analysis of the performance of strut models to simulate the seismic behaviour of masonry infills in partially infilled RC frames. Eng. Struct, 222, 111124.

114. Decanini, L.D.; Liberatore, L.; Mollaioli, F. (2014) Strength and stiffness reduction factors for infilled frames with openings. Earthq. Eng. Eng. Vib, 13, 437–454.

115. Asteris, P.G.; Cotsovos, D.M.; Chrysostomou, C.Z.; Mohebkhah, A.; Al-Chaar, G.K. (2013) Mathematical mi cromodeling of infilled frames: State of the art. Eng. Struct, 56, 1905–1921.

116. Hamburger, R.O.; Chakradeo, A.S. (1993) Methodology for seismic capacity evaluation of steel-frame buildings with infill unreinforced masonry. In Mitigation and Damage to the Built Environment; U.S. Central United States Earthquake Consortium (CUSEC): Memphis, TN, USA; pp. 173–182.

117. Thiruvengadam, V. (1985) On the natural frequencies of infilled frames. Earthq. Eng. Struct. Dyn. 13(3), 401–419.

118. Tripathy, D.; Singhal, V. (2019) Estimation of in-plane shear capacity of confined masonry walls with and without openings using strut-and-tie analysis. Eng. Struct 188, 290–304.

119. Anil, Ö.; Altin, S. (2007) An experimental study on reinforced concrete partially infilled frames. Eng. Struct, 29, 449–460.

120. Mughal, U.A.; Qazi, A.U.; Ahmed, A.; Abbass, W.; Abbas, S.; Salmi, A.; Sayed, M.M. (2022) Impact of Openings on the In-Plane Strength of Confined and

Unconfined Masonry Walls: A Sustainable Numerical Study. Sustainability, 14, 7467.

121. Kakaletsis, D. J. and C. G. Karayannis (2008) Influence of Masonry Strength and Openings on Infilled R/C Frames Under Cycling Loading. Journal of Earthquake Engineering 12(2), 197-221.

122. EN-998-2 (2001) Specification for Mortar for Masonry. European Committee for Standardization, Brussels, Belgium, 2001.

123. Furtado, A., Rodrigues, H., Arêde, A., Melo, J., & Varum, H. (2021). The use of textile-reinforced mortar as a strengthening technique for the infill walls out-of-plane behaviour. Composite Structures, 255, 113029.

124. Furtado A, Costa C, Arêde A, Rodrigues H. (2016) Geometric characterisation of Portuguese RC buildings with masonry infill walls. Eur J Environ Civil Eng :1–16.

125. CEN, NP EN10002-1 – (2006) Tensile testing of mettalic materials - Part 1: Method of test at ambient temperature. European Committee for Standardization.

126. NP EN206 (2000) - Concrete - Specification, performance, production and conformity (Portuguese version).

127. Agante, M., Furtado, A., Rodrigues, H., Arêde, A., Fernandes, P., & Varum, H. (2021). Experimental characterization of the out-of-plane behaviour of masonry infill walls made of lightweight concrete blocks. Engineering Structures, 244, 112755.

128. CEN. NP-EN 772-1 (2002) M´etodos de ensaio de bolocos para alvenaria Parte 1 : Determinaç˜ao da resistˆencia `a compressao;.

129. De Risi, M. T., Furtado, A., Rodrigues, H., Melo, J., Verderame, G. M., Arêde, A., ... & Manfredi, G. (2022). Influence of textile reinforced mortars strengthening on the in-plane/out of-plane response of masonry infill walls in RC frames. Engineering Structures, 254, 113887.

130. CEN, "NP EN 771-1 (2016) Especificaçoes ˜ para unidades de alvenaria Parte 1: Unidades cerˆamicas (tijolos ceramicos).

131. Messaoudi, A., Chebili, R., Mohamed, H., & Rodrigues, H. (2022). Influence of Masonry Infill Wall Position and Openings in the Seismic Response of Reinforced Concrete Frames. Applied Sciences, 12(19), 9477.

132. Kent, D. C. and Park, R. (1971) Flexural members with confined concrete. Journal of the Structural Division 97(7), 1969-1990.

133.   Niewiarowski, R.W.; Rojahn, C (2022) Seismic Evaluation and Retrofit of Concrete Buildings SEISMIC SAFE-TY COMMISSION State of California Products 1.2 and 1.3 of the Proposition 122 Seismic Retrofit Practices Improvement Program; 1996. Available online: https://www.atcouncil.org/pdfs/atc40toc.pdf (accessed on 29 April 2022).

134.   Sigmund, V., & Penava, D. (2013). Assessment of masonry infilled reinforced-concrete frames with openings. Tehnički vjesnik, 20(3), 459-466.

135.   Asteris, P. G., Cavaleri, L., Di Trapani, F., & Sarhosis, V. (2016). A macro-modelling approach for the analysis of infilled frame structures considering the effects of openings and vertical loads. Structure and Infrastructure Engineering, 12(5), 551-566.

136.   Kurmi, P. L., & Haldar, P. (2022, July). Modeling of opening for realistic assessment of infilled RC frame buildings. In Structures (Vol. 41, pp. 1700-1709). Elsevier.

137.   Yekrangnia, M., & Asteris, P. G. (2020). Multi-strut macro-model for masonry infilled frames with openings. Journal of Building Engineering, 32, 101683.

138.   Chaibedra, B., Benanane, S., Bahar, S., Benanane, A., Bourdim, S. M., & Titoum, M. (2019). Analyse de la performance sismique du patrimoine bâti de la ville de Mostaganem en Algérie. Academic Journal of Civil Engineering, 37(1), 445-449.

139.   Aschheim M, Hernández-Montes E, Vamvatsikos D. (2019) Design of Reinforced Concrete Buildings for Seismic Performance: Practical Deterministic and Probabilistic Approaches: Crc Press.

140.   Eads, L., Miranda, E., & Lignos, D. G. (2015). Average spectral acceleration as an intensity measure for collapse risk assessment. Earthquake Engineering & Structural Dynamics, 44(12), 2057-2073.

141.   Rossetto, T. and Elnashai, A. (2003) Derivation of vulnerability functions for European-type RC structures based on observational data. Engineering Structures 25(10), 1241-1263.

142.   Muntasir Billah, A. H. M., & Shahria Alam, M. (2015). Seismic fragility assessment of highway bridges: a state-of-the-art review. Structure and infrastructure engineering, 11(6), 804-832.

143.   Mohamed, H., & Romão, X. (2021). Seismic Fragility Functions for Non Seismically Designed RC Structures Considering Pounding Effects. Buildings, 11(12), 665.